이학박사 학위논문

C1 Functionalization Methods of Organic Compounds: N-Methylation, N-Formylation, and C(sp^3)–H Trifluoromethylation

유기물의 C1 작용기화 반응 개발: N-메틸화, N-포밀화, 그리고 C(sp^3)-H 트리플루오르메틸화 반응

2021 년 2 월

서울대학교 대학원

화학부 유기화학 전공

최 근 호

C1 Functionalization Methods of Organic Compounds: N-Methylation, N-Formylation, and C(sp^3)–H Trifluoromethylation

지도교수 이 홍 근

이 논문을 이학박사 학위논문으로 제출함
2020 년 11 월

서울대학교 대학원
화학부 유기화학 전공
최 근 호

최근호의 이학박사 학위논문을 인준함
2020 년 11 월

위 원 장 김 광 석 (인)
부위원장 이 홍 근 (인)
위 원 최 태 림 (인)
위 원 이 윤 철 (인)
위 원 홍 윤 혁 (인)

Abstract

C1 Functionalization Methods of Organic Compounds: N-Methylation, N-Formylation, and C(sp^3)–H Trifluoromethylation

Geunho Choi

Departments of Chemistry

The Graduate School

Seoul National University

Two C1 functionalization methods were developed using organometallic complexes. In Part I, catalytic utilizations of methanol as a C1 source are discussed. Methanol is an economical and sustainable chemical because of its wide applicability and biodegradability, which makes it environmentally friendly. Representative reported examples on organic syntheses using methanol were introduced in chapter 1. A selective N-monomethylation of various amines using methanol as the methylating reagent was achieved with ruthenium pincer complex (Chapter 2). Methanol is activated to formaldehyde by the acceptorless dehydrogenation, and kinetic reactivity control by additional hydrogen gas is suggested as the key of controlling the selectivity based on the mechanistic studies. With the same ruthenium

catalyst, selective N-formylation, N,N-dimethylation, and N,N-formylmethylation reactions of amines using methanol were realized through the simple tuning of reaction conditions (Chapter 3).

Part II describes the introduction of trifluoromethyl C1 group into organic molecules forming a $C(sp^3)$–CF_3 bond. Trifluoromethylation is a high demand functionalization in contemporary organic synthesis due to its widespread applicability, especially for drug development. Chapter 4 reviewed the current approaches for the $C(sp^3)$–CF_3 bond formation. C–H trifluoromethylation is an ideal method as direct introduction of the important trifluoromethyl group into complex bioactive molecules can be achieved in a single-step. A direct $C(sp^3)$–H trifluoromethylation of unactivated alkanes using a photo-induced bpy$Cu(CF_3)_3$ (bpy = 2,2'-bipyridine) complex was successfully achieved (Chapter 5). The method enabled the challenging reaction under mild conditions, and was applied for the functionalization of versatile bioactive or complex molecules in a single step.

Keywords: C1 chemistry, methanol, methylation, formylation, C–H activation, trifluoromethylation, copper, visible light

Student Number: 2016-20368

Table of Contents

Chapter 3. Selective N-Formylation and N-Methylation of Amines Using Methanol as a Sustainable C1 Source

Appendix

List of Tables

Chapter 2

Chapter 3

Chapter 5

List of Schemes

Chapter 1

Chapter 2

Chapter 3

Chapter 4

Chapter 5

List of Figures

Chapter 2

Chapter 3

Chapter 5

Chapter 1. Utilization of Methanol as a C1 Source for Organic Synthesis

1.1. Introduction

The development of sustainable chemical synthesis utilizing nontoxic, cheap, and renewable feedstocks, instead of using hazard and wasteful reagents, is a continuous challenge in organic synthesis. Methanol, which is the simplest alcohol with one carbon, is one of the sustainable chemicals to replace classical fossil fuels. Methanol has been widely used for a number of industrial applications, such as a feedstock for formaldehyde, acetic acid, and methyl tertiary-butyl ether (MTBE),[1] and is also a potential renewable energy source for the future.[2] About 2.3 billion liters of methanol is annually produced in the world.[3] Methanol is mainly produced from syngas using a suitable catalyst.[4] Recently sustainable resources such as biomasses and CO_2 were also used for production and further development is undergoing.[2b] Because methanol has much higher octane number than gasoline, it has higher compression ratios and increased combustion efficiency as a fuel.[5] For the sustainable chemical synthesis, methanol comes into the spotlight because it can be used as a valuable C1 source for that transformation. Especially the utilization of methanol via dehydrogenative activation generates dihydrogen as the sole byproduct with high atom-economy.

In this chapter, representative examples on organic synthesis using methanol are reviewed. The examples can be classified into three categories based on the reactivity and activation modes of methanol: oxygen nucleophile, electrophile activated by dehydrogenative pathway, and radical pathway (Scheme 1.1).

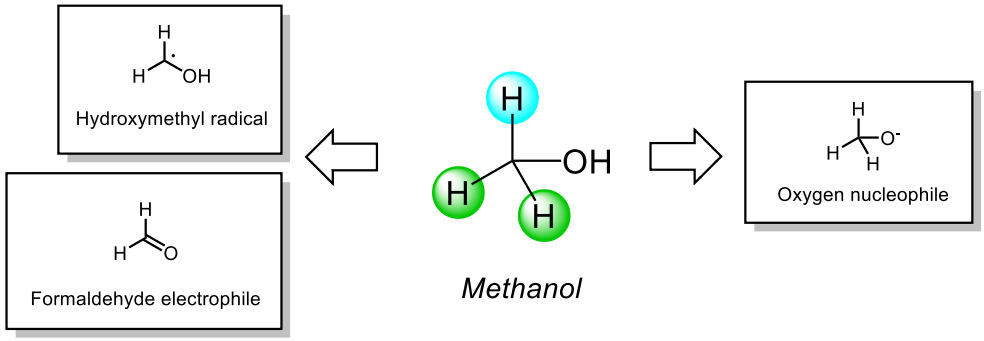

Scheme 1.1 Classification of methanol utility in organic synthesis based on its reactivity

1.2. Methanol utilization via oxygen nucleophile

Conventional reactivity of methanol originated from the electron-rich oxygen atom for methoxy group precursor. Methanol itself or deprotonated form can attack carbon electrophiles to generate C–O bonds. For example, nucleophilic attack of methoxy group to alkyl halides generates methyl ether (Williamson ether synthesis). Methyl ester can be synthesized via acid-catalyzed esterification of carboxylic acids in methanol as a solvent. However, the scope of such methods are limited because of the harsh reaction conditions, usage of toxic reagents, or low functional group tolerance.

Transition-metal catalyzed reactions have been developed to utilize methanol as an O-nucleophile overcoming those issues. Beller and co-workers firstly synthesized anisole moieties using palladium-catalyzed coupling reactions of aryl bromides or chlorides.[6] Because palladium(II) alkoxy complex showed faster β-hydride elimination than reductive elimination (similar mechanism to Scheme 1.2),

previous alkoxy aryl ether syntheses have two competitive pathways; the C–O bond forming reaction by reductive elimination and unwanted β-hydride elimination. They overcame the problem using bulky phosphine ligands to facilitate the reductive elimination to form C–O bond. Aryl halides and halopyridines could be transformed into methyl ether products. One year later, Buchwald and co-worker modified the conditions using *t*BuBrettPhos and palladacycle precatalyst (Scheme 1.2).[7] The reaction conditions were milder operating at room temperature to 50 °C, and various heterocycles could be used as the substrates.

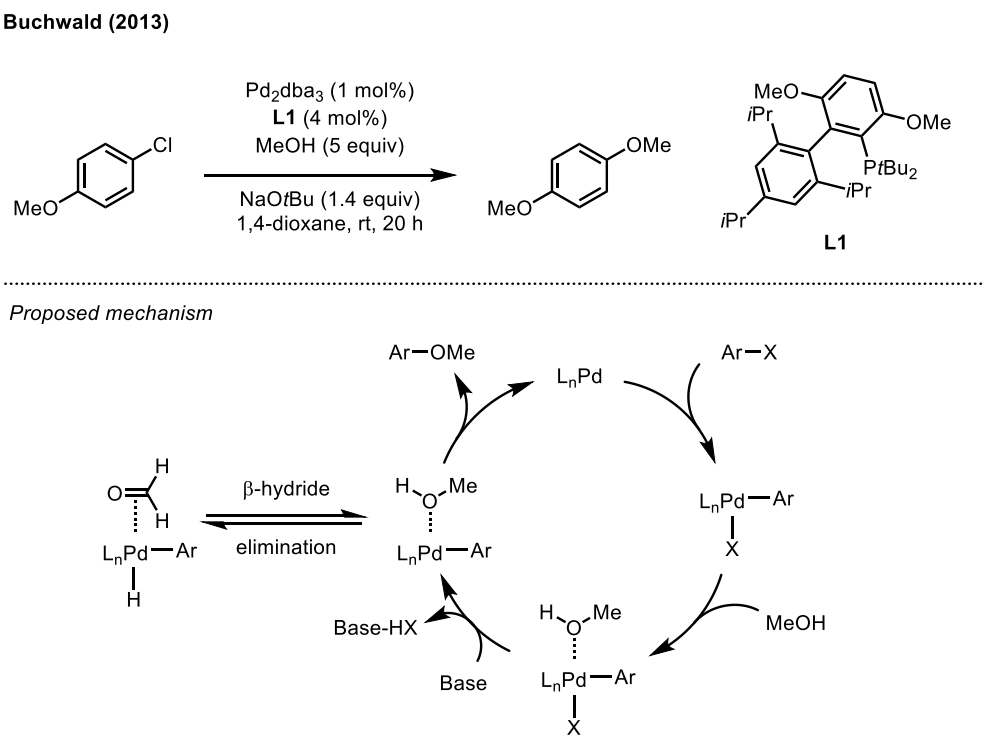

Scheme 1.2 Palladium catalyzed aryl methyl ether synthesis

Methyl ester syntheses with methanol as a methoxy group source were developed in catalytic manners. Other substrates rather than carboxylic acids could be used as an excellent esterification precursor. For example, palladium-catalyzed addition of carbon monoxide to alkenes and alkynes in the presence of methanol as a nucleophile is one of the well-developed methods for methyl ester synthesis.[8] Recently, Beller and co-workers utilized carbon dioxide, which is more abundant and non-toxic reagent, as a C1 source in the alkoxycarbonylation reaction with alkenes without using a strong external reductant (Scheme 1.3A).[9] The developed ruthenium catalytic system could perform dehydrogenation of alcohol, and the generated Ru-dihydrogen complex reduced carbon dioxide to carbon monoxide. It reacted with olefin and methanol to generate methyl ester products in two regioisomers.

The same group used aryl bromide and methanol including paraformaldehyde as a carbonyl source to synthesize aryl esters (Scheme 1.3B).[10] This CO-free palladium-catalyzed carbonylation protocol offers a practical method without using high-pressure reaction, but commercially available and cheap paraformaldehyde. Replacing methanol to silane, only serves as reductant, aryl bromide and paraformaldehyde led to aldehyde products, which strongly suggest the mechanism could follow the pathway in order of carbonylation-nucleophilic attack of alcohol.

The Garg group demonstrated challenging amide to ester transformation via carbon-nitrogen bonds cleavage using nickel catalysis (Scheme 1.3C).[11] Density functional theory (DFT) method suggested a plausible amide substrate by calculating

the thermodynamic preference (*Δ*G) and oxidative addition barrier. The reaction proceeded under mild conditions, and avoided the use of a large excess of methanol nucleophile.

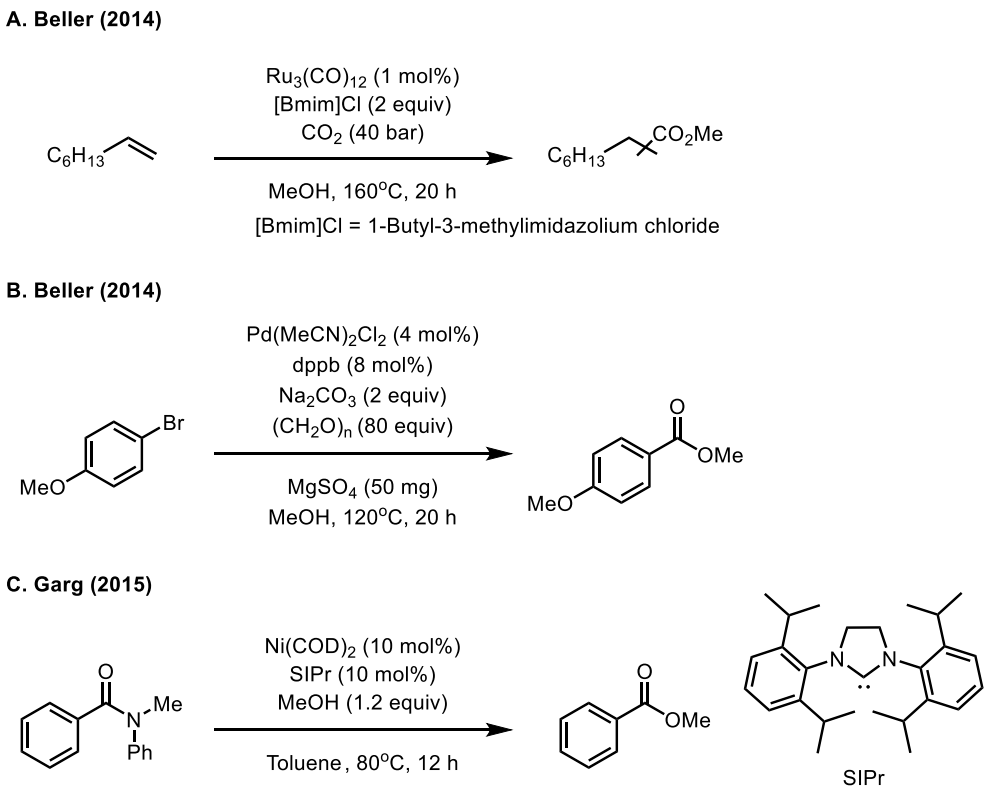

Scheme 1.3 Methyl ester synthesis from methanol

1.3. Methanol utilization via transition metal-catalyzed dehydrogenation

Alcohol dehydrogenation is one of the well-developed methods for organic synthesis using alcohols. Changing nucleophilic alcohols into electrophilic aldehydes or ketones by catalytic dehydrogenation enabled α-carbon of alcohols to participate in

C–X bond formations, broadening the applicability to various transformations. Due to the energetically uphill character of alcohol dehydrogenation,[12] previous activation required hydrogen acceptors to compensate for the thermodynamic hurdles (Scheme 1.4A). These stoichiometric amounts of oxidants lead to wasteful byproducts. To overcome this issue, an acceptorless dehydrogenation, which liberates only hydrogen gas to activate alcohol, has been actively pursued (Scheme 1.4B).[13] The absence of hydrogen acceptor avoids the toxic waste formation derived from external oxidants, maximizing the atom efficiency.

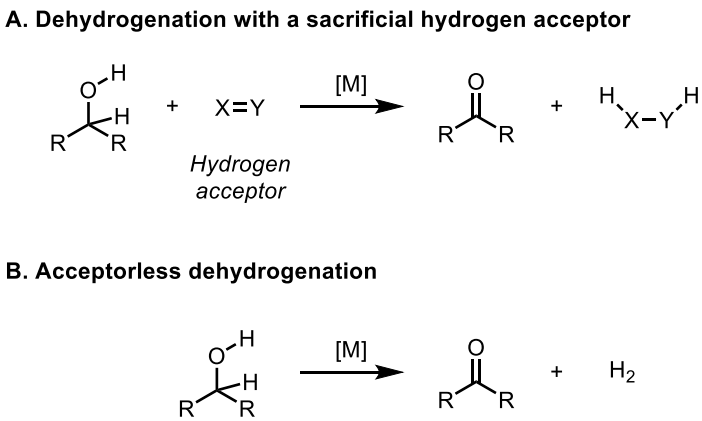

Scheme 1.4 Transition-metal catalyzed dehydrogenative alcohol activation modes

Methanol dehydrogenation was also developed in the same manner. In addition, current research was performed by the inexpensive and abundant first-row metals such as manganese and iron rather than precious transition metals like ruthenium, iridium, and rhodium.[14] In this chapter, organic transformation utilizing methanol via catalytic dehydrogenative is discussed with representative examples,

classified by the nucleophilic partner that attacks activated electrophile.

1.3.1. C–C1 functionalization with methanol

Methyl group on carbon atoms are ubiquitous in many biomolecules and pharmaceuticals, and such motif is known to have a vital influence on their reactivity.[15] Therefore, developing new synthetic methods for C–H methylation is of particular interest. Methanol has also been utilized for such C–C1 methyl functionalization using various nucleophiles. Generally, C–C1 functionalizations using methanol follow the pathway presented in Scheme 1.5; methanol is dehydrogenated to formaldehyde catalyzed by transition metal, followed by an attack of nucleophile generates hydroxymethylated product. Dehydration of such intermediate affords alkene, and reduction with hydrogen, which was generated by methanol dehydrogenation (borrowing hydrogen mechanism), forms C-methylated products.

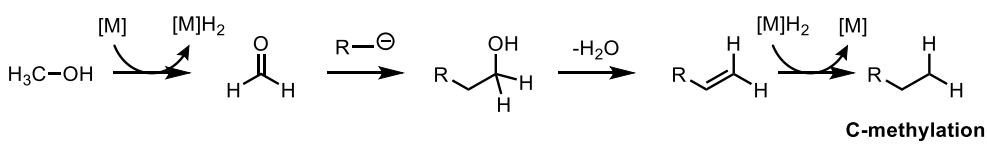

Scheme 1.5 General scheme for dehydrogenative C–C1 functionalization using methanol

Obora and co-worker conducted iridium-catalyzed selective α-methylation of ketones or phenylacetonitriles using methanol as the methylating agent (Scheme 1.6A).[16] Optimization with iridium precatalyst, methanol, and base successfully forms α-methylated products, and this system can be extended to three-component α-methylalkylation of methyl ketones using methanol and primary alcohols. The Seayad[17] and Donohoe[18] groups respectively developed the conditions using ruthenium and rhodium catalysts with methanol to synthesize α-methylated ketones. In particular, the Donohoe group developed a condition with relatively low temperature (65 °C for optimal condition) for the same reactivity. In 2019, Sortais and co-workers achieved the direct α-methylation of ketones with the first-row manganese catalyst (Scheme 1.6B).[19] Using a well-defined manganese PNP complex as precatalyst, the transformation proceeded smoothly with 1 equiv of a strong base. This protocol could be extended to the more challenging ester derivatives.

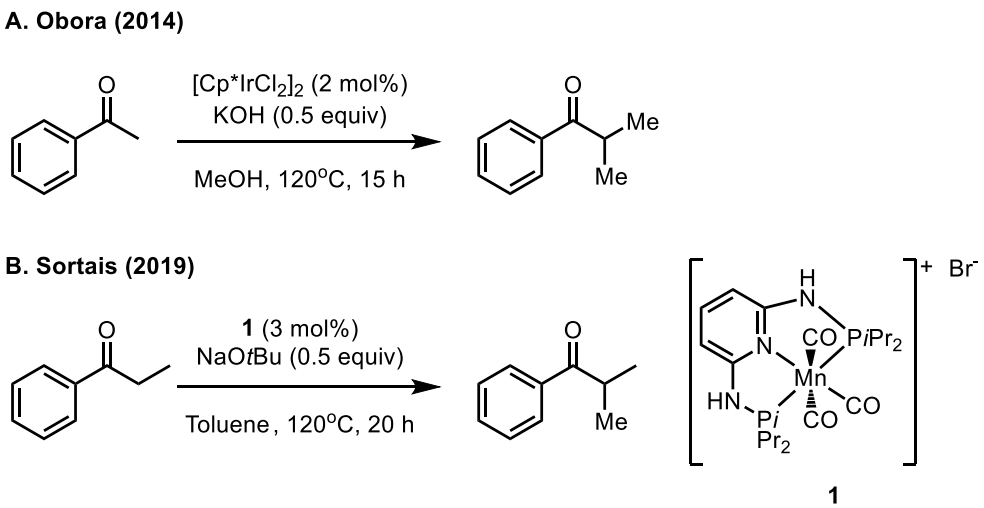

Scheme 1.6 α-Methylation of ketones using methanol

When alcohol is dehydrogenated, the produced ketone or aldehyde can function as enolate nucleophile, and β-methylation of alcohols can be achieved via a borrowing hydrogen strategy (Scheme 1.5). Leitner and co-workers achieved selective introduction of methyl group into the carbon chains of alcohols with low loading of ruthenium catalyst (TON, turn-over number = 18,000) (Scheme 1.7).[20] Ruthenium catalyst dehydrogenate both alcohol substrates and methanol, and aldol reaction-dehydration-hydrogenation of generated ketone forms desired β-methylated alcohols. Very recently, Morrill[21] and Kempe[22] respectively utilized cheaper iron and manganese catalysts for the same transformation using methanol as a C1 building block.

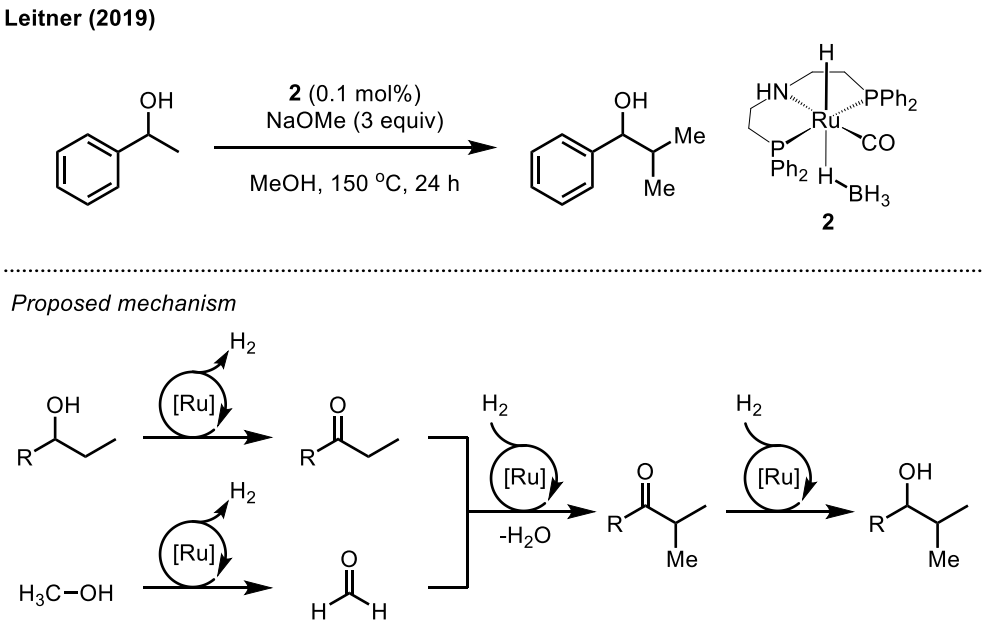

Scheme 1.7 β-Methylation of alcohols using methanol

Hong and co-worker developed ruthenium-catalyzed *ortho*-aminomethylation of phenol using methanol as methylene source (Scheme 1.8).[23] It should be noted that iminium intermediate, generated by dehydration of hemiaminal intermediate, is trapped by other phenol nucleophile to selectively form *ortho*-aminomethylated phenol. Using naphthol instead of phenols exhibited different selectivity toward methylation reaction.

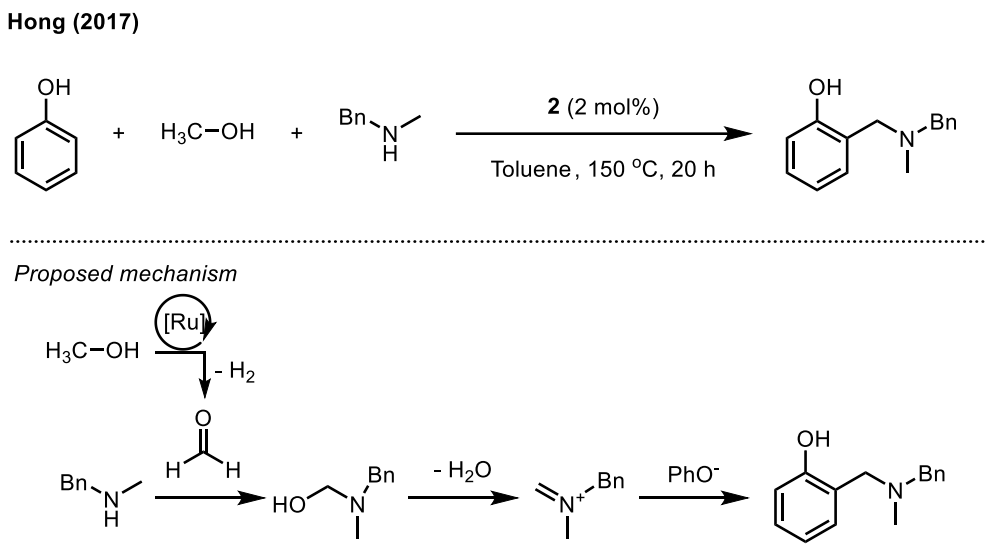

Scheme 1.8 Three-component reaction using methanol as methylene source

In 2017, Krische and co-workers used iridium precatalyst and (R)-PhanePhos ligand to synthesize hydrohydroxymethylated product with CF_3-allenes and methanol (Scheme 1.9).[24] The reaction enables catalytic enantioselective synthesis of acyclic CF_3-bearing carbon quaternary stereocenters, achieved by an allyliridium(III) intermediate conducting carbonyl addition in enantioselective

manner. This protocol has excellent yield and ee (about 90% ee) for various substrates.

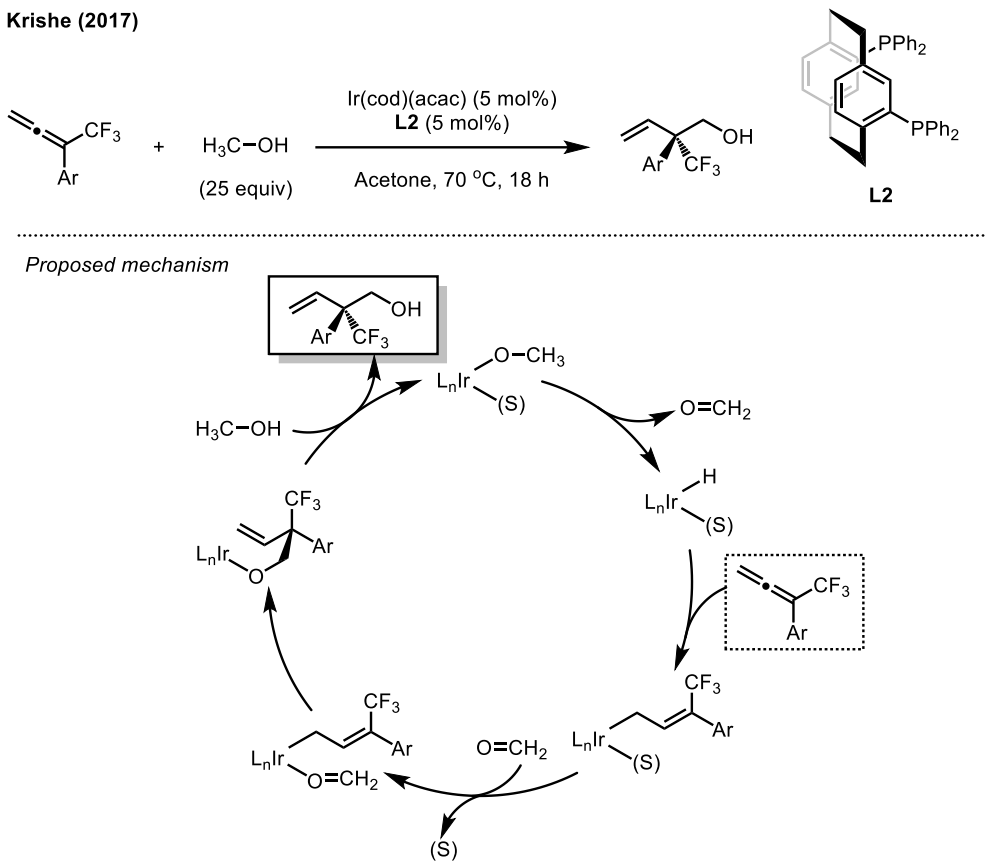

Scheme 1.9 Enantioselective hydroxymethylation of allenes

1.3.2. N–C1 functionalization with methanol

Like biologically important methyl group,[15] amide bonds also play a critical role in pharmaceutical chemistry and biochemistry. For example, amides are found in 25% of drug-like molecules[25] and 65% of drug-candidate molecules.[26] Amine C1

functionalization chemistries also focused on this point, and they are largely divided into two parts; N-methylation and N-formylation (Scheme 1.10).

Firstly, methanol is dehydrogenated into formaldehyde via transition-metal catalysis. Attacking formaldehyde with nitrogen nucleophile generates hemiaminal intermediate. This hemiaminal intermediate follows two possible pathways based on the reaction conditions. N-formylation is achieved when the hydroxyl group is once more dehydrogenated. Meanwhile, dehydration of hemiaminal, followed by hydrogenation of imine intermediate achieves N-methylation.

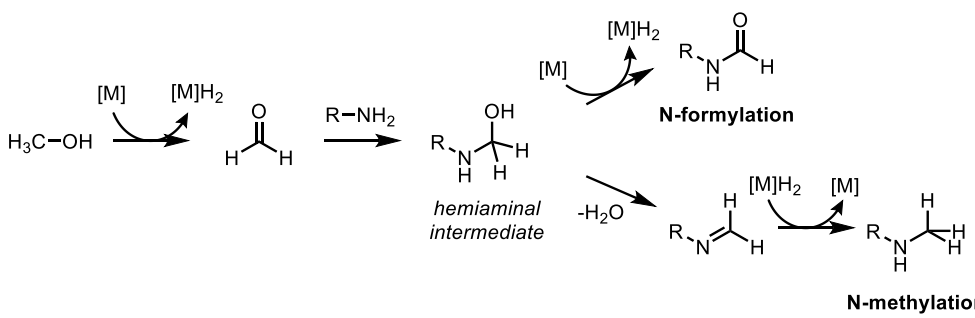

Scheme 1.10 General scheme for dehydrogenative N–C1 functionalization using methanol

Seayad and co-workers reported N-methylation of amines using methanol and ruthenium catalyst (Scheme 1.11A).[27] Different from previous reports that methylate only aromatic amines,[28] authors successfully methylated both aromatic and aliphatic amines. Selective N-monomethylation of aromatic amines and dimethylation of aliphatic amines were achieved in excellent yields. Although N-

monomethylated amines was selectively formed with aromatic amines using various catalytic system, only one example was reported for aliphatic amine by the Hong group, which will be discussed in Chapter 2.[29] Li and co-workers developed new type of Cp*iridium catalyst bearing a functional 2,2'-bibenzimidazole ligand, which was highly effective for N-methylation of aromatic and aliphatic amines, and sulfonamides (Scheme 1.11B). This catalytic system required only a weak base to be activated rather than a strong base which was required for previous catalytic systems.

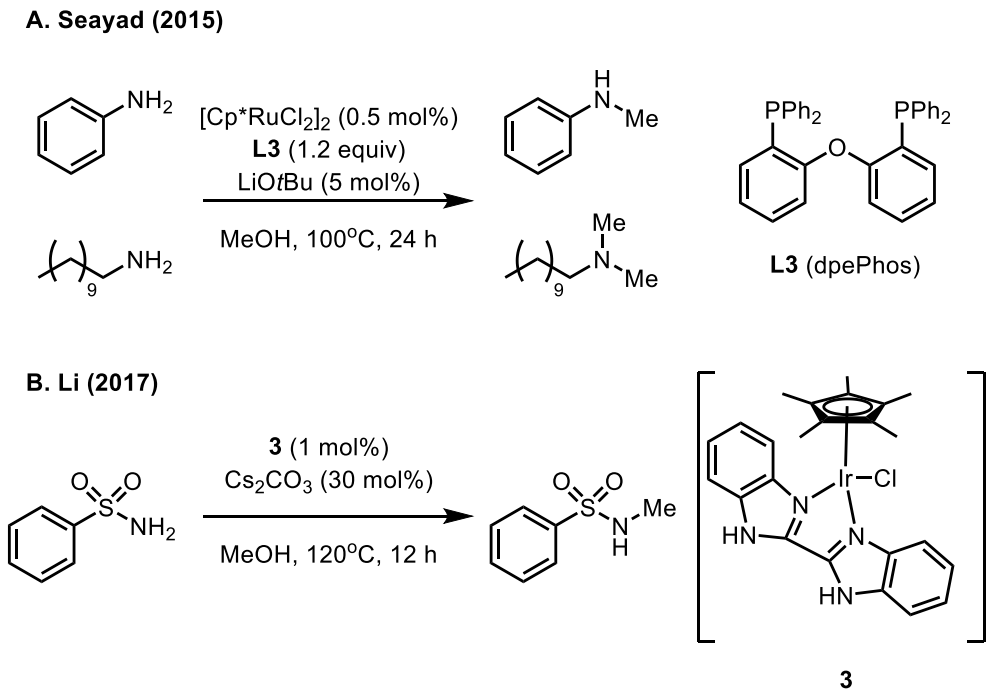

Scheme 1.11 Methylation of amines and sulfonamides using methanol

Kundu and co-workers developed 2-(2-pyridyl-2-methoxy)-1,10-

phenanthroline-based ruthenium catalytic system to broaden the scope of dehydrogenative N-methylation reaction. Rather than using amine, they utilized more oxidized substrates such as nitro or nitrile group as nitrogen source, which was *in-situ* reduced by hydrogen transfer from alcohols. In 2017, the Kundu group firstly transformed nitro compounds into N-methylated amines (Scheme 1.12A).[30] Interestingly, this catalytic system is applicable to not only aromatic or aliphatic nitro compounds, but also vinyl substituents. After one year, they modified the anion part of the catalyst to directly synthesize N,N-dimethylated amines from nitrile groups (Scheme 1.12B).[31] They proposed amine intermediate by reduction of nitriles via experimentally (amine intermediate detection) and computationally (thermodynamically favored 20.6 kcal/mol barrier reaction).

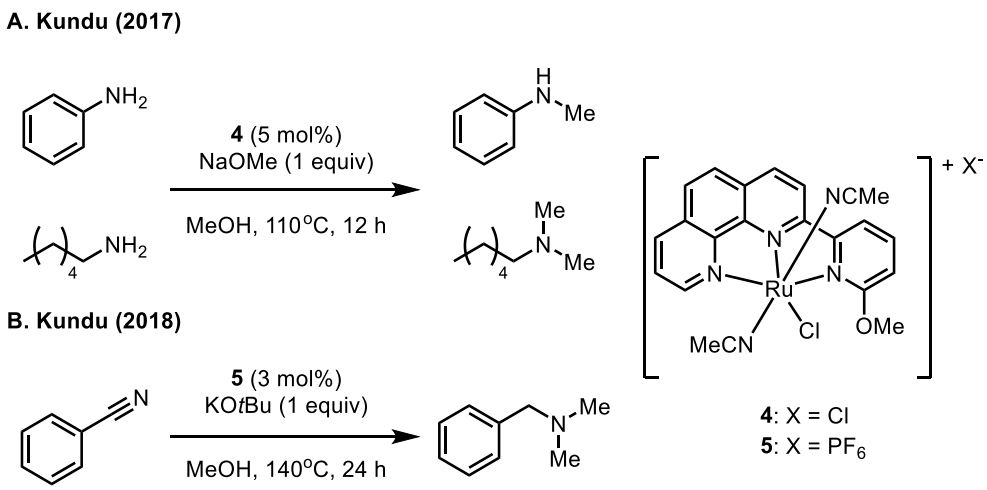

Scheme 1.12 Methylation of other nitrogen sources using methanol

Dehydrogenative catalysis for N-formylation is relatively less studied and has a shorter history than N-methylation cases. In 2013, the Glorius group reported the first amine N-formylation using methanol as a C1 source (Scheme 1.13 A).[32] The homogeneous ruthenium catalyst with NHC ligand can successfully conduct dehydrogenation of both methanol and hemiaminal intermediate to generate formamide (Scheme 1.10). However, this required styrene as an additional hydrogen acceptor which generates an equivalent amount of wastes. Hong and co-worker developed a ruthenium-dihydrogen-based catalytic system, which did not require any hydrogen acceptor or base (Scheme 1.13 B).[33] N-Formylation was successfully achieved with amines and nitriles.

Transition-metal pincer complexes exhibited high efficiency for N-formylation of amines. Ruthenium, manganese, and iron was used for such catalysts (Scheme 1.13 C–E). The Hong[34] and Milstein[35] group utilized ruthenium and manganese PNP-pincer complexes, respectively. The catalyst loading can be lowered to 2 mol%. Bernskoetter and co-workers reported an iron-based PNP pincer catalyst.[36] Turn over number (TON) up to 600 was achieved without any base or hydrogen acceptor. This efficiency is highly improved than previous catalytic systems, but it has critical limitation to substrate scopes; only secondary amines showed good yield, and poor conversion was observed for primary amines.

In 2020, the Prechtl group found that *in-situ* generated copper/TEMPO catalytic system could conduct N-formylation of a variety of amines (Scheme 1.13 F).[37] This catalytic system improved N-formylation reaction in several points; 1) O_2 was used as terminal oxidant, and water was generated as nontoxic byproduct, 2) it

firstly conduct N-formylation in high yield (up to 96%) with 1:1 ratio of amine and methanol, 3) reaction temperature is much milder than previous systems.

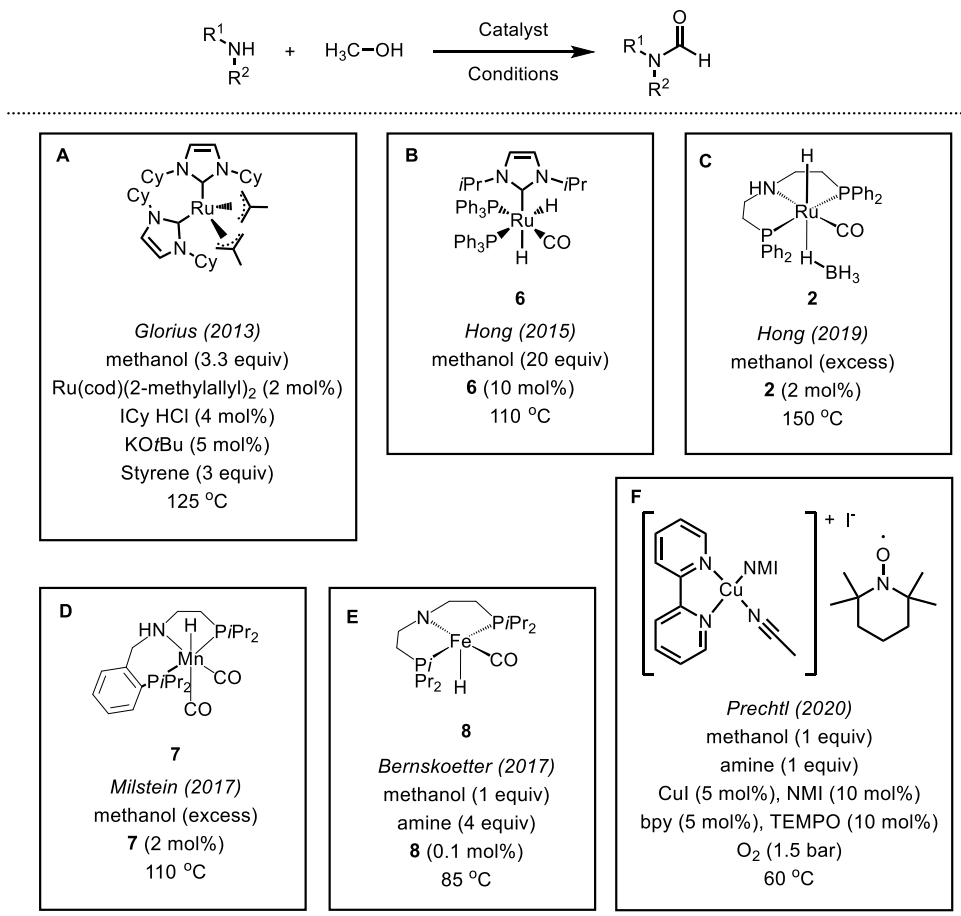

Scheme 1.13 Summary of N-formylation catalytic systems using methanol

1.4. Methanol utilization via radical pathway

Alcohol dehydrogenation is a powerful tool to utilize methanol as a C1 source in organic synthesis with various coupling partners. Unfortunately, it has a critical innate limitation that formaldehyde can only react with electron-rich nucleophilic partners, such as carbanions or amines.

Hydroxymethyl radical (CH_2OH), which loses one hydrogen atom from carbon, is proposed as a solution to overcome such limitation because such a radical has a nucleophilic character, which favors donating electron. However, the bond-dissociation energy (BDE) of C–H bond of methanol is 96 kcal/mol,[38] which is stronger than other alcohols and other activated C–H bonds. Despite the importance of the open-shell activation mode of methanol, examples utilizing hydroxymethyl radical into organic synthesis is very limited.

Early examples utilized titanium additives and equivalent amounts of oxidants for hydrogen atom transfer (HAT) of methanol, and furnished the hydroxymethyl products. The Punta and Porta group developed a one-pot multicomponent reaction of amine, aldehyde and methanol to synthesize 1,2-amino alcohol moieties (Scheme 1.14A).[39] The *tert*-butoxy radical, generated from Ti(III) and *tert*-butylhydroperoxide (TBHP), abstracts α-hydrogen of methanol to form hydroxymethyl radical. The radical inserted to *in-situ* generated iminium, and further reduction terminates the reaction into amino alcohol form. Griesbeck and co-worker utilized titanium as a homogeneous and heterogeneous photocatalyst under UV irradiation to insert hydroxymethyl radical into ketones (Scheme 1.14B).[40] Homogeneous titanium catalyst, $TiCl_2(O\textit{i}Pr)_2$, showed moderate yield of

hydroxymethylated alcohol from ketones. Meanwhile, heterogeneous titanium catalyst, TiO_2 P25, produced a dimerized product rather than the hydroxymethylated product. Although this work proposes that light can be utilized for hydroxymethyl radical generation, it has very limited scopes and yields.

Togo and co-workers treated quinolines and isoquinolines with a persulfate additive in a mixture of methanol and water to form hydroxymethylated products (Scheme 1.14C).[41] Persulfate can abstract hydrogen from α-hydrogen of methanol to form hydroxymethyl radical. It reacted with a protonated quinoline in Minisci type reaction, followed by oxidation to generate α-hydroxymethylated heterocyclic compounds. However, due to regioselectivity issues from the Minisci type reactivity, only 4-substituted quinolines or isoquinolines were utilized for the reaction. The Li group shed UV light to heteroarenes rather than using oxidant in methylene chloride solution.[42] Absence of an oxidant facilitates dehydration after inserting hydroxymethyl radical into heteroarenes, generating methylated product. This method also follows the Minisci type reactivity to make a dimethylated product on 1- and 4-position. These methods successfully used methanol as hydroxymethyl radical precursor. However, they also contain problems such as limited scopes, requirement of stoichiometric amount of oxidants, and solvent amount of methanol.

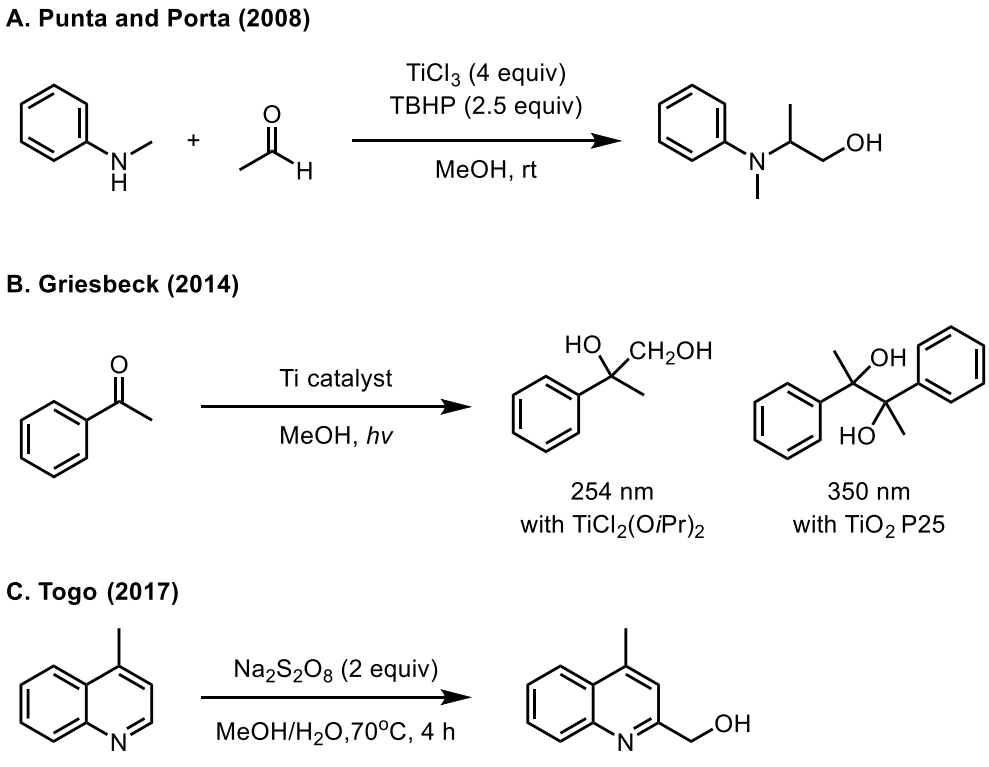

Scheme 1.14 Hydroxymethylation of electrophiles using hydroxymethyl radical

MacMillan and co-worker solved upper limitations utilizing photoredox/organo dual catalysis (Scheme 1.15).[43] The thiol organocatalyst was oxidized by iridium catalyst and it conducted HAT of methanol to generate hydroxymethyl radical. In addition, the Minisci type addition into protonated heteroarene, dehydration, then reduction formed desired 2-methylated heteroarenes. It showed much broader scopes, including medicinal late-stage functionalization, than previous hydroxymethyl radical reactions due to the absence of strong oxidant and mild room temperature condition.

MacMillan (2015)

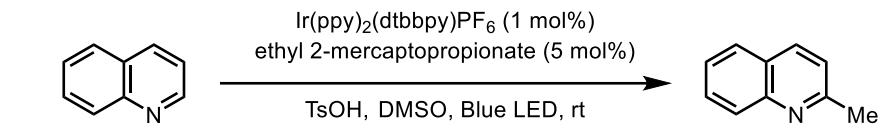

Proposed mechanism

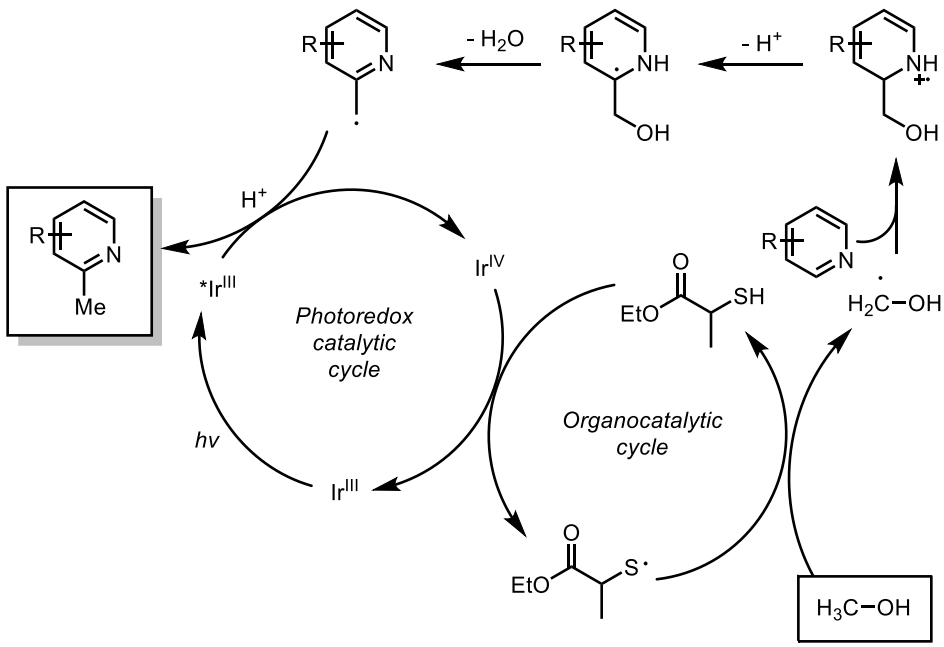

Scheme 1.15 Heteroarene methylation via hydroxymethyl radical intermediate

1.5. Conclusion

As sustainability becomes one of the major agenda in organic chemistry, the development of synthetic methods to utilize methanol have been actively pursued. Reactivity with oxygen nucleophile has been developed from classical simple substitution reactions to up-to-date cross coupling reactions. Through dehydrogenative activation to utilize methanol, a number of reactions have been developed with various nucleophilic coupling partners. Very recently, open-shell activation of methanol is under development to afford products that are difficult to access via previous activation modes.

Despite the advances, this research field still faces several challenges. First, catalytic N-formylation is relatively less developed than other reactions utilizing dehydrogenative activation modes. For example, there is no general method to formylate aromatic amines in homogeneous catalysis. Besides, in most reported cases, N-methylation of aliphatic amines was achieved in N,N-dimethylation form, which is caused by the more nucleophilic character of N-monomethylated amines. Only one example that can selectively synthesize N-monomethylated amine in aliphatic cases (Chapter 2) is reported, but it also required a harsh reaction condition (4 MPa of H_2 at 120 ^{o}C), which should be improved.

Finally, examples using open-shell activation of methanol are scarce, and most require harsh reaction conditions or toxic reagents. Although some catalytic improvement was recently achieved, the range of scope utilizing hydroxymethyl radical is very limited to a few substrates, such as heteroarene and iminium. Thus, expansion of the scope of the coupling partners is a remaining challenge.

1.6. References

(1) (a) Pérez-Fortes, M.; Schöneberger, J. C.; Boulamanti, A.; Tzimas, E., *Appl. Energy* **2016,** *161*, 718-732; (b) Ali, K. A.; Abdullah, A. Z.; Mohamed, A. R., *Renewable Sustainable Energy Rev.* **2015,** *44*, 508-518.

(2) (a) Nielsen, M.; Alberico, E.; Baumann, W.; Drexler, H.-J.; Junge, H.; Gladiali, S.; Beller, M., *Nature* **2013,** *495* (7439), 85-89; (b) Jaggai, C.; Imkaraaz, Z.; Samm, K.; Pounder, A.; Koylass, N.; Chakrabarti, D. P.; Guo, M.; Ward, K., *Green Chem.* **2020,** *22* (13), 4279-4294.

(3) https://www.methanol.org/methanol-production/ (accessed Sep 29, 2020).

(4) Natte, K.; Neumann, H.; Beller, M.; Jagadeesh, R. V., *Angew. Chem. Int. Ed.* **2017,** *56* (23), 6384-6394.

(5) Bellotti, D.; Rivarolo, M.; Magistri, L.; Massardo, A. F., *J. CO_2 Util.* **2017,** *21*, 132-138.

(6) Gowrisankar, S.; Neumann, H.; Beller, M., *Chemistry* **2012,** *18* (9), 2498-2502.

(7) Cheung, C. W.; Buchwald, S. L., *Org. Lett.* **2013,** *15* (15), 3998-4001.

(8) Brennführer, A.; Neumann, H.; Beller, M., *ChemCatChem* **2009,** *1* (1), 28-41.

(9) Wu, L.; Liu, Q.; Fleischer, I.; Jackstell, R.; Beller, M., *Nat. Commun.* **2014,** *5*, 3091.

(10) Natte, K.; Dumrath, A.; Neumann, H.; Beller, M., *Angew. Chem. Int. Ed.* **2014,** *53* (38), 10090-10094.

(11) Hie, L.; Fine Nathel, N. F.; Shah, T. K.; Baker, E. L.; Hong, X.; Yang, Y.-F.; Liu, P.; Houk, K. N.; Garg, N. K., *Nature* **2015,** *524* (7563), 79-83.

(12) Pandey, P.; Dutta, I.; Bera, J. K., *Proc. Nat. Acad. Sci. India Sect. A* **2016,** *86* (4), 561-579.

(13) (a) Gunanathan, C.; Milstein, D., *Science* **2013,** *341* (6143), 1229712; (b) Crabtree, R. H., *Chem. Rev.* **2017,** *117* (13), 9228-9246.

(14) Zhang, X.; Guo, C.; Wu, H., *Chin. J. Org. Chem.* **2019,** *39* (9), 2458.

(15) (a) Schönherr, H.; Cernak, T., *Angew. Chem. Int. Ed.* **2013,** *52* (47), 12256-12267; (b) Leung, C. S.; Leung, S. S. F.; Tirado-Rives, J.; Jorgensen, W. L., *J. Med. Chem.* **2012,** *55* (9), 4489-4500.

(16) Ogawa, S.; Obora, Y., *Chem. Commun.* **2014,** *50* (19), 2491-2493.

(17) Dang, T. T.; Seayad, A. M., *Adv. Synth. Catal.* **2016,** *358* (21), 3373-3380.

(18) Chan, L. K. M.; Poole, D. L.; Shen, D.; Healy, M. P.; Donohoe, T. J., *Angew. Chem. Int. Ed.* **2014,** *53* (3), 761-765.

(19) Bruneau-Voisine, A.; Pallova, L.; Bastin, S.; César, V.; Sortais, J.-B., *Chem. Commun.* **2019,** *55* (3), 314-317.

(20) Kaithal, A.; Schmitz, M.; Hölscher, M.; Leitner, W., *ChemCatChem* **2019,** *11* (21), 5287-5291.

(21) Polidano, K.; Williams, J. M. J.; Morrill, L. C., *ACS Catal.* **2019,** *9* (9), 8575-8580.

(22) Schlagbauer, M.; Kallmeier, F.; Irrgang, T.; Kempe, R., *Angew. Chem. Int. Ed.* **2020,** *59* (4), 1485-1490.

(23) Kim, S.; Hong, S. H., *Adv. Synth. Catal.* **2017,** *359* (5), 798-810.

(24) Holmes, M.; Nguyen, K. D.; Schwartz, L. A.; Luong, T.; Krische, M. J., *J. Am. Chem. Soc.* **2017,** *139* (24), 8114-8117.

(25) Ghose, A. K.; Viswanadhan, V. N.; Wendoloski, J. J., *J. Comb. Chem.* **1999,** *1* (1), 55-68.

(26) Carey, J. S.; Laffan, D.; Thomson, C.; Williams, M. T., *Org. Biomol. Chem.*

2006, *4* (12), 2337-2347.

(27) Dang, T. T.; Ramalingam, B.; Seayad, A. M., *ACS Catal.* **2015,** *5* (7), 4082-4088.

(28) (a) Elangovan, S.; Neumann, J.; Sortais, J.-B.; Junge, K.; Darcel, C.; Beller, M., *Nat. Commun.* **2016,** *7*, 12641; (b) Campos, J.; Sharninghausen, L. S.; Manas, M. G.; Crabtree, R. H., *Inorg. Chem.* **2015,** *54* (11), 5079-5084.

(29) Choi, G.; Hong, S. H., *Angew. Chem. Int. Ed.* **2018,** *57* (21), 6166-6170.

(30) Paul, B.; Shee, S.; Chakrabarti, K.; Kundu, S., *ChemSusChem* **2017,** *10* (11), 2370-2374.

(31) Paul, B.; Shee, S.; Panja, D.; Chakrabarti, K.; Kundu, S., *ACS Catal.* **2018,** *8* (4), 2890-2896.

(32) Ortega, N.; Richter, C.; Glorius, F., *Org. Lett.* **2013,** *15* (7), 1776-1779.

(33) Kang, B.; Hong, S. H., *Adv. Synth. Catal.* **2015,** *357* (4), 834-840.

(34) Choi, G.; Hong, S. H., *ACS Sustainable Chem. Eng.* **2019,** *7* (1), 716-723.

(35) Chakraborty, S.; Gellrich, U.; Diskin-Posner, Y.; Leitus, G.; Avram, L.; Milstein, D., *Angew. Chem. Int. Ed.* **2017,** *56* (15), 4229-4233.

(36) Lane, E. M.; Uttley, K. B.; Hazari, N.; Bernskoetter, W., *Organometallics* **2017,** *36* (10), 2020-2025.

(37) Pichardo, M. C.; Tavakoli, G.; Armstrong, J. E.; Wilczek, T.; Thomas, B. E.; Prechtl, M. H. G., *ChemSusChem* **2020,** *13* (5), 882-887.

(38) Luo, Y.-R., *Handbook of Bond Dissociation Energies in Organic Compounds*. CRC Press: 2002; p 392.

(39) Clerici, A.; Ghilardi, A.; Pastori, N.; Punta, C.; Porta, O., *Org. Lett.* **2008,** *10* (21), 5063-5066.

(40) Griesbeck, A. G.; Reckenthäler, M., *Beilstein J. Org. Chem.* **2014,** *10*, 1143-1150.

(41) Zhou, L.; Okugawa, N.; Togo, H., *Eur. J. Org. Chem.* **2017,** *2017* (41), 6239-6245.

(42) Liu, W.; Yang, X.; Zhou, Z.-Z.; Li, C.-J., *Chem* **2017,** *2* (5), 688-702.

(43) Jin, J.; MacMillan, D. W. C., *Nature* **2015,** *525* (7567), 87-90.

Chapter 2. Selective Monomethylation of Amines with Methanol as a C1 Source*

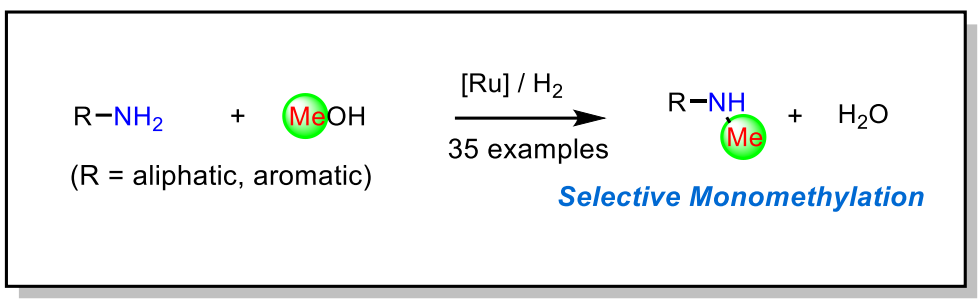

∗ The majority of this work has been published: Geunho Choi and Soon Hyeok Hong*, *Angew. Chem. Int. Ed.* **2018**, *57*, 6166-6170.

2.1. Introduction

N-methylation is one of the most fundamental C–N bond forming reactions in organic chemistry. The N-methyl group is commonly found in natural products and bioactive molecules[1] and plays an important role in various biological processes where some congeners show enhanced activity compared to that of non-methylated precursors.[2] Although N-monomethylation of amines seems to be relatively easily accomplished using a methylating reagent such as a methyl halide via an S_N2 mechanism, overmethylation presents a serious issue due to the increased nucleophilicity of the amine following monomethylation as well as the smallest size of the methyl group among the alkyl groups.[3] Therefore, to prevent the overmethylation, conventional syntheses of N-monomethylamines from primary amines require protection and deprotection steps that reduce the atom-efficiency of the overall process.[4]

The selectivity problem has been addressed in literature to some extent, yet most accounts have focused on the N-monomethylation of less nucleophilic aromatic amines.[5] Limited methods have been reported for aliphatic amines (Scheme 2.1a). For example, the Dalcanale group used a host-guest approach and MeI to achieve selective N-monomethylation of aliphatic amines.[6] N-monomethylation using other electrophiles, such as MeOTf, dimethyl phosphite, or dimethyl carbonate, have also been explored.[7] However, the aforementioned approaches could be viewed as non-environmentally benign or inefficient with regards to atom-economy. Recently, more atom-economical approaches that feature CO_2[8] and paraformaldehyde[9] as the methylating reagents were also reported, but these methods suffer from a narrow scope of aliphatic amines and low selectivity to N-monomethylamine.

a) Previous direct N-monomethylation method

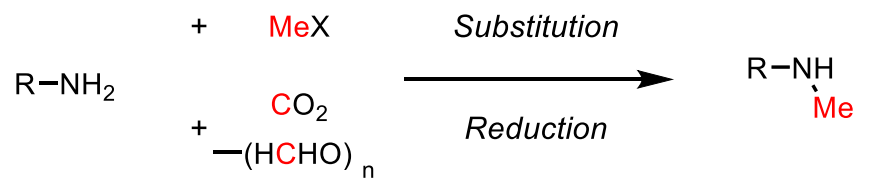

· Low selectivity · Narrow scopes · Non-atom economical

b) Previous MeOH reactivity with primary amines

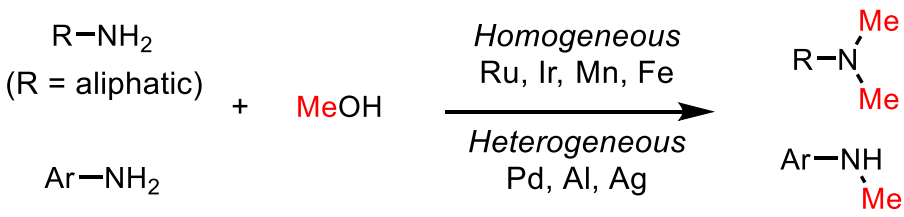

c) This work: N-monomethylation of amines with MeOH

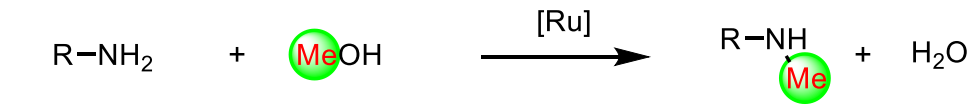

(R = aliphatic, aromatic)

Scheme 2.1 Synthetic strategies for N-monomethylation of primary amines

Methanol can serve as a sustainable and atom-economical C1 source for the methylation of amines as it only produces water as a byproduct when a borrowing hydrogen methodology is applied.[10] However, because of the higher enthalpy of the dehydrogenation of methanol (ΔH^o = +92.4 kJ mol^{-1} in gas phase) as compared with other alcohols such as ethanol (ΔH^o = +68.6 kJ mol^{-1} in gas phase), the use of methanol has been relatively limited as compared with that of other higher alcohols.[11] In addition, due to the significantly decreased steric effects, selective monomethylation is more difficult to achieve with methanol.[7a] Although the monoalkylation of aliphatic amines via dehydrogenative C–N coupling reactions has been well established with various alcohols,[12] N-methylation using methanol has only been developed for the dimethylation of aliphatic amines[10, 13] or the monomethylation or dimethylation of aromatic amines[10, 13c, 14] (Scheme 2.1b). Overall, the selective monomethylation of aliphatic amines using methanol has not been well presented. The first methylation using methanol was developed by the Grigg's group in 1981, yet a narrow substrate scope was reported.[15] Since then, to the best of our knowledge, only two examples of the monomethylation of amino alcohols using methanol were reported, albeit with poor selectivity and under harsh supercritical conditions (300 °C and a pressure greater than 8 MPa).[16] Herein, we describe the development of a selective N-monomethylation method using methanol as the C1 source with a commercially available Ru catalyst, which could be applied to structurally and functionally diverse aliphatic and aromatic amines, including biologically relevant substrates (Scheme 2.1c).

In the previous reports, formamide was synthesized using amine and methanol as the C1 source via the dehydrogenation of the hemiaminal intermediate.[17]

We hypothesized that the pathway for the monomethylamine could be controlled through the dehydration of the hemiaminal intermediate under reducing conditions. Hydrogen gas was chosen as the reducing agent because H_2 could retard the dehydrogenation of hemiaminal **A**, and could facilitate the hydrogenation of imine **B**, which would form via dehydration of hemiaminal **A** (Scheme 2.2). It was envisioned that further methylation of the secondary amine could be kinetically controlled by suitable catalytic conditions, as the formation of the charged iminium intermediate **D** could have a higher activation barrier than that of the neutral imine **B**.

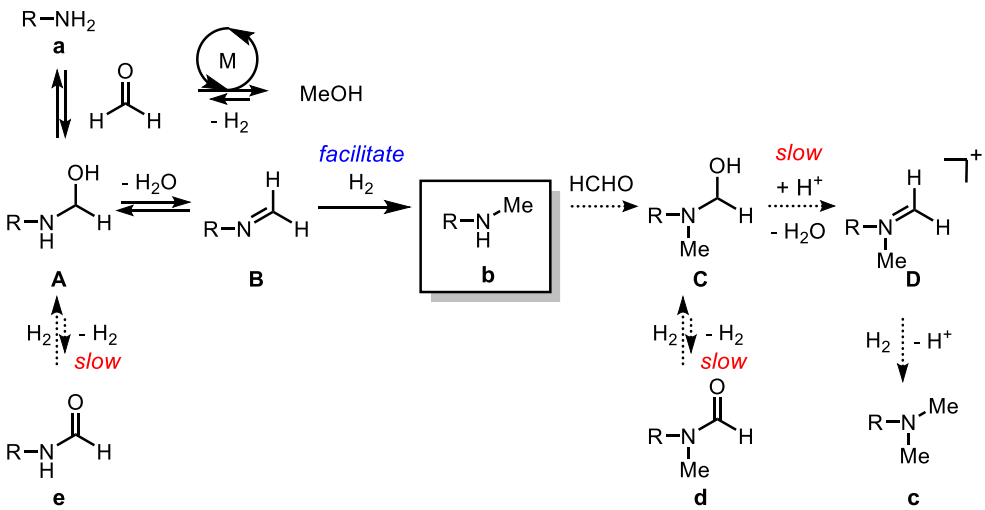

Scheme 2.2 Proposed reaction pathway

2.2. Results and discussion

2.2.1. Reaction condition optimization

Initial attempts using benzylamine (**1a**) and methanol in the presence of Ru-MACHO-BH (**1**, Table 2.2) did not yield any of the methylated product. Instead, *N*,*N*-benzylmethylformamide (**1d**) and *N*-benzylformamide (**1e**) resulting from the formylation of the amine were obtained (Scheme 2.3). Consistent with our previous assumption, in the presence of H_2, the formamide formation reactions were dramatically suppressed and monomethylated *N*-methyl benzylamine (**1b**) was produced in 61% yield (entry 1, Table 2.3). Inspired by this result, various transition metal complexes, which are known to mediate hydrogen transfer reactions, were screened, and **1** was identified as the most efficient catalyst with the highest yield of **1b**. No products were detected in the absence of the catalyst (entry 9, Table 2.3).

Further optimization studies were performed using complex **1** (Table 2.1). Increasing the hydrogen pressure (from 2.0 to 4.0 MPa) improved the selectivity (entries 1–2, Table 2.1). Although prolonged reaction times (from 6 to 12 h) led to the complete conversion of the amine, the selectivity of the monomethylated product **1b** (33%) decreased significantly, with dimethylated product **1c** (55%) being the major product (entry 3). The reaction temperature critically affected both conversion and selectivity (entries 3–6). Reducing the temperature to 120 °C and extending the reaction time to 24 h afforded both the best selectivity and yield of **1b** (82%, entry 7). Decreasing the catalyst loading by half resulted in a decreased conversion (34%, entry 8).

Table 2.1 Optimization of N-monomethylation[a]

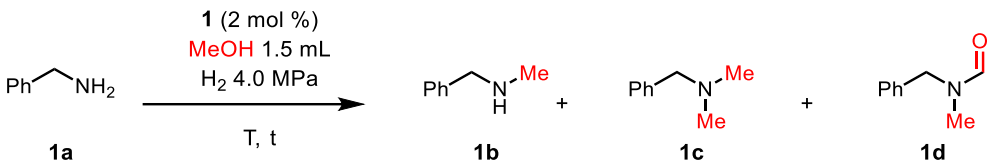

Entry	Time (h)	T (°C)	Conv.(%)	**1b** (%)	**1c** (%)	**1d** (%)
1[b]	6	150	95	61	5	29
2	6	150	65	57	-	7
3	12	150	>99	33	55	12
4	12	130	>99	55	32	9
5	12	120	51	41	-	1
6	12	110	18	13	-	-
7	24	120	93	82	5	6
8[c]	24	120	34	30	-	-

[a]Reaction conditions: **1a** (1 mmol), methanol (1.5 mL), **1** (2 mol %), and H_2 (4.0 MPa) in a closed vessel; yields were determined by ^{1}H NMR using *p*-xylene as an internal standard. [b]H_2 2.0 MPa. [c]Catalyst **1** (1 mol %)

2.2.2. Substrate scope of amines

With the optimal conditions in hand (entry 7, Table 2.1), the scope of the N-monomethylation reaction was investigated (Table 2.2 and Table 2.5). For aliphatic amines, the resulting reaction mixture was directly subjected to a Boc protection protocol for facile isolation of the products (Table 2.2). Benzylamine gave 77% of the N-monomethylated amine (**1bb**). Benzylamine derivatives in the 2, 3, and 4-position with methyl substituents afforded the corresponding secondary amines in excellent yields (**2bb**–**4bb**). Benzylamines with both electron donating and deficient groups resulted in the corresponding products (**5bb**–**7bb**) in good yields. Other aliphatic amines (**8a**–**12a**), including cyclic (**10bb**) and acetal-containing (**11bb**) substrates provided moderate to good yields of the desired products. To our delight, amines with pyridine and thiophene heterocycles were also tolerated to afford the monomethyl amines in excellent yields (**13bb** and **14bb**). Methylation of 1-adamantylamine (**15bb**), which is bulky α-tertiary amine, took place with good selectivity upon addition of 3 equiv of water.[18] It is also worth mentioning that no epimerization occurred at the stereogenic center of the amine (α-position; **16bb**). Interestingly, secondary amines were smoothly converted into tertiary amines (**17b** and **18b**). Aromatic amines exhibited little reactivity under the optimal catalytic conditions,[19] such that a primary aliphatic amine could also be selectively methylated in an excellent yield even in the presence of a secondary aromatic amine (**20bb**). Further investigations revealed that aromatic amines could also be selectively methylated, with no formamide product, under the modified reaction conditions without H_2 in excellent yields (**19b** and Table 2.4). Various aromatic amines were smoothly methylated (**22b**–**28b**) including amines with heterocycles (**26b** and **27b**)

and bulky naphthylamine (**28b**) without H_2. Substrates with reducible functional groups such as olefin, alkyne, nitrile, and ester were not tolerant under the reaction conditions. To our surprise, when aliphatic primary and secondary amines were present in the same molecule, the primary amine underwent selective methylation to secondary amines (**21bb**) with only a trace amount (<2%) of the undesired methylated product (**21c',** Table 2.5). To the best of our knowledge, this is the first example among N-methylation protocols that highlighted the reactivity difference between aliphatic primary and secondary amines. Overall, the protocols could be applicable to both aliphatic and aromatic amines with an appropriate level of chemo-selectivity with respect to N-methylation.

Next, the developed methodology was applied for the monomethylation of bio-related compounds or pharmaceuticals. For example, putrescine, a diamine that is involved in a biological pathway,[20] was monomethylated to give a moderate yield (**29bb**). Tyramine, a noradrenaline transporter,[21] exhibited poor reactivity (10% yield of **30b**) under the optimized conditions, most likely due to the presence of an acidic phenol. The addition of 0.3 equiv of K_2CO_3 provided the methylated product **30bb** in a moderate yield (34%). Memantine (**31a**) and mexiletine (**32a**), a commercially available Alzheimer drug[22] and anesthetic reagent,[23] respectively, were successfully converted into methylated products in good yields (64% and 71%, respectively). 1,3-Dimethylbutylamine (DMBA) (**33a**), which was reported as a pressor substance,[24] also showed moderate reactivity (35%). Oenethyl (**34bb**)[25] was synthesized from the precursor in a good yield (76%) using the developed methodology. Finally, the methylation protocol was applied for the last step in a

multi-step synthesis of atomoxetine (**35bb**), which is among the top 100 best-selling ADHD drugs,[26] resulting in a good yield (65%).

Table 2.2 Monomethylation of amines using methanol as C1 source[a]

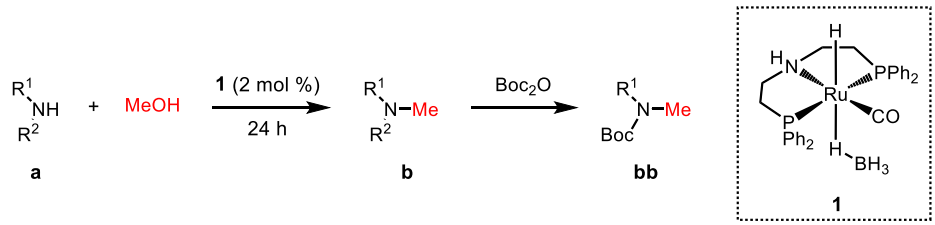

Aliphatic amines

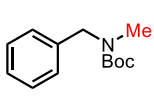

1bb, 77%

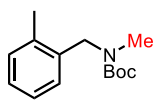

2bb, 85%

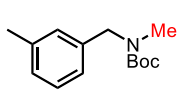

3bb, 72%

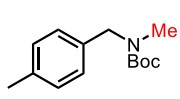

4bb, 75%

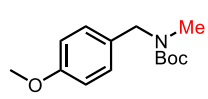

5bb, 82%

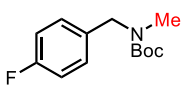

6bb[c], 64%

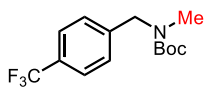

7bb[d], 76%

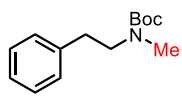

8bb, 79%

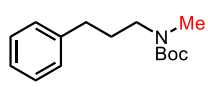

9bb[e], 74%

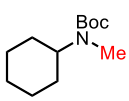

10bb, 45%

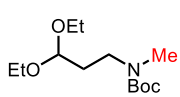

11bb[c], 70%

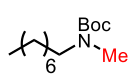

12bb[e], 68%

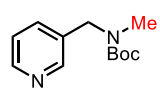

13bb[c, d], 71%

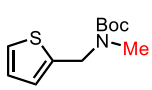

14bb[f], 84%

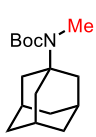

15bb[d, g], 58%

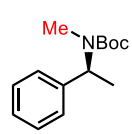

16bb[d], 88%

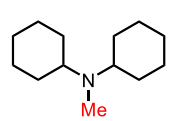

17b[f], 63%

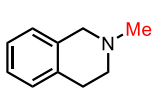

18b, 74%

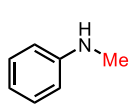

19b[b], 77%

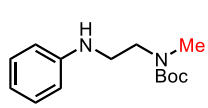

20bb, 83%

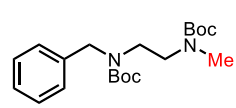

21bb[e], 63%

Aromatic amines[b]

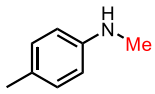

22b, 63%

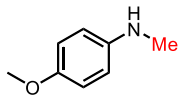

23b[d, h], 62%

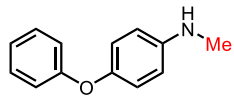

24b[d], 70%

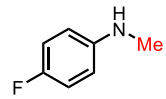

25b[i], 58%

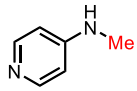

26b, 90%

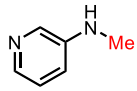

27b, >99%

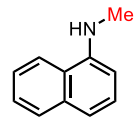

28b, 80%

Beio-related compounds[f]

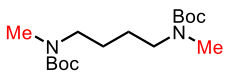

Putrescine-Me (**29bb**)
43%

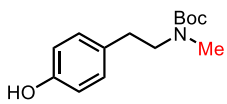

Tyramine-Me (**30bb**)[a, j]
34%

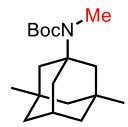

Memantine-Me (**31bb**)[g]
64%

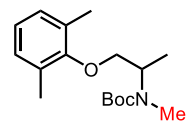

Mexiletine-Me (**32bb**)[d]
71%

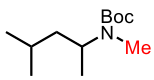

DMBA-Me (**33bb**)
35%

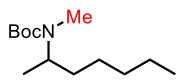

Oenethyl (**34bb**)[d]
76%

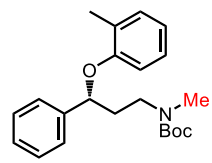

Atomoxetine (**35bb**)
65%

[a]Aliphatic amine conditions: amine (1 mmol), methanol (1.5 mL), **1** (2 mol %), and H_2 (4 MPa) at 120 °C oil bath for 24 h in a closed vessel; Boc-protection was conducted after the reaction for facile isolation of the product; isolated yields after Boc protection. [b]Aromatic amine conditions: amine (1 mmol), methanol (2 mL), and **1** (5 mol %) at 150 °C oil bath for 24 h in a closed vessel. [c]2.0 MPa of H_2. [d]140 °C. [e]110 °C. [f]130 °C. [g]3 eq. of H_2O. [h]12 h. [i]160 °C. [j]0.3 eq. of K_2CO_3.

2.2.3. Mechanistic studies

To understand the unusual selectivity of primary amines over secondary N-methyl amines, the reaction profile was investigated. Complete conversion of primary amine **1a** to N-methyl amine **1b** was observed under the developed conditions (Figure 2.2). Dehydrogenation of methanol was suggested as the rate-limiting step based on the primary KIE of methanol (k_H/k_D = 4.51) and the zeroth order to the concentration of **1a** (Figures 2.2 and 2.3). In the absence of H_2, formamide was formed as the major product (Figure 2.4 and Scheme 2.3), which is consistent with the literature.[27] When **1d** was subjected to the developed reaction conditions, the formation of **1b** and **1c** was observed, suggesting that the amide reduction and amine formylation reactions were reversible (Scheme 2.4). These results indicated that the addition of H_2 inhibited the dehydrogenation steps to generate **e** and **d**, letting the dehydration pathways more productive (Scheme 2.2). As no amide product was generated in the case of the aromatic amine without H_2 (**19a**), dehydrogenation of the hemiaminal intermediates from aromatic amines may be less favored than dehydration even in the absence of H_2, which would lead to the selective methylation.[28]

In order to assess the difference in reactivity between primary and secondary amines, which is critical for modulating the selectivity, several control experiments using secondary amines were conducted. When 1,2,3,4-tetrahydroisoquinoline (**18a**) was subjected to the optimal reaction conditions, formation of the tertiary *N*-methyl amine **18b** took place (Figure 2.5). However, when primary amine **1a** (0.5 equiv) was added to the reaction mixture, **1a** was the only amine that underwent the reaction, with virtually no conversion of **18a** taking place until **1a** was completely consumed (Figure 2.1). The results indicated that

primary amines were more reactive in the methylation when both primary and secondary amines were present in the reaction mixture. A moderately low temperature was preferred for selectivity, as the initially formed monomethylated product could be further methylated at a higher temperature of 150 °C (Figure 2.6) implying that kinetic control is critical to the reaction.

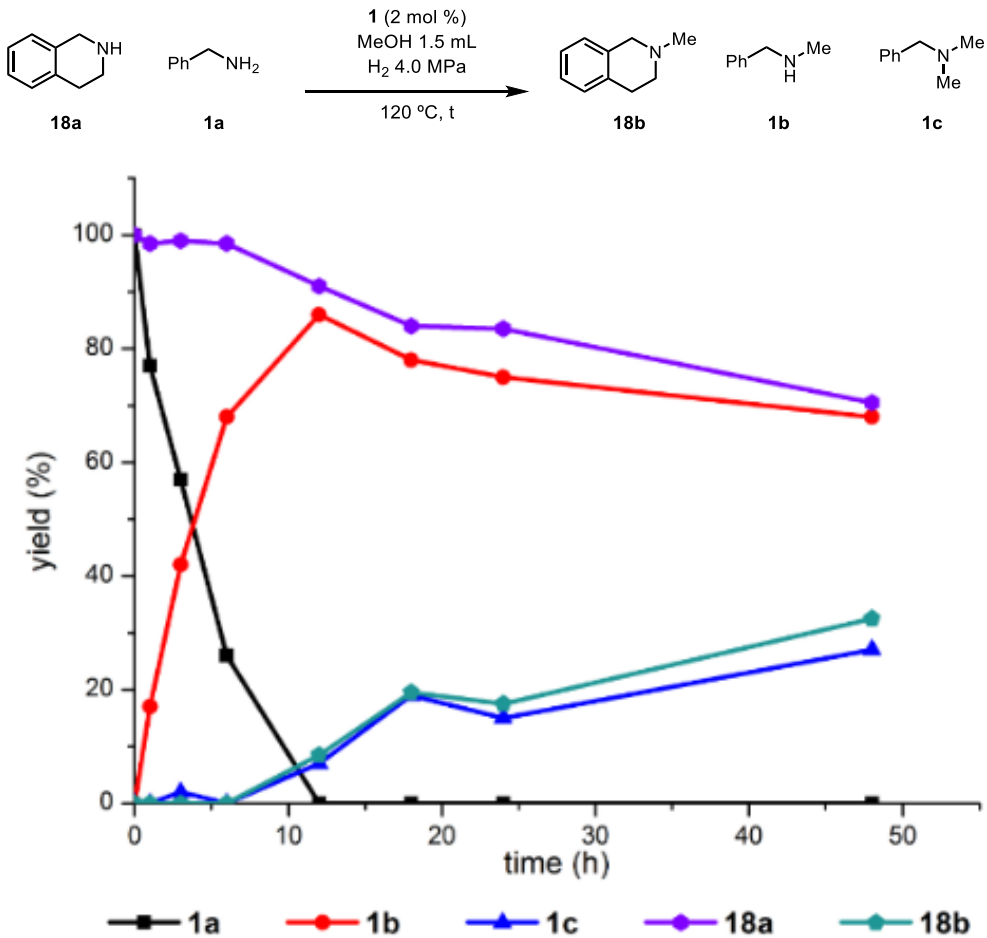

Figure 2.1 Reaction profile of competition reaction between primary and secondary amines

2.3. Conclusion

In conclusion, N-monomethylation of amines was achieved in a highly selective manner using methanol as the C1 source. Various amines including challenging aliphatic primary amines, aromatic amines, and bio-related compounds were selectively monomethylated in moderate to excellent yields with good functional group tolerance. By adjusting the reaction conditions, aliphatic amines were selectively methylated in the presence of aromatic amines. In addition, primary amines were also selectively monomethylated even in the presence of secondary amine moieties. Control experiments indicated that the presence of hydrogen was essential to control dehydration over dehydrogenation of the hemiaminal intermediate. Reaction temperature was found to be important for kinetically controlling the selectivity between N-monomethylation and N,N-dimethylation. The present study demonstrated that selectivity control in N-methylation—a fundamentally challenging task in traditional organic synthesis—can be achieved via transition metal catalysis with high atom-economy using methanol as the methylating reagent.

2.4. Experimental section

2.4.1. General information

Unless otherwise noted, all reactions were carried out using standard Schlenk techniques or in an argon-filled glove box. High purity H_2 (99.999%) was used. All amine monomethylation reactions were performed in an oven-dried stainless steel vessel under an argon atmosphere. Unless otherwise noted, all commercially available chemicals were purchased from Strem Chemicals, Sigma Aldrich, Alfa Aesar, or Tokyo Chemical Industry (TCI), and used as received. Methanol was purified by vacuum distillation to remove water and oxygen. Analytical TLC was performed on Merck 60 F254 silica gel plates (0.25mm thickness). Column chromatography was performed using Merck 60 silica gel (230-400 mesh). NMR spectra were recorded in $CDCl_3$ on a Bruker DPX-300 (300 MHz) spectrometer or Varian 400 and 500 NMR (400 and 500 MHz). Chemical shifts are reported in ppm and coupling constants are given in Hz. Chiral compounds were analyzed using an Agilent LC chromatographer with a CHIRALPAK AS-H column (particle size 5 μm, dimensions 4.6 mm x 250 mm). High-resolution mass spectrometry (HRMS) was performed at the Organic Chemistry Research Center in Sogang University using the ESI method.

2.4.2. General reaction procedures

General procedure for aliphatic amine N-monomethylation

A stainless steel vessel (50 mL) was charged with complex **1** (0.020 mmol, 2.0 mol %), amine (1.0 mmol), and methanol (1.5 mL) in an argon-filled glove box. Then the vessel was purged three times and charged with H_2 (4.0 MPa). The vessel was placed in an oil bath heated to 120 °C. After 24 h, the reaction was cooled to room temperature, and H_2 was carefully released in a fumehood. The crude reaction mixture was concentrated using a rotary evaporator. Unless otherwise noted, di-*tert*-butyl dicarbonate (3.0 mmol), triethylamine (5.0 mmol), and dichloromethane (5 mL) were sequentially added to the oily residue, and the reaction mixture was stirred at room temperature overnight, followed by concentration using a rotary evaporator. The residue was purified by column chromatography to afford the desired product.

General procedure for aromatic amine N-monomethylation

A stainless steel vessel (50 mL) was charged with complex **1** (0.050 mmol, 5.0 mol %), amine (1.0 mmol), and methanol (2 mL) in an argon-filled glove box. The vessel was placed in an oil bath heated to 150 °C. After 24 h, the reaction was cooled to room temperature, and H_2 was carefully released in a fumehood. The crude reaction mixture was concentrated using a rotary evaporator. The residue was purified by column chromatography to afford the desired product.

2.4.3. Supplementary optimizations

Table 2.3 Optimization experiments of homogeneous dehydrogenation catalysts[a]

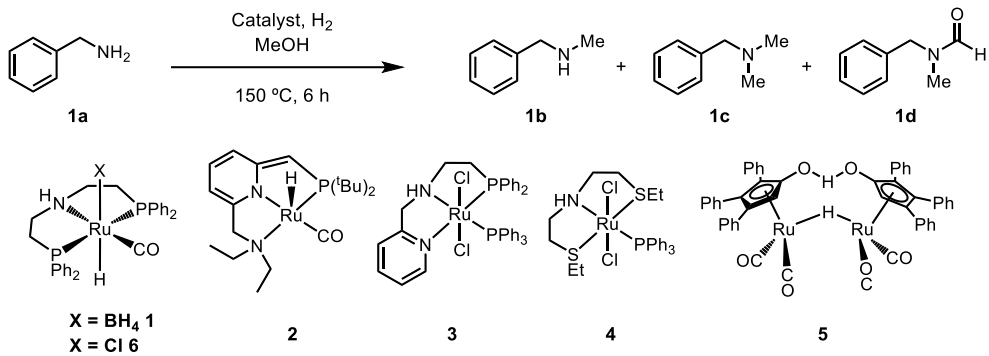

Entry	Catalyst	Additive	**1b** (%)	**1c** (%)	**1d**(%)
1	**1**	-	61	5	29
2	**2**	-	8	-	-
3	**3**	-	19	-	4
4	**4**	K_2CO_3	19	-	-
5	**5**	-	-	-	-
6	$RuH_2(CO)(PPh_3)_3$	-	17	-	-
7	$[Cp^*IrCl_2]_2$	$NaHCO_3$	-	-	-
8	**6**	K_2CO_3	45	26	29
9	-	-	-	-	-

[a]Reaction conditions: **1a** (1.0 mmol), methanol (1.5 mL), catalyst (2.0 mol %), additive (2.0 mol %), and H_2 (2.0 MPa) at 150 °C oil bath for 6 h; yields were determined by ^1H NMR using *p*-xylene as an internal standard.

Table 2.4 Optimization experiments of aromatic amine[a]

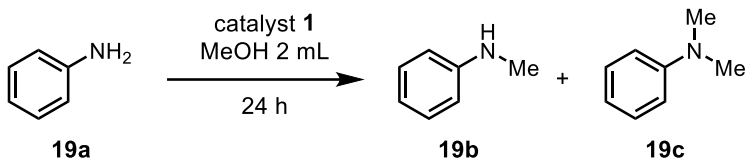

Entry	Temperature (°C)	**1** (mol %)	Additive	**19b** (%)	**19c** (%)
1	160	5	NaOMe	92	2
2	160	5	-	91	2
3	150	5	-	90	2
4	140	5	-	61	-
5	150	2	-	46	-

[s]Reaction conditions: **19a** (1.0 mmol), methanol (2.0 mL), and catalyst **1** at 150 °C oil bath for 24 h; yields were determined by ^{1}H NMR using *p*-xylene as an internal standard.

2.4.4. Control experiments and byproduct yield

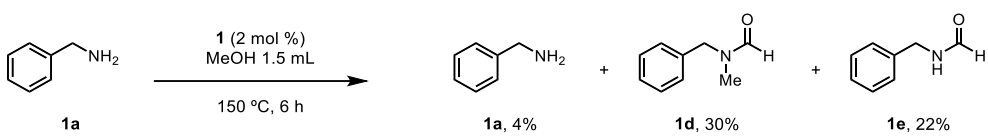

Scheme 2.3. Control experiment; reaction without H_2 gas

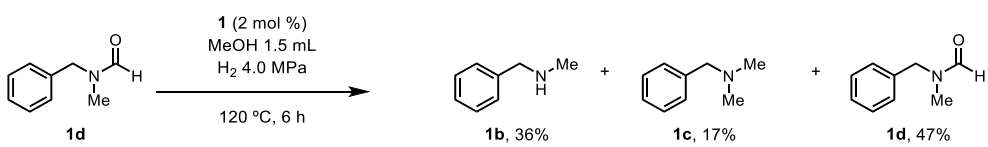

Scheme 2.4 Control experiment to check possible reactions of an intermediate **1d**

Table 2.5 N,N-dimethylamine byproduct[a]

Aliphatic amines

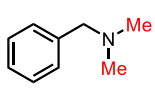

1c, 7%

2c, 13%

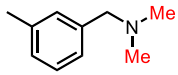

3c, N.D.

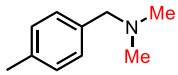

4c, N.D.

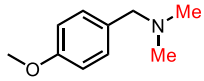

5c, 5%

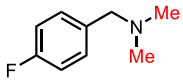

6c, 5%

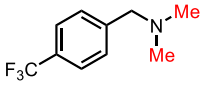

7c, N.D.

8c, 16%

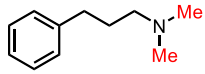

9c, 2%

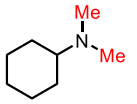

10c, 31%

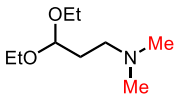

11c, 24%

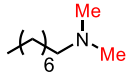

12c, 7%

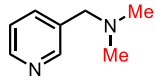

13c, 10%

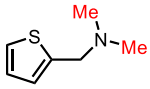

14c, 8%

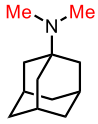

15c, 13%

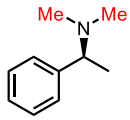

16c, 6%

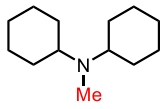

-

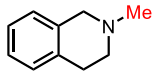

-

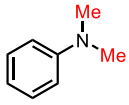

19c, N.D.

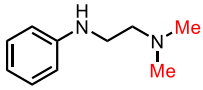

20c[b], 5%

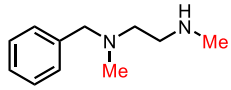

21c'[c], <2%

Aromatic amines

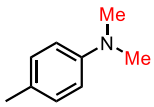

22c, 4%

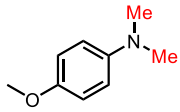

23c, N.D.

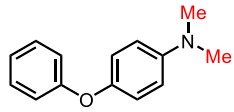

24c, N.D.

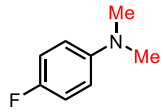

25c, 25%

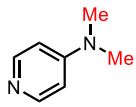

26c, N.D.

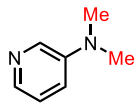

27c, N.D.

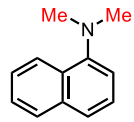

28c, N.D.

Beio-related compounds

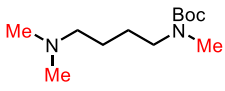

29c'[c]
24%

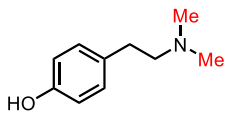

30c
10%

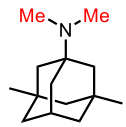

31c
35%

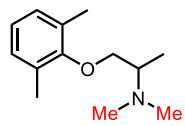

32c
20%

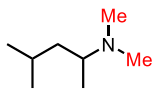

33c
11%

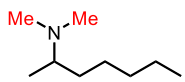

34c
21%

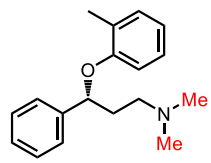

35c
34%

N.D. = Not detected [a]Yields were determined by ^{1}H NMR using *p*-xylene as an internal standard. [b]No methylation of aromatic amine was observed. [c]Isolated yields.

2.4.5. Kinetic profiling studies

Reaction under optimized conditions

A stainless steel vessel (50 mL) was charged with complex **1** (0.020 mmol, 2.0 mol %), **1a** (1.0 mmol), and methanol (1.5 mL) in an argon-filled glove box. Then the vessel was purged three times and charged with H_2 (4.0 MPa). The vessel was placed in an oil bath heated to 120 °C. After specific time, the reaction mixture was cooled to room temperature, and H_2 was carefully released in a fumehood. The crude reaction mixture was concentrated using a rotary evaporator, and the yields were determined by ^{1}H NMR using *p*-xylene as an internal standard.

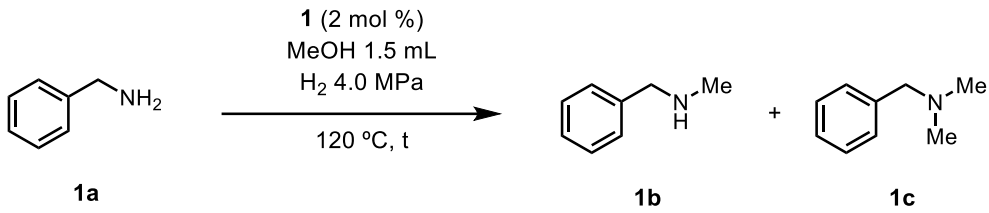

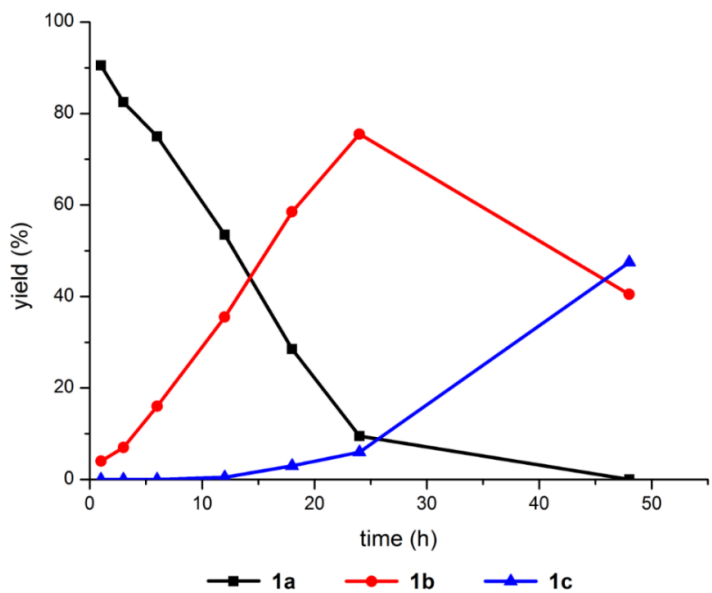

Figure 2.2 Reaction profile under optimized conditions

Reaction with CD_3OD

A stainless steel vessel (50 mL) was charged with complex **1** (0.020 mmol, 2.0 mol %), **1a** (1.0 mmol), and CD_3OD (1.5 mL) in an argon-filled glove box. Then the vessel was purged three times and charged with H_2 (4.0 MPa). The vessel was placed in an oil bath heated to 120 °C. After specific time, the reaction mixture was cooled to room temperature, and H_2 was carefully released in a fumehood. The crude reaction mixture was concentrated using a rotary evaporator, and the yields were determined by ^1H NMR using *p*-xylene as an internal standard. KIE value was measured by the ratio of the slope from Figures 2.2 and 2.3; k_H/k_D = (-3.56) / (-0.79) = 4.51.

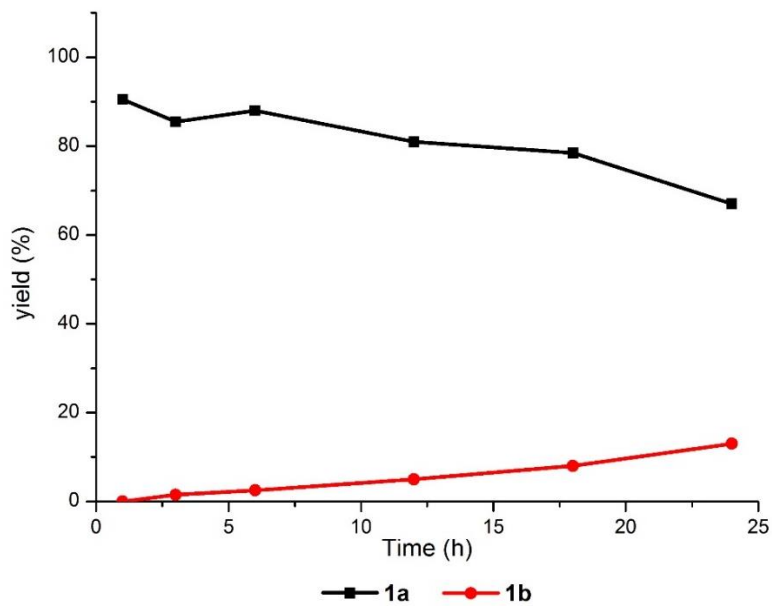

Figure 2.3 Reaction profile with CD_3OD

Reaction without H_2

A stainless steel vessel (50 mL) was charged with complex **1** (0.020 mmol, 2.0 mol %), **1a**(1.0 mmol), and methanol (1.5 mL) in an argon-filled glove box. The vessel was placed in an oil bath heated to 120 °C. After specific time, the reaction mixture was cooled to room temperature, and generated H_2 was carefully released in a fumehood. The crude reaction mixture was concentrated using a rotary evaporator, and the yields were determined by ^{1}H NMR using *p*-xylene as an internal standard.

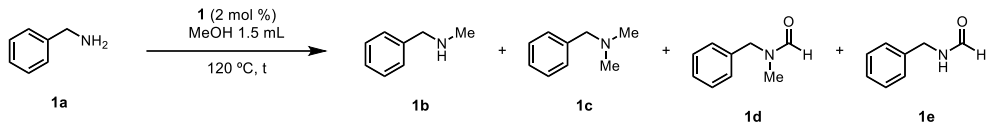

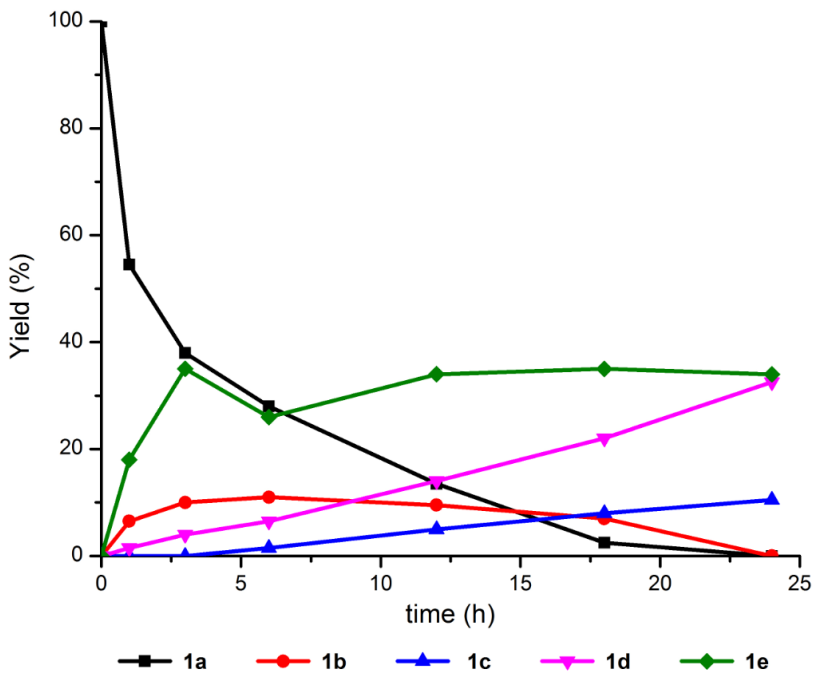

Figure 2.4 Reaction profile without H_2 gas

Reaction of secondary amine as starting reagent

A stainless steel vessel (50 mL) was charged with complex **1** (0.020 mmol, 2.0 mol %), **18a** (1.0 mmol), and methanol (1.5 mL) in an argon-filled glove box. Then the vessel was purged three times and charged with H_2 (4.0 MPa). The vessel was placed in an oil bath heated to 120 °C. After specific time, the reaction mixture was cooled to room temperature, and H_2 was carefully released in a fumehood. The crude reaction mixture was concentrated using a rotary evaporator, and the yields were determined by ^{1}H NMR using *p*-xylene as an internal standard.

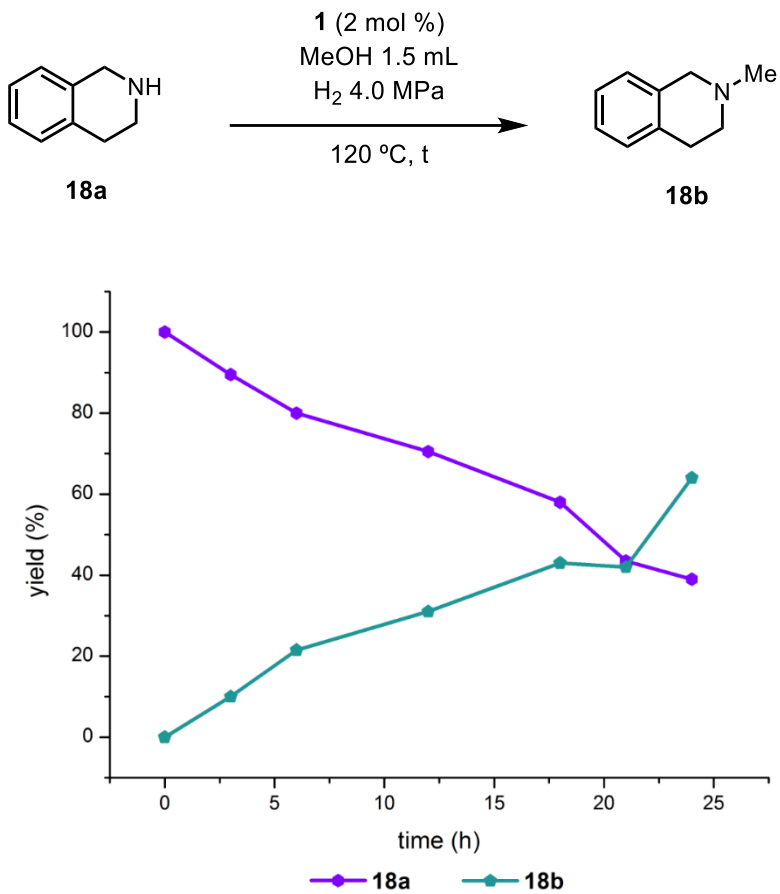

Figure 2.5 Reaction profile of secondary amine

Competition reaction of primary and secondary amines

A stainless steel vessel (50 mL) was charged with complex **1** (0.020 mmol, 2.0 mol %), **18a** (1.0 mmol), **1a** (0.5 mmol), and methanol (1.5 mL) in an argon-filled glove box. Then the vessel was purged three times and charged with H_2 (4.0 MPa). The vessel was placed in an oil bath heated to 120 °C. After specific time, the reaction mixture was cooled to room temperature, and H_2 was carefully released in a fumehood. The crude reaction mixture was concentrated using a rotary evaporator, and the yields were determined by ^{1}H NMR using *p*-xylene as an internal standard.

Reaction under a relatively high temperature

A stainless steel vessel (50 mL) was charged with complex **1** (0.020 mmol, 2.0 mol %), **1a** (1.0 mmol), and methanol (1.5 mL) in an argon-filled glove box. Then the vessel was purged three times and charged with H_2 (4.0 MPa). The vessel was placed in an oil bath heated to 150 °C. After specific time, the reaction mixture was cooled to room temperature, and H_2 was carefully released in a fumehood. The crude reaction mixture was concentrated using a rotary evaporator, and the yields were determined by ^{1}H NMR using *p*-xylene as an internal standard.

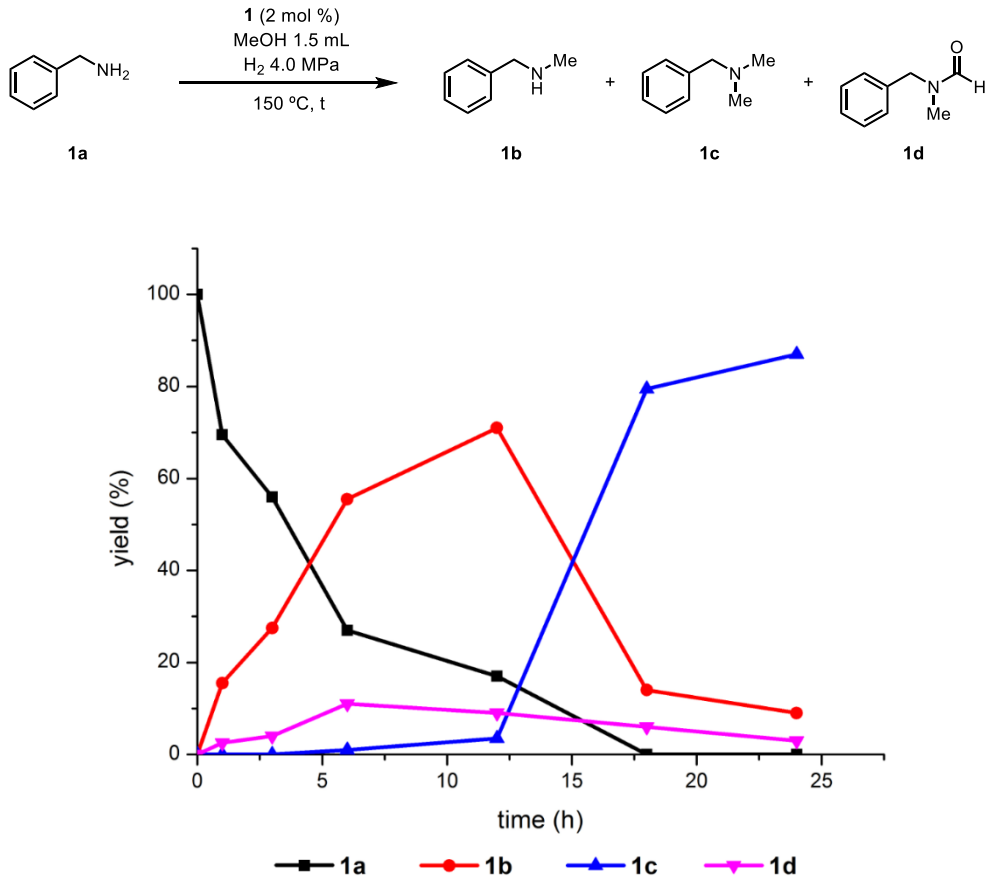

Figure 2.6 Reaction profile under high temperature

2.4.6. Characterization of newly reported compounds

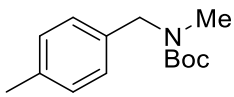

***N*-(*tert*-butoxycarbonyl)-*N*-methyl(*p*-methylbenzyl)amine (4bb)**

Colorless oil. ^{1}H NMR (300 MHz, $CDCl_3$) δ = 7.15 (s, 4H), 4.41 (s, 2H), 2.84 (s, 3H), 2.36 (s, 3H), 1.52 (s, 9H); ^{13}C NMR (75 MHz, $CDCl_3$) δ = 155.88, 136.76, 135.04, 129.19, 127.75, 127.29, 79.52, 52.32, 51.63, 33.74, 28.48, 21.08; HRMS-ESI (m/z): $[M+Na]^+$ calcd for $C_{14}H_{21}NNaO_2$: 258.1470. Found: 258.1464

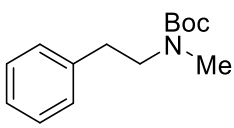

***tert*-butyl methyl(phenethyl)carbamate (8bb)**

Colorless oil. ^{1}H NMR (500 MHz, $CDCl_3$) δ = 7.28 (dd, J=14.2, 6.7, 2H), 7.20 (dd, J=14.4, 7.1, 2H), 3.42 (t, J=7.4, 2H), 2.89 – 2.72 (m, 5H), 1.41 (s, 9H); ^{13}C NMR (75 MHz, $CDCl_3$) δ = 155.57, 139.26, 128.88, 128.46, 126.23, 79.16, 50.85, 34.59, 34.29, 28.39; HRMS-ESI (m/z): $[M+Na]^+$ calcd for $C_{14}H_{21}NNaO_2$: 258.1470. Found: 258.1464

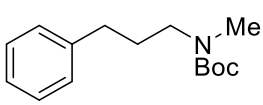

***tert*-butyl methyl(3-phenylpropyl)carbamate (9bb)**

Colorless oil. ^{1}H NMR (300 MHz, $CDCl_3$) δ = 7.37 – 7.13 (m, 5H), 3.27 (s, 2H), 2.86 (s, 3H), 2.68 – 2.53 (m, 2H), 1.94 – 1.77 (m, 2H), 1.48 (s, 9H); ^{13}C NMR (75 MHz, $CDCl_3$) δ = 155.78, 141.75, 128.39, 128.30, 125.87, 79.13, 48.49, 34.11, 33.09, 29.49, 28.47; HRMS-ESI (m/z): $[M+Na]^+$ calcd for $C_{15}H_{23}NNaO_2$: 272.1626. Found: 272.1621

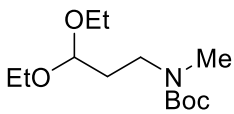

3,3-diethoxy-*N*-methylpropan-1-amine (11bb)

Colorless oil. ^{1}H NMR (500 MHz, $CDCl_3$) δ = 4.49 (t, J=5.6, 1H), 3.64 (m, 2H), 3.54 – 3.41 (m, 2H), 3.25 (s, 2H), 2.83 (s, 3H), 1.83 (dd, J=14.6, 5.9, 2H), 1.44 (s, 9H), 1.19 (t, J=7.1, 5H); ^{13}C NMR (125 MHz, $CDCl_3$) δ = 155.57, 101.01, 79.09, 61.04, 44.96, 34.34, 32.03, 28.35, 15.20; HRMS-ESI (m/z): $[M+Na]^+$ calcd for $C_{13}N_{27}NNaO_4$: 284.1838. Found: 284.1832

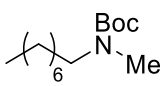

***tert*-butyl methyl(octyl)carbamate (12bb)**

Colorless oil. ^{1}H NMR (300 MHz, $CDCl_3$) δ = 3.10 (br, 2H), 2.75 (s, 3H), 1.43 – 1.34 (m, 10H), 1.19 (m, 10H), 0.79 (br, J=6.0, 3H); ^{13}C NMR (75 MHz, $CDCl_3$) δ = 155.65, 78.81, 48.63, 33.85, 31.72, 29.23, 29.19, 28.33, 27.71, 26.59, 22.54, 13.95; HRMS-ESI (m/z): $[M+Na]^+$ calcd for $C_{14}H_{29}NNaO_2$: 266.2096. Found: 266.2090.

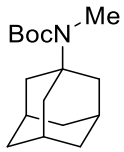

***N*-*t*-butoxycarbonyl-*N*-methyl-1-adamantylamine (15bb)**

For Boc protection, di-*tert*-butyl dicarbonate (1.5 mmol) and ehtnaol (5 mL) was added to the crude oil. The mixture was stirred at room temperature overnight. Colorless oil. ^{1}H NMR (500 MHz, $CDCl_3$) δ = 2.85 (s, 1H), 2.11 – 2.05 (m, 3H), 1.67 – 1.62 (m, 2H), 1.46 (s, 3H); ^{13}C NMR (125 MHz, $CDCl_3$) δ = 155.87, 79.03, 55.96, 40.25, 36.45, 30.09, 30.00, 28.60; HRMS-ESI (m/z): $[M+Na]^+$ calcd for $C_{16}H_{27}NNaO_2$: 288.1939. Found: 288.1934

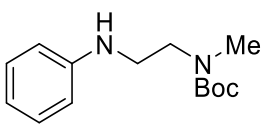

***tert*-butyl methyl(2-(phenylamino)ethyl)carbamate (20bb)**

For Boc protection, di-*tert*-butyl dicarbonate (1.2 mmol) and methanol (5 mL) was added to the crude oil. The mixture was stirred at room temperature overnight. Colorless oil. ^{1}H NMR (300 MHz, $CDCl_3$) δ = 7.21 (t, J=7.8, 2H), 6.78 – 6.67 (m, 1H), 6.64 (d, J=8.0, 2H), 4.19 (br, 1H), 3.50 (s, 2H), 3.30 (t, J=6.0, 2H), 2.92 (s, 3H), 1.52 (s, 9H); ^{13}C NMR (75 MHz, $CDCl_3$) δ = 156.80, 155.78, 148.38, 129.30, 117.27, 112.41, 79.77, 47.97, 42.49, 41.83, 34.92, 34.57, 28.46; HRMS-ESI (m/z): $[M+H]^+$ calcd for $C_{14}H_{23}N_2O_2$: 251.1760. Found: 251.1754

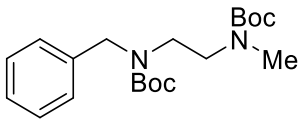

***tert*-butyl benzyl(2-((*tert*-butoxycarbonyl)(methyl)amino)ethyl)carbamate (21bb)**

For Boc protection, di-*tert*-butyl dicarbonate (5 mmol), trimethylamine (3 mmol), and dichloromethane (5 mL) was added to the crude oil. The mixture was stirred at room temperature overnight. Colorless oil. ^{1}H NMR (500 MHz, $CDCl_3$) δ = 7.37 – 7.13 (m, 5H), 4.45 (d, J=21.5, 2H), 3.30 (d, J=41.5, 4H), 2.86 (d, J=17.6, 3H), 1.53 – 1.39 (m, 18H); ^{13}C NMR (75 MHz, $CDCl_3$) δ = 155.61, 138.21, 128.45, 127.70, 127.16, 79.78, 79.30, 51.17, 50.63, 50.08, 46.73, 46.00, 44.32, 43.73, 34.86, 34.45, 28.36; HRMS-ESI (m/z): $[M+Na]^+$ calcd for $C_{20}H_{32}N_2NaO_4$: 387.2260. Found: 387.2254

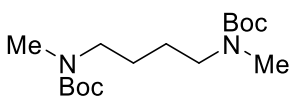

***N*-*t*-butoxycarbonyl-*N*-methylputrescine (di-*tert*-butyl butane-1,4-diylbis(methyl)carbamate, 29bb)**

For Boc protection, di-*tert*-butyl dicarbonate (4 mmol), trimethylamine (5 mmol), and dichloromethane (5 mL) was added to the crude oil. The mixture was stirred at room temperature overnight. Colorless oil. ^{1}H NMR (500 MHz, $CDCl_3$) δ = 3.20 (s, 4H), 2.81 (s, 6H), 1.49 – 1.46 (m, 4H), 1.44 (d, J=1.6, 18H); ^{13}C NMR (75 MHz, $CDCl_3$) δ = 155.57, 78.91, 48.20, 33.92, 33.87, 28.32, 28.27, 24.78; HRMS-ESI (m/z): $[M+Na]^+$ calcd for $C_{16}H_{32}N_2NaO_4$: 339.2260. Found: 339.2254

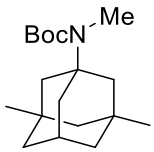

_N_-t-butoxycarbonyl-_N_-methylmemantine (_tert_-butyl (3,5-dimethyladamantan-1-yl)(methyl)carbamate, 31bb)

Free memantine was prepared from its hydrochloride form, commercially purchased. Memantine hydrochloride was dissolved in a minimum amount of distilled water with constant magnetic stirring. An aqueous solution of 10% sodium hydroxide was slowly added until the reaction medium reached a pH of 10. The reaction was left under stirring for 10 min. The mixture was extracted with dichloromethane and dried over anhydrous magnesium sulfate to give an oily product, which was used for the monomethlyation reaction.

Colorless oil. ^{1}H NMR (500 MHz, $CDCl_3$) δ = 2.84 (s, 3H), 2.14 (br, 1H), 1.92 (br, 2H), 1.72 (br, 3H), 1.45 (s, 9H), 1.42 (s, 1H), 1.34 (d, J=12.3, 2H), 1.25 (d, J=12.3, 2H), 1.12 (br, 2H), 0.84 (s, 6H); ^{13}C NMR (125 MHz, $CDCl_3$) δ = 155.73, 78.96, 57.70, 50.57, 46.24, 42.67, 38.66, 32.67, 30.60, 30.46, 30.17, 28.59; HRMS-ESI (m/z): $[M+Na]^+$ calcd for $C_{18}H_{31}NNaO_2$: 316.2252. Found: 316.2247

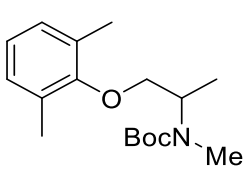

_N_-t-butoxycarbonyl-_N_-methylmexiletine (_tert_-butyl (1-(2,6-dimethylphenoxy)propan-2-yl)(methyl)carbamate, 32bb)

Free mexiletine was prepared from its hydrochloride form, commercially purchased. Mexiletine hydrochloride was dissolved in a minimum amount of distilled water with constant magnetic stirring. An aqueous solution of 10% sodium hydroxide was slowly added until the reaction medium reached a pH of 10. The reaction was left under stirring for 10 min. The mixture was extracted with dichloromethane and dried over anhydrous magnesium sulfate to give an oily product, which was used for the monomethlyation reaction.

Colorless oil. ^{1}H NMR (500 MHz, $CDCl_3$) δ = 7.00 (d, J=7.3, 2H), 6.91 (t, J=7.2, 1H), 4.48 (d, J=46.3, 1H), 3.82 – 3.65 (m, 2H), 2.88 (s, 3H), 2.27 (s, 6H), 1.48 (s, 9H), 1.31 (d, J=7.0, 3H); ^{13}C NMR (75 MHz, $CDCl_3$) δ = 155.70, 155.54, 130.68, 128.86, 123.93, 123.82, 79.38, 73.46, 51.38, 50.73, 29.92, 29.04, 28.47, 16.16, 15.13, 14.71; HRMS-ESI (m/z): $[M+Na]^+$ calcd for $C_{17}H_{27}NNaO_3$: 316.1889. Found: 316.1883

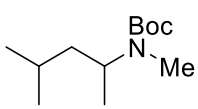

***N*-t-butoxycarbonyl-*N*-methyl-1,3-dimethylbutanamine (33bb)**

Colorless oil. ^{1}H NMR (500 MHz, $CDCl_3$) δ = 4.24 (brm, 1H), 2.62 (s, 3H), 1.43 (m, 11H), 1.13 – 0.98 (m, 4H), 0.92 – 0.81 (m, 6H); ^{13}C NMR (125 MHz, $CDCl_3$) δ = 155.73, 78.89, 48.63, 43.30, 28.43, 24.90, 23.04, 22.10, 18.65; HRMS-ESI (m/z): $[M+Na]^+$ calcd for $C_{12}H_{25}NNaO_2$: 238.1783. Found: 238.1777

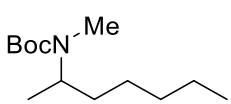

***N*-t-butoxycarbonyloenethyl (*tert*-butyl heptan-2-yl(methyl)carbamate, 34bb)**

Colorless oil. ^{1}H NMR (500 MHz, $CDCl_3$) δ = 4.08 (brm, 1H), 2.58 (s, 3H), 1.38 (s, 9H), 1.31 – 1.04 (m, 8H), 0.98 (d, J=6.9, 3H), 0.80 (dd, J=9.6, 4.0, 3H); ^{13}C NMR (125 MHz, $CDCl_3$) δ = 155.78, 78.76, 49.83, 33.96, 31.50, 28.37, 26.89, 26.00, 22.48, 18.23, 13.82; HRMS-ESI (m/z): $[M+Na]^+$ calcd for $C_{13}H_{27}NNaO_2$: 252.1939. Found: 252.1934

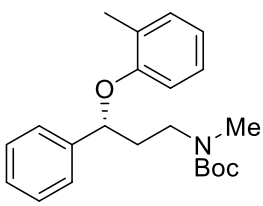

***N*-t-butoxycarbonylatomoxetine (*tert*-butyl methyl(3-phenyl-3-(o-tolyloxy)propyl)carbamate, 35bb)**

Starting noratomoxetine was prepared by following previous works.[30]

Colorless oil. ^{1}H NMR (300 MHz, $CDCl_3$) δ = 7.32 (m, 5H), 7.16 (d, J=7.2, 1H), 6.99 (t, J=7.8, 1H), 6.81 (t, J=7.3, 1H), 6.62 (d, J=8.1, 1H), 5.20 (dd, J=8.4, 4.1, 1H), 3.49 (br, 2H), 2.89 (s, 3H), 2.39 (s, 3H), 2.18 (m, 2H), 1.44 (s, 9H); ^{13}C NMR (75 MHz, $CDCl_3$) δ = 155.83, 155.79, 141.84, 130.64, 128.69, 127.55, 126.90, 126.61, 125.65, 120.28, 112.59, 79.36, 46.02, 37.20, 34.54, 28.39, 16.58; HRMS-ESI (m/z): $[M+Na]^+$ calcd for $C_{22}H_{29}NNaO_3$: 378.2045. Found: 378.2040

2.5. References

(1) (a) Ke, Z.; Cui, X.; Shi, F., *ACS Sustainable Chem. Eng.* **2016,** *4* (7), 3921-3926; (b) Barreiro, E. J.; Kümmerle, A. E.; Fraga, C. A. M., *Chem. Rev.* **2011,** *111* (9), 5215-5246.

(2) (a) Sagan, S.; Karoyan, P.; Lequin, O.; Chassaing, G.; Lavielle, S., *Curr. Med. Chem.* **2004,** *11* (21), 2799-2822; (b) Subtelny, A. O.; Hartman, M. C. T.; Szostak, J. W., *J. Am. Chem. Soc.* **2008,** *130* (19), 6131-6136.

(3) Salvatore, R. N.; Yoon, C. H.; Jung, K. W., *Tetrahedron* **2001,** *57* (37), 7785-7811.

(4) (a) Lebleu, T.; Kotsuki, H.; Maddaluno, J.; Legros, J., *Tetrahedron Lett.* **2014,** *55* (2), 362-364; (b) Le Pera, A.; Leggio, A.; Liguori, A., *Tetrahedron* **2006,** *62* (25), 6100-6106.

(5) (a) Jacquet, O.; Frogneux, X.; Das Neves Gomes, C.; Cantat, T., *Chem. Sci.* **2013,** *4* (5), 2127-2131; (b) González, I.; Mosquera, J.; Guerrero, C.; Rodríguez, R.; Cruces, J., *Org. Lett.* **2009,** *11* (8), 1677-1680.

(6) Yebeutchou, R. M.; Dalcanale, E., *J. Am. Chem. Soc.* **2009,** *131* (7), 2452-2453.

(7) (a) Lebleu, T.; Ma, X.; Maddaluno, J.; Legros, J., *Chem. Commun.* **2014,** *50* (15), 1836-1838; (b) Kundu, S. K.; Mitra, K.; Majee, A., *RSC Adv.* **2013,** *3* (23), 8649-8651; (c) Selva, M.; Tundo, P., *Tetrahedron Lett.* **2003,** *44* (44), 8139-8142.

(8) (a) Liger, F.; Eijsbouts, T.; Cadarossanesaib, F.; Tourvieille, C.; Le Bars, D.; Billard, T., *Eur. J. Org. Chem.* **2015,** *2015* (29), 6434-6438; (b) González-Sebastián, L.; Flores-Alamo, M.; García, J. J., *Organometallics* **2015,** *34* (4), 763-769.

(9) (a) Wang, H.; Huang, Y.; Dai, X.; Shi, F., *Chem. Commun.* **2017,** *53* (40), 5542-5545; (b) Hajipour, A. R.; Mohammadpoor-Baltork, I.; Noroallhi, M., *Indian J.*

Chem., Sect B **2001,** *40* (2), 152-156; (c) Guyon, C.; Duclos, M.-C.; Métay, E.; Lemaire, M., *Tetrahedron Lett.* **2016,** *57* (27), 3002-3005.

(10) Natte, K.; Neumann, H.; Beller, M.; Jagadeesh, R. V., *Angew. Chem. Int. Ed.* **2017,** *56* (23), 6384-6394.

(11) Moran, J.; Preetz, A.; Mesch, R. A.; Krische, M. J., *Nat. Chem.* **2011,** *3*, 287.

(12) (a) Gunanathan, C.; Milstein, D., *Science* **2013,** *341* (6143); (b) Bähn, S.; Imm, S.; Neubert, L.; Zhang, M.; Neumann, H.; Beller, M., *ChemCatChem* **2011,** *3* (12), 1853-1864; (c) Yamaguchi, R.; Fujita, K.; Zhu, M. W., *Heterocycles* **2010,** *81* (5), 1093-1140; (d) Celaje, J. J. A.; Zhang, X.; Zhang, F.; Kam, L.; Herron, J. R.; Williams, T. J., *ACS Catal.* **2017,** *7* (2), 1136-1142; (e) Lee, H.; Yi, C. S., *Organometallics* **2016,** *35* (11), 1973-1977.

(13) (a) Tsarev, V. N.; Morioka, Y.; Caner, J.; Wang, Q.; Ushimaru, R.; Kudo, A.; Naka, H.; Saito, S., *Org. Lett.* **2015,** *17* (10), 2530-2533; (b) Liang, R.; Li, S.; Wang, R.; Lu, L.; Li, F., *Org. Lett.* **2017,** *19* (21), 5790-5793; (c) Dang, T. T.; Ramalingam, B.; Seayad, A. M., *ACS Catal.* **2015,** *5* (7), 4082-4088.

(14) (a) Zhao, Y.; Foo, S. W.; Saito, S., *Angew. Chem. Int. Ed.* **2011,** *50* (13), 3006-3009; (b) Campos, J.; Sharninghausen, L. S.; Manas, M. G.; Crabtree, R. H., *Inorg. Chem.* **2015,** *54* (11), 5079-5084; (c) Elangovan, S.; Neumann, J.; Sortais, J.-B.; Junge, K.; Darcel, C.; Beller, M., *Nat. Commun.* **2016,** *7*, 12641.

(15) Grigg, R.; Mitchell, T. R. B.; Sutthivaiyakit, S.; Tongpenyai, N., *J. Chem. Soc., Chem. Commun.* **1981,** (12), 611-612.

(16) (a) Oku, T.; Ikariya, T., *Angew. Chem. Int. Ed.* **2002,** *41* (18), 3476-3479; (b) Oku, T.; Arita, Y.; Tsuneki, H.; Ikariya, T., *J. Am. Chem. Soc.* **2004,** *126* (23), 7368-7377.

(17) (a) Kang, B.; Hong, S. H., *Adv. Synth. Catal.* **2015,** *357* (4), 834-840; (b) Chakraborty, S.; Gellrich, U.; Diskin-Posner, Y.; Leitus, G.; Avram, L.; Milstein, D., *Angew. Chem. Int. Ed.* **2017,** *56* (15), 4229-4233; (c) Ortega, N.; Richter, C.; Glorius, F., *Org. Lett.* **2013,** *15* (7), 1776-1779.

(18) N,N-dimethyladamantanamine **15c** was obtained in 12% yield; without water, **15b** was formed in a low yield (15%) along with **15c** (67%) as the major product. It is plausible that water suppressed the dehydration step during dimethylation, while having less of an effect on the dehydrogenation step in the monomethylation.

(19) Under these conditions, **19a** was converted to **19b** in 4% yield.

(20) Wang, X.; Wu, G.; Bazer, F. W., Chapter 2 - mTOR: The Master Regulator of Conceptus Development in Response to Uterine Histotroph During Pregnancy in Ungulates A2 - Maiese, Kenneth. In *Molecules to Medicine with mTOR*, Academic Press: Boston, 2016; pp 23-35.

(21) Finberg, J. P. M.; Gillman, K., Selective inhibitors of monoamine oxidase type B and the "cheese effect". In *International Review of Neurobiology*, Youdim, M. B. H.; Douce, P., Eds. Academic Press: 2011; Vol. 100, pp 169-190.

(22) Mount, C.; Downton, C., *Nat. Med.* **2006,** *12*, 780.

(23) Jarvis, B.; Coukell, A. J., *Drugs* **1998,** *56* (4), 691-707.

(24) Rohrmann, E.; Shonle, H. A., *J. Am. Chem. Soc.* **1944,** *66* (9), 1516-1520.

(25) Shaffer, F. E.; Knoefel, P. K., *J. Am. Pharm. Assoc.* **1950,** *39* (1), 12-15.

(26) (a) McGrath, N. A.; Brichacek, M.; Njardarson, J. T., *J. Chem. Educ.* **2010,** *87* (12), 1348-1349; (b) Kielbasa, W.; Lobo, E., *J. Clin. Pharmacol.* **2015,** *55* (12), 1422-1431.

(27) Oldenhuis, N. J.; Dong, V. M.; Guan, Z., *Tetrahedron* **2014,** *70* (27), 4213-4218.

(28) It has been reported that amidation of aromatic amines with alcohol via dehydrogenation of the hemiaminal intermediates is not facile in homogeneous Ru-catalyzed dehydrogenative C–N bond formation reactions, see representative examples

(29) Václavík, J.; Zschoche, R.; Klimánková, I.; Matoušek, V.; Beier, P.; Hilvert, D.; Togni, A., *Chem. Eur. J.* **2017,** *23* (27), 6490-6494.

(30) (a) Vogl, M.; Kratzer, R.; Nidetzky, B.; Brecker, L., *Chirality* **2012,** *24* (10), 847-853; (b) Kuo, F.; Clodfelter, D. K.; Wheeler, W. J., *J. Labelled Compd. Radiopharm.* **2004,** *47* (9), 615-625.

Chapter 3. Selective N-Formylation and N-Methylation of Amines Using Methanol as a Sustainable C1 source*

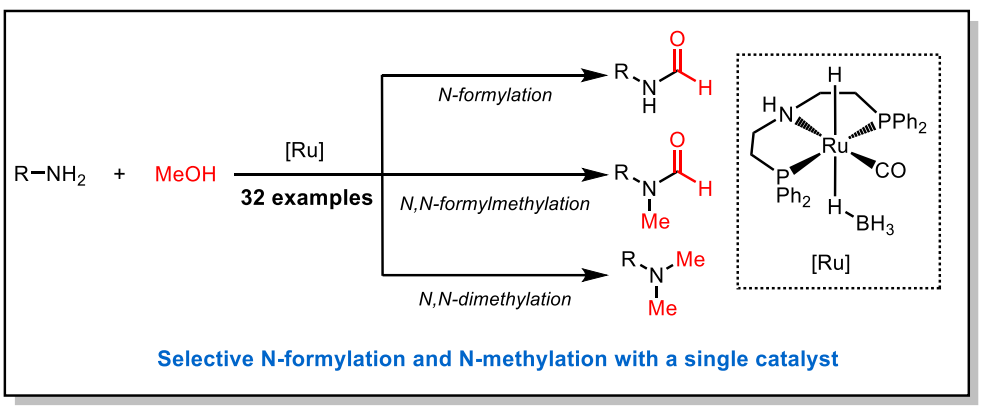

* The majority of this work has been published: Geunho Choi and Soon Hyeok Hong*, *ACS Sustainable Chem. Eng.*.**2019**, *7*, 716-723.

3.1. Introduction

Methanol is a widely used chemical that is increasingly in demand because it can be efficiently produced, widely applicable, and biodegradable, which reduces its environmental impact.[1] A recent survey highlighted that its demand will reach about 100 million metric tons per year by 2020, and continue to increase.[2] The current primary feedstock for methanol production is syngas, which is obtained from fossil fuels such as natural gas and coal. Extensive research to produce methanol from more sustainable sources such as carbon dioxide or biomass is ongoing.

Methanol is generally used as a common solvent in organic chemistry. Recently, it has been actively investigated as a C1 reagent for organic transformations such as C-methylation, C-methoxylation, and C–N bond formation.[1] Achieving this goal would enable the replacement of conventional C1 reagents in organic synthesis,[3] such as methyl halides, carbon monoxide, phosgene, methyl formate, and formaldehyde with economical, abundant, non-toxic, and prospectively sustainably producible methanol.[1]

Acceptorless dehydrogenation of alcohol is known to be an environmentally benign and atom-economical method for the synthesis of various value-added products from alcohols. This method converts alcohols to electrophilic aldehydes or ketones through catalytic dehydrogenation without an external oxidant, producing H_2 as the only by-product.[4] N–C1 functional groups, such as N-formyl and N-methyl, are commonly found in a variety of biomolecules, pharmaceuticals, and enzymes.[5] However, acceptorless dehydrogenative N-formylation and N-methylation reactions using methanol have not been reported as frequently as those for higher alcohols[6] because of the higher enthalpy of dehydrogenation of methanol

(ΔH^o = +92.4 kJ mol^{-1}) compared with those of other alcohols such as ethanol (ΔH^o = +68.6 kJ mol^{-1}).[7]

a) N-Formylation of amines using methanol

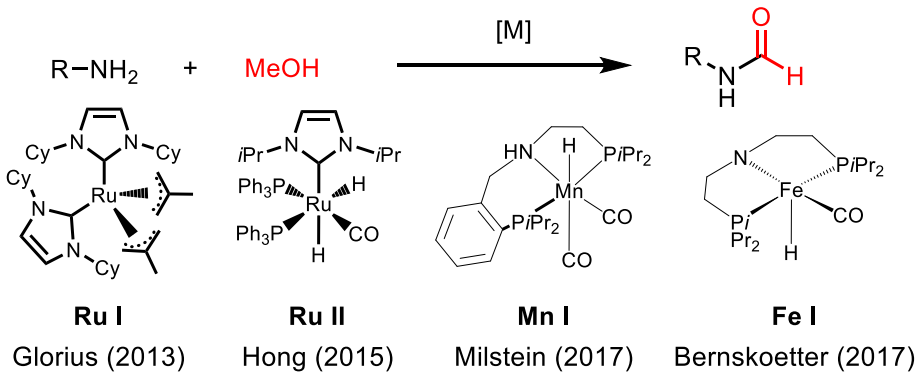

b) N-Methylation of aliphatic amines using methanol

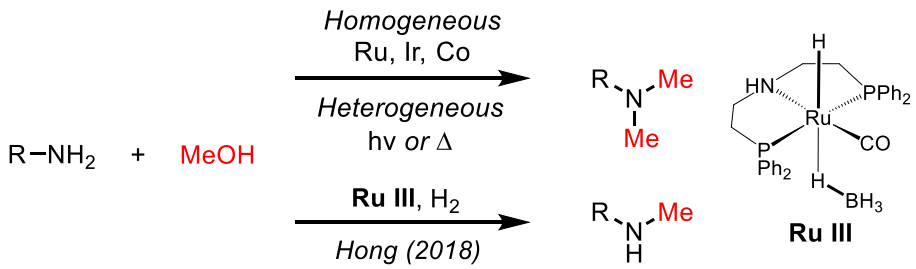

c) This work: Tunable N-formylation & methylation using a single catalyst

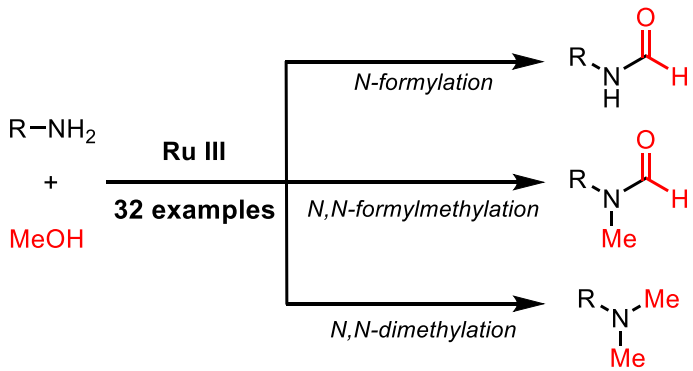

Scheme 3.1 N-Formylation and N-methylation of aliphatic amines using methanol

For the N-formylation of aliphatic or aromatic amines with methanol, Au- or Cu-nanoparticle-mediated heterogeneous catalytic systems have been reported using oxygen as an oxidant.[5, 8] The Glorius group reported the first homogeneously catalyzed dehydrogenative N-formylation of aliphatic amines with methanol using **Ru I** (2 mol %) with KO^{t}Bu (5 mol %) as the base and styrene (3 equiv) as the hydrogen acceptor (Scheme 3.1a).[9] Hong and Kang developed an N-formylation reaction using Ru dihydride complex **Ru II** (10 mol %) without any external reagents such as a base or hydrogen acceptor.[10] The Milstein and the Bernskoetter groups also respectively reported homogeneous **Mn I**[5] (2 mol %) and **Fe I**[11](0.1 mol %) catalysts for the same transformation.

N-Methylation of aromatic amines with using Ru, Ir, Mn, Fe, or inorganic catalysts such as the triazotriphosphorine compound is well-developed.[12] In the case of aliphatic amines, N,N-dimethylation has been primarily reported. The Seayad group[13] used a catalytic amount of [RuCp*Cl_2]$_2$/dpePhos (0.5 mol %) with LiO^{t}Bu (5 mol %), while the Kundu group[14] used [Ru(phenpy-OMe)-(MeCN)$_2$Cl]Cl (1 mol %) with NaOMe (1 equiv) to achieve N,N-dimethylation of aliphatic amines and N-monomethylation of aromatic amines. Similarly, Li and co-workers reported that [Cp*Ir(BiBzImH_2)Cl]Cl (BiBzIm = 2,2'-bibenzimidazole, 1 mol %) catalyzed methylation of amines with Cs_2CO_3 (0.3 equiv) through a thermal route (Scheme 3.1b).[15] Recently, the Liu group reported N,N-dimethylation of primary amines and N-monomethylation of secondary amines using an earth-abundant Co catalyst (5 mol %) in combination with tetradentate phosphine and an equivalent of K_3PO_4.[16] The Saito and the Shi groups used Ag and Pd heterogeneous catalysts, respectively, for N,N-dimethylation of amines with methanol under UV irradiation.[17] To achieve

the challenging N-monomethylation of aliphatic amines using methanol, Hong and Choi recently reported Ru-catalyzed selective N-monomethylation adding external hydrogen gas to kinetically control the reaction.[7]

It has been well-reported that N-alkylation and N-amidation reactions of amines by dehydrogenative activation of alcohols proceed through a common hemiaminal intermediate, which is generated from the reaction of an amine with an aldehyde (Scheme 3.2).[18] Dehydrogenative oxidation of the hemiaminal produces the amide product, while dehydration of the same intermediate to an imine followed by hydrogenation generates the alkylated amine. Typically, different catalytic systems are required to control the selectivity by promoting each reaction pathway.

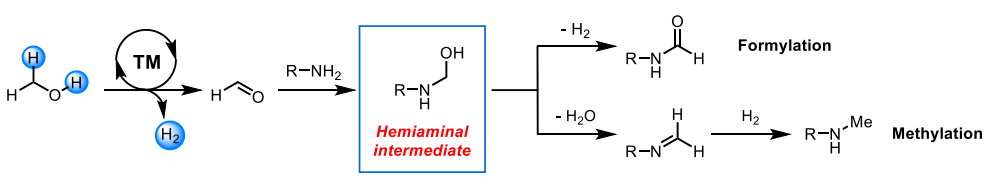

Scheme 3.2 N-Formylation and N-methylation pathway including the hemiaminal intermediate

Herein, we report a tunable catalytic system for selective formylation and methylation reactions using methanol as the C1 source based on a single dehydrogenative Ru precatalyst, Ru-MACHO-BH (**Ru III**) (Scheme 3.1c). Recently, the Huynh[18b] and the Mashima[18a] groups respectively reported the selectivity controlled amidation, imidation, and alkylation reactions of amines using higher alcohols; these reactions can be tuned by controlling the reaction conditions including Ru catalyst, bases, solvents, and ligands. However, to the best of our knowledge, selective formylation and methylation reactions using methanol have not been achieved yet. Notably, the N,N-formylmethylation reaction, which has not been reported using previous catalytic systems, was achieved.

3.2. Results and discussion

3.2.1. Proposed strategy to control the selectivity

To realize selective C1 functionalization of amines, the reaction of benzylamine (**1a**) with methanol (2.0 mL) and **Ru III** (2.0 mol %) was initially monitored at 150 °C (Figure 3.1): Both formylated and methylated products were observed. As the reaction proceeded, the concentrations of *N*-benzylformamide (**1b**) and *N*-benzylmethylamine (**1c**) increased. Subsequently, the concentrations of *N,N*-benzylmethylformamide (**1d**) and *N,N*-dimethylbenzylamine (**1e**) increased with a corresponding decrease in the concentrations of **1b** and **1c**. Finally, the concentration of **1d** decreased as **1e** was generated as the final product.

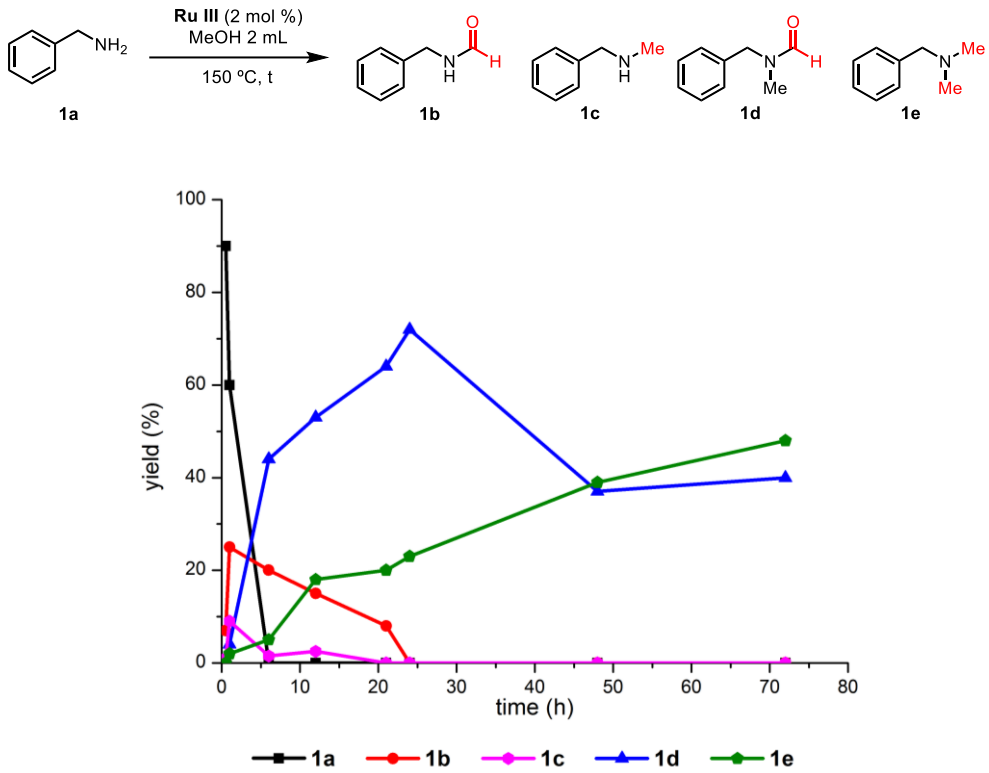

Figure 3.1 Reaction profile using **1a** and the **Ru III** catalyst

Based on the reaction profile and results of previous studies, possible reaction pathways are proposed (Scheme 3.3). Methanol is initially oxidized to formaldehyde by the Ru catalyst, followed by attack of the amine to form hemiaminal **A**; **A** can then be further transformed to formamide **b** or imine **B** by dehydrogenation or dehydration, respectively. During the early stage of the reaction, **A** is dehydrogenated to the more stable formamide **b**. However, as H_2 gas is generated during dehydrogenation of methanol, **b** can be reversibly reduced back to **A**. Dehydration of **A** to **B** and hydrogenation of **B** produce N-methylated amine **c**. Further formylation or methylation of the secondary methylamine **c** will follow similar pathways as those of primary amines to generate **d** or **e** depending on the pressure of the generated hydrogen. The kinetic control of the reaction progress that is achieved by tuning the reaction conditions is key to achieving high selectivity to generate the desired products. Accordingly, various catalytic reaction conditions were screened to identify the optimal conditions for N-formylation, N,N-formylmethylation, and N,N-dimethylation using **Ru III**.

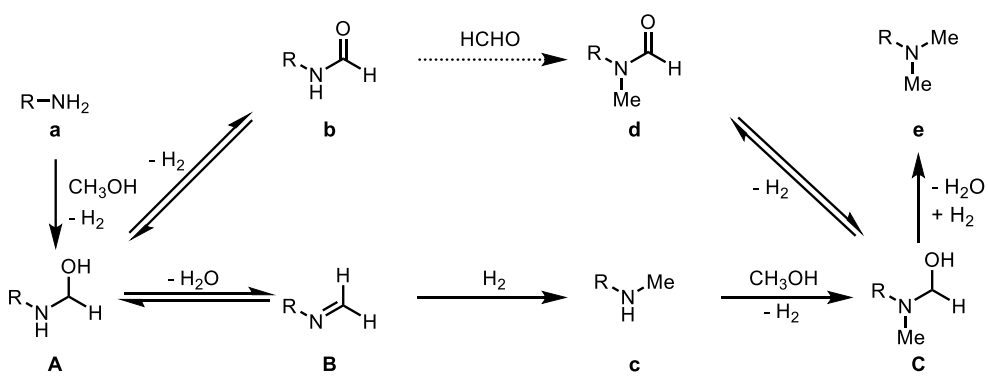

Scheme 3.3 Possible reaction pathways

3.2.2. Reaction condition optimization

Selective Formylation of Amines. The reaction of benzylamine (**1a**, 0.5 mmol) with **Ru III** (3 mol %) in methanol (1.0 mL) at 130 °C produced formamide **1b** (33%) after 12 h (Table 3.1, entry 1). The reaction temperature significantly impacted the yields of **1b**: A higher temperature (150 °C) resulted in 82% **1b** (entries 2 and 3). In contrast, decreasing the catalyst loading to 2 mol % reduced the yield of **1b** to 64% (entry 4). Increasing the methanol amount to 2 mL improved the yield of **1b** to 87% (entries 5 and 6); however, further increasing the amount of methanol (3 mL) slightly decreased the yield of **1b** (82%, entry 7).

Table 3.1 Optimization of N-formylation[a]

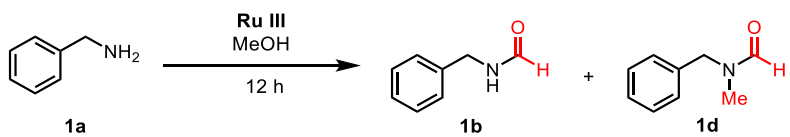

Entry	T (°C)	**Ru III** (mo l %)	MeOH (mL)	**1b** (%)	**1d** (%)
1	130	3	1	33	-
2	140	3	1	48	-
3	150	3	1	82	13
4	150	2	1	64	6
5	150	2	1.5	83	7
6	150	2	2	87	8
7	150	2	3	82	-

[a]Reaction conditions: **1a** (0.5 mmol), **Ru III**, and methanol in a closed screw cap round-bottom flask; yields were determined by ^{1}H NMR using *p*-xylene as an internal standard.

Selective Formylmethylation of Amines. To identify the optimal conditions for N,N-formylmethylation, reactions of **1a** (1 mmol), **Ru III**, and methanol were again investigated (Table 3.2). Under similar conditions as those used for N-formylation, the targeted N,N-formylmethylation product **1d** was obtained in a 9% yield after an extended reaction time in a screw-cap round-bottom flask; the major product was **1b** (68%, Table 3.2, entry 1). To our delight, running the reaction in an autoclave resulted in a dramatically higher yield of **1d** (43%, entry 2); this is likely because a stainless steel autoclave can be heated much more efficiently than a glass round-bottom flask. Increasing the catalyst loading to 5 mol % increased the yield of the product to 56% (entry 3). In contrast, a higher reaction temperature to 150 °C resulted in a slightly lower yield of **1d (**48%, entry 4). Further decreasing the amount of methanol (1.5 mL) resulted in a 79% yield of **1d** (entries 4-7). The yield of dimethylated amine **1e** increased when the reaction time was extended to 48 h (entry 8).

Table 3.2 Optimization of N,N-formylmethylation[a]

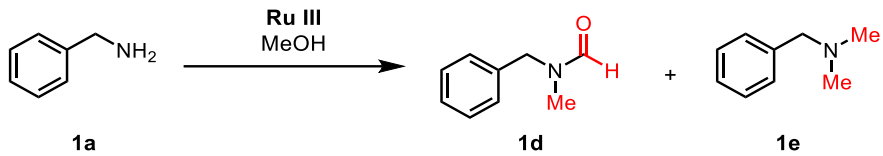

1a **1d** **1e**

Entry	time (h)	T (°C)	**Ru III** (mol %)	MeOH (mL)	**1d** (%)	**1e** (%)
1[b]	24	140	2	2	9	-
2	24	140	2	2	43	22
3	24	140	5	2	56	30
4	24	150	5	2	48	45
5	24	150	5	1.9	49	45
6	24	150	5	1.7	56	34
7	24	150	5	1.5	79	10
8	48	150	5	1.5	57	43

[a]Reaction conditions: **1a** (1.0 mmol), **Ru III**, and methanol in an autoclave; yields were determined by ^{1}H NMR using *p*-xylene as an internal standard. [b]Screw cap round-bottom flask. 68% **1b** was observed.

Selective Dimethylation of Amines. Next, we investigated the optimal conditions for N,N-dimethylation. A reaction of **1a** (1 mmol) and **Ru III** (5 mol %**)** in methanol (2 mL) at 160 °C for 48 h provided *N,N*-dimethylbenzylamine (**1e**) in a 41% yield (Table 3.3, entry 1). When the experiment was carried out with the addition of NaOMe (15 mol %), the yield of **1e** significantly increased to 70% (entry 2). However, the addition of other bases (Table 3.5) did not improve the yield of **1e**. The yield of **1e** was observed to decrease when the amount of the base was more or less than 15 mol % (entries 2-4, Table 3.3). Decreasing the temperature to 150 °C lowered the yield of **1e** to 61%, but a further increase to 170 °C did not affect the yield (entries 5 and 6). To our delight, increasing of the reaction scale to 2 mmol of **1a** only slightly decreased the yield of **1e** (68%, entry 7). Further, good yields were still obtained under reduced catalyst loading (1 mol %) and reaction times (entries 8-10).

Table 3.3 Optimization of N,N-dimethylation[a]

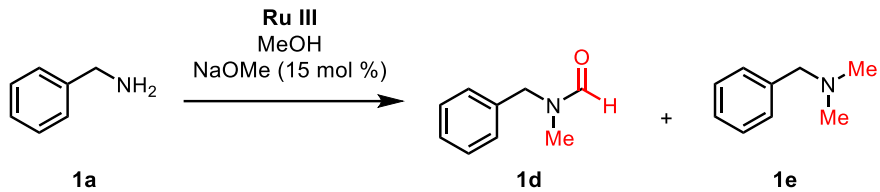

Entry	Scale (mmol)	T (°C)	**Ru III** (mol %)	MeOH (mL)	**1d** (%)	**1e** (%)
1[b]	1	160	5	2	44	41
2	1	160	5	2	26	70
3[c]	1	160	5	2	40	41
4[d]	1	160	5	2	41	59
5	1	150	5	2	26	61
6	1	170	5	2	27	70
7	2	160	5	4	15	68
8	2	160	2.5	4	12	72
9[e]	2	160	1	4	9	71
10[e]	2	160	0.2	4	12	58

[a]Reaction conditions: **1a** (1.0 mmol), **Ru III**, methanol, and NaOMe (15 mol %) in an autoclave for 48 h; yields were determined by ^{1}H NMR using *p*-xylene as an internal standard. [b]Without NaOMe. [c]NaOMe 10 mol %. [d]NaOMe 30 mol %. [e]24 h.

3.2.3. Substrate scope of amines

Scope of the Reactions. Using the optimized conditions for each reaction, the scopes of the reactions were examined (Table 3.4). Benzylamine (**1a**) gave good yields of formyl (**1b**), formylmethyl (**1d**), and dimethyl (**1e**) products under each reaction condition. Electron-donating groups (**2a**) or halide substituents at the *para* positions (**3a**-**4a**) of the benzylamines selectively afforded the C1-functionalized products in good to excellent yields, although *N*-(4-chlorobenzyl)-*N*-methylformamide (**4d**) was not observed under the N,N-formylmethylating conditions.[19] *Ortho*-substituted 1-phenylmethanamine (**5a**) was also smoothly converted to three products in excellent yields. In addition to benzylamines, more challenging aliphatic amines, such as phenethylamine (**6a**), cyclohexylamine (**7a**), and 1-octylamine (**8a**), were functionalized selectively in moderate to good yields. To our delight, heterocycles, such as 3-picolylamine (**9a**) and 2-thiophenmethylamine (**10a**), also afforded selectively C1-functionalized products. The N-formylation reactions were not effective for sterically bulky adamantylamine (**11a**) and secondary amines (**12a**-**13a**); however, N-methylations proceeded smoothly in excellent to quantitative yields.

Table 3.4 C1 functionalizations of amines using methanol[a]

N-formylation[b]

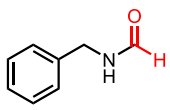
1b, 76%

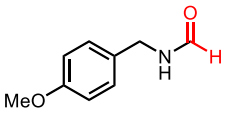

2b, 83%

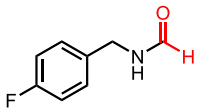

3b, 74%

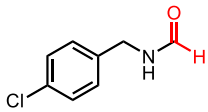

4b, 63%

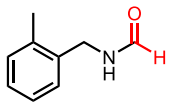
5b, 83%

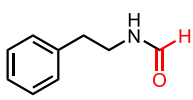
6b, 67%

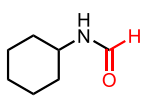
7b, 90%

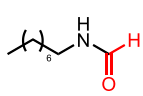
8b, 84%

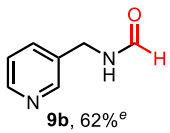
9b, 62%[e]

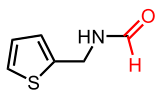
10b, 73%

N,N-formylmethylation[c]

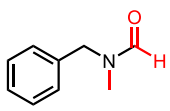
1d, 63%

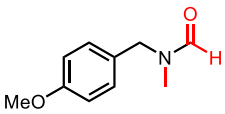

2d, 62%

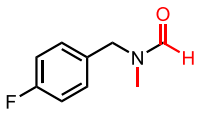

3d, 61%

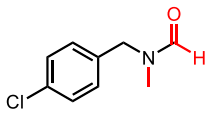

4d, trace

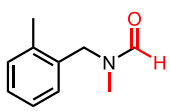
5d, 77%

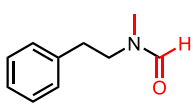
6d, 71%

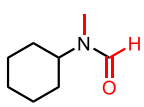
7d, 34%

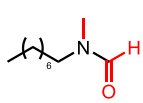
8d, 66%

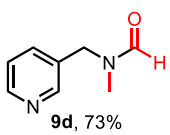
9d, 73%

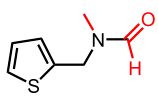
10d, 81%

N,N-dimethylation[d]

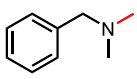

1e, 65%

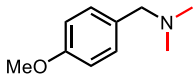

2e, 73%

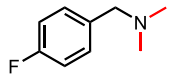

3e, 62%

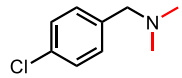

4e, 51%

5e, 71%

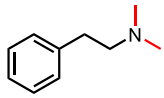

6e, 89%

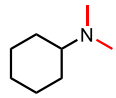

7e, 76%

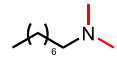

8e, 68%

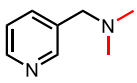

9e, 37%

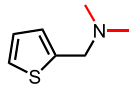

10e, 46%

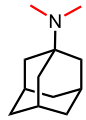

11e, 97%

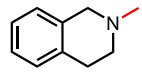

12e, 79%

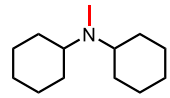

13e, >99%

[a]Yields of isolated products are given. [b]N-Formylation conditions: amine (0.5 mmol), methanol (2 mL), and **1** (2 mol %) at 150 °C in an oil bath for 12 h in a closed screw cap round-bottom flask. [c]N,N-Formylmethylation conditions: amine (1.0 mmol), methanol (1.5 mL), and **1** (5 mol %) at 150 °C in an oil bath for 24 h in a closed autoclave. [d]N,N-Dimethylation conditions: amine (2.0 mmol), methanol (4 mL), **1** (1 mol %), and NaOMe (15 mol %) at 160 °C in an oil bath for 24 h in a closed autoclave. [e]160 °C.

3.2.4. Mechanistic studies

Further investigations were performed to elucidate the mechanisms of the developed formylation and methylation reactions of amines with methanol. Mechanistic investigations were mainly performed to answer the following questions: (1) How can both formylation and methylation reactions be performed by a single catalytic system; (2) what factors influence the selectivity for formylation and methylation; and (3) what factors influence the selective reduction of formamide to N-methylamine?

Reversible Reduction of Formamide to the Hemiaminal Intermediate. Initially, we investigated how both formylation and methylation reactions proceed under the same catalytic conditions (Scheme 3.3). Although **Ru III** has often been reported as a catalyst for amide synthesis via dehydrogenation of hemiaminals, it is possible to perform the methylation reaction through dehydration of heminaminal **A** (Scheme 3.3). For the methylation reaction, the reaction between **A** and formylated product **b** should be reversible as formylation usually occurs faster than methylation. Therefore, under the optimized formylmethylating conditions, **b** should transform to **d** or **e** if the N-formyl group can be reversibly transformed to hemiaminal intermediate **A** and dehydration occurs. As expected, **1b** converted to **1d** under the optimized formylmethylating conditions (Scheme 3.4a). Possible intermediate **1c** was also converted to **1d** and **1e** under the optimal dimethylating conditions (Scheme 3.4b).

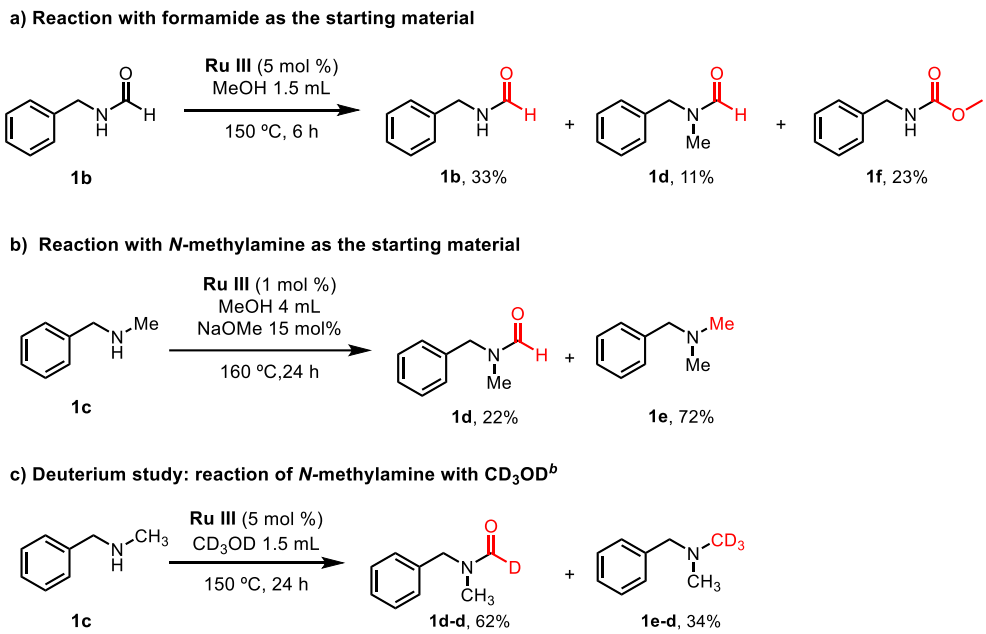

Yields were determined by ^{1}H NMR using *p*-xylene as an internal standard. [b]The products were confirmed by GC-MS.

Scheme 3.4 Control experiments to confirm the reversibility of the products

Next, to identify whether **d** was generated by reversible hydrogenation (Scheme 3.3, solid line from **b** to **A**) or direct methylation (Scheme 3.3, dotted line from **b** to **d**), a control experiment using δ-valerolactam (**14b**) was conducted (Scheme 3.5a). If methylation from **14b** occurred through hydrogenation to **14A** and dehydration to **14B**, intermediate **14c** will generate **14d** or **14e** as the products. In contrast, the route involving direct methylation will generate a different product: **14d'**. Reaction of **14b** under the optimal formylmethylating conditions generated **14d** without any observation of **14d'**; this indirectly suggests reversible dehydration from intermediate **A** is more feasible than direct methylation to generate formylmethylamine **d**. To elucidate this further, another experiment with a linear amide, *N*-benzylacetamide (**15b'**), was conducted (Scheme 3.5b). The control experiment with **15b'** under the same conditions revealed **1b** and **1d** as the products, which could have been generated by reduction of **15b'** to **1a**. The direct methylation product of **15b'**, *N,N*-benzylmethylacetamide (**15d'**), was not observed. It could be possible to generate **1d** from **15b'** by direct methylation (**15d'**), reduction (**1c**), and formylation. However, when used as a starting material, **15d'** did not exhibit any conversion to the product, which conclusively confirms that direct methylation from the amide is not possible (Scheme 3.5b).

a) Proposed reaction pathway with δ-valerolactam (14b) and result[a]

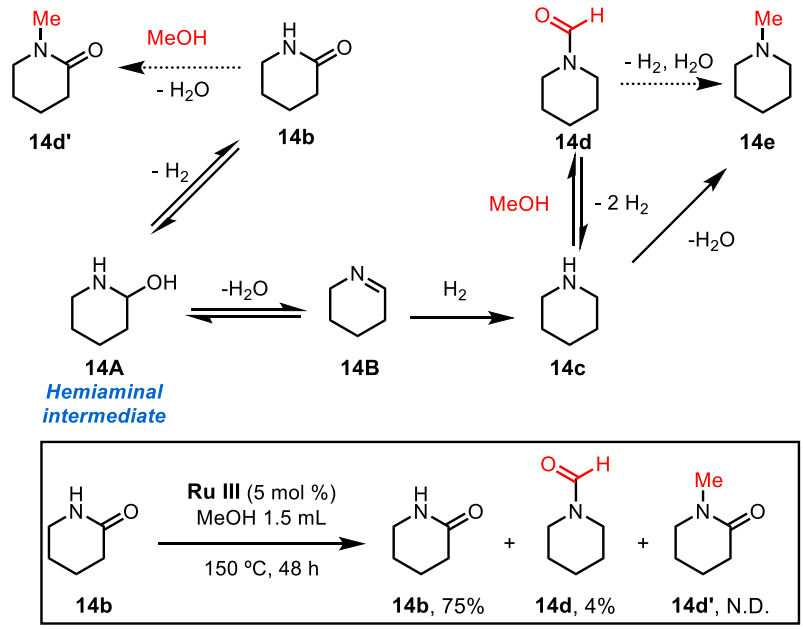

b) Proposed reaction pathway with *N*-benzylacetamide (15b) and result[b]

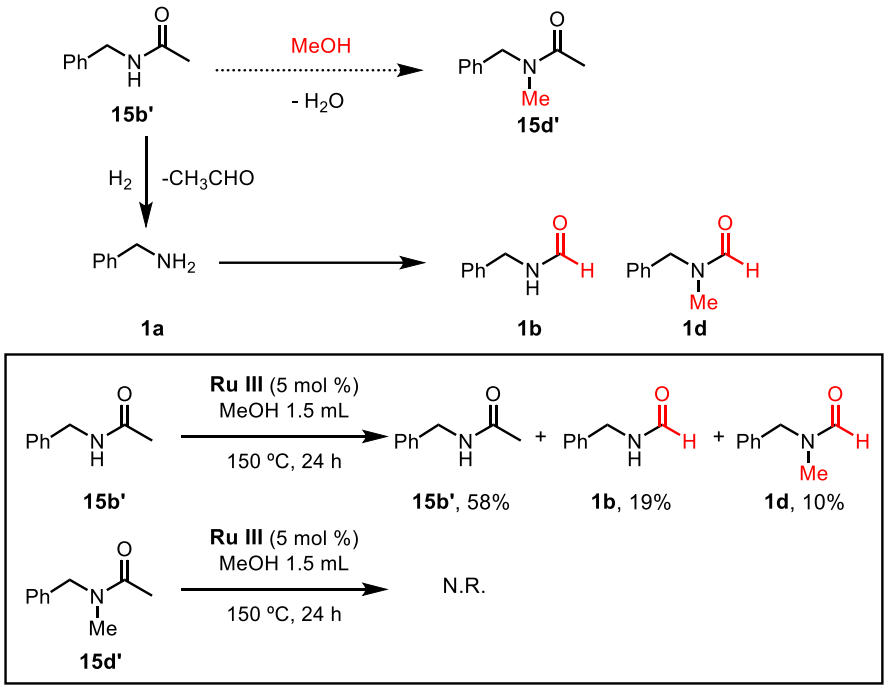

[a]Yields were determined by GC using *p*-xylene as an internal standard. [b]Yields were determined by ^{1}H NMR using *p*-xylene as an internal standard.

Scheme 3.5 Reaction of secondary amides

The possibility of dehydrogenation of the N-methyl group between **B** and **c** was assessed through a deuterium-labelling study with *N*-benzylmethylamine (**1c**) and methanol-d_4 (Scheme 3.4c). Exposure of **1c** to the formylmethylating conditions with methanol-d_4 did not result in any product with deuterated methyl groups. In this reaction, only the newly formed formyl and methyl groups were deuterated, which implies that reversible dehydrogenation of the methyl group does not occur.

Selectivity Between Formylation and Methylation. Next, we questioned what factors critically affect the selectivity between formylation and methylation. As previously reported, H_2 pressure can be used to control the equilibrium of the reaction pathways.[7] It was observed that dehydrogenation of methanol caused the H_2 pressure to gradually increase during the reaction (Figure 3.2), which affected the reaction selectivity for primary amine **1a** (Scheme 3.6a). At a higher H_2 pressure (4 MPa), dehydrogenation of **A** to **1b** was suppressed, and the dehydration product **1c** was the major product, which is consistent with the previous report.[7] Similarly, when **1b** was reacted at a higher pressure of H_2 (4 MPa), its reduction was accelerated and the formation of dehydrogenated product **1d** was suppressed (Scheme 3.6b). *N*-Methylformamide **1d** showed less conversion (42%, Scheme 3.6c) than formamide **1b** (72%) under the same reducing conditions, which suggests that reduction of more electron-rich **1d** is less facile than that of **1b**. The reactivity difference could result in the selective production of **1d** under reducing conditions in the presence of H_2, which can hydrogenate **1b**. The reaction temperature is also a critical factor that controls the reaction progress. A control experiment at lower temperature (140 °C) under dimethylation conditions using NaOMe resulted in a reduced yield (53%) of **1e** and the production of **1b** (9%), which was not observed at 160 °C (Scheme 3.6d).

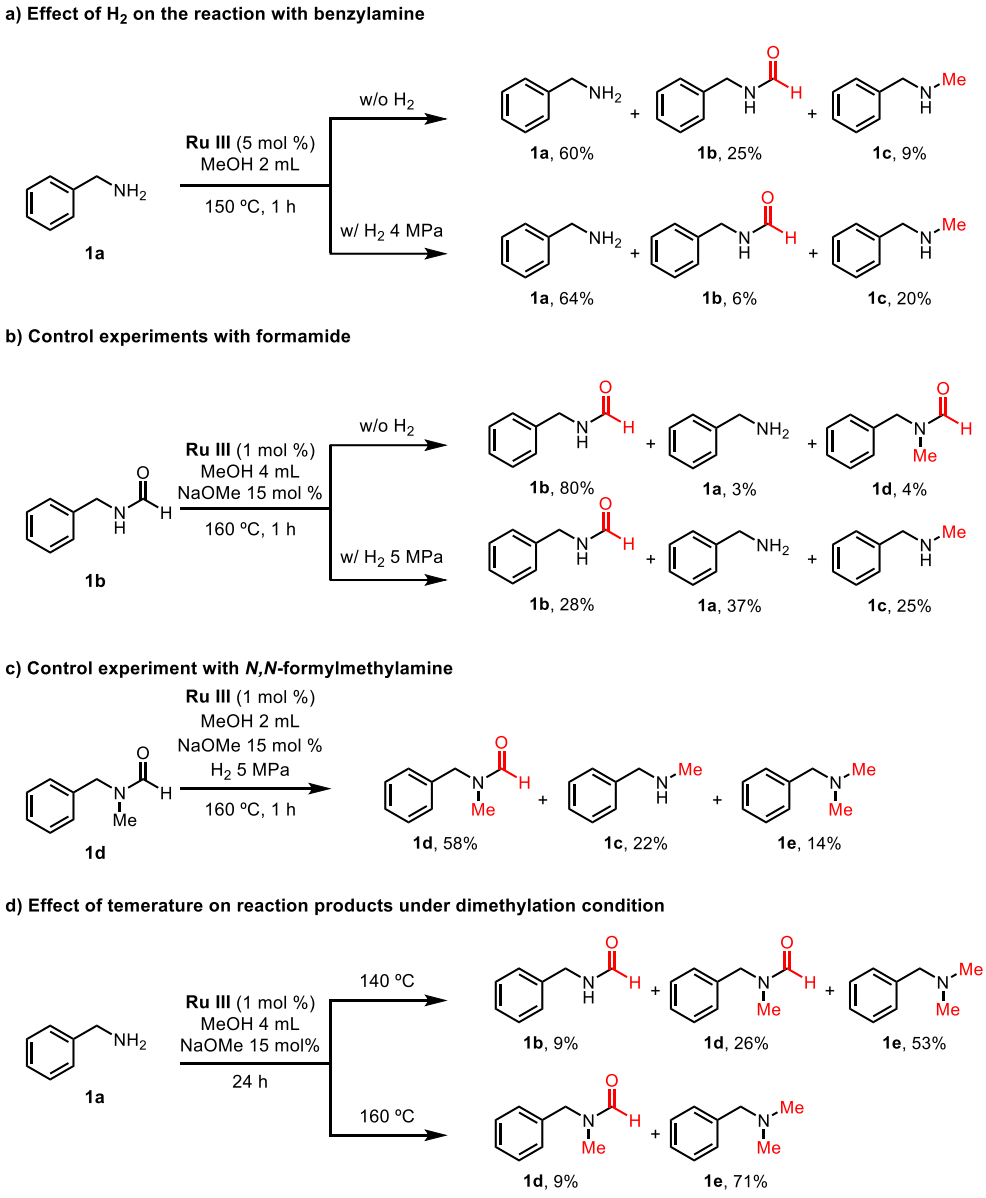

Scheme 3.6 Effect of hydrogen and temperature

Reduction Selectivity from Formamide. The factors that affect the pathway for formamide reduction were investigated. In previous reports, formamide was generally reduced to the corresponding amine and methanol.[20] In contrast, under the developed catalytic conditions, formamide **b** was reduced to N-methylamine **c** as the major product (Scheme 3.7a). Generation of methanol from the reduction of **b** could be thermodynamically disfavored under the developed conditions because of the presence of significant amounts of methanol. Under the same reaction conditions with THF as the solvent, **1b** was primarily converted to **1a**, as expected, and only trace amounts of methylated **1c** were observed (Scheme 3.7b). These data suggest that the amount of methanol solvent makes hemiaminal **A** more susceptible to dehydration than reduction to primary amines.

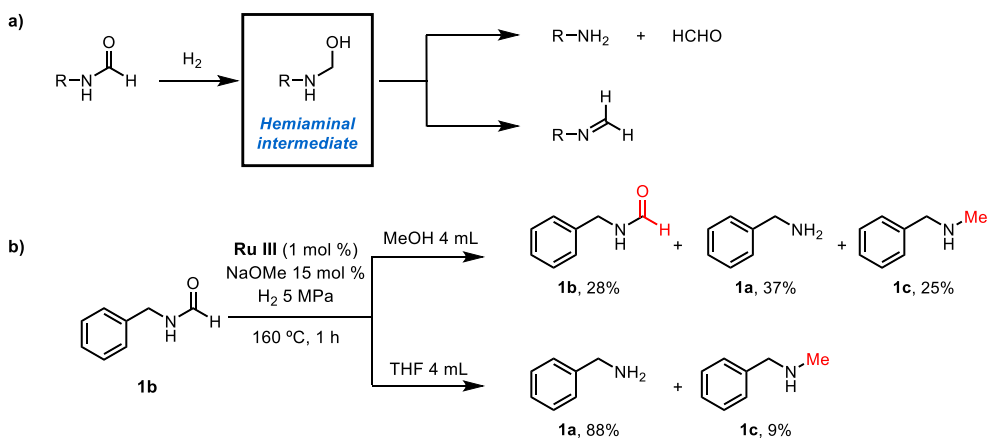

Scheme 3.7 a) Reduction pathway from formamide **b**, b) Reduction of formamide in THF solvent

The proposed reaction pathway is illustrated in Scheme 3.8. Primary amine **a** reacts with formaldehyde, which is generated via dehydrogenation of methanol, forming hemiaminal **A**. In the early stage of the reaction, **A** is primarily oxidized to **b**. However, as the hydrogen pressure increases, it reverts to **A**, which is dehydrated to generate imine **B**, followed by hydrogenation to obtain **c**. Reduction of **A** to primary amine **a** is suppressed because of the presence of a significant amount of methanol. The more nucleophilic secondary amine **c** further reacts to generate formylmethyl amine (**d**) and dimethylamine (**e**). The methyl groups on the amine are not reactive to further dehydrogenation under the developed catalytic conditions, as proven by deuterium-labelling studies.

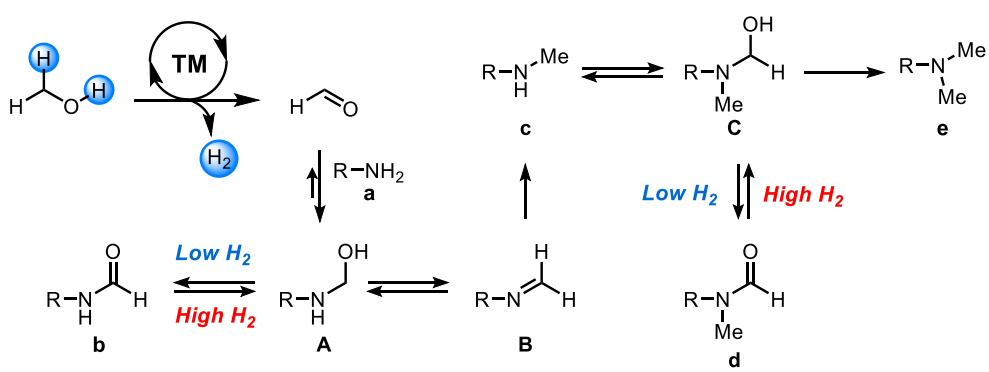

Scheme 3.8 Reaction pathway to various N-functional groups

3.3. Conclusion

We developed a catalytic system based on a Ru-MACHO-BH complex that kinetically controls the selectivity between formylation and methylation of amines. Various formamides, dimethylamines, and N,N-formylmethylamines were effectively and selectively synthesized in moderate to good yields. Mechanistic studies revealed that formylation and methylation were controlled by the reversibility of the reaction of the formyl group. Hydrogen generated from methanol and the reaction temperature controlled the reversibility of the reaction of the formyl group enabling the selectivity among various products to be tuned. In addition, using a solvent amount of methanol facilitated reduction in a productive amine-functionalization pathway.

3.4. Experimental section

3.4.1. General information

All reactions were carried out in an oven-dried screw cap round-bottom flask or stainless-steel autoclave under inert conditions. All reagents were purchased from commercial suppliers and used as received. **Ru III** (98% purity) was purchased from Strem Chemical and used as received. Methanol was purified by vacuum distillation to remove any adventitious water and oxygen. Analytical TLC was performed on Merck 60 F254 silica gel plates (0.25mm thick). Column chromatography was performed using Merck 60 silica gel (230–400 mesh). NMR spectra were recorded in $CDCl_3$ or CD_3OD on a Bruker DPX-300 (300 MHz) spectrometer or Varian 400 and 500 NMR (400 and 500 MHz). The chemical shifts are reported in ppm and the coupling constants are given in Hertz. High-resolution mass spectrometry (HRMS) was performed at the Organic Chemistry Research Center at Sogang University using the ESI method and Korea Basic Science Institute using the EI method.

3.4.2. General reaction procedures

General Procedure for N-Formylation of Amine. A screw cap round-bottom flask was charged with **Ru III** (0.010 mmol, 2.0 mol %), amine (0.5 mmol), and methanol (2 mL) in an argon-filled glove box. The reaction vessel was taken out of the glove box, placed in an oil bath, and heated to 150 °C. After 12 h, the reaction was cooled to room temperature, and H_2 was carefully released in a fume hood. The crude reaction mixture was concentrated using a rotary evaporator. The residue was purified by column chromatography to afford the desired product.

General Procedure for N,N-Formylmethylation of Amine. A stainless-steel autoclave (50 mL) was charged with **Ru III** (0.050 mmol, 5.0 mol %), amine (1.0 mmol), and methanol (1.5 mL) in an argon-filled glove box. The vessel was taken out of the glove box, placed in an oil bath, and heated to 150 °C. After 24 h, the reaction was cooled to room temperature, and H_2 was carefully released in a fume hood. The crude reaction mixture was concentrated using a rotary evaporator. The residue was purified by column chromatography to afford the desired product.

General Procedure for N,N-Dimethylation of Amine. A stainless-steel autoclave (50 mL) was charged with **Ru III** (0.020 mmol, 1.0 mol %), amine (2.0 mmol), and methanol (4.0 mL) in an argon-filled glove box. The vessel was taken out of the glove box, placed in an oil bath, and heated to 160 °C. After 24 h, the reaction was cooled to room temperature, and H_2 was carefully released in a fume hood. The crude reaction mixture was concentrated using a rotary evaporator. Unless otherwise noted, the residue was extracted with dilute HCl. An aqueous solution of NaOH (40%) was added to the water layer, and the aqueous phase was extracted with methylene chloride, then dried with $MgSO_4$. The residue was concentrated using a rotary evaporator to afford the desired product.

3.4.3. Supplementary optimizations and data

Table 3.5 Base screening for N,N-dimethylation[a]

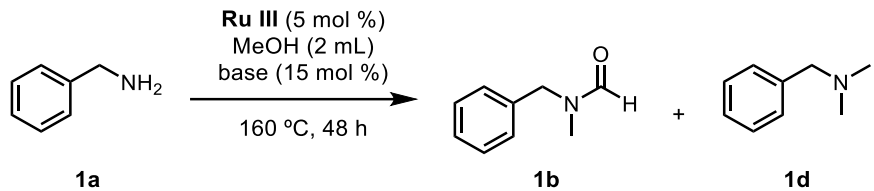

Entry	base	**1b** (%)	**1d** (%)
1	LiO^{t}Bu	12	11
2	LiOH	40	46
3	NaOMe	26	70
4	NaO^{t}Bu	43	56
5	KO^{t}Bu	15	68
6	KOH	24	65
7	K_2CO_3	5	63
8	$KHCO_3$	21	57
9	K_3PO_4	13	64
10	Ce_2CO_3	15	55

[a]Reaction conditions: **1a** (1.0 mmol), **Ru III** (5 mol %), methanol (2 mL), and base (15 mol %) in an autoclave at 160 °C for 48 h; yields were determined by ^{1}H NMR using *p*-xylene as an internal standard.

Pressure change during the reaction

A stainless steel autoclave (50 mL) was charged with complex **Ru III** (0.020 mmol, 1.0 mol %), benzylamine **1a** (2.0 mmol), sodium methoxide (15 mol %), and methanol (4.0 mL) in an argon-filled glove box. The vessel was placed in an oil bath heated to 160 °C. At each time, pressure gauge at autoclave was checked. In the absence of **Ru III**, pressure under 2 bar was observed.

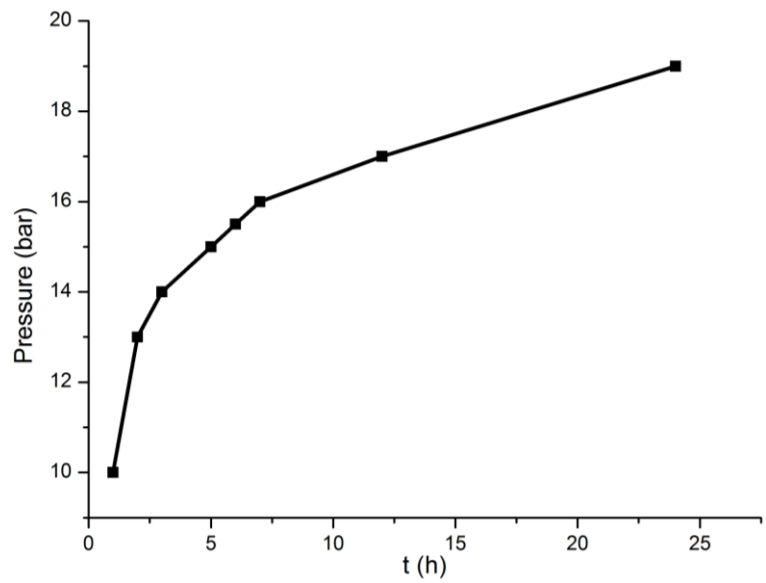

Figure 3.2 Change of internal pressure in a closed reactor

3.4.4. Characterization of newly reported compounds

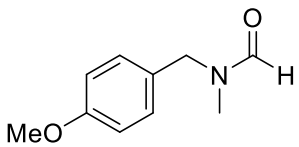

***N*-(4-methoxybenzyl)-*N*-methylformamide (2d)**

Yellow oil. Mixture of rotamers were observed. ^{1}H NMR (300 MHz, $CDCl_3$) Major rotamer: δ 8.24 (s, 1H), 7.13 (dd, *J* = 17.7, 8.5 Hz, 2H), 6.91 – 6.79 (m, 2H), 4.30 (s, 2H), 3.77 (m, 3H), 2.73 (s, 3H). Minor rotamer: δ 8.10 (s, 1H), 7.13 (dd, *J* = 17.7, 8.5 Hz, 2H), 6.91 – 6.79 (m, 2H), 4.43 (s, 2H), 3.77 (m, 3H), 2.80 (s, 3H).; ^{13}C NMR (125 MHz, $CDCl_3$) Major rotamer: δ 162.5, 159.4, 128.7,127.6, 114.2, 55.2, 52.8, 33.8. Minor rotamer: δ 162.4,159.1, 129.5, 128.1, 114.0, 55.2, 47.1, 29.1.; HRMS-ESI (m/z): $[M+Na]^+$ calcd for $C_{10}H_{13}NNaO_2$: 202.0844. Found: 202.0838.

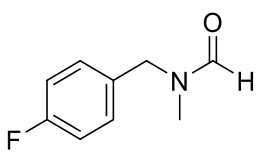

***N*-(4-fluorobenzyl)-*N*-methylformamide (3d)**

Yellow oil. Mixture of rotamers were observed. ^{1}H NMR (400 MHz, $CDCl_3$) Major rotamer: δ 8.26 (s, 1H), 7.24 – 7.16 (m, 2H), 7.09 – 6.94 (m, 2H), 4.34 (s, 2H), 2.74 (s, 3H). Minor rotamer: δ 8.12 (s, 1H), 7.24 – 7.16 (m, 2H), 7.09 – 6.94 (m, 2H), 4.46 (s, 2H), 2.82 (s, 3H).; ^{13}C NMR (100 MHz, $CDCl_3$) Major rotamer: δ 162.4 (*J* = 245.66 Hz), 162.5, 131.7 (J = 37.21 Hz), 129.5 (*J* = 81.57 Hz), 115.7 (*J* = 28.60 Hz), 52.6, 33.9. Minor rotamer: δ 162.2 (J = 245.66 Hz), 162.4, 131.6 (*J* = 37.21 Hz), 129.4 (*J* = 81.57 Hz). 115.5 (*J* = 28.60 Hz), 46.9, 29.2.; ^{19}F NMR (375 MHz, $CDCl_3$)

δ -114.02, -114.78.; HRMS-ESI (m/z): $[M+Na]^+$ calcd for $C_9H_{10}FNNaO$: 190.0644. Found: 190.0639.

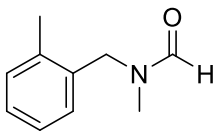

***N*-(2-methybenzyl)-*N*-methylformamide (5d)**

Yellow oil. Mixture of rotamers were observed. ^{1}H NMR (300 MHz, $CDCl_3$) Major rotamer: δ 8.20 (s, 1H), 7.26 – 7.02 (m, 4H), 4.35 (s, 2H), 2.75 (s, 3H), 2.30 (s, 3H). Minor rotamer: δ 8.11 (s, 1H), 7.26 – 7.02 (m, 4H), 4.50 (s, 2H), 2.75 (s, 3H), 2.30 (s, 3H).; ^{13}C NMR (125 MHz, $CDCl_3$) Major rotamer: δ 162.9, 136.1, 133.5, 130.7, 127.9, 127.8, 126.2, 51.1, 33.8, 19.0. Minor rotamer: δ 162.3, 136.6, 133.4, 130.5, 128.6, 127.6, 126.0, 45.5, 29.4, 19.0.; HRMS-ESI (m/z): $[M+Na]^+$ calcd for $C_{10}H_{13}NNaO$: 186.0895. Found: 186.0889.

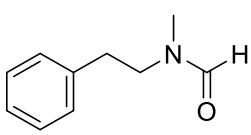

***N*-methyl-*N*-phenethylformamide (6d)**

Yellow oil. Mixture of rotamers were observed. ^{1}H NMR (400 MHz, $CDCl_3$) Major rotamer: δ 7.78 (s, 1H), 7.32 – 7.16 (m, 3H), 7.11 (d, J = 7.2 Hz, 1H), 3.44 (t, J = 7.0 Hz, 2H), 2.92 – 2.76 (m, 5H). Minor rotamer: δ 7.99 (s, 1H), 7.32 – 7.16 (m, 3H), 7.11 (d, J = 7.2 Hz, 1H), 3.54 (t, J = 7.5 Hz, 2H), 2.92 – 2.76 (m, 5H).; ^{13}C NMR (100 MHz, $CDCl_3$) Major rotamer: δ 162.6, 137.7, 128.7, 128.6, 126.8, 51.2, 34.8,

33.2. Minor rotamer: δ 162.4, 138.5, 128.7, 128.5, 126.4, 45.9, 35.0, 29.7.; HRMS-EI (m/z): calcd for $C_{10}H_{13}NO$: 163.0997. Found: 163.0999.

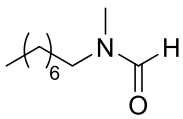

***N*-methyl-*N*-octylformamide (8d)**

Yellow oil. Mixture of rotamers were observed. 1H NMR (300 MHz, CDCl3) Major rotamer: δ 8.07 (s, 1H), 3.23 (t, *J* = 7.0 Hz, 2H), 2.87 (s, 3H), 1.59 – 1.52 (m, 2H), 1.29 (m, 10H), 0.92 – 0.88 (m, 3H). Minor rotamer: δ 8.07 (s, 1H), 3.34 (t, *J* = 7.6 Hz, 2H), 2.94 (s, 3H), 1.59 – 1.52 (m, 2H), 1.29 (m, 10H), 0.92 – 0.88 (m, 3H).; 13C NMR (75 MHz, $CDCl_3$) δ 162.4, 162.3, 49.4, 44.0, 34.3, 31.6, 29.2, 29.1, 29.0, 27.8, 26.6, 26.5, 26.2, 22.5, 13.9.; HRMS-ESI (m/z): $[M+Na]^+$ calcd for $C_{10}H_{21}NNaO$: 194.1521. Found: 194.1515.

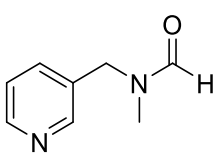

***N*-((pyridine-2-yl)methyl)-*N*-methylformamide (9d)**

Yellow oil. Mixture of rotamers were observed. ^1H NMR (300 MHz, $CDCl_3$) Major rotamer: δ 8.64 – 8.49 (m, 2H), 8.18 (s, 1H), 7.64 (d, *J* = 7.9 Hz, 1H), 7.38 – 7.27 (m, 1H), 4.54 (s, 2H), 2.89 (s, 3H). Minor rotamer: δ 8.64 – 8.49 (m, 2H), 8.32 (s, 1H), 7.55 (d, *J* = 7.9 Hz, 1H), 7.38 – 7.27 (m, 1H), 4.44 (s, 2H), 2.80 (s, 3H).; ^{13}C NMR (75 MHz, $CDCl_3$) Major rotamer: δ 162.5, 148.9,134.9, 131.6, 123.6, 45.0, 33.8. Minor rotamer: δ 162.5, 149.3, 135.7, 131.3, 123.5, 50.6, 29.1.; HRMS-ESI (m/z): $[M+H]^+$ calcd for $C_8H_{11}N_2O$: 151.0871. Found: 151.0886.

3.5. References

(1) Natte, K.; Neumann, H.; Beller, M.; Jagadeesh, R. V., *Angew. Chem. Int. Ed.* **2017,** *56* (23), 6384-6394.

(2) Alvarado, M. The changing face of the global methanol industry. Insights of IHS Chemical Bulletin; IHS Markit: London, 2016; http://www.methanol.org/wp-content/uploads/2016/07/IHS-ChemicalBulletin-Issue3-Alvarado-Jun16.pdf

(3) Keim, W., *Pure and Applied Chemistry* **1986,** *58* (6), 825-832.

(4) Gunanathan, C.; Milstein, D., *Science* **2013,** *341* (6143), 1229712.

(5) Chakraborty, S.; Gellrich, U.; Diskin-Posner, Y.; Leitus, G.; Avram, L.; Milstein, D., *Angew. Chem. Int. Ed.* **2017,** *56* (15), 4229-4233.

(6) Kawahara, R.; Fujita, K.-i.; Yamaguchi, R., *J. Am. Chem. Soc.* **2010,** *132* (43), 15108-15111.

(7) Choi, G.; Hong, S. H., *Angew. Chem. Int. Ed.* **2018,** *57* (21), 6166-6170.

(8) Tumma, H.; Nagaraju, N.; Reddy, K. V., *J. Mol. Catal. A: Chem.* **2009,** *310* (1), 121-129.

(9) Ortega, N.; Richter, C.; Glorius, F., *Org. Lett.* **2013,** *15* (7), 1776-1779.

(10) Kang, B.; Hong, S. H., *Adv. Synth. Catal.* **2015,** *357* (4), 834-840.

(11) Lane, E. M.; Uttley, K. B.; Hazari, N.; Bernskoetter, W., *Organometallics* **2017,** *36* (10), 2020-2025.

(12) (a) Elangovan, S.; Neumann, J.; Sortais, J.-B.; Junge, K.; Darcel, C.; Beller, M., *Nat. Commun.* **2016,** *7*, 12641; (b) Du, Y.; Oishi, S.; Saito, S., *Chem. Eur. J.* **2011,** *17* (44), 12262-12267.

(13) Dang, T. T.; Ramalingam, B.; Seayad, A. M., *ACS Catal.* **2015,** *5* (7), 4082-4088.

(14) Paul, B.; Shee, S.; Chakrabarti, K.; Kundu, S., *ChemSusChem* **2017,** *10* (11), 2370-2374.

(15) Liang, R.; Li, S.; Wang, R.; Lu, L.; Li, F., *Org. Lett.* **2017,** *19* (21), 5790-5793.

(16) Liu, Z.; Yang, Z.; Yu, X.; Zhang, H.; Yu, B.; Zhao, Y.; Liu, Z., *Adv. Synth. Catal.* **2017,** *359* (24), 4278-4283.

(17) Tsarev, V. N.; Morioka, Y.; Caner, J.; Wang, Q.; Ushimaru, R.; Kudo, A.; Naka, H.; Saito, S., *Org. Lett.* **2015,** *17* (10), 2530-2533.

(18) (a) Higuchi, T.; Tagawa, R.; Iimuro, A.; Akiyama, S.; Nagae, H.; Mashima, K., *Chem. Eur. J.* **2017,** *23* (52), 12795-12804; (b) Xie, X.; Huynh, H. V., *ACS Catal.* **2015,** *5* (7), 4143-4151.

(19) 4e was observed as the major product in formylmethylating condition.

(20) (a) Rasu, L.; John, J. M.; Stephenson, E.; Endean, R.; Kalapugama, S.; Clément, R.; Bergens, S. H., *J. Am. Chem. Soc.* **2017,** *139* (8), 3065-3071; (b) Zhang, L.; Han, Z.; Zhao, X.; Wang, Z.; Ding, K., *Angew. Chem. Int. Ed.* **2015,** *54* (21), 6186-6189.

Chapter 4. Direct C(sp^3)–H Trifluoromethylation of Unactivated Alkanes

4.1. Introduction

Trifluoromethyl group (CF_3) has a strong electron-withdrawing ability and a large dipole moment, which results in properties such as lipophilicity, permeability, and metabolic stability when it is installed to a molecule. This makes the trifluoromethyl group play an important role in various fields such as agrochemical[1], pharmaceutical[2], and material[3] chemistries. Therefore, the development of efficient synthetic methods to install the trifluoromethyl group is an important goal in organic synthesis.

Since the McLoughlin-Thrower reaction (Scheme 4.1A)[4], an early developed practical trifluoromethylation reaction of aryl iodides, significant progress has been achieved in this field using nucleophilic, electrophilic, and radical trifluoromethylation methods. These methods mainly focused on the construction of arene-CF_3 moieties, such as transition metal-catalyzed cross-coupling reactions.[5] In the case of direct trifluoromethylation of C–H bonds, C(sp^2)–H trifluoromethylation was mainly developed. In spite of the well-developed C(sp^2)–CF_3 trifluoromethylation reactions, the introduction of the aliphatic trifluoromethyl group has been underdeveloped. The implementation of the trifluoromethyl group has also been widely studied in medicinal chemistry, but most examples focused on aryl–CF_3 drug. There are only a few examples with C(sp^3)–CF_3, such as Dexlansoprazole, Efavirenz, and Flumedroxone acetate.

In this chapter, recently developed representative synthetic strategies for $C(sp^3)$–CF_3 bond formation are overviewed. The examples are categorized based on the reaction types: substitution, addition, and $C(sp^3)$–H activation reactions.

4.2. $C(sp^3)$–CF_3 bond formation via diverse synthetic methods

4.2.1. $C(sp^3)$–CF_3 bond formation via substitution of CF_3 source

Since the development of the McLoughlin-Thrower reaction (Scheme 4.1A), $C(sp^2)$–trifluoromethylation reactions of aromatic compounds have been extensively studied; however, $C(sp^3)$–trifluoromethylation of unactivated alkane is less studied. In classical reactions, a $CuCF_3$ complex displays good reactivities for substitution reactions. Development for the methods to form the proper trifluoromethyl copper complex has been focused. In 1979, Kobayashi and co-workers initially examined the trifluoromethylation of alkyl halides (X = Br, I) with $CuCF_3$ generated from CF_3I and Cu powder under mechanical stirring and high reaction temperature in a stainless steel tube (Scheme 4.1B).[6] Yagupolskii and co-workers used $Hg(CF_3)_2$ and excess amount of Cu powder at 140 °C for 2 h to get moderate yield of benzylic trifluoromethylated product from benzyl bromide moieties.[7] To avoid harsh reaction conditions and toxic reagent, the generation of reactive $CuCF_3$ was examined in mild conditions like the combination of R_3SiCF_3/KF/CuI[8] or XCF_2CO_2Me/CuI.[9] Since the development of trifluoromethylation of alkyl halides, substitution of other leaving groups, such as alkyl boronate, carboxylic acid, alkyl azo compounds, were variously discovered. Herein, the recent methods to generate trifluoromethylated alkanes using substitution reaction will be discussed, categorized by the character of starting

materials.

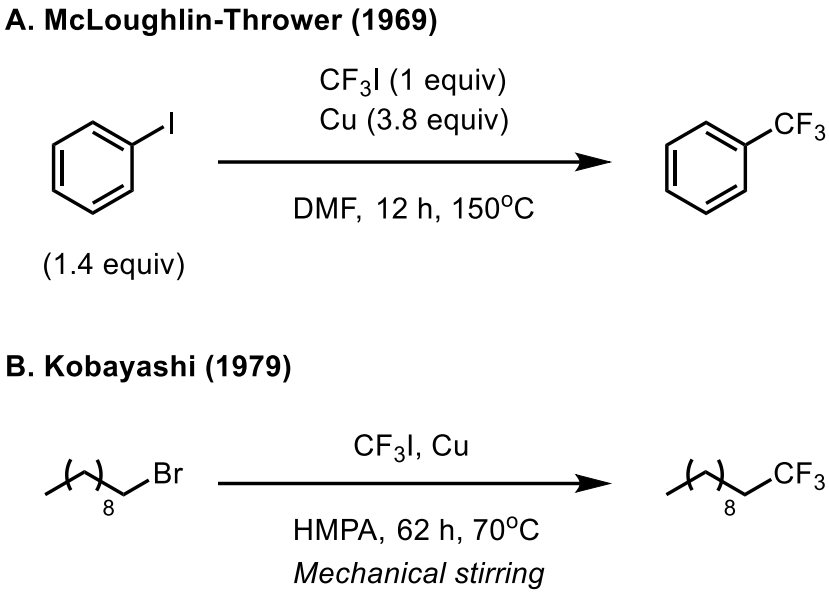

Scheme 4.1. Classical organic trifluoromethylation chemistries using Cu and CF_3I

For a long time, trifluoromethylation has been addressed using alkyl halides and in-situ generated $CuCF_3$ species. Recently, Grushin and co-workers generated $CuCF_3$ using HCF_3 that is a by-product and waste from manufacturing Teflon, of which destruction is costly (Scheme 4.2A).[10] Using low-cost CuCl and *t*BuOK with $Et_3N \cdot 3HF$ as a stabilizer at room temperature and under atmospheric pressure of HCF_3, almost quantitative yield of $CuCF_3$ was synthesized. This reagent was used for nucleophilic trifluoromethylation of α-haloketone in a regioselective pathway.

Although in-situ generated $CuCF_3$ showed good reactivity, instability of the complex limits the versatile utility. Other ligand-binding trifluoromethylated coppers were synthesized as new trifluoromethylation reagents. Szabó and co-workers

utilized tris(triphenylphosphine) and trifluoromethyl copper complex for allylic chloride and bromide trifluoromethylation (Scheme 4.2B).[11] The reaction was highly regio- and stereoselective to terminal trifluoromethylation, even internal allylic alkyl chloride generated a terminal product. Copper center mediated the reaction via a nucleophilic substitution mechanism involving allyl copper intermediates. Recently, Trost and co-workers developed an asymmetric allylic trifluoromethylation catalyzed by CpPd(η^3-C_3H_5) and diamidophosphite ligand.[12] Using allyl fluoride as a precursor for generation of π-allyl complexes enabled the synergistic interplay of the fluoride leaving group to activate trifluoromethylating reagent, $TMSCF_3$. Various allylic fluoride substrates could be transformed in excellent enantioselectivity and functional group tolerance.

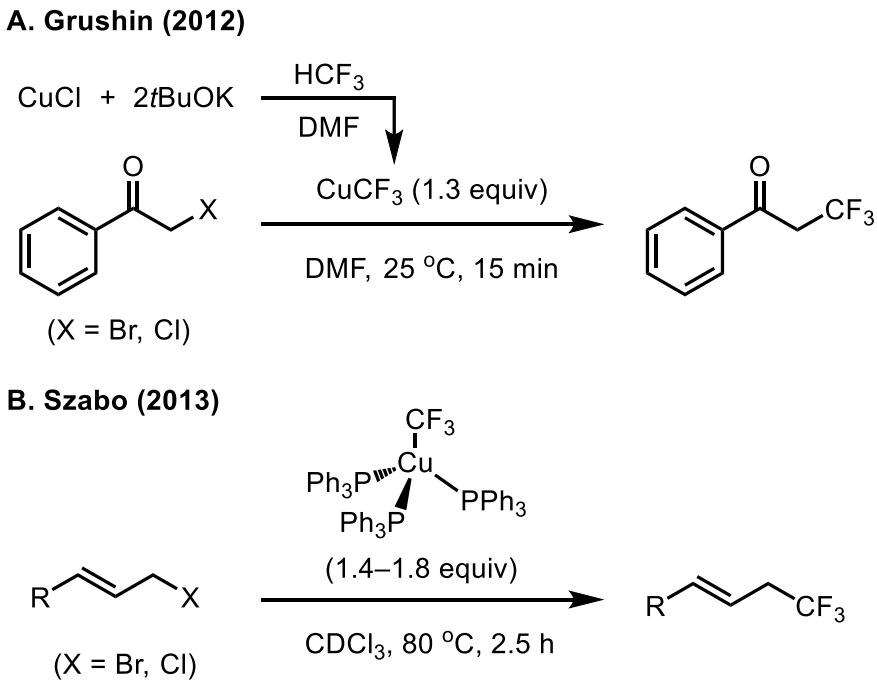

Scheme 4.2. Trifluoromethylation using stoichiometric copper complex

Furthermore, trifluoromethylation of unactivated alkyl halides was also realized using transition metal-mediated radical reaction pathways. The Ma and Gong group illustrated a reductive cross-electrophile coupling protocol of alkyl iodides under copper catalyzed/nickel-promoted conditions using the Togni reagent as electrophilic trifluoromethylating source (Scheme 4.3A).[13] Exact role of nickel additive is not clear, but it may promote the reaction by inhibiting undesired C-B bond formation from Cu(III) complex. Primary alkyl iodide delivered the coupling product in good yields with excellent functional group tolerance, but efficiencies were found to be lower when secondary iodide was used.

Li and co-workers developed unactivated alkyl bromide trifluoromethylation method utilizing air-stable bpyCu(CF_3)$_3$ (bpy = 2,2'-bipyridine) at room temperature (Scheme 4.3B).[14] Et_3SiH and $K_2S_2O_8$ initiated the radical reaction of alkyl bromides or iodides to generate alkyl radical, and reaction with Cu(II)–CF_3 generated C(sp^3)–CF_3 bonds. This method could be applicable secondary alkyl halides as well as primary ones with high efficiencies and wide scopes under mild conditions. Recently, MacMillan and co-worker realized trifluoromethylation of unactivated alkyl bromide in catalytic methods using copper/photoredox dual catalysis.[15] They proposed silyl radical, generated from the oxidation of silanol, could abstracts bromine to generate alkyl radical. This catalytic protocol converted a variety of alkyl, allyl, benzyl, and heterobenzyl bromides, including complex drug derivatives into alkyl trifluoromethane.

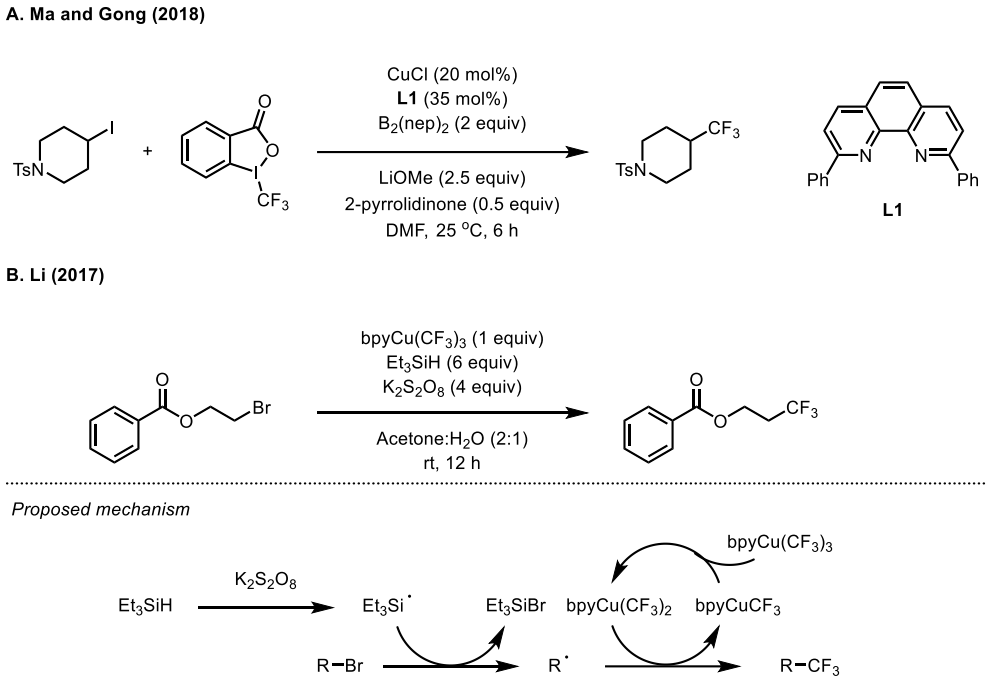

Scheme 4.3. Trifluoromethylation of unactivated alkyl halides

Aliphatic carboxylic acids are ideal raw materials for chemical synthesis due to its high stability, availability, and low costs. For this reason, utilization of carboxylic acid in catalytic transformation has been widely studied in last decades.[16] Conversion of the carboxylic acid group into trifluoromethyl group has also been well researched. Hu and co-workers achieved copper-catalyzed trifluoromethylation of polysubstituted acrylic acid derivatives (Scheme 4.4A).[17] Electrophilic Togni reagent was attacked by olefin, and copper Lewis acid catalyzed decarboxylative rearrangement to generate allylic and vinylic products. Although this transformation tolerated water, oxygen in practical issues, it was only applicable to β,γ-unsaturated carboxylic acids, which limited the scope of the reaction. After one year, the Li group

reported trifluoromethylation of unactivated carboxylic acids using bpyCu(CF_3)$_3$ as an efficient reagent (Scheme 4.4B).[18] Using persulfate ($K_2S_2O_8$) as terminal oxidant assisted by catalytic amount of silver ($AgNO_3$), generated alkyl radical can combine with Cu(II)(CF_3)$_2$ complex, which was activated by $ZnMe_2$. The scope is broader than previous decarboxylative trifluoromethylating methods in operational and mild room temperature reactions. Further improvement was done in 2018 by MacMillan and co-workers. They utilized iridium/copper photoredox dual catalysis for decarboxylative trifluoromethylation of unactivated carboxylic acids in the catalytic pathway (Scheme 4.4C).[19] Not only primary, secondary, tertiary acids, but also medicinal agents and natural products were successfully trifluoromethylated at room temperature. The Mykhailiuk group showed sulfur tetrafluoride can be utilized as a decarboxylative trifluoromethylating reagent without any metal-additive at 55 ^{o}C.[20]

A. Hu (2016)

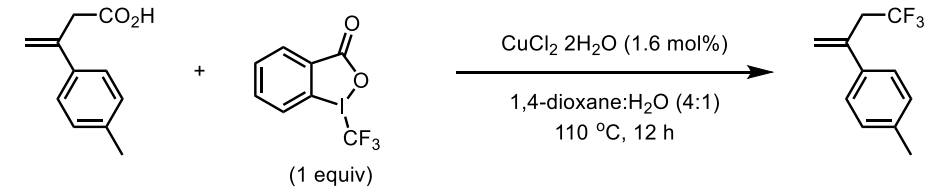

Proposed mechanism

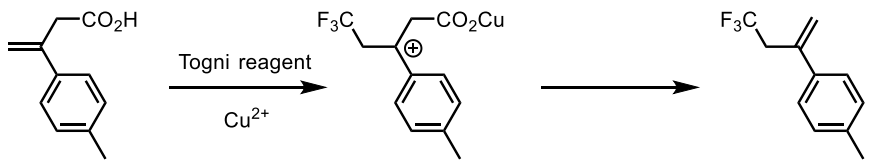

B. Li (2017)

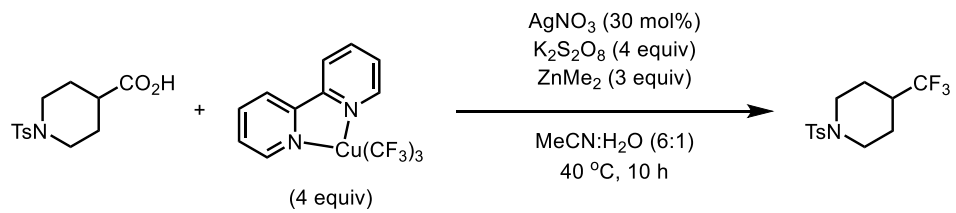

Proposed mechanism

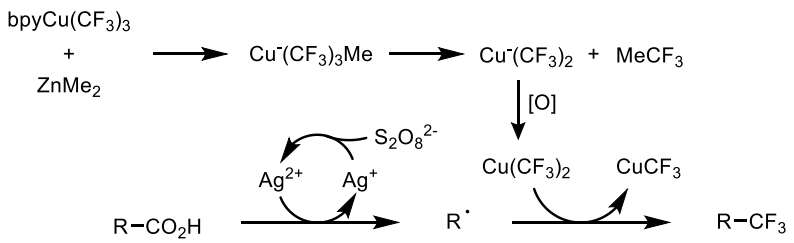

C. MacMillan (2018)

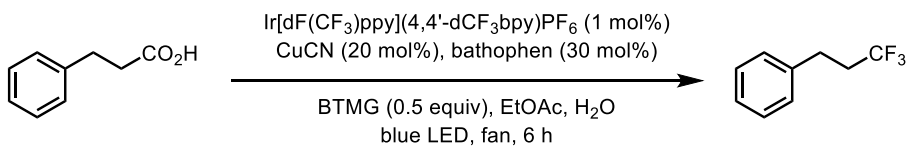

BTMG = 2-*tert*-butyl-1,1,3,3-tetramethylguanidine

Scheme 4.4. Decarboxylative trifluoromethylation of unactivated carboxylic acids

Transition metal-mediated trifluoromethylation reaction extends the concept and scope of $C(sp^3)–CF_3$ bond formation utilizing other alkyl leaving groups than alkyl halides and carboxylic acids. Fu and co-workers reported an copper-promoted trifluoromethylation reaction of primary and secondary alkylboronic acids with $TMSCF_3$ (Scheme 4.5A).[21] Both cyclic and acyclic boronic acids were trifluoromethylated with good tolerance to amine, amide, ketone groups.

C=N double bond functional groups, such as diazo or hydrazone moieties, can be attacked by trifluoromethyl reagent with generation of nitrogen gas as the leaving group. In 2012, Hu and co-workers developed the trifluoromethylation of α-diazo esters with $TMSCF_3$ reagent to prepare α-trifluoromethyl esters (Scheme 4.5B).[22] It requires one-pot two step reaction; synthesis of $CuCF_3$ was firstly conducted, and addition of diazo compound can successfully generate trifluoromethylated ester. Meanwhile, Zeng and Li reported metal-free trifluoromethylation of hydrazones with electrophilic Togni reagent.[23] This method only required solvent and mild heating (80 ^oC), which has potential to synthesize trifluoromethylated products in a greener protocol.

OX groups have been modified by many chemists to design better leaving groups under mild conditions. The Altman group utilized $–OCS_2Me$,[24] $–OCOCF_2Br$,[25] and the Sun group utilized $–OCO_2Me$[26] as the leaving group. Recently, the Zhang group utilized stereospecific $–OSO_2Ar$ substituted propargyl sulfonates, and stereoselectively inverted trifluoromethyl product could be obtained (Scheme 4.5C).[27]

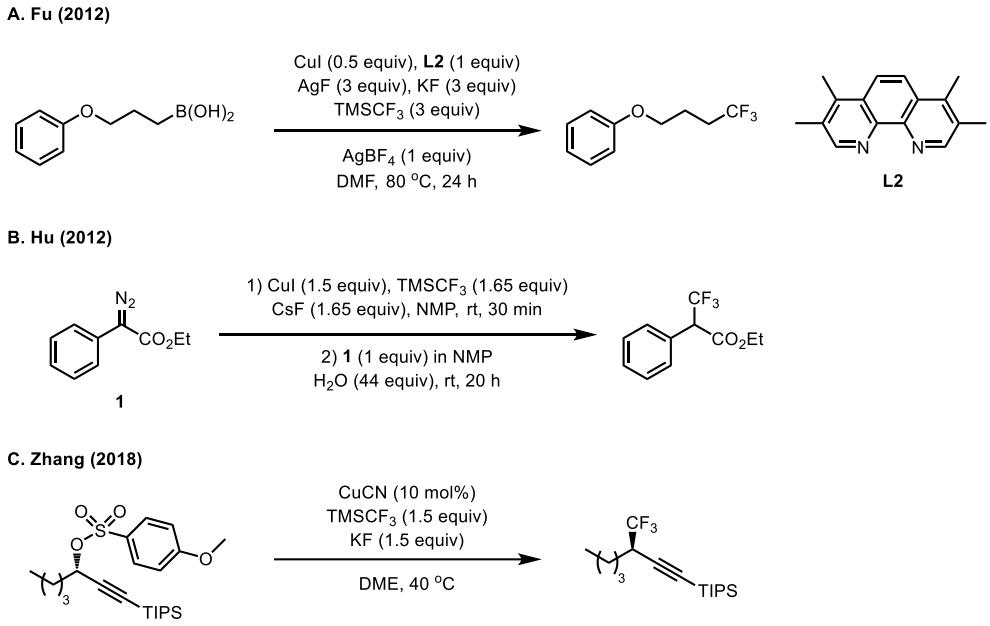

Scheme 4.5. Other trifluoromethylation reactions with substitution mechanism

4.2.2. C(sp^3)–CF_3 bond formation via addition of CF_3 source

Trifluoromethyl group can also be introduced to unsaturated bonds. For example, nucleophilic enamines or enolates can attack electrophilic trifluoromethyl sources.[28] Meanwhile, trifluoromethyl anion conducts the nucleophilic addition to carbonyl or imine moieties. Recently, dual functionalization of alkenes by addition of trifluoromethyl anion or radical is one of promising approaches for the construction of multi-functional C(sp^3)–CF_3 bonds. Utilizing various terminal reagents, hydro-. carbo-, nitro-, oxo-, halo-, acyltrifluoromethylation of olefins, even three component reactions, have been realized. Herein, recent development of carbonyl addition reactions, and representative dual functionalization of olefins with addition mechanism are reviewed (Scheme 4.6).

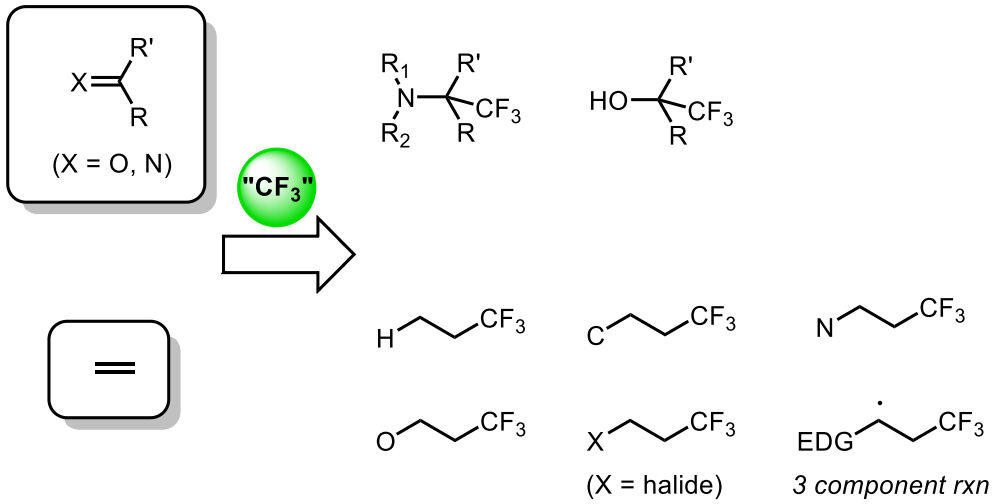

Scheme 4.6 Summary of trifluoromethylation via addition mechanism

Colby and co-workers discovered a new trifluoromethylating reagent, an amidinate salt of hexafluoroacetone hydrate (Scheme 4.7A).[29] This non-hygroscopic and air-stable reagent was activated by deprotonation of hydroxyl group. The generated trifluoromethyl anion conducted nucleophilic trifluoromethylation. A reaction with the reagent was applicable to carbonyl and disulfide electrophiles in excellent yields. Also, Shibata and co-workers firstly developed enantioselective trifluoromethylation of imines (Scheme 4.7B).[30] By using bromide salts of cinchona alkaloids and KOH as a chiral catalyst, azomethine imines and $TMSCF_3$ provided α-trifluoromethyl amine in excellent enantioselectivity.

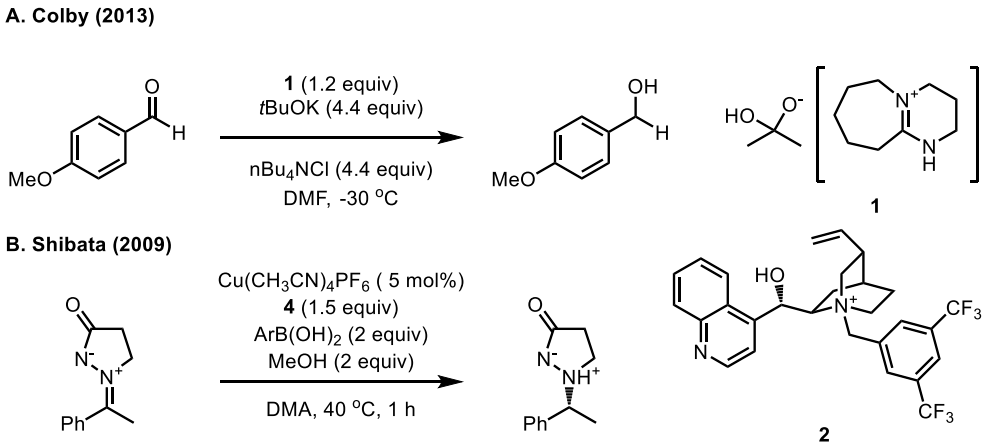

Scheme 4.7 Trifluoromethylation of carbonyl and imine substrates

Dual trifluoromethylation of alkenes mainly takes place through a radical pathway. Generally, trifluoromethyl radical undergoes anti-Markovnikov type addition with an alkene to give internal carbon-centered radical intermediate. Varying the coupling substrates can diversify the functional group on the β-position of trifluoromethyl group. Hydrotrifluoromethylation is one of the simplest alkene addition-based transformations. Nicewicz and co-workers reported an organic photoredox catalysis system for the hydrotrifluoromethylation of styrenes and unactivated aliphatic alkenes with $NaSO_2CF_3$ (Scheme 4.8).[31] Under blue light irradiation, $NaSO_2CF_3$ is oxidized by highly oxidizing mesityl acridinium photoredox catalyst to generate trifluoromethyl radical, and it inserted to alkene in anti-Markovnikov pathway, followed by hydrogen abstraction from thiophenol.

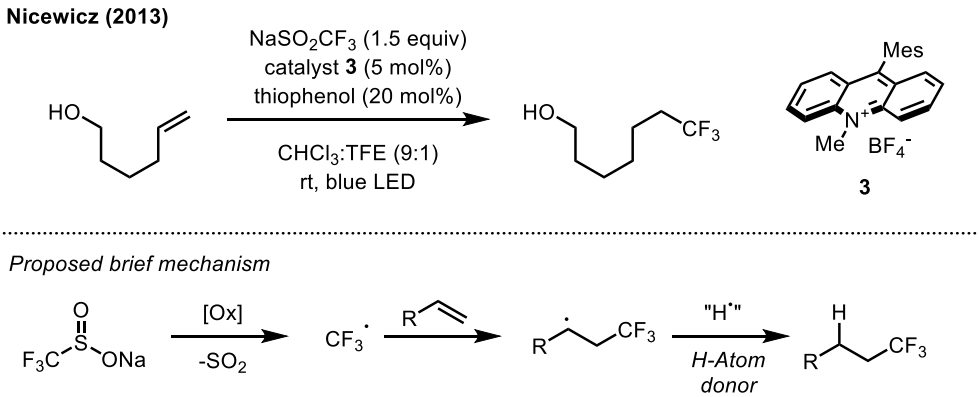

Scheme 4.8 Hydrotrifluoromethylation of olefins

Carbotrifluoromethylation has been mainly studied in an intramolecular pathway, including olefin and the other unsaturated bonds which can be attacked by the intermediate carbon-centered radical. Tan and Liu demonstrated the first example of metal-free direct carbotrifluoromethylation of alkenes including aryl rings (Scheme 4.9A).[32] Inexpensive $TMSCF_3$ with $PhI(OAc)_2$ as the oxidant furnished diverse heterocyclic compounds. In 2014, copper-catalyzed intermolecular trifluoroarylation of alkenes was investigated by the Liu group (Scheme 4.9B).[33] The reaction afforded trifluoromethyl-containing diarylmethane derivatives using the combination of arylboronic acid and Togni reagent. Especially, arylboronic acid conducted both roles; transmetallating reagent and activator to generate trifluoromethyl radical, which achieved the intermolecular reaction.

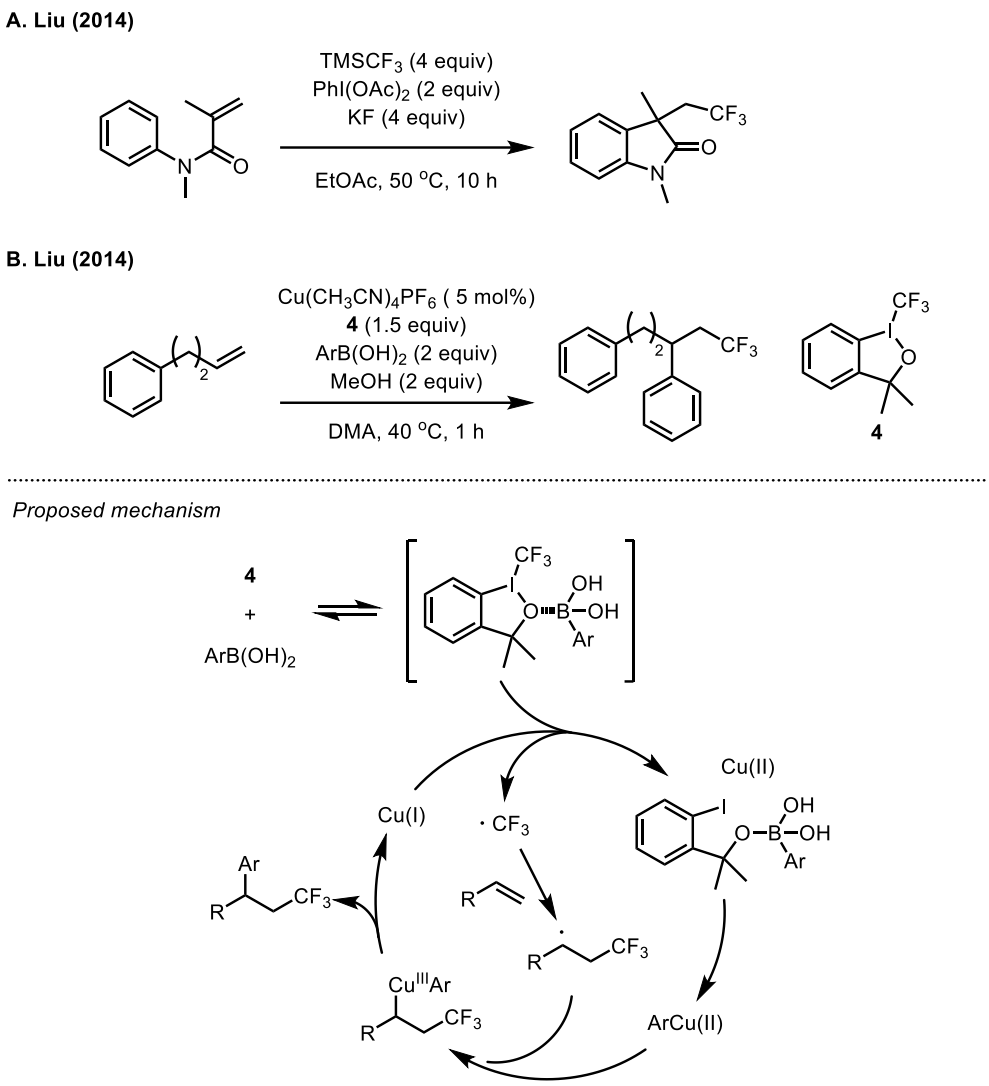

Scheme 4.9 Carbotrifluoromethylation of olefins

Using nitrogen-containing substrates as the coupling partners afforded aminotrifluoromethylation of olefins. Magnier and Masson reported azidotrifluoromethylation using photocatalysis and $TMSN_3$, which attacked trifluoromethylated alkyl cation oxidized from carbon-centered radical intermediate

(Scheme 4.10A).[34] Gong and co-workers used azo derivatives to generate hydrazine products under blue light photoredox catalysis conditions.[35] Recently, Li and co-workers developed a new copper-catalyzed aminotrifluoromethyation system using bpyZn(CF_3)$_2$ as a trifluoromethylating reagent (Scheme 4.10B).[36] Driven by addition of N-centered radical to alkene and avoiding the generation of trifluoromethyl radical generation, the reaction exhibited a regioselectivity opposite to those mediated by typical trifluoromethyl radical addition reactions; trifluoromethylation of internal carbon. The N-centered radical firstly added to terminal position, and the generated alkyl radical was trapped by Cu intermediate with CF_3 ligand, following reductive elimination which afforded inner-trifluoromethylated product.

A. Magnier and Masson (2014)

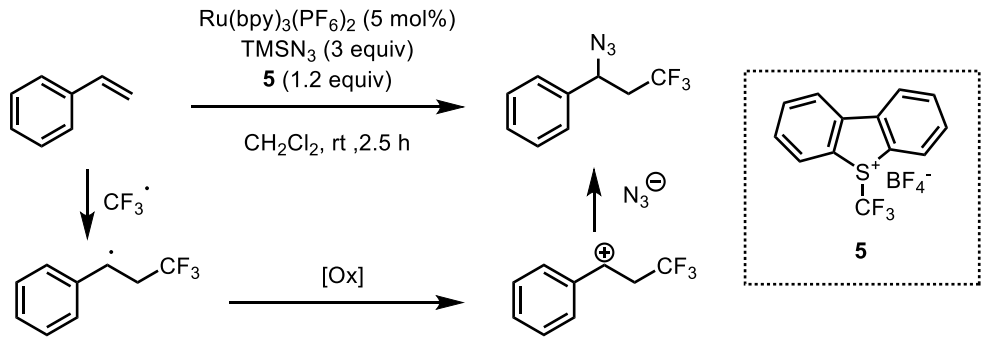

B. Li (2019)

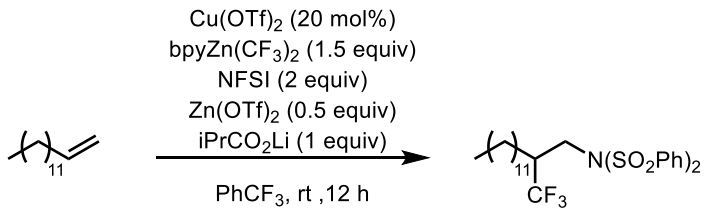

Proposed mechanism

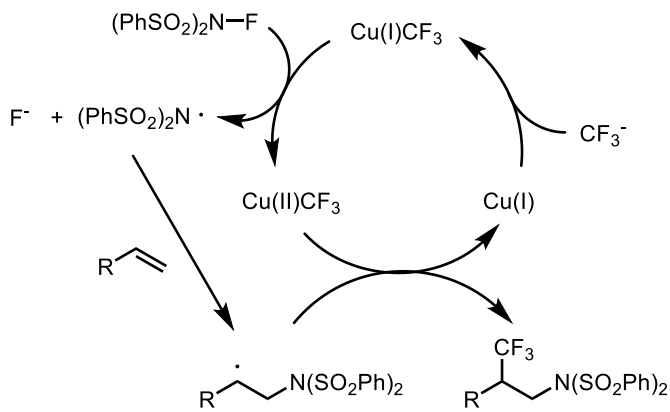

Scheme 4.10 Aminotrifluoromethylation of olefins

Using similar mechanism as scheme 4.10A (trifluoromethyl radical addition and generation of alkyl radical intermediate–oxidation–nucleophilic addition of coupling partner), other dual functionalizations such as oxotrifluoromethylation and halotrifluoromethylation can be achieved. In 2012, the Buchwald group developed copper-catalyzed intramolecular oxotrifluoromethylation under mild and operatively simple conditions (Scheme 4.11A).[37] Oxo-nucleophiles such as alcohols, carboxylic acids, and phenols were used to derive heterocycles and lactones in high yields. The Jung and Han group used CF_3SO_2Cl under visible light irradiation with Ru photocatalyst to conduct chlorotrifluoromethylation of alkenes regioselectively (Scheme 4.11B).[38] Oxidation of the reagent generated trifluoromethyl radical and chloride anion, which added to alkene in order. Complex and biologically active molecules could be well-functionalized to afford chlorotrifluoromethyl compounds in high yields.

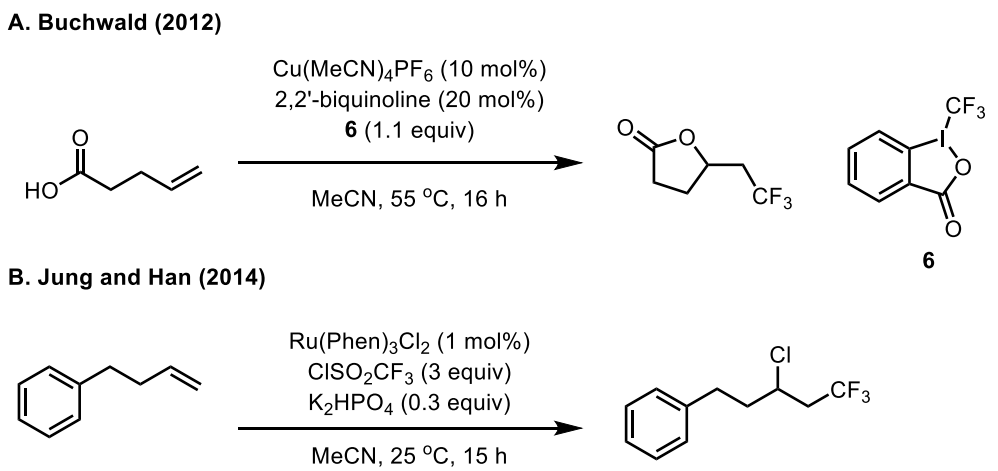

Scheme 4.11 Oxotrifluoromethylation and halotrifluoromethylation of olefins

Using the character of polarity, Yang and co-workers achieved three-component reaction of two different alkenes to provide chain elongated and trifluoromethylated aromatic alkenes (Scheme 4.12).[39] Good chemoselectivity can be achieved by polarity-match concept; electrophilic trifluoromethyl radical favors electron-rich alkenes, and further generated nucleophilic radical intermediate favors electron-deficient alkenes. Decarboxylative radical oxidation produced elongated alkene.

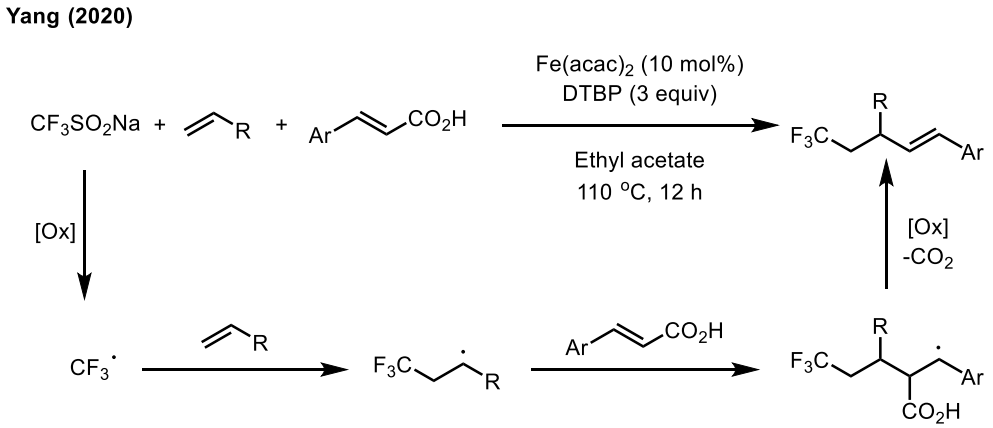

Scheme 4.12 Three-component reaction of different olefins

4.3. C(sp^3)–CF_3 bond formation via C–H activation

Different from classical organic transformations, C–H activation enables the direct introduction of a functional group into the desired C–H bond without prefunctionalization of the starting material, providing significant atom-economic and environmental advantages. In this context, C(sp^2)–H trifluoromethylation has

been extensively developed from olefins to unactivated arenes. However, only a few methods have been developed for the direct trifluoromethylation of C(sp^3)–H bonds. Herein, representative examples of C(sp^3)–H trifluoromethylation methods are discussed (Scheme 4.13).

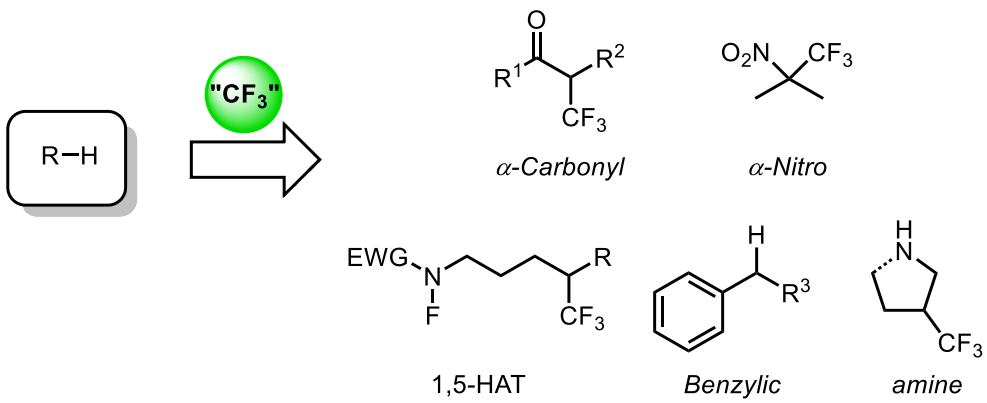

Scheme 4.13 Summary of trifluoromethylation via C–H activation

Early C(sp^3)–H trifluoromethylation was studied with weak and acidic bonds such as α-carbonyl C–H bonds, which can be easily activated by base or catalyst. Cahard and co-workers developed an efficient protocol for trifluoromethylation of chiral imide enolates using electrophilic Togni reagent (Scheme 4.14A).[40] Using oxazolidinone substituent, Evans-type lithium imide enolates were generated using LiHMDS at -78ºC, and attacked electrophilic Togni reagent in excellent diastereomeric selectivity. The resulting product could be further transformed into alcohol and carboxylic acids without racemization.

In 2010, the MacMillan group introduced a new mechanistic approach to the enantioselective α-trifluoromethylation of aldehydes using Lewis acid-organocatalysis (Scheme 4.14B).[41] Amine catalyst with aldehydes should generate enamine that is sufficiently π-electron-rich to participate in an enantioselective formation of C–CF_3 bond with Togni reagent via nucleophilic attack.

Not only aldehydes, β-ketoester derivatives can be used as substrates. Gade and co-workers reported enantioselective copper-catalyzed trifluoromethylation of β-ketoester using electrophilic Umemoto reagent (Scheme 4.14C).[42] Both five- and six-membered ring β-ketoesters were converted to the corresponding quaternary-carbon centered trifluoromethylated products in high yields with up to 99% ee under mild conditions.

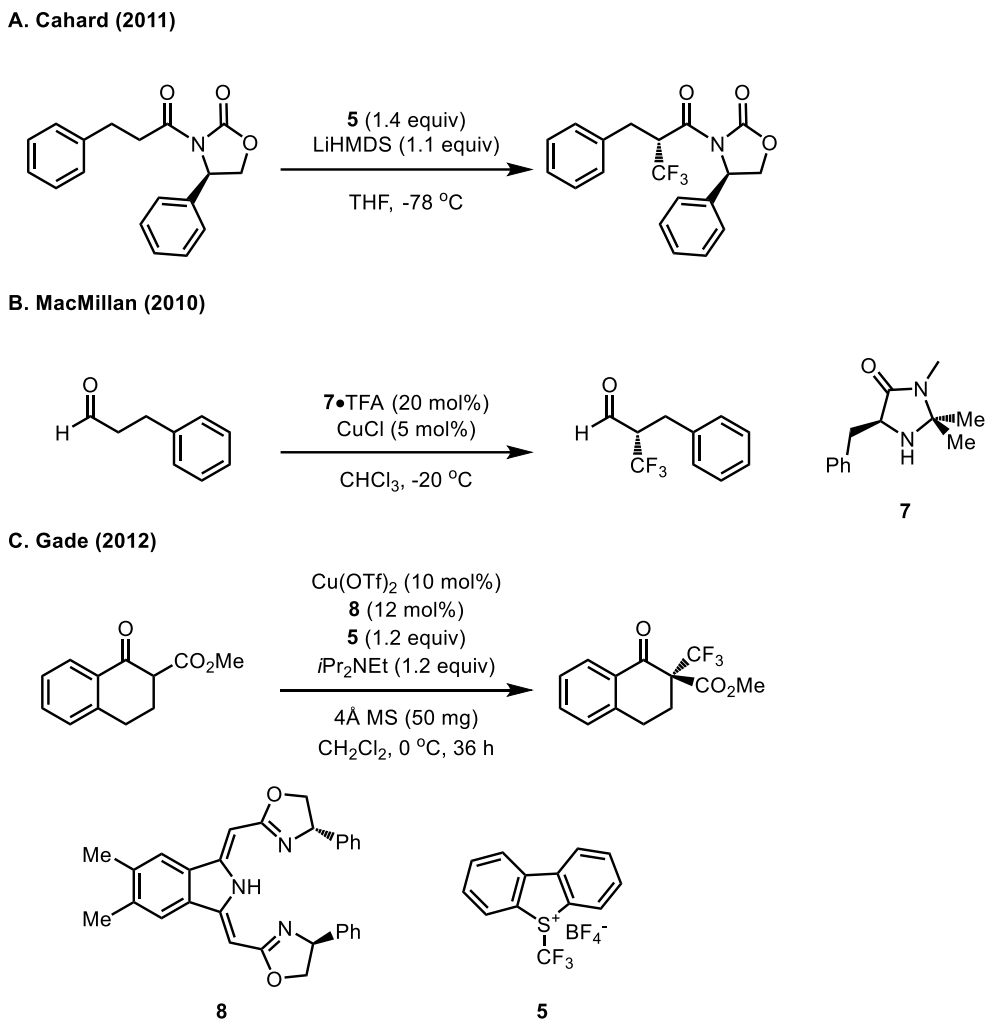

Scheme 4.14 Trifluoromethylation via α-carbonyl C–H bond activation

The α-amino C(sp^3)–H trifluoromethylation was developed via nitroalkane functionalization. Watson and co-workers provided a synthesis of quaternary α-(trifluoromethyl)nitroalkane via a metal-free method (Scheme 4.15).[43] This high-yielding and diastereoselective method was conducted via a radical pathway generated through slow electron-transfer of substrate and trifluoromethylating

reagent.

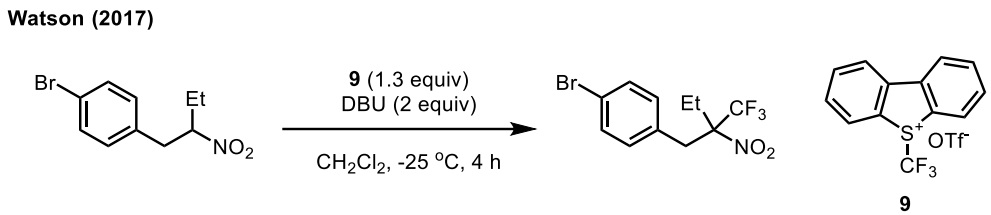

Scheme 4.15 Trifluoromethylation via α-amino C–H bond activation

Activation of an unactivated strong C–H bond is a crucial challenge in the development of C–H functionalization. The Li and Zhu group developed unactivated δ-trifluoromethylation of amine substrates via the similar mechanism proposed in Scheme 4.10B. It is known that aminyl radical can conduct facile rearrangement to generate alkyl radical by hydrogen atom transfer of C–H bonds at δ-position. After generating an aminyl radical by the reduction of N-fluoroamine substrate, 1,5-HAT took place to give carbon-centered radical and trifluoromethyl group transfer from Cu(II)–CF_3 provided the desired product (Scheme 4.16). Except α-amino or α-carbonyl positions, only few examples were reported for non-directed C(sp^3)–H trifluoromethylation, focusing on benzylic C–H bonds. Benzylic C(sp^3)–H trifluoromethylations were mainly developed by using copper complexes, such as bpyCu$(CF_3)_3$[44] or bpyZn$(CF_3)_2$[45], as trifluoromethylating reagent. In 2020, the MacMillan group firstly reported unactivated C(sp^3)–H trifluoromethylation of amine substrates in the absence of a directing group.[46] These methods are more discussed in chapter 5.

Li (2019)

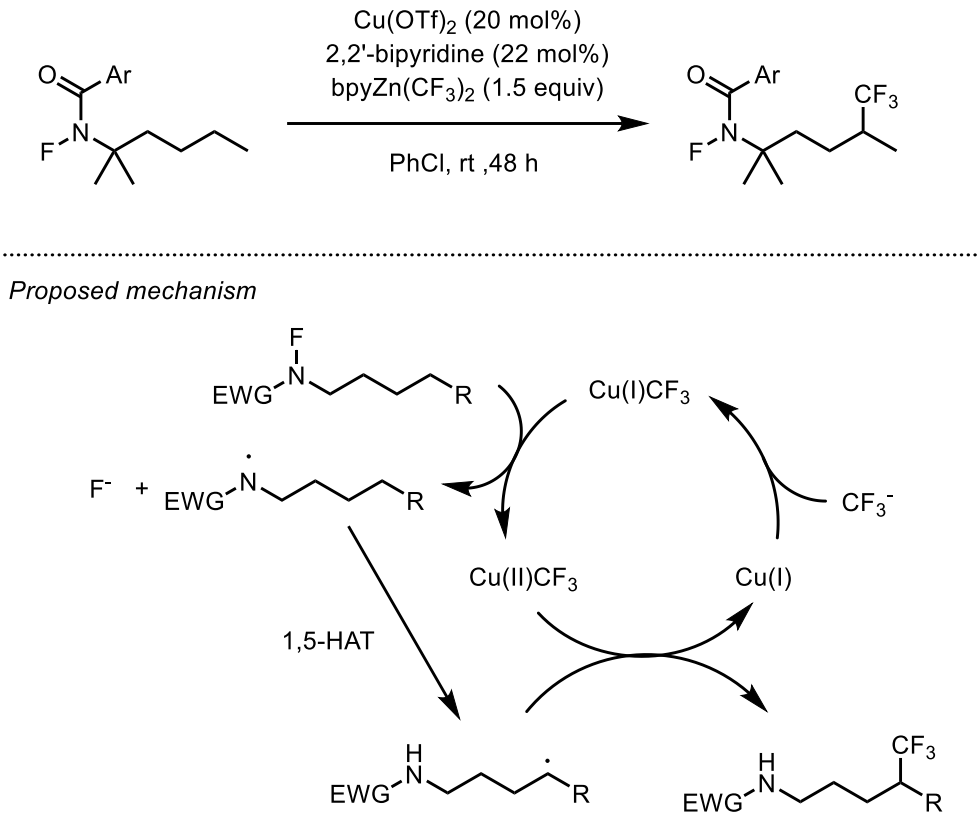

Scheme 4.16 Trifluoromethylation via 1,5-HAT and C–H bond activation

4.4. Conclusion

Over the past decades, remarkable progress has been made in trifluoromethylation to enable C(sp^3)–CF_3 bond formation to overcome the problem that is mainly limited to C(sp^2)–CF_3 formation. Easily accessible substrates such as alkyl halide and carboxylic acids were utilized for high-yield trifluoromethylation via substitution reaction. Addition of various trifluoromethyl anion or radical to unsaturated bonds expanded the reactions to dual-functionalization. Recent progress in C(sp^3)–H

trifluoromethylation makes the strategy more economical and practical.

However, dual functionalization of olefins are mainly focused on anti-Markovnikov type reactions, and only a few strategies have been reported for the opposite regioselectivity. Also, though tertiary and α-heteroatom $C(sp^3)$–H activation is widely reported for other functionalizations, regioselective trifluoromethylation of those positions remains still elusive. Finally, the detailed operating mechanism is still in question regarding what happens on the copper center and the exact structure of copper intermediates for trifluoromethylation of alkyl radicals, which can offer new insight of $C(sp^3)$–CF_3 bond formations.

4.5. References

(1) Fujiwara, T.; O'Hagan, D., *J. Fluor. Chem.* **2014,** *167*, 16-29.

(2) Meanwell, N. A., *J. Med. Chem.* **2018,** *61* (14), 5822-5880.

(3) Zhao, Y.; Schwab, M. G.; Kiersnowski, A.; Pisula, W.; Baumgarten, M.; Chen, L.; Müllen, K.; Li, C., *J. Mater. Chem.* **2016,** *4* (21), 4640-4646.

(4) McLoughlin, V. C. R.; Thrower, J., *Tetrahedron* **1969,** *25* (24), 5921-5940.

(5) (a) Cho, E. J.; Senecal, T. D.; Kinzel, T.; Zhang, Y.; Watson, D. A.; Buchwald, S. L., *Science* **2010,** *328* (5986), 1679-1681; (b) Keaveney, S. T.; Schoenebeck, F., *Angew. Chem. Int. Ed.* **2018,** *57* (15), 4073-4077.

(6) Kobayashi, Y.; Yamamoto, K.; Kumadaki, I., *Tetrahedron Lett.* **1979,** *20* (42), 4071-4072.

(7) Kondratenko, N. V.; Vechirko, E. P.; Yagupolskii, L. M., *Synthesis* **1980,** *11*, 932-933.

(8) Urata, H.; Fuchikami, T., *Tetrahedron Lett.* **1991,** *32* (1), 91-94.

(9) (a) Chen, Q.-Y.; Wu, S.-W., *J. Chem. Soc. Chem. Commun.* **1989,** (11), 705-706;

(b) Chen, Q.-Y.; Duan, J.-X., *Tetrahedron Lett.* **1993,** *34* (26), 4241-4244.

(10) Novák, P.; Lishchynskyi, A.; Grushin, V. V., *J. Am. Chem. Soc.* **2012,** *134* (39), 16167-16170.

(11) Larsson, J. M.; Pathipati, S. R.; Szabó, K. J., *J. Org. Chem.* **2013,** *78* (14), 7330-7336.

(12) Trost, B. M.; Gholami, H.; Zell, D., *J. Am. Chem. Soc.* **2019,** *141* (29), 11446-11451.

(13) Chen, Y.; Ma, G.; Gong, H., *Org. Lett.* **2018,** *20* (15), 4677-4680.

(14) Shen, H.; Liu, Z.; Zhang, P.; Tan, X.; Zhang, Z.; Li, C., *J. Am. Chem. Soc.* **2017,** *139* (29), 9843-9846.

(15) Kornfilt, D. J. P.; MacMillan, D. W. C., *J. Am. Chem. Soc.* **2019,** *141* (17), 6853-6858.

(16) (a) Rodríguez, N.; Goossen, L. J., *Chem. Soc. Rev.* **2011,** *40* (10), 5030-5048;

(b) Moon, P. J.; Lundgren, R. J., *ACS Catal.* **2020,** *10* (3), 1742-1753.

(17) He, Z.; Tan, P.; Hu, J., *Org. Lett.* **2016,** *18* (1), 72-75.

(18) Tan, X.; Liu, Z.; Shen, H.; Zhang, P.; Zhang, Z.; Li, C., *J. Am. Chem. Soc.* **2017,** *139* (36), 12430-12433.

(19) Kautzky, J. A.; Wang, T.; Evans, R. W.; MacMillan, D. W. C., *J. Am. Chem. Soc.* **2018,** *140* (21), 6522-6526.

(20) Bugera, M.; Trofymchuk, S.; Tarasenko, K.; Zaporozhets, O.; Pustovit, Y.; Mykhailiuk, P. K., *J. Org. Chem.* **2019,** *84* (24), 16105-16115.

(21) Xu, J.; Xiao, B.; Xie, C.-Q.; Luo, D.-F.; Liu, L.; Fu, Y., *Angew. Chem. Int. Ed.*

2012, *51* (50), 12551-12554.

(22) Hu, M.; Ni, C.; Hu, J., *J. Am. Chem. Soc.* **2012,** *134* (37), 15257-15260.

(23) Zeng, H.; Luo, Z.; Han, X.; Li, C.-J., *Org. Lett.* **2019,** *21* (15), 5948-5951.

(24) Zhu, L.; Liu, S.; Douglas, J. T.; Altman, R. A., *Chem. Eur. J.* **2013,** *19* (38), 12800-12805.

(25) Ambler, B. R.; Zhu, L.; Altman, R. A., *J. Org. Chem.* **2015,** *80* (16), 8449-8457.

(26) Yang, W.; Ma, D.; Zhou, Y.; Dong, X.; Lin, Z.; Sun, J., *Angew. Chem. Int. Ed.* **2018,** *57* (37), 12097-12101.

(27) Gao, X.; Xiao, Y.-L.; Wan, X.; Zhang, X., *Angew. Chem. Int. Ed.* **2018,** *57* (12), 3187-3191.

(28) (a) Ma, J.-A.; Cahard, D., *J. Fluor. Chem.* **2007,** *128* (9), 975-996; (b) Zheng, Y.; Ma, J.-A., *Adv. Synth. Catal.* **2010,** *352* (16), 2745-2750; (c) Shimizu, R.; Egami, H.; Hamashima, Y.; Sodeoka, M., *Angew. Chem. Int. Ed.* **2012,** *51* (19), 4577-4580; (d) Pham, P. V.; Nagib, D. A.; MacMillan, D. W. C., *Angew. Chem. Int. Ed.* **2011,** *50* (27), 6119-6122.

(29) Riofski, M. V.; Hart, A. D.; Colby, D. A., *Org. Lett.* **2013,** *15* (1), 208-211.

(30) Kawai, H.; Kusuda, A.; Nakamura, S.; Shiro, M.; Shibata, N., *Angew. Chem. Int. Ed.* **2009,** *48* (34), 6324-6327.

(31) Wilger, D. J.; Gesmundo, N. J.; Nicewicz, D. A., *Chem. Sci.* **2013,** *4* (8), 3160-3165.

(32) Li, L.; Deng, M.; Zheng, S.-C.; Xiong, Y.-P.; Tan, B.; Liu, X.-Y., *Org. Lett.* **2014,** *16* (2), 504-507.

(33) Wang, F.; Wang, D.; Mu, X.; Chen, P.; Liu, G., *J. Am. Chem. Soc.* **2014,** *136* (29), 10202-10205.

(34) Dagousset, G.; Carboni, A.; Magnier, E.; Masson, G., *Org. Lett.* **2014,** *16* (16), 4340-4343.

(35) Wang, P.; Zhu, S.; Lu, D.; Gong, Y., *Org. Lett.* **2020,** *22* (5), 1924-1928.

(36) Xiao, H.; Shen, H.; Zhu, L.; Li, C., *J. Am. Chem. Soc.* **2019,** *141* (29), 11440-11445.

(37) Zhu, R.; Buchwald, S. L., *J. Am. Chem. Soc.* **2012,** *134* (30), 12462-12465.

(38) Oh, S. H.; Malpani, Y. R.; Ha, N.; Jung, Y.-S.; Han, S. B., *Org. Lett.* **2014,** *16* (5), 1310-1313.

(39) Zhao, J.; Liu, R.-X.; Luo, C.-P.; Yang, L., *Org. Lett.* **2020,** *22* (17), 6776-6779.

(40) Matoušek, V.; Togni, A.; Bizet, V.; Cahard, D., *Org. Lett.* **2011,** *13* (21), 5762-5765.

(41) Allen, A. E.; Macmillan, D. W. C., *J. Am. Chem. Soc.* **2010,** *132* (14), 4986-4987.

(42) Deng, Q.-H.; Wadepohl, H.; Gade, L. H., *J. Am. Chem. Soc.* **2012,** *134* (26), 10769-10772.

(43) Gietter-Burch, A. A. S.; Devannah, V.; Watson, D. A., *Org. Lett.* **2017,** *19* (11), 2957-2960.

(44) (a) Guo, S.; AbuSalim, D. I.; Cook, S. P., *J. Am. Chem. Soc.* **2018,** *140* (39), 12378-12382; (b) Paeth, M.; Carson, W.; Luo, J.-H.; Tierney, D.; Cao, Z.; Cheng, M.-J.; Liu, W., *Chem. Eur. J.* **2018,** *24* (45), 11559-11563.

(45) Xiao, H.; Liu, Z.; Shen, H.; Zhang, B.; Zhu, L.; Li, C., *Chem* **2019,** *5* (4), 940-949.

(46) Sarver, P. J.; Bacauanu, V.; Schultz, D. M.; DiRocco, D. A.; Lam, Y.-H.; Sherer, E. C.; MacMillan, D. W. C., *Nat. Chem.* **2020,** *12* (5), 459-467.

Chapter 5. Direct C(sp^3)–H Trifluoromethylation of Unactivated Alkanes Enabled by Multifunctional Trifluoromethyl Copper Complexes*

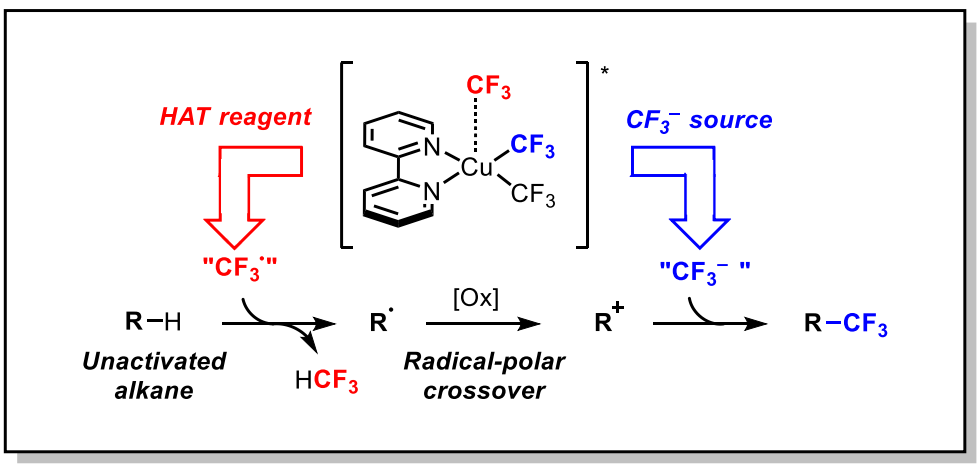

* The majority of this work has been published: Geunho Choi and Soon Hyeok Hong*, *Under revision.*

5.1. Introduction

The introduction of a trifluoromethyl group to organic molecules is important for metabolic stability, lipophilicity, and hydrophobicity. Therefore, trifluoromethylation has attracted significant attention in the field of material, pharmaceutical, and agricultural chemistry to conveniently modulate the polarity, solubility, and chemical reactivity of desired compounds.[1] Various synthetic methods to form C–CF_3 bonds have been developed using nucleophilic,[2] electrophilic,[3] or radical[4] trifluoromethyl sources.

Direct formation of C–CF_3 bonds via C–H activation is ideal for trifluoromethylation in consideration of atom- and step-efficiencies. C(sp^2)–H trifluoromethylation reactions have been extensively developed to introduce trifluoromethyl groups on arenes,[5] heteroarenes,[6] olefins, [7] and aldehydes.[8] Although C(sp^2)–H trifluoromethylation has been significantly investigated, very few examples of C(sp^3)–H trifluoromethylation have been reported, employing a directing group,[9] and being only applicable to relatively more activated C(sp^3)–H bonds such as α-carbonyl,[10] α-nitrogen,[11] and benzylic C–H bonds (Scheme 5.1a).[12] Therefore, direct C(sp^3)–H trifluoromethylation of unactivated alkanes under mild conditions is highly desired to facilitate a streamlined synthesis of various trifluoromethylated compounds, obviating the need for pre-functionalization. During the preparation of this manuscript, MacMillan and co-workers reported trifluoromethylation of aliphatic C(sp^3)–H bonds combining decatungstate photocatalysis and copper catalysis by using the Togni reagent.[13] The elegant dual catalysis enabled the direct C–CF_3 bond formation at aliphatic and benzylic C(sp^3)–

H bonds.

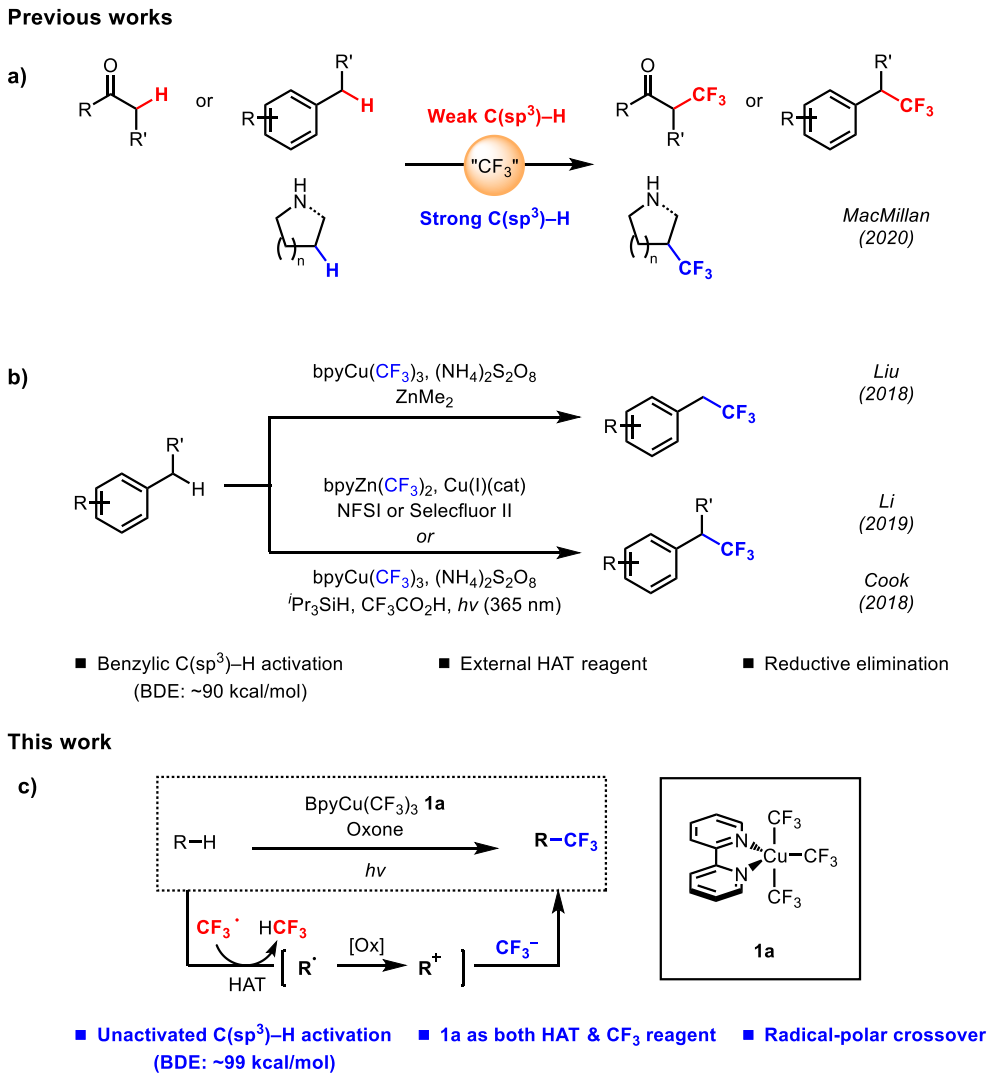

Scheme 5.1 Undirected C(sp^3)–CF_3 trifluoromethylation via C(sp^3)–H activation

Considering a novel strategy for the direct trifluoromethylation of normal C(sp^3)–H bonds, we were inspired by the recently highlighted bpyM(CF_3)$_x$ (M = Cu, Zn; bpy = 2,2'-bipyridine) complexes[8, 9b, 14] due to their exceptional reactivity toward benzylic C(sp^3)–CF_3 trifluoromethylation (Scheme 5.1b). Li and co-workers introduced copper-catalyzed benzylic C(sp^3)–H trifluoromethylation using bpyZn(CF_3)$_2$ as the anionic trifluoromethyl source and *N*-fluorobenzenesulfonimide (NFSI) or Selectfluor as the oxidant and hydrogen atom transfer (HAT) reagent precursor.[12b] Liu and Cheng trifluoromethylated benzylic C(sp^3)–H bond by combining bpyCu(CF_3)$_3$ **1a** and Zn(Me)$_2$ to activate **1a** to bpyCu(II)(CF_3)$_2$ with the generation of MeCF_3.[12c] Cook and co-workers reported the trifluoromethylation of benzylic C(sp^3)–H with **1a** using persulfate, silane, and acid in acetone/water.[12a] UV-irradiation induces homolysis of **1a** to form the active bpyCu(II)(CF_3)$_2$ and CF_3 radical, while the sulfate radical anion performs the HAT from the benzylic C–H bond, generating the benzyl radical which is recombined with bpyCu(II)(CF_3)$_2$, followed by reductive elimination, for the desired trifluoromethylation. Especially, silane is required to capture the CF_3 radical to control the reactivity.

The ingenious strategy developed by Cook led us to consider a different strategy to functionalize unactivated C(sp^3)–H bonds in order to expand the scope from benzylic C(sp^3)–H bonds. Instead of using an externally added persulfate as the HAT reagent and trapping the reactive CF_3 radical with a silane to control the reactivity, we envisioned direct utilization of the highly reactive CF_3 radical without using an external HAT reagent. Based on the bond-dissociation energy (BDE) of fluoroform (106 kcal/mol),[15] the CF_3 radical is hypothesized to perform the HAT from unactivated C(sp^3)–H bonds of alkanes to generate alkyl radicals, which can

further undergo Cu-complex-mediated trifluoromethylation. Although the CF_3 radical has been reported to perform the HAT from C–H bonds of various hydrocarbons to generate fluoroform,[16] to the best of our knowledge, no C–H functionalization reaction utilizing the CF_3 radical as the HAT reagent has been reported. Herein, a novel trifluoromethylation of unactivated C(sp^3)–H bonds was achieved by photo-induced bpyCu(CF_3)$_3$ **1a** based on the newly designed strategy (Scheme 5.1c). A series of control experiments and computational studies suggested that the reaction occurs via an ionic pathway enabled by an oxidative radical-polar crossover with the aid of an Oxone additive. Notably, the bench-stable Cu complex **1a** plays multiple roles of the photo-induced reaction initiator, trifluoromethyl radical source for HAT, and trifluoromethyl anion source, thus enabling direct trifluoromethylation of strong C(sp^3)–H bonds under mild conditions.

5.2. Result and discussion

5.2.1. Reaction condition optimization

Cyclohexane **2a** was chosen as a model hydrocarbon substrate to evaluate the feasibility of the designed strategy with **1a** (Table 5.1). When **2a** (5.0 equiv) was reacted with **1a** (1.0 equiv) in the presence of Oxone (3.0 equiv) in CH_3CN (0.5 mL), (trifluoromethyl)cyclohexane **3a** was produced in 93% yield under blue light irradiation for 3 h (entry 1). Reducing the amount of **2a** (1 or 3 equiv) resulted in diminished yield (50% and 73%, entries 2–3, respectively), and further increasing **2a** content showed quantitative yield (>96%, entries 4–5). Decreased yield was afforded without Oxone (16%, entry 6) and with less than 3.0 equiv of Oxone (39 or

70%, entries 7–8, respectively). Control experiments in the dark demonstrated the critical role of irradiation to produce **3a** (entry 9). Altering the light source to the near ultraviolet region (390 nm) was not effective (21%, entry 10). A lower yield was obtained when the reaction was conducted under air (63%, entry 11). Another oxidant including a persulfate salt, $(NH_4)_2S_2O_8$, resulted in a lower yield (60%, entry 12). Other solvents, except CH_3CN, afforded lower product yield (Table 5.6). The conditions reported by Cook were not effective to afford **3a** in good yield (14%, entry 13) likely because the HAT from silane to the generated sulfate radical anion is faster than that from a C(sp^3)–H bond of **1a**, which has a higher BDE than a benzylic C(sp^3)–H bond.[12a]

Under optimized conditions, the reactivity of various Cu(III)–CF_3 complexes bearing other *N,N*-bidentate ligands, bipyridines, and phenanthrolines, were investigated (Table 5.2). Among the bipyridine ligands tested, the simplest bipyridine performed best. Introduction of any substituent on the *ortho*, *meta*, or *para* positions to modify the steric and electronic characters of the ligand resulted in lower product yield (**1b**–**1h**). No clear correlation between electronic and steric characters of the ligand and reaction outcome were observed. The absorption of the Cu(III) complexes was also examined, but no specific correlations between the absorptions and λ_{max} of the screened Cu complexes and the reaction yields were observed (Figure 5.2–3).

Table 5.1 Variation of the reaction conditions[a]

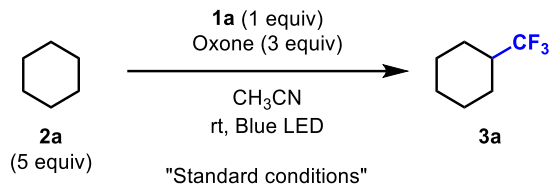

Entry	Variation from the "standard conditions"	**3a** (%)
1[b]	None	93
2	1.0 equiv **2a**	50
3	3.0 equiv **2a**	73
4	16.0 equiv **2a**	>96
5	32.0 equiv **2a**	>96
6[c]	No Oxone	16
7	1.0 equiv Oxone	39
8	2.0 equiv Oxone	70
9	No light	N. D.
10	390 nm, instead of blue light	21
11	Under air in a closed vial	63
12	$(NH_4)_2S_2O_8$, instead of Oxone	60
13[d]	Cook conditions	14

[a]Yields were determined by GC analysis using hexafluorobenzene as an internal standard. [b]Reaction conditions: **2a** (0.25 mmol, 5.0 equiv), **1a** (0.050 mmol, 1.0 equiv), Oxone (0.15 mmol, 3.0 equiv), and CH_3CN (0.5 mL) under 40 W blue LED irradiation with fan cooling (30±5 °C) for 3 h. [c]12 h. [d]Reaction conditions: **2a** (0.10 mmol, 2.0 equiv), **1a** (0.05 mmol, 1.0 equiv), $(NH_4)_2S_2O_8$ (0.15 mmol, 3.0 equiv), *i*Pr_3SiH (0.15 mmol, 3.0 equiv), trifluoroacetic acid (0.40 mmol, 8.0 equiv), acetone (0.3 mL), and water (0.3 mL) under 43 W 370 nm LED irradiation with fan cooling (30±5 °C) for 18 h. N. D. = not detected.

Table 5.2 Reactivity of various copper complexes[a]

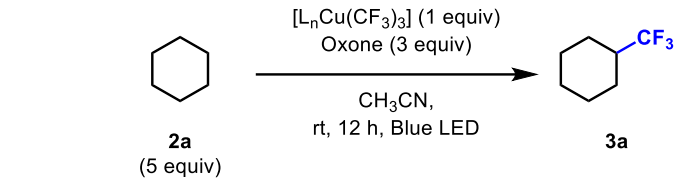

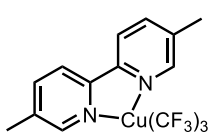

1b, 63%

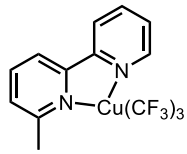

1c, 51%

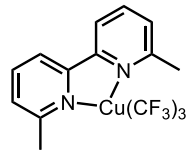

1d, 13%

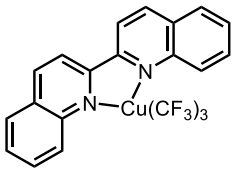

1e, 7%

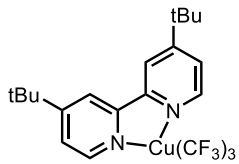

1f, 53%

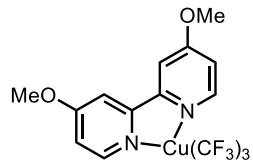

1g, 58%

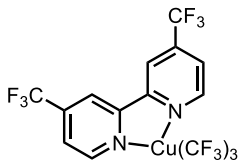

1h, 45%

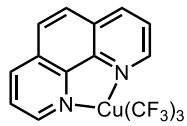

1i, 47%

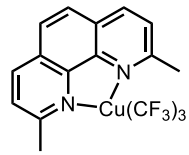

1j, 14%

[a]Reaction conditions: **2a** (0.25 mmol, 5.0 equiv), **1** (0.050 mmol, 1.0 equiv), Oxone (0.15 mmol, 3.0 equiv), and CH_3CN (0.5 mL) under 40 W blue LED irradiation with fan cooling (30±5 °C) for 12 h; Yields were determined by GC analysis using hexafluorobenzene as an internal standard.

5.2.2. Substrate scope of alkanes

After investigating the reaction conditions, various hydrocarbon substrates were investigated to evaluate the generality of the newly developed photo-induced C–H trifluoromethylation protocol (Table 5.3). Although the conditions using anhydrous acetonitrile solvent performed best for **2a**, co-solvent conditions with water (CH_3CN/H_2O, 5:1 (v/v)) using 6.0 equiv hydrocarbon substrates were more effective for other C–H substrates, presumably due to increased solubility of Oxone. For instance, **2c** produced (trifluoromethyl)cycloheptane **3c** in 10% yield under the conditions without water. With the co-solvent conditions with water, the yield was dramatically increased to 84%, although 10% of cycloheptanone **4c** was observed as the by-product. Cyclic alkanes with varied ring sizes were efficiently converted to the corresponding trifluoromethylated products (**3a**–**3e**). The reactions with some substrates (**3e, 3j, 3l, 3m, 3q, 3u**) proceeded smoothly in hexafluoroisopropanol (HFIP) instead of CH_3CN. For example, cyclododecane **3e** furnished the desired product in 30% yield when HFIP was used as the solvent, whereas unidentified complex mixtures were obtained in CH_3CN solvent. Linear alkanes, including hexane (**2f**) and pentane (**2g**), readily underwent trifluoromethylation in very good yields with a preponderance on methylene positions (76% and 87% yield; 88 and 85% methylene selectivity, respectively), likely due to the enhanced stability of methylene radicals compared to primary methyl radicals. Benzylic C–H bonds in toluene could also be functionalized, but in a low yield (39%, **3h**) due to competing CF_3 radical addition to the aryl ring, which was suppressed when silane was used as a trapping reagent under Cook's conditions.[12a] Increased steric hindrance around the arene ring inhibited the undesired addition, affording the desired product in excellent yield

(91%, **3i**). Carboxylic acids (**2j** and **2k**), an ester (**2l**), and an amide (**2m**) were also tolerated in this transformation. 1-Propanoic acid (**2j**) and methyl propanoate (**2l**) mostly underwent α-methylene C–H trifluoromethylation (47 and 71% yield; 85 and 82% α-selectivity, respectively), consistently demonstrating preference for the methylene C–H bond over terminal methyl C–H bond. Propanamide (**2m**) afforded the α-methylene C–H trifluoromethylated product (37%, **3m**) without significant byproduct formation. With 1-butanoic acid (**2k**), the more hydric β-methylene position was preferred over the α-methylene C–H bond (62% yields; 62% beta selectivity, **3k**). Other hydrocarbons containing a carbonyl group were trifluoromethylated with satisfactory yields, favoring functionalization on the more electron-rich C–H bonds due to the preference of the electrophilic CF_3 radical for HAT (**3n**–**3q**). Cyclic ketones including cyclopentanone (**2n**) and cyclohexanone (**2o**) afforded trifluoromethylated products favoring the β-methylene C–H position (58 and 80% yield; 79 and 73% β-selectivity, respectively). Especially, the linear carbonyl 4-heptanone (**2p**) was exclusively trifluoromethylated at the β-position of the carbonyl group rather than the α-methylene or ϒ-methyl position (88%, **3p**). The β-ketoester was also compatible with a major β-trifluoromethylation on the carbonyl group (48%, **3q**). Unfortunately, reactions using aliphatic amines, such as *N*-Boc-pyrrolidine and *N*-acetylpyrrolidine, and aliphatic ethers, such as THF, were not successful. This may due to the coordination of heteroatoms to electron-deficient copper center, which hampers the trifluoromethylation reactivity.

Trifluoromethyl group introduction can reportedly regulate bioactivity.[1b] Previously studied late-stage C–H trifluoromethylation mainly focused on C(sp^2)–H[6a, 17] and weak C(sp^3)–H bonds.[12a, 12b, 13] The applicability of the newly developed

reaction was further examined with direct C(sp^3)–H trifluoromethylations of well-known natural products and bioactive molecule derivatives (Table 3). Eucalyptol, which has anti-inflammatory and antioxidant effects,[18] was smoothly trifluoromethylated with high regio- and diastereo-selectivities at the less sterically hindered position (41%, **3r**). Other bicyclic terpenoids such as norcamphor, the analog of the naturally occurring terpenoid camphor, and fenchone, which exhibits antifungal activity,[19] also delivered the desired C–H trifluoromethylated products (47%, **3s** and 31%, **3t**). Additionally, a cubane core, whose derivatives have not been trifluoromethylated, afforded **3u** in moderate yield (14%). Ambroxide, a naturally occurring terpenoid that is commonly used in the fragrance industry,[20] was trifluoromethylated to furnish a major 2-functionalized regioisomer albeit with low efficiency (20%, **3v**). It should be noted that trifluoromethylation was conducted in the sterically less-hindered cyclohexyl ring, but not at the α-oxy position, exhibiting an unusual trend compared to other radical-based C–H functionalization reactions.[21] Sclareolide, an antifungal plant compound,[22] showed a similar selectivity to ambroxide with higher yield (38%, **3w**). Finally, camphoric acid, which is often used as a precursor of bioactive molecules,[23] was used as a dimethyl ester derivative (**2x**) and was selectively trifluoromethylated at the least sterically hindered methylene position in a moderate yield (32%, **3x**). These results demonstrated the potential applicability of the developed reaction for late-stage, direct C–H trifluoromethylation of functional molecules with reasonable regio- and diastereo-selectivities favoring less-sterically hindered positions.

Table 5.3 Substrate scope of unactivated C(sp^3)–H trifluoromethylation[a]

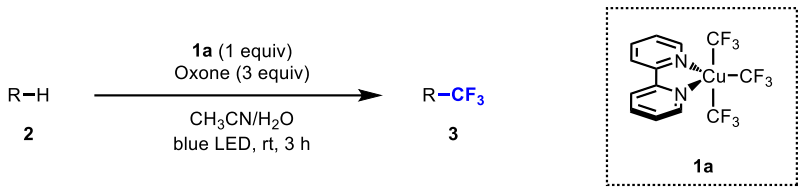

Substrate scopes

minor isomers

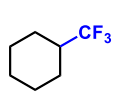

3a, 82% (93%[b])

3b, >96%

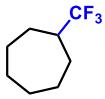

3c, 84%

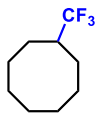

3d, 57%

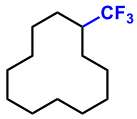

3e, 30%[c]

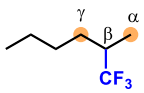

3f, 76%
(α : β : γ = 12 : 50 : 38)

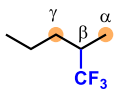

3g, 87%
(α : β : γ =15 : 58 : 27)

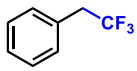

3h, 39%

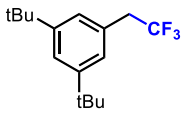

3i, 91%

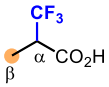

3j, 47%[c]
(α : β = 85 : 15)

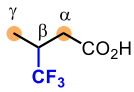

3k, 62%
(α : β : γ = 19 : 62 :19)

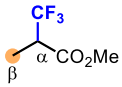

3l, 71%[c]
(α : β = 82 : 18)

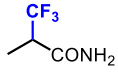

3m, 37%[c, d]

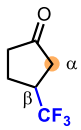

3n, 58%
(α : β = 21 : 79)

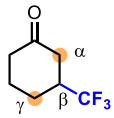

3o, 80%
(α : β : γ = 9 : 73 : 18)

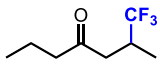

3p, 88%

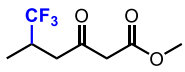

3q, 48%[c, d]

Late-stage functionalization[d]

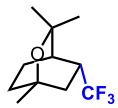

3r, Eucalyptol–CF_3
41%

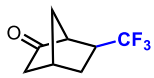

3s, Norcamphor–CF_3
47%

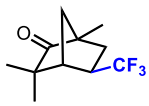

3t, Fenchone–CF_3
31%

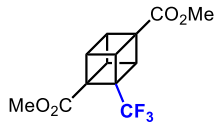

3u, Dimethyl Cubane-1,4-dicarboxylate–CF_3
14%[c]

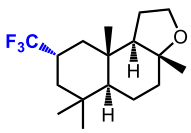

3v, Ambroxide–CF_3
20%

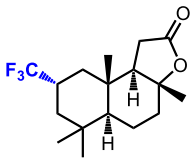

3w, Sclareolide–CF_3
38%[e]

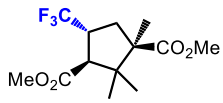

3x, (+)-Camphoric acid dimethyl ester–CF_3
32%

[a]Reaction conditions: **2** (0.60 mmol, 6.0 equiv), **1a** (0.10 mmol, 1.0 equiv), Oxone (0.30 mmol, 3.0 equiv), CH_3CN (1.0 mL), and H_2O (0.2 mL) under 40 W blue LED irradiation with fan cooling (30±5 °C) for 3 h; Yields and selectivities (%) were determined by ^{19}F NMR using fluorobenzene as an internal standard unless otherwise noted. [b]Reaction conditions: **2a** (0.25 mmol, 5.0 equiv), **1a** (0.050 mmol, 1.0 equiv), Oxone (0.15 mmol, 3.0 equiv), and CH_3CN (0.5 mL) under 40 W blue LED irradiation with fan cooling (30±5 °C) for 3 h; Yields were determined by GC analysis using hexafluorobenzene as internal standard. [c]HFIP (2.0 mL) as a solvent. [d]Isolated yield. [e]**2w** (0.30 mmol, 3.0 equiv).

5.2.3. Mechanistic studies

To determine the underlying reaction mechanism, several control experiments and computational studies were conducted. The intermediary of the CF_3 radical in the reaction was first examined (Table 5.4a). The liberation of the CF_3 radical from **1a** is experimentally and computationally well-documented. [12a, 14a, 14b] In agreement with the previous reports, introduction of a radical scavenger, TEMPO (2,2,6,6-tetramethylpiperidine-*N*-oxyl radical) or BHT (2,6-di-*tert*-butyl-4-methylphenol), suppressed the trifluoromethylation of **2a**, with simultaneous formation of the **TEMPO–CF_3** adduct in 94% yield, clearly indicating that CF_3 radical formation is involved in the product-forming pathway.

Next, deuterium labelling experiments using deuterated cyclohexane (**2a-d_{12}**) and acetonitrile were conducted to determine the applicability of the generated CF_3 radical as the HAT reagent against the aliphatic C–H bonds (Table 5.4b). A sulfate radical, which can be generated from Oxone additive, was also reported as a HAT reagent that can activate C–H bonds.[8, 12a, 12c] However, as the reaction proceeded without Oxone, albeit in a lower yield (16%, Table 5.1, entry 6), it is unlikely that the HAT mediated by the sulfate radical is the major C–H activating process. With **2a** and **2a-d_{12}** as C–H substrates in a CD_3CN solvent, fluoroforms (HCF_3, >34% and DCF_3, >12%) were observed by ^{19}F NMR spectroscopy (entries 1–2). It should be noted that no DCF_3 was detected in the reaction with **2a** in CD_3CN indicating the reaction between a trifluoromethyl source and CD_3CN is not facile. Without cyclohexane, DCF_3 was not observed from the reaction between **1a** and CD_3CN, confirming that hydrogen or deuterium in the generated fluoroforms mainly

originated from cyclohexane (entry 3). When the reaction was performed with **2a-d_{12}** in CH_3CN, DCF_3 (>8%) was observed along with a non-negligible amount of HCF_3 (>12%, entry 4). This may originate from HAT from CH_3CN because the reaction between **1a** and CH_3CN without cyclohexane generated HCF_3 (>40%, entry 5). These results clearly indicate that the trifluoromethyl radical serves as the HAT reagent in the reaction.

Table 5.4 Control experiments regarding the CF_3 radical as a HAT reagent

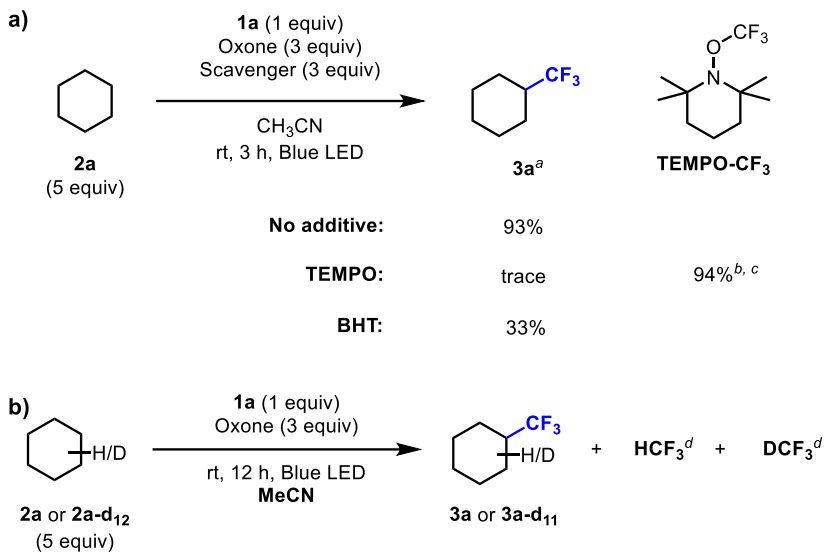

Entry	**2a**/**2a-d$_{12}$**	Solvent	**3a**/**3a-d$_{11}$** (%)	HCF_3 (%)	DCF_3 (%)
1	**2a**	CD_3CN	35	>34	N. D.
2	**2a-d$_{12}$**	CD_3CN	17	>9	>12
3	-	CD_3CN	-	>5	N. D.
4	**2a-d$_{12}$**	CH_3CN	12	>12	>8
5	-	CH_3CN	-	>40	-

[a]Yields determined by GC analysis using hexafluorobenzene as an internal standard. [b]Yields determined by ^{19}F NMR analysis using fluorobenzene as an internal standard. [c]Product was confirmed by HRMS. [d]NMR tube reactions were performed. The amount of dissolved gaseous fluoroform was only determined by ^{19}F NMR analysis using fluorobenzene as an internal standard. N. D. = not detected.

After identification of the CF_3 radical as the HAT reagent, three product forming pathways were proposed; (1) direct coupling between the alkyl and CF_3 radicals, (2) C–CF_3 reductive elimination via a Cu(III)–alkyl complex similar to recent reports on **1a**-mediated trifluoromethylation reactions,[12a, 12c, 14a, 14c] and (3) radical polar crossover involving ionic coupling between an alkyl cation and trifluoromethyl anion. The first possibility, involving the selective coupling of two transient radical species, is unlikely because no homodimerization product was observed with or without Oxone. This indicates that the free alkyl radical species may not be sufficiently generated for the radical-radical coupling reaction. Secondly, reductive elimination is a viable pathway for C–CF_3 bond formation with **1a** as the trifluoromethylating reagent. A Cu(II) complex has been proposed to trap a carbon-centered radical, subsequently forming the desired C–CF_3 bond via concerted reductive elimination.[12a, 12c, 14a, 14c] Recently, anionic or neutral alkyl-$Cu^{III}(CF_3)_x$ complexes were investigated to disclose that C(sp^3)–CF_3 bonds can be formed via concerted reductive elimination from a high-valent copper species.[24] Lastly, a radical-polar crossover pathway for the ionic coupling was proposed. In this case, alkyl radical, which has low oxidation potential ($E^o_{calc}(Cy^{\cdot}/Cy^+)$ = +0.46 V), is oxidized to generate an alkyl cation, followed by ionic coupling with a CF_3 anion for bond formation. C–X (X = F, CF_3) bonds can be formed via electron transfer from the alkyl radical to Cu^{II}–X.[14d, 25] We hypothesized that the oxidant can accelerate electron transfer from the alkyl radical, facilitating the radical-polar crossover pathway.

To determine the most viable pathway, density-functional theory (DFT) studies of the two proposed pathways were conducted with **2a** as model substrate at

the B3LYP-D3/6-311++G**/SDD level of theory (Figure 5.1). Time-dependent density functional theory (TD-DFT) computations on complex **1a** revealed relevant singlet transitions in the blue light region, giving rise to **1a*** (Figure 5.11). This complex would then undergo intersystem crossing (ISC), traversing the triplet excited ^{3}**1a** to release CF_3 radical **CF_3-rad** and ^{2}**I**, as previously reported by the Cook group.[14a] Beginning with this species, HAT of **CF_3-rad** against cyclohexane **2a** is facile with a barrier of only 10.9 kcal/mol. This is reasonable considering the relative instability of the CF_3 radical and its electrophilic nature. After the HAT event, the reaction pathway could follow one of the two aforementioned mechanisms. The reductive elimination pathway (orange trace) involving the Cy–Cu(III) complex ^{1}**II** exhibited an overall barrier of 20.8 kcal/mol. All attempts to find alternative pathways of reductive elimination from ^{1}**II** with a lower energy barrier which can compete with the oxidative pathway (*vide infra*) were unsuccessful. The bisulfate ligand-assisted reductive elimination process, as proposed by the Cook group, has a computed activation barrier of 14.8 kcal/mol (Figure 5.10).[14a]

In contrast, the DFT computation suggested that chemical oxidation of ^{2}**I** with Oxone affords a Cu(III)–bisulfate species ^{1}**IV** (blue trace), located at –35.1 kcal/mol. This is due to the strong oxidation power of Oxone, providing results analogous to previous work by the Cook group where persulfate served as the oxidant to produce the identical Cu species ($E°_{calc}$[^{2}**I**/^{1}**IV**] = +0.98 V, E°(Oxone) = +1.81 V).[14a] With this Cu species, single-electron oxidation of cyclohexyl radical was modeled using the Marcus theory, and the energy barrier of the electron transfer was 5.3 kcal/mol. The exotherm of the oxidation was –5.0 kcal/mol, indicating a good match in terms of redox potentials ($E°_{calc}$[^{1}**IV**/^{2}**IV-anion**] = +0.67 V,

$E°_{calc}(Cy^{\cdot}/Cy^{+})$ = +0.46 V). The generated transient Cu(II) complex **^{2}IV-anion** will undergo structural rearrangement to liberate a trifluoromethyl anion, which can spontaneously recombine with the cyclohexyl cation **Cy-cat** to furnish the desired product with a strong driving force of 67.8 kcal/mol. It should be noted that the oxidation of other Cu species, including **^{1}II**, could eventually generate the **^{2}IV-anion** and **Cy-cat**. Overall, for unactivated alkanes, the activation barrier was much lower for the radical-polar crossover pathway (5.3 kcal/mol) compared to the reductive elimination pathway (20.8 kcal/mol), accounting for the improved reaction efficiency with an oxidant. Although we cannot rule out the possibility of a direct single electron oxidation between **Cy-rad** and Oxone, we think that the proposed Cu(III)-bisulfate mediated oxidation of **Cy-rad** is more reasonable for providing an anionic CF_3 source via reduction of the resulting Cu(III) species for the trifluoromethylation.

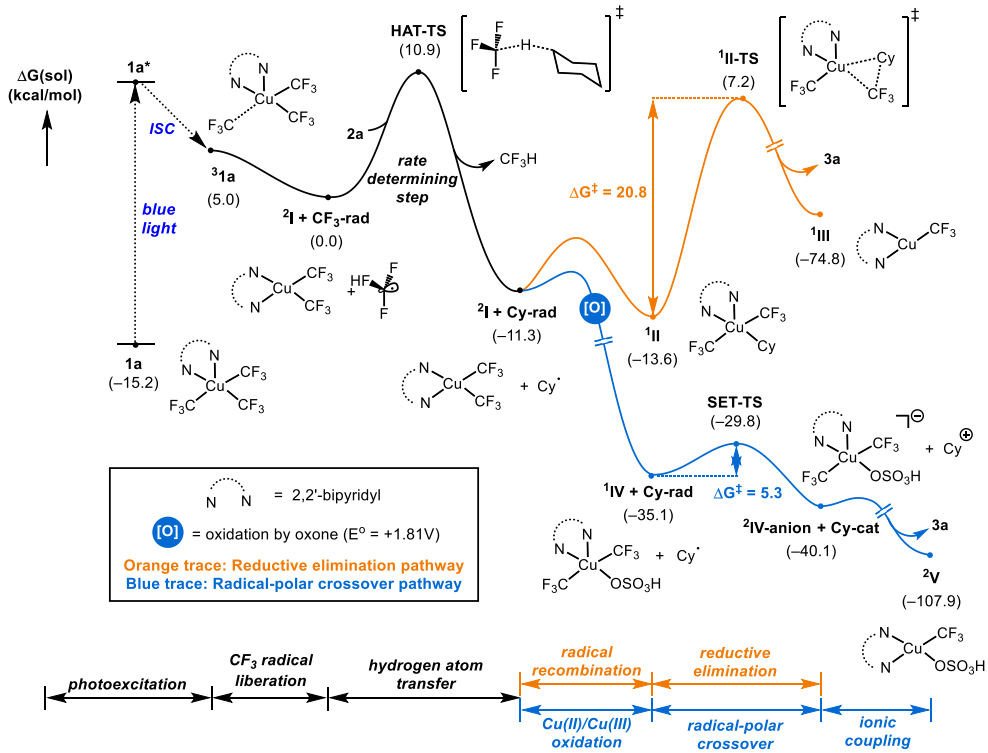

Figure 5.1. Computational results following the proposed reaction pathway

Based on the computational study, further experiments were performed to verify the proposed mechanism. First, the kinetic isotope effect (KIE) was measured using **2a** and **2a-d$_{12}$** to elucidate the rate-determining step (Scheme 5.2). Primary KIE values of 4.2 (parallel reaction) and 5.2 (intermolecular competition) were obtained, clearly indicating that the HAT step is rate-determining, in good accordance with the DFT studies. If the reductive elimination were the major product forming pathway, a primary KIE would not be observed as the reductive elimination should be the rate-determining step (Figure 5.1). Besides, as the only masses of the products obtained from the intermolecular competition experiment were *m/z* 152.1 (**3a**) and 163.2 (**3a-d$_{11}$**), we could conclude that the C–H cleavage is irreversible. This phenomenon is in good agreement with our DFT-computed energy profile

where reverse hydrogen atom transfer possesses a higher barrier compared to the forward reactions.

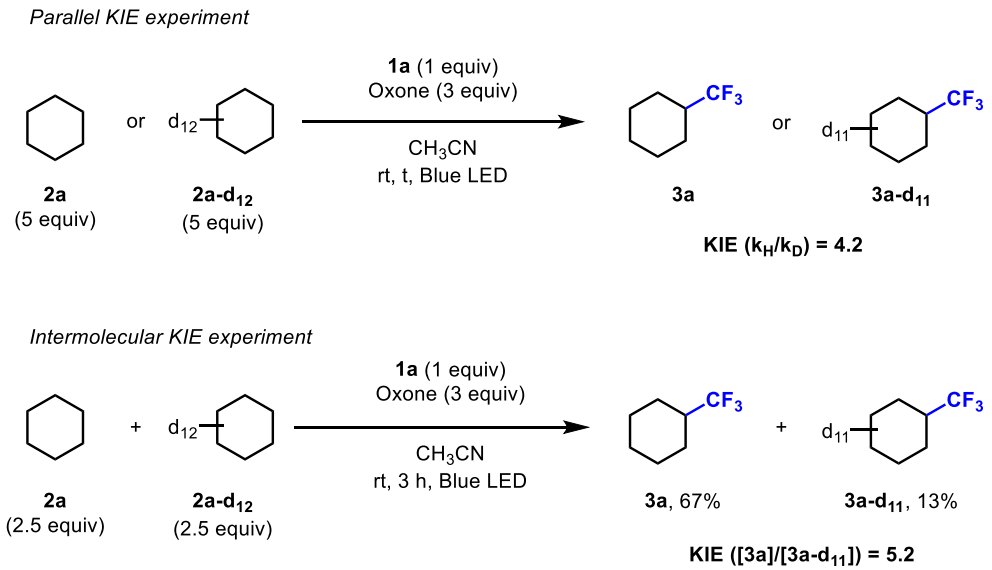

Scheme 5.2 H/D kinetic isotope effect

Secondly, we attempted to trap an alkyl cation intermediate that could arise from the radical-polar crossover pathway (Table 5.5). From Table 5.1, the standard reaction with **2a** under anhydrous conditions produced **3a** without significant by-product production (entry 1). Upon water addition, a significant amount of cyclohexanone **4a** (14%) was observed, which can be generated from the reaction between the cyclohexyl cation and water to furnish cyclohexanol, followed by subsequent oxidation to form the ketone (entry 2). Increased water contents facilitated the formation of **4a** (20%, entry 3) and without Oxone, no **4a** was generated (entry 4). Cycloheptane **2c** also produced **3c** in a decreased yield (25%) with increased cycloheptanone by-product **4c** (16%) under the co-solvent conditions of increased amount of water (CH_3CN/H_2O, 1:1 (v/v)). This clearly suggested that a

carbocation is generated under the reaction conditions. It has been reported that a persulfate can be homolytically cleaved via UV irradiation, acting as a HAT reagent.[12a, 26] However, under the reaction conditions without **1a**, neither oxidation nor dimerized products were observed, indicating that Oxone itself cannot perform the HAT from **2a** under the blue light irradiation conditions used herein (entry 5).

Table 5.5 Oxidation product detection[a]

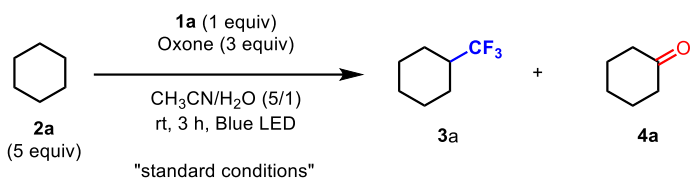

Entry	Variation from the "standard conditions"	**3a** (%)	**4a** (%)
1	Anhydrous condition	93	N. D.
2	None	63	14
3	CH_3CN/H_2O (1/1)	19	20
4	No Oxone	31	N. D.
5	No **1a**	-	N. D.

[a]Yields determined by GC analysis using hexafluorobenzene as an internal standard.

In summary, driven by the photo irradiation of **1a**, the homolytically cleaved CF_3 radical conducts the HAT from a C(sp^3)–H bond of alkane substrate, as experimentally supported by trapping CF_3 radical and detection of fluoroform HCF_3. Oxone dramatically increased the reaction efficiency by oxidizing the resulting Cu(II) complex ^{2}**I** to Cu(III) ^{1}**IV** which can oxidize the alkyl radical to form an alkyl cation. Formation of **4a** in presence of water supports the existence of an alkyl cation. The produced anionic Cu(II) complex ^{2}**IV-anion** acts as a CF_3 anion source that undergoes ionic coupling with the alkyl cation to form the C(sp^3)–CF_3 bond.

5.3. Conclusion

In conclusion, a novel C(sp^3)–H trifluoromethylation was developed using a photo-induced high-valent Cu–CF_3 complex. Diverse unactivated alkanes including bioactive molecules were trifluoromethylated using bench-stable bpyCu(CF_3)$_3$ **1a** under mild reaction conditions, favoring the methylene and less-sterically hindered C(sp^3)–H bonds. The experimental and computational mechanistic studies suggested that the reaction proceeds via the CF_3 radical-mediated HAT reaction to activate C(sp^3)–H bonds, followed by radical-polar crossover and ionic coupling. Notably, **1a** performs multiple roles as the photo-induced reaction initiator, precursor of the CF_3 radical as a unique HAT reagent, and trifluoromethylating source. It is anticipated that the developed operatively simple reaction will have wide-scale applications especially for late-stage, single-step trifluoromethylation of functional molecules.

5.4. Experimental section

5.4.1. General information

Unless otherwise noted, all reactions were performed under inert conditions. All chemicals were purchased from commercial sources (Sigma-Aldrich, Alfa Aesar, TCI, or Strem) and used without further purification. Unless otherwise noted, all reactions were conducted under irradiation by 40 W blue LED lamps purchased from Kessil (Kessil A160WE) using a maximum light intensity and the shortest wavelength setup. Reactions were monitored by thin-layer chromatography (TLC) on EMD Silica Gel 60 F254 plates, and visualized by staining with potassium permanganate and heating. Nuclear magnetic resonance (NMR) spectra were recorded in $CDCl_3$ and acetone-d_6 on a Bruker DPX-300 (300 MHz) spectrometer, Varian 400 and 500 NMR (400 and 500 MHz), Bruker AVANCE 300 (300 MHz), Bruker AVANCE 400 (400 MHz), Bruker AVANCE III HD (400 MHz), Bruker AVANCE NEO (500 MHz), or Agilent DD-2 (600 MHz). The residual solvent signal was used as a reference. Chemical shifts are reported in ppm, and coupling constants are given in Hz. Gas chromatography (GC) was carried out using a 7890A or 7890B GC system (Agilent Technologies) equipped with an HP-5ms column and a flame ionization detector (FID). UV-Vis spectra were recorded using Shimadzu UV-2600. X-ray diffraction data were collected on a Bruker D8 QUEST by using APEX III software. High-resolution mass spectrometry (HRMS) was performed at the Korea Basic Science Institute (KBSI) for EI and FAB methods.

5.4.2. Optimization of reaction condition

Optimization of reaction conditions

"Standard conditions" reaction was performed under the following procedure. To a 4 mL vial equipped with a PTFE-coated stirrer bar were added bpyCu(CF_3)$_3$ **1a** (0.050 mmol, 1.0 equiv), Oxone (0.15 mmol, 3.0 equiv), cyclohexane (0.25 mmol, 5.0 equiv), and CH_3CN (0.5 mL) in an argon-filled glove box. The resulting mixture was stirred for 3 h under 40 W blue LED irradiation with fan cooling (30±5 °C). Hexafluorobenzene was added as an internal standard, and the crude mixture was analyzed by GC to determine the product yields. For entry 10, the reaction was conducted under irradiation by 52 W 390 nm LED lamps purchased from Kessil (Kessil PR160L-390) using a maximum light intensity and the shortest wavelength setup.

Optimization of solvents

To a 4 mL vial equipped with a PTFE-coated stirrer bar were added bpyCu(CF_3)$_3$ **1a** (0.050 mmol, 1.0 equiv), Oxone (0.15 mmol, 3.0 equiv), cyclohexane (0.25 mmol, 5.0 equiv), and solvent (0.5 mL) in an argon-filled glove box. The resulting mixture was stirred for 3 h under 40 W blue LED irradiation with fan cooling (30±5 °C). Hexafluorobenzene was added as an internal standard, and the crude mixture was analyzed by GC to determine the product yields. N. D. = not detected.

Table 5.6 Solvent optimization

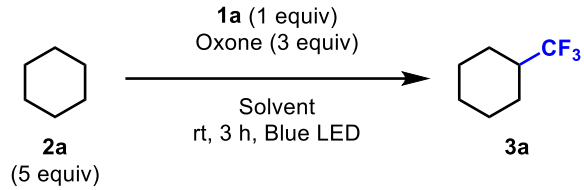

Entry	Solvent	Yield **3a** (%)
1	CH_3CN	93
2	CH_2Cl_2	21
3	*N,N*-Dimethylformamide (DMF)	10
4	*N,N*-Dimethylacetamide (DMA)	10
5	Tetrahydrofuran (THF)	N. D.
6	1,4-dioxane	N. D.
7	Dichloroethane (DCE)	16
8	Dimethyl sulfoxide (DMSO)	23
9	Acetone	15
10	Hexafluoroisopropanol (HFIP)	19

Optimization of copper complexes

To a 4 mL vial equipped with a PTFE-coated stirrer bar were added copper complex (0.050 mmol, 1.0 equiv), Oxone (0.15 mmol, 3.0 equiv), cyclohexane (0.25 mmol, 5.0 equiv), and CH_3CN (0.5 mL) in an argon-filled glove box. The resulting mixture was stirred for 12 h under 40 W blue LED irradiation with fan cooling (30±5 °C).

Hexafluorobenzene was added as an internal standard, and the crude mixture was analyzed by GC to determine the product yields.

Reported condition by Cook using 2a[12a]

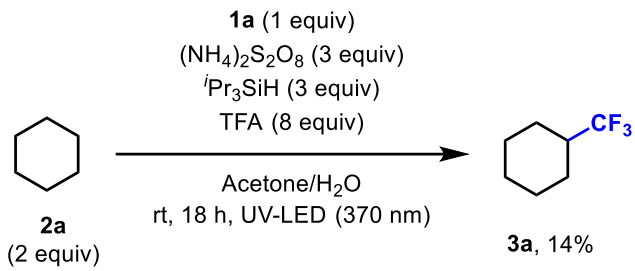

To a 4 mL vial equipped with a PTFE-coated stirrer bar were added bpyCu(CF_3)$_3$ **1a** (0.050 mmol, 1.0 equiv), $(NH_4)_2S_2O_8$ (0.15 mmol, 3.0 equiv), cyclohexane **2a** (0.10 mmol, 2.0 equiv), and acetone (0.3 mL), followed by $^{i}Pr_3SiH$ (0.15 mmol, 3.0 equiv) in an argon-filled glove box. Water (0.3 mL) and trifluoroacetic acid (0.40 mmol, 8.0 equiv) were added outside the glove box. The resulting mixture was stirred for 18 h under 43 W 370 nm LED lamps purchased from Kessil (Kessil PR160-370) using a maximum light intensity and the shortest wavelength set up with fan cooling. The reaction mixture was quenched with saturated aqueous $NaHCO_3$. Hexafluorobenzene was added as an internal standard, and the crude mixture was analyzed by GC to determine **3a** as 14%.

5.4.3. Cu complex preparation and characterization

Synthesis of bpyCu(CF_3)$_3$ (1a)

Reaction procedure was modified from reported procedure.[27] To a 250 mL Schlenk round-bottom flask were added copper (I) iodide (10 mmol), 2,2'-bipyridine (10 mmol), silver (I) fluoride (40 mmol) in an argon-filled glove box. DMF (13 mL) was added outside of glove box, and stirred for 30 min. $TMSCF_3$ (65 mmol) was slowly added (10 mL/h) under argon flow. The resulting mixture was stirred for 18 h at room temperature. The resulting mixture was filtered through a pad of Celite®, eluted with acetone, and concentrated under reduced pressure. Methanol was added (200 mL) to the resulting residue, and recrystallized under –20 ºC overnight. Recrystallized yellow solid was filtered with glass-filter funnel, and dried to afford pure **1a** bpyCu(CF_3)$_3$ as the product.

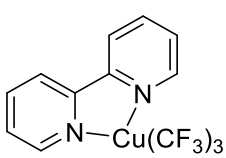

^{1}H NMR (400 MHz, DMSO-d_6) δ 9.20 (d, J = 5.2 Hz, 2H), 8.77 (d, J = 8.1 Hz, 2H), 8.35 (td, J = 7.9, 1.6 Hz, 2H), 7.88 (ddd, J = 7.7, 5.2, 1.1 Hz, 2H). ^{19}F NMR (376 MHz, DMSO-d_6) δ -23.97 (hept, J = 9.3 Hz), -36.11 (q, J = 9.1 Hz).

Synthesis of $L_nCu(CF_3)_3$ complexes

Reaction procedure was modified from reported procedure.[27] To a 100 mL or 50 mL Schlenk round-bottom flask were added copper (I) iodide (1 mmol), ligand (1 mmol), silver (I) fluoride (4 mmol) in an argon-filled glove box. DMF (3 mL) was added outside of glove box, and stirred for 30 min. $TMSCF_3$ (6.5 mmol) was slowly added under argon flow. The resulting mixture was stirred for 18 h at room temperature. The resulting mixture was filtered through a pad of Celite®, eluted with acetone, and concentrated under reduced pressure. The resulting residue was purified by flash column chromatography to afford the desired product.

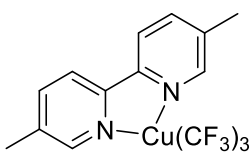

(5,5'-Dimethyl-2,2'-dipyridyl)$Cu(CF_3)_3$ (1b)

^{1}H NMR (400 MHz, Acetone-d_6) δ 9.17 – 8.98 (m, 2H), 8.57 (d, J = 8.3 Hz, 2H), 8.19 (d, J = 8.2 Hz, 2H), 2.63 (s, 6H). ^{19}F NMR (376 MHz, Acetone-d_6) δ -24.74 (hept, J = 9.5 Hz), -37.63 (q, J = 9.4 Hz). ^{13}C NMR (101 MHz, Acetone-d_6) δ 148.72, 147.68, 140.87, 137.34, 121.88, 17.38. HRMS-FAB (*m/z*): $[M\text{-}CF_3]^+$ calcd for $C_{14}H_{12}CuF_6N_2$: 385.0201. Found: 385.0197.

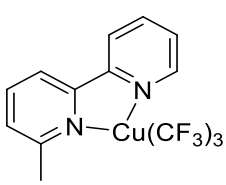

(6-Methyl-2,2'-dipyridyl)$Cu(CF_3)_3$ (1c)

^{1}H NMR (400 MHz, $CDCl_3$) δ 9.23 (d, *J* = 4.4 Hz, 1H), 8.23 (d, *J* = 8.1 Hz, 1H), 8.19 – 8.08 (m, 2H), 8.02 (t, *J* = 7.8 Hz, 1H), 7.72 (ddd, *J* = 7.6, 5.0, 1.1 Hz, 1H), 7.56 (d, *J* = 7.5 Hz, 1H), 3.25 (s, 3H). ^{19}F NMR (376 MHz, $CDCl_3$) δ -24.30 (hept, *J* = 8.8 Hz), -35.83 (q, *J* = 9.7 Hz).^{13}C NMR (101 MHz, Acetone-d_6) δ 158.80, 149.90, 149.57, 148.84, 140.99, 140.44, 127.06, 126.74, 122.62, 120.50, 24.06. HRMS-FAB (*m/z*): $[M\text{-}CF_3]^+$ calcd for $C_{13}H_{10}CuF_6N_2$: 371.0044. Found: 371.0042.

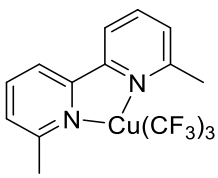

(6,6'-Dimethyl-2,2'-dipyridyl)Cu(CF_3)$_3$ (1d)

^{1}H NMR (400 MHz, $CDCl_3$) δ 7.96 (d, *J* = 7.9 Hz, 2H), 7.89 (t, *J* = 7.8 Hz, 2H), 7.45 (d, *J* = 7.6 Hz, 2H), 3.10 (s, 6H). ^{19}F NMR (376 MHz, $CDCl_3$) δ -25.73 (hept, *J* = 9.8 Hz), -34.38 (q, *J* = 9.7 Hz). ^{13}C NMR (101 MHz, Acetone-d_6) δ 158.93, 149.57, 140.68, 126.92, 120.22, 23.58. HRMS-FAB (*m/z*): $[M\text{-}CF_3]^+$ calcd for $C_{14}H_{12}CuF_6N_2$: 385.0201. Found: 385.0204.

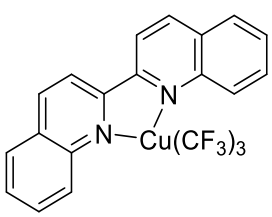

(2,2'-Biquinoline)Cu(CF_3)$_3$ (1e)

^{1}H NMR (400 MHz, Acetone-d_6) δ 9.08 – 9.03 (m, 4H), 9.01 (d, *J* = 8.5 Hz, 2H), 8.34 (d, *J* = 8.2 Hz, 2H), 8.25 (ddd, *J* = 8.5, 6.9, 1.4 Hz, 2H), 8.02 – 7.93 (m, 2H). ^{19}F NMR (376 MHz, Acetone-d_6) δ -21.32 (hept, *J* = 9.9 Hz), -30.47 (q, *J* = 10.0 Hz).

^{13}C NMR (101 MHz, Acetone-d_6) δ 150.58, 145.60, 141.73, 132.99, 129.71, 129.49, 128.90, 127.83, 119.98. HRMS-FAB (*m/z*): $[M\text{-}CF_3]^+$ calcd for $C_{20}H_{12}CuF_6N_2$: 457.0201. Found: 457.0202.

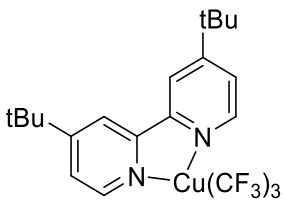

(4,4'-Di-*tert*-butyl-2,2'-dipyridyl)Cu(CF_3)$_3$ (1f)

^{1}H NMR (400 MHz, Acetone-d_6) δ 9.15 (d, *J* = 5.6 Hz, 2H), 8.80 (d, *J* = 1.3 Hz, 2H), 7.96 (dd, *J* = 5.6, 1.9 Hz, 2H), 1.50 (s, 18H). ^{19}F NMR (376 MHz, Acetone-d_6) δ -24.81 (hept, *J* = 9.2 Hz), -37.51 (q, *J* = 9.4 Hz). ^{13}C NMR (101 MHz, Acetone-d6) δ 165.09, 150.05, 148.54, 123.76, 119.95, 35.54, 29.65. HRMS-FAB (*m/z*): $[M\text{-}CF_3]^+$ calcd for $C_{20}H_{24}CuF_6N_2$: 469.1140. Found: 469.1141.

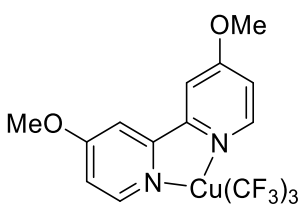

(4,4'-Dimethoxy-2,2'-dipyridyl)Cu(CF_3)$_3$ (1g)

^{1}H NMR (400 MHz, $CDCl_3$) δ 8.93 (d, *J* = 6.1 Hz, 2H), 7.59 (d, *J* = 2.5 Hz, 2H), 7.13 (dd, *J* = 6.1, 2.4 Hz, 2H), 4.03 (s, 6H). ^{19}F NMR (376 MHz, $CDCl_3$) δ -23.95 (hept, *J* = 9.5 Hz), -37.28 (q, *J* = 9.4 Hz). ^{13}C NMR (101 MHz, Acetone-d_6) δ 168.90, 151.79, 149.88, 112.20, 109.37, 56.25. HRMS-FAB (*m/z*): $[M\text{-}CF_3]^+$ calcd for $C_{14}H_{12}CuF_6N_2O_2$: 417.0099. Found: 417.0097.

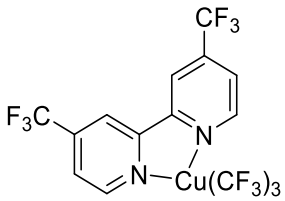

(4,4'-Bis(trifluoromethyl)-2,2'-dipyridyl)Cu(CF_3)$_3$ (1h)

^{1}H NMR (400 MHz, CD_2Cl_2) δ 9.45 (d, *J* = 5.4 Hz, 2H), 8.62 (s, 2H), 8.10 (d, *J* = 6.1 Hz, 2H). ^{19}F NMR (376 MHz, CD_2Cl_2) δ -23.40 (hept, *J* = 10.2 Hz), -37.26 (q, *J* = 9.7 Hz), -65.20. ^{13}C NMR (101 MHz, CD_2Cl_2) δ 150.55, 150.12, 142.25 (d, *J* = 35.6 Hz), 123.37 (q, *J* = 3.7 Hz), 121.85 (q, *J* = 274.2 Hz), 118.92 (q, *J* = 3.0 Hz). HRMS-FAB (*m/z*): $[M\text{-}CF_3]^+$ calcd for $C_{14}H_6CuF_{12}N_2$: 492.9635. Found: 492.9639.

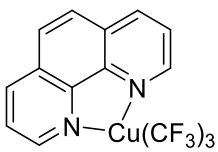

(1,10-Phenanthroline)Cu(CF_3)$_3$ (1i)[28]

^{1}H NMR (400 MHz, CD_2Cl_2) δ 9.47 (dd, *J* = 4.8, 1.5 Hz, 2H), 8.67 (dd, *J* = 8.2, 1.5 Hz, 2H), 8.10 (s, 2H), 8.06 (dd, *J* = 8.2, 4.8 Hz, 2H). ^{19}F NMR (376 MHz, CD_2Cl_2) δ -24.46 (hept, *J* = 10.4 Hz), -37.46 (q, *J* = 9.6 Hz).

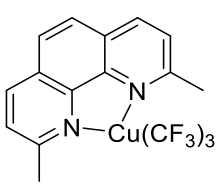

(2,9-Dimethyl-1,10-phenanthroline)Cu(CF_3)$_3$ (1j)

^{1}H NMR (400 MHz, $CDCl_3$) δ 8.42 (d, J = 8.3 Hz, 2H), 7.91 (s, 2H), 7.81 (d, J = 8.3 Hz, 2H), 3.37 (s, 6H). ^{19}F NMR (376 MHz, Acetone-d_6) δ -26.23 (hept, J = 9.6 Hz), -34.81 (q, J = 9.7 Hz). ^{13}C NMR (101 MHz, $CDCl_3$) δ 159.92, 141.05, 138.40, 127.40, 125.83, 125.79, 25.14. HRMS-FAB (*m/z*): $[M\text{-}CF_3]^+$ calcd for $C_{16}H_{12}CuF_6N_2$: 409.0201. Found: 409.0200.

5.4.4. General procedure for substrate scopes

To a 8 mL vial equipped with a PTFE-coated stirrer bar were added bpy$Cu(CF_3)_3$ (0.1 mmol), Oxone (0.3 mmol), the corresponding C-H substrate (0.6 mmol), and appropriate solvent (CH_3CN or HFIP) (1.0 mL or 2.0 mL) in an argon-filled glove box. Water (0.2 mL) was added outside of glove box. The resulting mixture was stirred for 3 h under 40 W blue LED irradiation with fan cooling (30±5 °C). Magnesium sulfate was added to the resulting mixture to trap water, and filtered through a short pad of Celite®, eluted with CH_2Cl_2. If possible, the crude mixture was concentrated under reduced pressure, and the resulting residue was purified by flash column chromatography to afford the desired product.

5.4.5. Characterization of newly reported compounds

Some products (**3f** and **3g**) were not able to be isolate due to its volatility. As such, ^{1}H NMR and ^{13}C NMR of the isolated compounds could not be obtained. The crude ^{19}F NMR spectra, using C_6H_5F as an internal standard, were obtained and compared with authentic samples, along with HRMS analysis.[29]

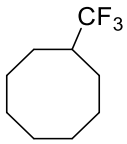

(Trifluoromethyl)cyclooctane (3d)

^{1}H NMR (400 MHz, $CDCl_3$) δ 2.32 – 2.13 (m, 1H), 1.92 – 1.73 (m, 4H), 1.65 – 1.45 (m, 10H). ^{19}F NMR (376 MHz, $CDCl_3$) δ -73.39 (d, J = 10.0 Hz). ^{13}C NMR (101 MHz, $CDCl_3$) δ 128.96 (q, J = 279.5 Hz), 41.91 (q, J = 24.3 Hz), 26.37, 26.28, 25.56 (q, J = 2.6 Hz), 25.10. HRMS-EI (*m/z*): $[M]^+$ calcd for $C_9H_{15}F_3$: 180.1126. Found: 180.1123.

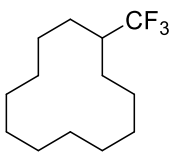

(Trifluoromethyl)cyclododecane (3e)

^{1}H NMR (400 MHz, $CDCl_3$) δ 2.24 – 2.11 (m, 1H), 1.64 – 1.28 (m, 22H). ^{19}F NMR (376 MHz, $CDCl_3$) δ -70.57 (d, J = 9.5 Hz). ^{13}C NMR (101 MHz, $CDCl_3$) δ 129.07 (q, J = 280.1 Hz), 38.66 (q, J = 24.4 Hz), 29.71, 24.04, 23.66 (q, J = 2.5 Hz), 23.60, 23.42, 22.27. HRMS-EI (*m/z*): $[M]^+$ calcd for $C_{13}H_{23}F_3$: 236.1752. Found: 236.1752.

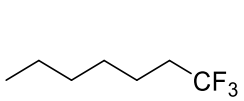

3fa

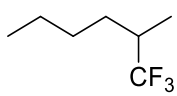

3fb

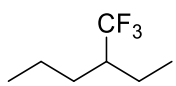

3fc

1-(Trifluoromethyl)hexane (3fa), 2-(trifluoromethyl)hexane (3fb), and 3-(trifluoromethyl)hexane (3fc)

HRMS-EI (*m/z*): $[M]^+$ calcd for $C_7H_{13}F_3$: 154.0969. Found: 154.0967.

1-(Trifluoromethyl)hexane (3fa)

^{19}F NMR (376 MHz, $CDCl_3$) δ -66.56 (t, *J* = 10.9 Hz).

2-(Trifluoromethyl)hexane (3fb)

^{19}F NMR (376 MHz, $CDCl_3$) δ -73.43 (d, *J* = 9.3 Hz).

3-(Trifluoromethyl)hexane (3fc)

^{19}F NMR (376 MHz, $CDCl_3$) δ -70.21 (d, *J* = 9.7 Hz).

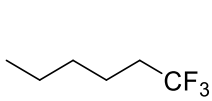

3ga

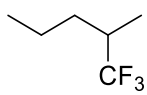

3gb

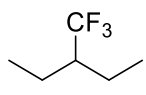

3gc

1-(Trifluoromethyl)pentane (3ga), 2-(trifluoromethyl)pentane (3gb), and 3-(trifluoromethyl)pentane (3gc)

HRMS-EI (*m/z*): $[M]^+$ calcd for $C_6H_{11}F_3$: 140.0813. Found: 140.0811.

1-(Trifluoromethyl)pentane (3ga)

^{19}F NMR (376 MHz, $CDCl_3$) -66.54 (t, *J* = 11.0 Hz).

2-(Trifluoromethyl)pentane (3gb)

^{19}F NMR (376 MHz, $CDCl_3$) δ -73.48 (d, *J* = 9.3 Hz).

3-(Trifluoromethyl)pentane (3gc)

^{19}F NMR (376 MHz, $CDCl_3$) δ -69.82 (d, *J* = 9.7 Hz).

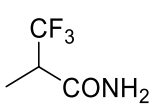

3,3,3-Trifluoro-2-methylpropanamide (3m)

^{1}H NMR (400 MHz, $CDCl_3$) δ 5.64 (s, 2H), 3.17 – 3.00 (m, 1H), 1.42 (d, *J* = 7.2 Hz, 3H). ^{19}F NMR (376 MHz, $CDCl_3$) δ -69.69 (d, *J* = 8.8 Hz). ^{13}C NMR (101 MHz, $CDCl_3$) δ 168.42, 125.40 (q, *J* = 279.2 Hz), 45.38 (q, *J* = 27.5 Hz), 11.03 (q, *J* = 2.9 Hz). HRMS-EI (*m/z*): $[M]^+$ calcd for $C_4H_6F_3NO$: 141.0401. Found: 141.0403.

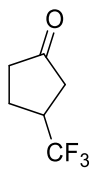

3nb

3-(trifluoromethyl)cyclopentan-1-one (3nb)

^{1}H NMR (400 MHz, $CDCl_3$) δ 3.02 – 2.88 (m, 1H), 2.61 – 2.18 (m, 5H), 2.16 – 2.01 (m, 1H). ^{19}F NMR (376 MHz, $CDCl_3$) δ -72.41 (d, *J* = 8.7 Hz). ^{13}C NMR (101 MHz, $CDCl_3$) δ 214.55, 127.26 (q, *J* = 276.9 Hz), 40.08 (q, *J* = 28.6, 28.1 Hz), 37.91, 37.06, 22.40. HRMS-EI (*m/z*): $[M]^+$ calcd for $C_6H_7F_3O$: 152.0449. Found: 152.0450.

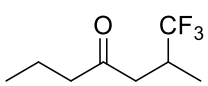

1,1,1-Trifluoro-2-methylheptan-4-one (3p)

^{1}H NMR (400 MHz, $CDCl_3$) δ 2.90 – 2.79 (m, 1H), 2.74 (dd, *J* = 17.7, 3.6 Hz, 1H), 2.54 – 2.29 (m, 3H), 1.70 – 1.52 (m, 2H), 1.10 (d, *J* = 6.9 Hz, 3H), 0.92 (t, *J* = 7.4 Hz, 3H). ^{19}F NMR (376 MHz, $CDCl_3$) δ -73.67 (d, *J* = 9.1 Hz). ^{13}C NMR (101 MHz, $CDCl_3$) δ 207.17, 128.10 (q, *J* = 278.7 Hz), 45.23, 42.39 (q, *J* = 2.2 Hz), 33.49 (q, *J* = 27.5 Hz), 17.18, 13.62, 13.17 (q, *J* = 3.0 Hz). HRMS-EI (*m/z*): $[M]^+$ calcd for $C_8H_{13}F_3O$: 182.0918. Found: 182.0916.

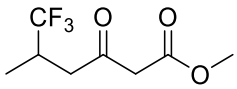

Methyl 6,6,6-trifluoro-5-methyl-3-oxohexanoate (3q)

^{1}H NMR (400 MHz, $CDCl_3$) δ 3.75 (s, 3H), 3.48 (s, 2H), 3.05 – 2.75 (m, 2H), 2.60 (q, *J* = 8.9 Hz, 1H), 1.13 (d, *J* = 6.9 Hz, 3H). ^{19}F NMR (376 MHz, $CDCl_3$) δ -73.66 (d, *J* = 8.8 Hz). ^{13}C NMR (151 MHz, $CDCl_3$) δ 199.04, 167.10, 127.81 (q, *J* = 278.7 Hz), 52.49, 49.11, 42.75 (q, *J* = 3.7 Hz), 33.42 (q, *J* = 27.8 Hz), 12.98 (q, *J* = 3.7 Hz). HRMS-EI (*m/z*): $[M]^+$ calcd for $C_8H_{11}F_3O_3$: 212.0660. Found: 212.0656.

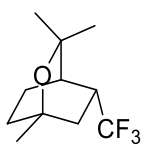

(1S,4R,5R)-1,3,3-Trimethyl-5-(trifluoromethyl)-2-oxabicyclo[2.2.2]octane (3r)

^{1}H NMR (600 MHz, $CDCl_3$) δ 2.99 – 2.82 (m, 1H), 1.95 – 1.82 (m, 3H), 1.73 – 1.64 (m, 2H), 1.56 (dd, *J* = 13.8, 5.8 Hz, 1H), 1.53 – 1.47 (m, 1H), 1.31 (s, 3H), 1.27 (s, 3H), 1.11 (s, 3H). ^{19}F NMR (376 MHz, $CDCl_3$) δ -68.87 (d, *J* = 10.6 Hz). ^{13}C NMR (101 MHz, $CDCl_3$) δ 127.14 (q, *J* = 278.0 Hz), 73.99, 70.18, 36.67 (q, *J* = 26.7 Hz), 33.09 (q, *J* = 2.1 Hz), 31.74 (q, *J* = 2.0 Hz), 31.05, 28.82, 28.55, 27.26, 16.46. HRMS-EI (*m/z*): $[M]^+$ calcd for $C_{11}H_{17}F_3O$: 222.1231. Found: 222.1232.

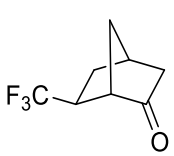

(1S,4S,5R)-5-(Trifluoromethyl)bicyclo[2.2.1]heptan-2-one (3s)

^{1}H NMR (400 MHz, $CDCl_3$) δ 2.85 – 2.77 (m, 2H), 2.52 – 2.36 (m, 1H), 2.21 – 2.07 (m, 1H), 1.99 – 1.89 (m, 3H), 1.86 – 1.77 (m, 1H), 1.75 – 1.66 (m, 1H). ^{19}F NMR (376 MHz, $CDCl_3$) δ -69.67 (d, *J* = 9.9 Hz). ^{13}C NMR (101 MHz, $CDCl_3$) δ 213.96, 127.47 (q, *J* = 278.1 Hz), 50.75 (q, *J* = 1.8 Hz), 44.04, 40.09 (q, *J* = 28.9 Hz), 35.41, 35.03, 30.02 (q, *J* = 2.0 Hz). HRMS-EI (*m/z*): $[M]^+$ calcd for $C_8H_9F_3O$: 178.0605. Found: 178.0607.

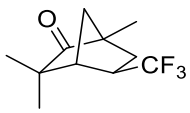

(1S,4R,5R)-1,3,3-Trimethyl-5-(trifluoromethyl)bicyclo[2.2.1]heptan-2-one (3t)

^{1}H NMR (600 MHz, $CDCl_3$) δ 2.78 – 2.63 (m, 1H), 2.38 (s, 1H), 1.91 (d, *J* = 11.5 Hz, 1H), 1.81 (d, *J* = 11.5 Hz, 1H), 1.74 – 1.65 (m, 2H), 1.17 (s, 3H), 1.11 (s, 3H), 1.08 (s, 3H). ^{19}F NMR (376 MHz, $CDCl_3$) δ -68.96 (d, *J* = 10.3 Hz). ^{13}C NMR (101 MHz, $CDCl_3$) δ 221.31, 128.02 (q, *J* = 278.2 Hz), 53.66, 48.10, 46.31 (q, *J* = 2.0 Hz), 40.99 (q, *J* = 27.7 Hz), 38.86 (q, *J* = 2.0 Hz), 33.26, 23.59, 21.42, 14.24. HRMS-EI (*m/z*): $[M]^+$ calcd for $C_{11}H_{15}F_3O$: 220.1075. Found: 220.1076.

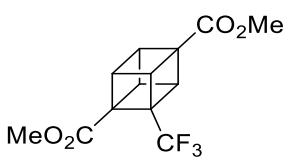

Dimethyl (1R,2S,3S,8S)-2-(trifluoromethyl)cubane-1,4-dicarboxylate (3u)

^{1}H NMR (600 MHz, $CDCl_3$) δ 4.38 (br, 2H), 4.26 – 4.22 (m, 2H), 4.18 (br, 1H), 3.73 (s, 3H), 3.71 (s, 3H). ^{19}F NMR (376 MHz, $CDCl_3$) δ -75.12. ^{13}C NMR (151 MHz, $CDCl_3$) δ 170.33, 168.81, 123.52 (q, *J* = 273.9 Hz), 56.06 (q, *J* = 3.3 Hz), 54.59 (q,

J = 37.1 Hz), 53.19, 52.05, 51.94, 47.82, 46.20 (q, *J* = 2.7 Hz), 44.76. HRMS-FAB (*m/z*): $[M+H]^+$ calcd for $C_{13}H_{12}F_3O_4$: 289.0682. Found: 289.0690.

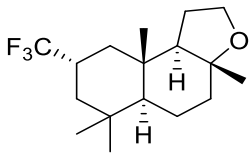

(3aR,5aS,8S,9aS,9bR)-3a,6,6,9a-Tetramethyl-8-(trifluoromethyl)dodecahydronaphtho[2,1-b]furan (3v)

^{1}H NMR (400 MHz, $CDCl_3$) δ 3.94 (td, *J* = 8.5, 4.5 Hz, 1H), 3.84 (q, *J* = 8.2 Hz, 1H), 2.49 – 2.28 (m, 1H), 1.97 (dt, *J* = 11.4, 3.1 Hz, 1H), 1.81 – 1.60 (m, 5H), 1.49 – 1.28 (m, 3H), 1.24 – 1.20 (m, 1H), 1.12 – 1.07 (m, 1H), 1.10 (s, 3H), 1.02 – 0.98 (m, 1H), 0.97 (s, 3H), 0.87 (s, 3H), 0.87 (s, 3H). ^{19}F NMR (376 MHz, $CDCl_3$) δ -72.93 (d, *J* = 8.3 Hz). ^{13}C NMR (101 MHz, $CDCl_3$) δ 127.07 (q, *J* = 277.8 Hz), 79.88, 65.11, 60.00, 56.90, 40.41 (q, *J* = 2.2 Hz), 39.65, 38.43 (q, *J* = 2.3 Hz), 36.17, 35.01 (q, *J* = 26.0 Hz), 33.46, 33.19, 22.71, 21.53, 21.33, 20.60, 15.69. HRMS-FAB (*m/z*): $[M-H]^+$ calcd for $C_{17}H_{26}F_3O$: 303.1930. Found: 303.1935.

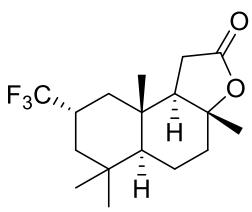

(3aR,5aS,8S,9aS,9bR)-3a,6,6,9a-Tetramethyl-8-(trifluoromethyl)decahydronaphtho[2,1-b]furan-2(1H)-one (3w)[29a]

^{1}H NMR (400 MHz, $CDCl_3$) δ 2.52 – 2.37 (m, 2H), 2.30 (dd, *J* = 16.2, 6.5 Hz, 1H), 2.14 (dt, *J* = 12.0, 3.3 Hz, 1H), 2.04 (dd, *J* = 14.7, 6.5 Hz, 1H), 1.96 (dq, *J* = 14.3,

3.2 Hz, 1H), 1.79 – 1.62 (m, 3H), 1.48 – 1.39 (m, 1H), 1.37 (s, 3H), 1.31 – 1.25 (m, 1H), 1.17 – 1.07 (m, 2H), 1.01 (s, 3H), 0.97 (s, 3H), 0.91 (s, 3H). ^{19}F NMR (376 MHz, $CDCl_3$) δ -72.98 (d, *J* = 8.2 Hz). ^{13}C NMR (101 MHz, $CDCl_3$) δ 176.22, 128.14 (q, *J* = 278.8 Hz), 86.01, 58.91, 56.30, 40.25 (q, *J* = 2.0 Hz), 38.63, 38.04 (q, *J* = 2.2 Hz), 36.02, 35.02 (q, *J* = 26.3 Hz), 33.26, 33.08, 28.74, 21.81, 21.34, 20.49, 15.75. HRMS-FAB (*m/z*): $[M-H]^+$ calcd for $C_{17}H_{24}F_3O_2$: 317.1723. Found: 317.1725.

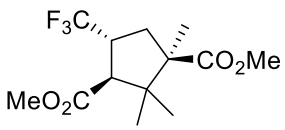

Dimethyl(1R,3S,4R)-1,2,2-trimethyl-4-(trifluoromethyl)cyclopentane-1,3-dicarboxylate (3x)

^{1}H NMR (600 MHz, $CDCl_3$) δ 3.73 (s, 3H), 3.69 (s, 3H), 3.42 – 3.29 (m, 1H), 2.99 – 2.91 (m, 2H), 1.67 (dd, *J* = 14.9, 5.0 Hz, 1H), 1.28 (s, 3H), 1.24 (s, 3H), 0.78 (s, 3H). ^{19}F NMR (376 MHz, $CDCl_3$) δ -70.82 (d, *J* = 9.6 Hz). ^{13}C NMR (151 MHz, $CDCl_3$) δ 175.13, 171.83, 127.69 (q, *J* = 277.5 Hz), 55.66, 53.40, 52.04, 51.89, 47.51, 41.21 (q, *J* = 28.2 Hz), 32.66, 22.38, 21.99, 21.35. HRMS-EI (*m/z*): $[M]^+$ calcd for $C_{13}H_{19}F_3O_4$: 296.1235. Found: 296.1232.

5.4.6. Mechanistic studies

UV-Vis absorption of copper complexes

UV-Vis spectra of $L_nCu(CF_3)_3$ (390 nm–460 nm)

UV-Vis absorption spectra of $L_nCu(CF_3)_3$ **1** were examined. Stock solutions of **1** were prepared by dissolving complexes in CH_3CN (0.4 mM). Absorption spectra were illustrated in the visible light range (390 nm–460 nm).

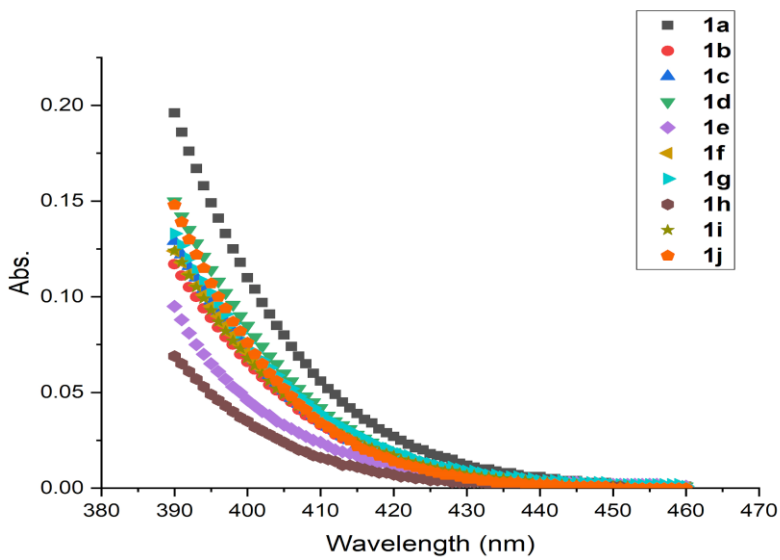

Figure 5.2 Absorption spectra (390 nm–460 nm) of **1a–1j** in 0.4 mM of CH_3CN

UV-Vis spectra of $L_nCu(CF_3)_3$ (250 nm–400 nm)

UV-Vis absorption spectra of $L_nCu(CF_3)_3$ **1** were examined. Stock solutions of **1** were prepared by dissolving complexes in CH_3CN (0.04 mM). Absorption spectra were illustrated in the light range of 250 nm–400 nm.

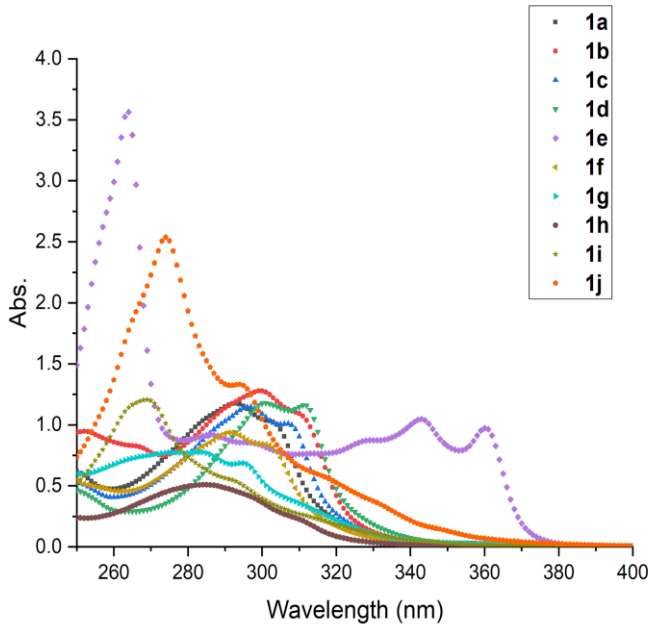

Figure 5.3 Absorption spectra (250 nm–400 nm) of **1a–1j** in 0.04 mM of CH_3CN

Reaction with radical scavenger

TEMPO as a radical scavenger

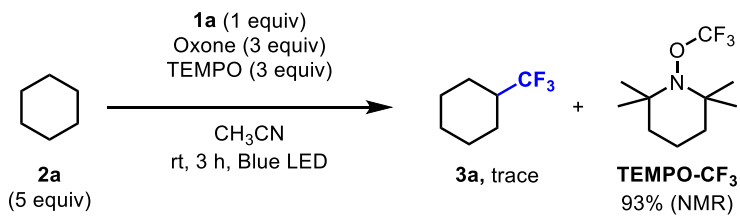

To a 4 mL vial equipped with a PTFE-coated stirrer bar were added bpyCu(CF_3)$_3$ **1a** (0.050 mmol, 1.0 equiv), Oxone (0.15 mmol, 3.0 equiv), cyclohexane **2a** (0.25 mmol, 5.0 equiv), 2,2,6,6-tetramethylpiperidine-*N*-oxyl radical (TEMPO, 0.15 mmol, 3.0

equiv), and CH_3CN (0.5 mL) in an argon-filled glove box. The resulting mixture was stirred for 3 h under 40 W blue LED irradiation with fan cooling (30±5 °C). Hexafluorobenzene was added as an internal standard to determine the yield of **3a** through GC analysis, and only a trace amount of **3a** was generated. The crude mixture was then concentrated under reduced pressure. Fluorobenzene was added as an internal standard, and the mixture was analyzed by ^{19}F NMR to determine the yields of **TEMPO–CF_3**. Based on ^{19}F-NMR, the yield of **TEMPO–CF_3** (376 MHz, $CDCl_3$: δ -55.71) was 93%. Generated **TEMPO–CF_3** was identified by comparison with reported chemical shift value,[30] and further confirmed with HRMS (HRMS-EI (m/z): $[M]^+$ calcd for $C_{10}H_{18}F_3NO$: 225.1340. Found: 225.1337).

BHT as a radical scavenger

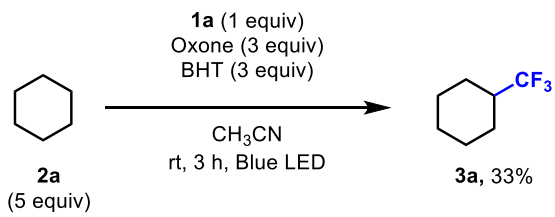

To a 4 mL vial equipped with a PTFE-coated stirrer bar were added bpyCu$(CF_3)_3$ **1a** (0.050 mmol, 1.0 equiv), Oxone (0.15 mmol, 3.0 equiv), cyclohexane **2a** (0.25 mmol, 5.0 equiv), 2,6-di-*tert*-butyl-4-methylphenol (BHT, 0.15 mmml, 3.0 equiv), and CH_3CN (0.5 mL) in an argon-filled glove box. The resulting mixture was stirred for 3 h under 40 W blue LED irradiation with fan cooling (30±5 °C). Hexafluorobenzene was added as an internal standard to determine the yield of **3a** through GC analysis (33%).

Detection of fluoroform (HCF_3 / DCF_3)

*Reaction of cyclohexane **2a** in CD_3CN*

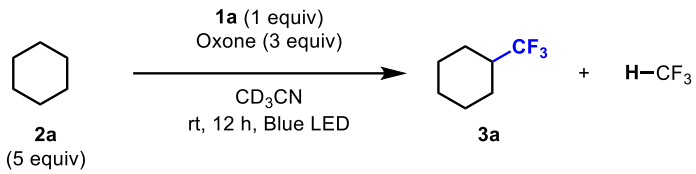

To a screw-cap NMR tube were added bpyCu(CF_3)$_3$ **1a** (0.020 mmol, 1.0 equiv), Oxone (0.060 mmol, 3.0 equiv), cyclohexane **2a** (0.10 mmol, 5.0 equiv), and CD_3CN (0.5 mL) in an argon-filled glove box. The resulting mixture was exposed to 40 W blue LED irradiation for 12 h with fan cooling (30±5 °C). Fluorobenzene was added as an internal standard in the resulting crude mixture, and was subjected to ^{19}F-NMR analysis. **3a** (35%) and HCF_3 (>34%) were observed in ^{19}F-NMR, confirmed by previously reported NMR data.[31]

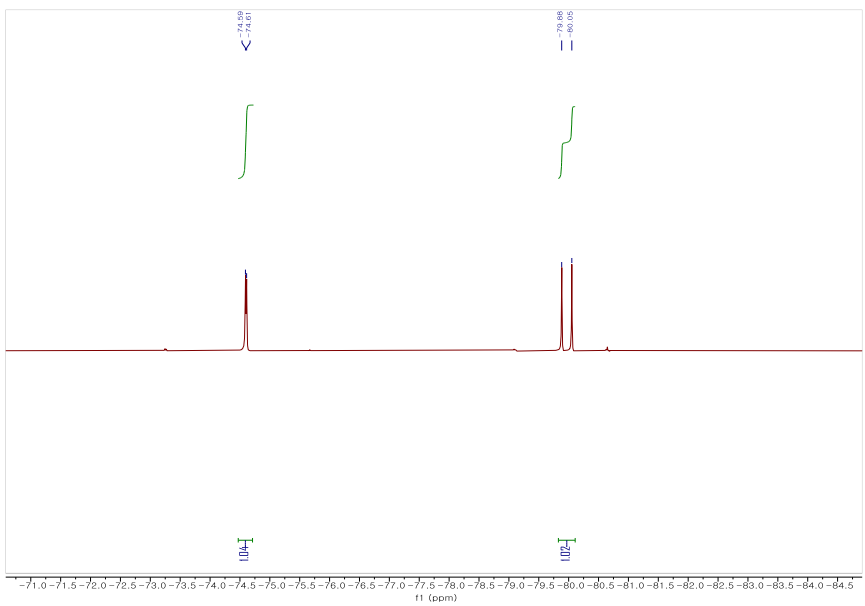

Figure 5.4 Reaction of cyclohexane **2a** in CD_3CN

*Reaction of cyclohexane **2a-d$_{12}$** in CD_3CN*

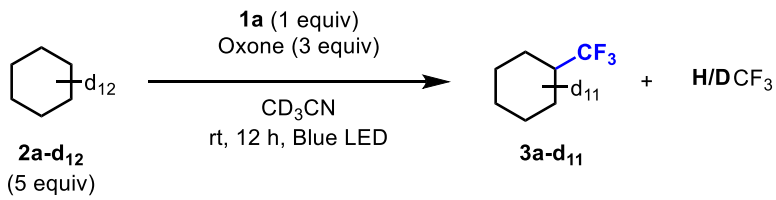

To a screw-cap NMR tube were added bpyCu(CF_3)$_3$ **1a** (0.020 mmol, 1.0 equiv), Oxone (0.060 mmol, 3.0 equiv), cyclohexane **2a-d$_{12}$** (0.10 mmol, 5.0 equiv), and CD_3CN (0.5 mL) in an argon-filled glove box. The resulting mixture was exposed to 40 W blue LED irradiation for 12 h with fan cooling (30±5 °C). Fluorobenzene was added as an internal standard in the resulting crude mixture, and was subjected to ^{19}F-NMR analysis. **3a-d$_{11}$** (17%), HCF_3 (>9%), and DCF_3 (>12%) were observed in ^{19}F-NMR, confirmed by previously reported NMR data.[31]

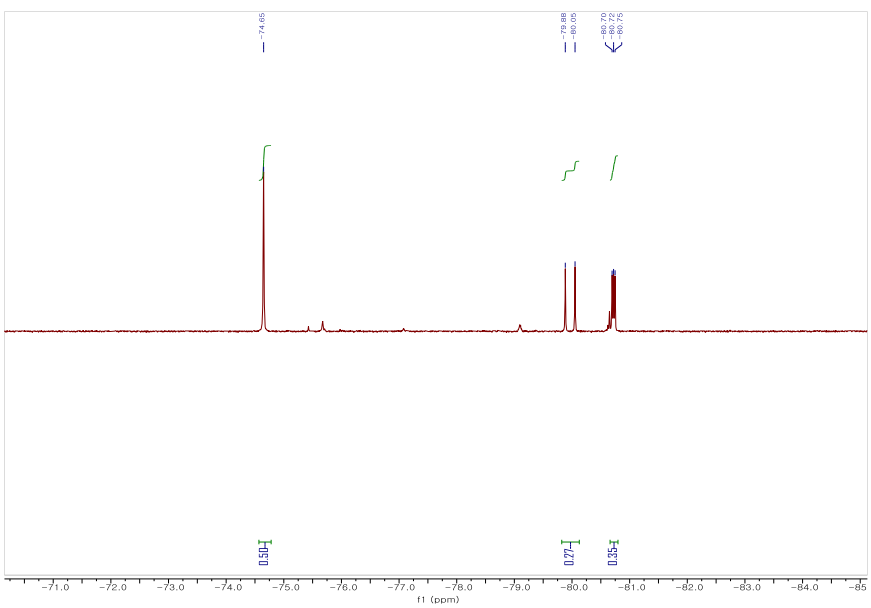

Figure 5.5 Reaction of cyclohexane **2a-d$_{12}$** in CD_3CN

Reaction without C–H substrate in CD_3CN

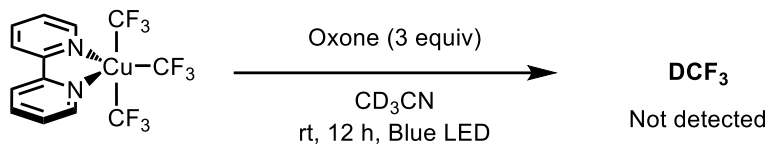

To a screw-cap NMR tube were added bpyCu(CF_3)$_3$ **1a** (0.020 mmol, 1.0 equiv), Oxone (0.060 mmol, 3.0 equiv), and CD_3CN (0.5 mL) in an argon-filled glove box. The resulting mixture was exposed to 40 W blue LED irradiation for 12 h with fan cooling (30±5 °C). Fluorobenzene was added as an internal standard in the resulting crude mixture, and was subjected to ^{19}F-NMR analysis. HCF_3 (>5%) was observed, and no DCF_3 was detected in ^{19}F-NMR, confirmed by previously reported NMR data.[31]

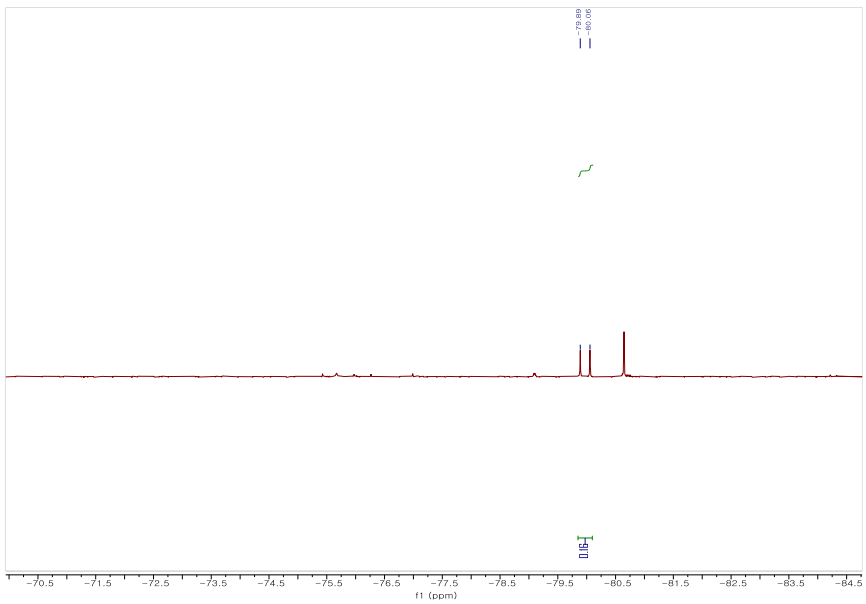

Figure 5.6 Reaction without C–H substrate in CD_3CN

*Reaction of cyclohexane **2a-d$_{12}$** in CH_3CN*

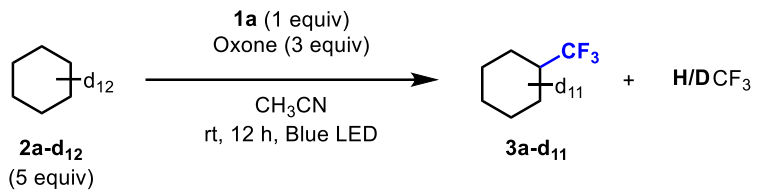

To a screw-cap NMR tube were added bpyCu(CF_3)$_3$ **1a** (0.020 mmol, 1.0 equiv), Oxone (0.060 mmol, 3.0 equiv), cyclohexane **2a-d$_{12}$** (0.10 mmol, 5.0 equiv), and CH_3CN (0.5 mL) in an argon-filled glove box. The resulting mixture was exposed to 40 W blue LED irradiation for 12 h with fan cooling (30±5 °C). Fluorobenzene and CD_3CN (0.1 mL) were added as internal standard and NMR lock solvent. The resulting crude mixture was subjected to ^{19}F-NMR analysis. **3a-d$_{11}$** (12%), HCF_3 (>12%), and DCF_3 (>8%) were observed in ^{19}F-NMR, confirmed by previously reported NMR data.[31]

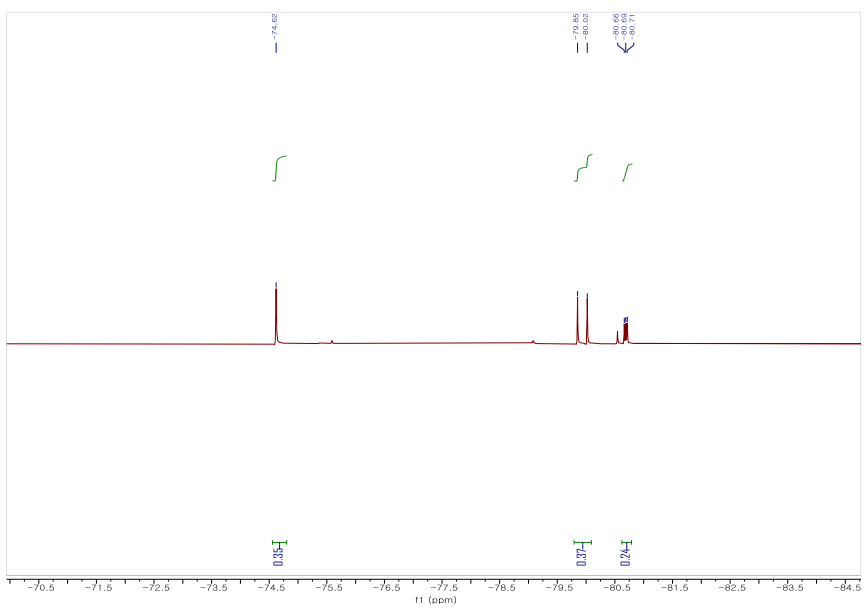

Figure 5.7 Reaction of cyclohexane **2a-d$_{12}$** in CH_3CN

Reaction without C–H substrate in CH_3CN

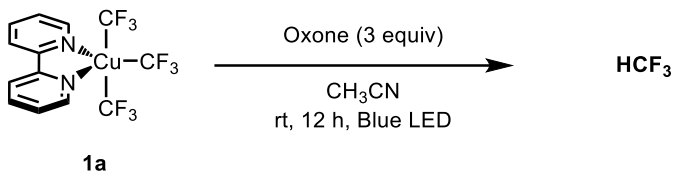

1a

To a screw-cap NMR tube were added bpyCu(CF_3)$_3$ **1a** (0.020 mmol, 1.0 equiv), Oxone (0.060 mmol, 3.0 equiv), and CH_3CN (0.5 mL) in an argon-filled glove box. The resulting mixture was exposed to 40 W blue LED irradiation for 12 h with fan cooling (30±5 °C). Fluorobenzene and CD_3CN (0.1 mL) were added as an internal standard and NMR lock solvent. The resulting crude mixture was subjected to ^{19}F-NMR analysis. HCF_3 (>40%) was detected in ^{19}F-NMR, confirmed by previously reported NMR data.[31]

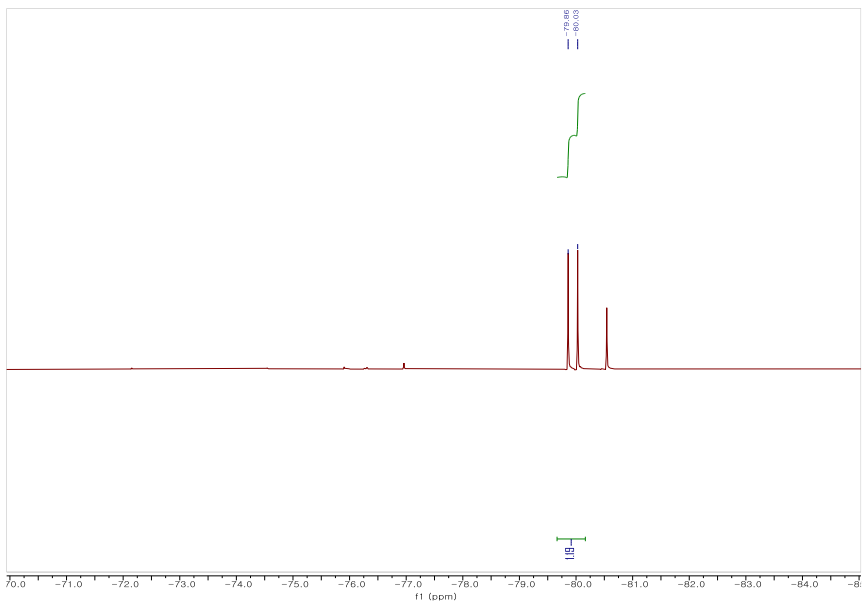

Figure 5.8 Reaction without C–H substrate in CH_3CN

Kinetic isotope effect (KIE) experiments

KIE with two parallel reactions

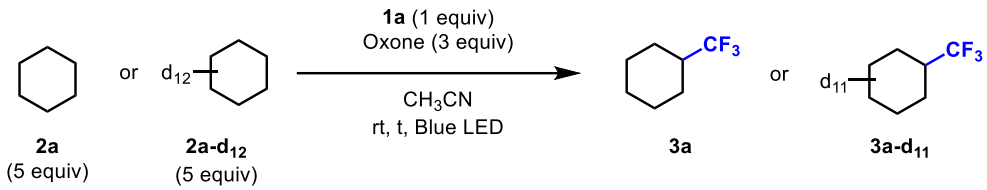

The KIE was determined by comparing the initial reaction rates of the C–H trifluoromethylation with cyclohexane **2a** or deuterated cyclohexane **2a-d$_{12}$**. To a 8 mL vial equipped with a PTFE-coated stirrer bar were added bpyCu(CF$_3$)$_3$ **1a** (0.050 mmol, 1.0 equiv), Oxone (0.15 mmol, 3.0 equiv), **2a** or **2a-d$_{12}$** (0.25 mmol, 5.0 equiv), hexafluorobenzene, and CH$_3$CN (4.0 mL) in an argon-filled glove box. The resulting mixture was exposed to 40 W blue LED irradiation with fan cooling (30±5 °C). Aliquots of the reaction mixture were obtained every 2 min (for **2a**) and 5 min (for **2a-d$_{12}$**), and analyzed by GC to determine the yields of the product. Three independent runs were conducted, and the average values were used for the rate calculation. The KIE was determined to be 4.2.

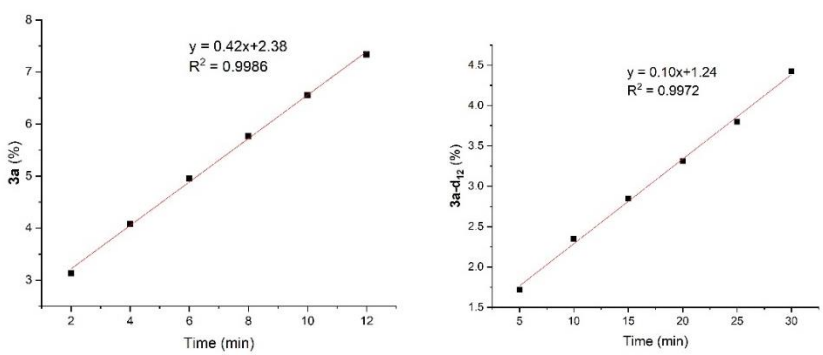

Figure 5.9 KIE with two parallel reactions

KIE with intermolecular competition

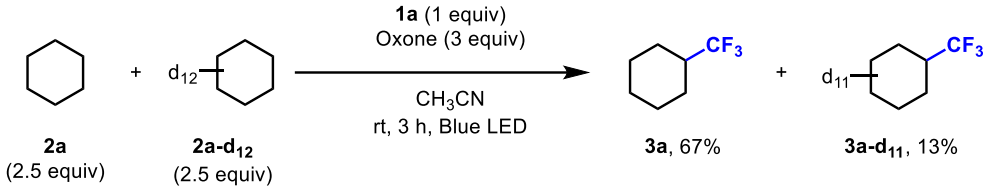

The KIE was determined by comparing product yields of the C–H trifluoromethylation with cyclohexane **2a** and deuterated cyclohexane **2a-d$_{12}$** in a single reaction vessel. To a 4 mL vial equipped with a PTFE-coated stirrer bar were added bpyCu(CF_3)$_3$ **1a** (0.050 mmol, 1.0 equiv), Oxone (0.15 mmol, 3.0 equiv), **2a** and **2a-d$_{12}$** (0.125 mmol, 2.50 equiv each), hexafluorobenzene, and CH_3CN (0.5 mL) in an argon-filled glove box. The resulting mixture was exposed to 40 W blue LED irradiation with fan cooling for 3 h (30±5 °C). The resulting mixture was analyzed by GC to determine the yields of **3a** and **3a-d$_{11}$**. The ratio of products [**3a**]/[**3a-d$_{11}$**] was observed to be 5.2. GC/MS analysis showed no proton/deuterium scrambling of the product and showed only the masses of the products 152.1 (**3a**) and 163.2 (**3a-d$_{11}$**).

Detection of oxidation product

Reaction with water co-solvent system

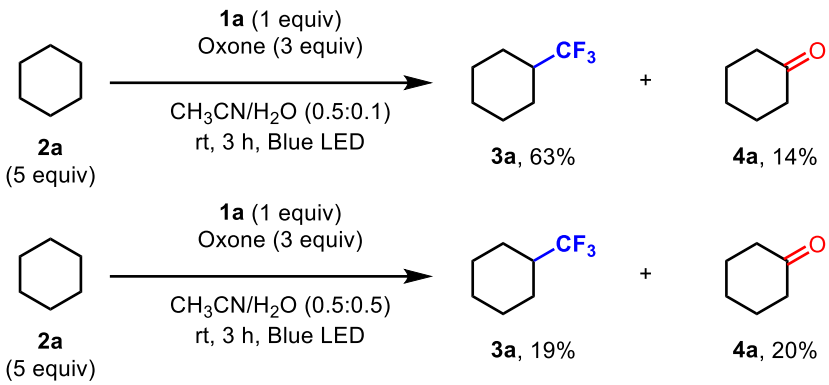

To a 4 mL vial equipped with a PTFE-coated stirrer bar were added bpyCu(CF_3)$_3$ **1a** (0.050 mmol, 1.0 equiv), Oxone (0.15 mmol, 3.0 equiv), cyclohexane **2a** (0.25 mmol, 5.0 equiv), and CH_3CN (0.5 mL) in an argon-filled glove box. Water (0.1 or 0.5 mL) was added outside the glove box. The resulting mixture was stirred for 3 h under 40 W blue LED irradiation with fan cooling (30±5 °C). Hexafluorobenzene was added as an internal standard and filtered with magnesium sulfate. Yields of the products were determined by GC analysis.

*Reaction without **1a***

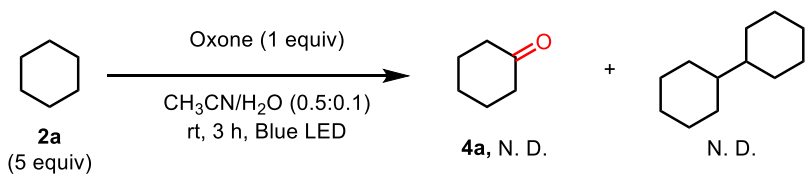

To a 4 mL vial equipped with a PTFE-coated stirrer bar were added Oxone (0.15 mmol, 1.0 equiv), cyclohexane **2a** (0.25 mmol, 5.0 equiv), and CH_3CN (0.5 mL) in

an argon-filled glove box. Water (0.1 mL) was added outside the glove box. The resulting mixture was stirred for 3 h under 40 W blue LED irradiation with fan cooling (30±5 °C). Hexafluorobenzene was added as an internal standard and filtered with magnesium sulfate. Yields of the products were determined by GC analysis.

5.5. Computational section

5.5.1. General considerations

All calculations were carried out using DFT as implemented in the Gaussian 09[32] program packages. Gas phase geometry optimizations were conducted with the B3LYP[33] hybrid functional, including Grimme's D3[34] dispersion correction and the 6-31G**/LanL2DZ(Cu)[35] basis set. The energies of the optimized structures were reevaluated by additional single point calculations using B3LYP hybrid functional including Grimme's D3 dispersion correction and the 6-311++G**/SDD(Cu) basis set. The integral equation formalism variant of the Polarizable Continuum Model (IEFPCM) was employed as implemented to account for the solvation effects for acetonitrile (ε = 35.688). Analytical vibrational frequencies within the harmonic approximation were computed with the 6-31G**/LanL2DZ(Cu) basis set to confirm proper convergence to well-defined minima (no imaginary frequency) or saddle points (one and only one imaginary frequency) on the potential energy surface. Time-dependent density functional theory (TD-DFT) calculations were performed with the Gaussian 09 program using the hybrid exchange-correlation CAM-B3LYP[36] functional with long-range corrections and the 6-311++G**/SDD(Cu) basis set under the integral equation formalism variant of the Polarizable Continuum Model (IEFPCM) for acetonitrile (ε = 35.688).

Redox potentials were calculated from computed solution-phase electron attachment energies of the oxidized species and employing the absolute potential of the standard hydrogen electrode –4.43 V.[37]

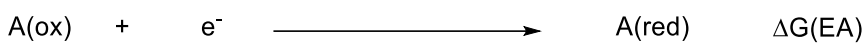

$$E^{o}_{calc} = -\Delta G(EA) - 4.43\ (V)$$

The barrier of electron transfer was computed with the Marcus theory of electron transfer following the protocol reported by Murphy and Tuttle.[38] Oxidation exotherm of Oxone was calculated using the reported standard oxidation potential of Oxone.

5.5.2. Reductive elimination from bisulfate Cu(III) complexes

Computations to verify the reductive elimination barrier from bisulfate-Cu(III) species **^{1}VI** were performed. Even with a bisulfate ligand on the Cu center, the reductive elimination showed a barrier of 14.8 kcal/mol. This energy diagram is also not in agreement with the kinetic experiments where the hydrogen atom transfer was determined to be rate-determining.

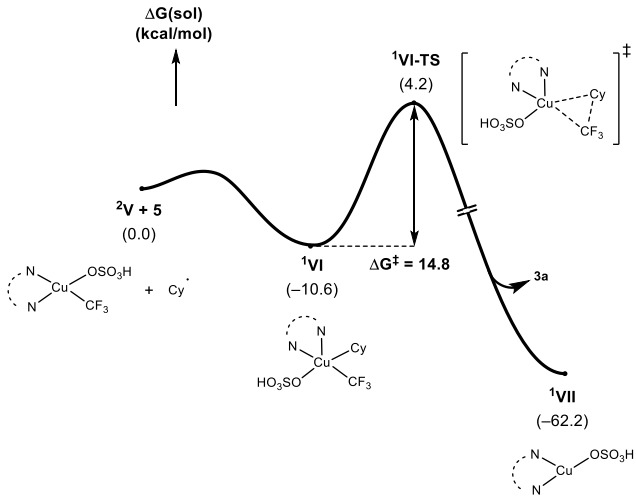

Figure 5.10 Reductive Elimination from Bisulfate Cu(III) Complex

5.5.3. Time-dependent density functional theory calculation

TD-DFT computations were performed on **1a**. Information on the first singlet excitation is shown below. Transitions of >5% contribution are presented.

Figure 5.11 TD-DFT Computations on **1a**

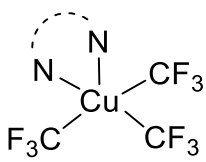

1a

λ (nm)	f	Transition
382.29	0.0081	HOMO–2 → LUMO (75.4%)

HOMO-2 **LUMO**

5.6. References

(1) (a) Fujiwara, T.; O'Hagan, D., *J. Fluor. Chem.* **2014,** *167*, 16-29; (b) Meanwell, N. A., *J. Med. Chem.* **2018,** *61* (14), 5822-5880; (c) Zhao, Y.; Schwab, M. G.; Kiersnowski, A.; Pisula, W.; Baumgarten, M.; Chen, L.; Müllen, K.; Li, C., *J. Mater. Chem. C* **2016,** *4* (21), 4640-4646.

(2) (a) Liu, X.; Xu, C.; Wang, M.; Liu, Q., *Chem. Rev.* **2015,** *115* (2), 683-730; (b) Chu, L.; Qing, F.-L., *Acc. Chem. Res.* **2014,** *47* (5), 1513-1522.

(3) (a) Prieto, A.; Baudoin, O.; Bouyssi, D.; Monteiro, N., *Chem. Commun.* **2016,** *52* (5), 869-881; (b) Barata-Vallejo, S.; Lantaño, B.; Postigo, A., *Chem. Eur. J.* **2014,** *20* (51), 16806-16829; (c) Charpentier, J.; Früh, N.; Togni, A., *Chem. Rev.* **2015,** *115* (2), 650-682; (d) Tomita, R.; Koike, T.; Akita, M., *Angew. Chem. Int. Ed.* **2015,** *54* (44), 12923-12927.

(4) (a) Koike, T.; Akita, M., *Acc. Chem. Res.* **2016,** *49* (9), 1937-1945; (b) Studer, A., *Angew. Chem. Int. Ed.* **2012,** *51* (36), 8950-8958; (c) Sato, A.; Han, J.; Ono, T.; Wzorek, A.; Aceña, J. L.; Soloshonok, V. A., *Chem. Commun.* **2015,** *51* (27), 5967-5970.

(5) (a) Sladojevich, F.; McNeill, E.; Börgel, J.; Zheng, S.-L.; Ritter, T., *Angew. Chem. Int. Ed.* **2015,** *54* (12), 3712-3716; (b) Zhang, X.-G.; Dai, H.-X.; Wasa, M.; Yu, J.-Q., *J. Am. Chem. Soc.* **2012,** *134* (29), 11948-11951; (c) Wang, X.; Truesdale, L.; Yu, J.-Q., *J. Am. Chem. Soc.* **2010,** *132* (11), 3648-3649; (d) Litvinas, N. D.; Fier, P. S.; Hartwig, J. F., *Angew. Chem. Int. Ed.* **2012,** *51* (2), 536-539; (e) Shang, M.; Sun, S.-Z.; Wang, H.-L.; Laforteza, B. N.; Dai, H.-X.; Yu, J.-Q., *Angew. Chem. Int. Ed.* **2014,** *53* (39), 10439-10442; (f) Li, L.; Mu, X.; Liu, W.; Wang, Y.; Mi, Z.; Li, C.-J., *J. Am. Chem. Soc.* **2016,** *138* (18), 5809-5812.

(6) (a) Nagib, D. A.; MacMillan, D. W. C., *Nature* **2011,** *480* (7376), 224-228; (b) O'Brien, A. G.; Maruyama, A.; Inokuma, Y.; Fujita, M.; Baran, P. S.; Blackmond, D. G., *Angew. Chem. Int. Ed.* **2014,** *53* (44), 11868-11871; (c) Nishida, T.; Ida, H.; Kuninobu, Y.; Kanai, M., *Nat. Commun.* **2014,** *5*, 3387; (d) Fujiwara, Y.; Dixon, J. A.; O'Hara, F.; Funder, E. D.; Dixon, D. D.; Rodriguez, R. A.; Baxter, R. D.; Herlé, B.; Sach, N.; Collins, M. R.; Ishihara, Y.; Baran, P. S., *Nature* **2012,** *492* (7427), 95-99; (e) Chu, L.; Qing, F.-L., *J. Am. Chem. Soc.* **2012,** *134* (2), 1298-1304; (f) Nagase, M.; Kuninobu, Y.; Kanai, M., *J. Am. Chem. Soc.* **2016,** *138* (19), 6103-6106.

(7) (a) Feng, C.; Loh, T.-P., *Angew. Chem. Int. Ed.* **2013,** *52* (47), 12414-12417; (b) Straathof, N. J. W.; Cramer, S. E.; Hessel, V.; Noël, T., *Angew. Chem. Int. Ed.* **2016,** *55* (50), 15549-15553; (c) Yang, C.; Hassanpour, A.; Ghorbanpour, K.; Abdolmohammadi, S.; Vessally, E., *RSC Adv.* **2019,** *9* (47), 27625-27639.

(8) Zhang, P.; Shen, H.; Zhu, L.; Cao, W.; Li, C., *Org. Lett.* **2018,** *20* (22), 7062-7065.

(9) (a) Ide, T.; Masuda, S.; Kawato, Y.; Egami, H.; Hamashima, Y., *Org. Lett.* **2017,** *19* (17), 4452-4455; (b) Liu, Z.; Xiao, H.; Zhang, B.; Shen, H.; Zhu, L.; Li, C., *Angew. Chem. Int. Ed.* **2019,** *58* (8), 2510-2513.

(10) (a) Allen, A. E.; Macmillan, D. W. C., *J. Am. Chem. Soc.* **2010,** *132* (14), 4986-4987; (b) Herrmann, A. T.; Smith, L. L.; Zakarian, A., *J. Am. Chem. Soc.* **2012,** *134* (16), 6976-6979; (c) Nagib, D. A.; Scott, M. E.; MacMillan, D. W. C., *J. Am. Chem. Soc.* **2009,** *131* (31), 10875-10877; (d) Deng, Q.-H.; Wadepohl, H.; Gade, L. H., *J. Am. Chem. Soc.* **2012,** *134* (26), 10769-10772; (e) Matoušek, V.; Togni, A.; Bizet, V.; Cahard, D., *Org. Lett.* **2011,** *13* (21), 5762-5765.

(11) (a) Gietter-Burch, A. A. S.; Devannah, V.; Watson, D. A., *Org. Lett.* **2017,** *19* (11), 2957-2960; (b) Chu, L.; Qing, F.-L., *Chem. Commun.* **2010,** *46* (34), 6285-6287;

(c) Mitsudera, H.; Li, C.-J., *Tetrahedron Lett.* **2011,** *52* (16), 1898-1900.

(12) (a) Guo, S.; AbuSalim, D. I.; Cook, S. P., *J. Am. Chem. Soc.* **2018,** *140* (39), 12378-12382; (b) Xiao, H.; Liu, Z.; Shen, H.; Zhang, B.; Zhu, L.; Li, C., *Chem* **2019,** *5* (4), 940-949; (c) Paeth, M.; Carson, W.; Luo, J.-H.; Tierney, D.; Cao, Z.; Cheng, M.-J.; Liu, W., *Chem. Eur. J.* **2018,** *24* (45), 11559-11563; (d) Egami, H.; Ide, T.; Kawato, Y.; Hamashima, Y., *Chem. Commun.* **2015,** *51* (93), 16675-16678.

(13) Sarver, P. J.; Bacauanu, V.; Schultz, D. M.; DiRocco, D. A.; Lam, Y.-H.; Sherer, E. C.; MacMillan, D. W. C., *Nat. Chem.* **2020,** *12* (5), 459-467.

(14) (a) Guo, S.; AbuSalim, D. I.; Cook, S. P., *Angew. Chem. Int. Ed.* **2019,** *58* (34), 11704-11708; (b) Shen, H.; Liu, Z.; Zhang, P.; Tan, X.; Zhang, Z.; Li, C., *J. Am. Chem. Soc.* **2017,** *139* (29), 9843-9846; (c) Tan, X.; Liu, Z.; Shen, H.; Zhang, P.; Zhang, Z.; Li, C., *J. Am. Chem. Soc.* **2017,** *139* (36), 12430-12433; (d) Xiao, H.; Shen, H.; Zhu, L.; Li, C., *J. Am. Chem. Soc.* **2019,** *141* (29), 11440-11445; (e) Romine, A. M.; Nebra, N.; Konovalov, A. I.; Martin, E.; Benet-Buchholz, J.; Grushin, V. V., *Angew. Chem. Int. Ed.* **2015,** *54* (9), 2745-2749.

(15) Amphlett, J. C.; Coomber, J. W.; Whittle, E., *J. Phys. Chem.* **1966,** *70* (2), 593-594.

(16) (a) Gray, P.; Herod, A. A.; Jones, A., *Chem. Rev.* **1971,** *71* (3), 247-294; (b) Bullock, G.; Cooper, R., *Trans. Faraday Soc.* **1970,** *66* (0), 2055-2064; (c) Bell, T. N.; Zucker, U. F., *Can. J. Chem.* **1970,** *48* (8), 1209-1213; (d) Fass, R. A.; Willard, J. E., *J. Chem. Phys.* **1970,** *52* (4), 1874-1882.

(17) Ye, F.; Berger, F.; Jia, H.; Ford, J.; Wortman, A.; Börgel, J.; Genicot, C.; Ritter, T., *Angew. Chem. Int. Ed.* **2019,** *58* (41), 14615-14619.

(18) Seol, G. H.; Kim, K. Y., Eucalyptol and Its Role in Chronic Diseases. In *Drug*

Discovery from Mother Nature, Gupta, S. C.; Prasad, S.; Aggarwal, B. B., Eds. Springer International Publishing: Cham, 2016; pp 389-398.

(19) Sukhchain, S.; Pawan, G.; Jeena, G., *Curr. Drug Discov. Technol.* **2019,** *16*, 1-12.

(20) Zerbe, P.; Bohlmann, J., Enzymes for Synthetic Biology of Ambroxide-Related Diterpenoid Fragrance Compounds. In *Biotechnology of Isoprenoids*, Schrader, J.; Bohlmann, J., Eds. Springer International Publishing: Cham, 2015; pp 427-447.

(21) (a) Morton, C. M.; Zhu, Q.; Ripberger, H.; Troian-Gautier, L.; Toa, Z. S. D.; Knowles, R. R.; Alexanian, E. J., *J. Am. Chem. Soc.* **2019,** *141* (33), 13253-13260; (b) Mukherjee, S.; Maji, B.; Tlahuext-Aca, A.; Glorius, F., *J. Am. Chem. Soc.* **2016,** *138* (50), 16200-16203.

(22) Jasiński, M.; Stukkens, Y.; Degand, H.; Purnelle, B.; Marchand-Brynaert, J.; Boutry, M., *Plant Cell* **2001,** *13* (5), 1095-1107.

(23) Chernyshov, V. V.; Yarovaya, O. I.; Fadeev, D. S.; Gatilov, Y. V.; Esaulkova, Y. L.; Muryleva, A. S.; Sinegubova, K. O.; Zarubaev, V. V.; Salakhutdinov, N. F., *Mol. Divers.* **2020,** *24* (1), 61-67.

(24) (a) Paeth, M.; Tyndall, S. B.; Chen, L.-Y.; Hong, J.-C.; Carson, W. P.; Liu, X.; Sun, X.; Liu, J.; Yang, K.; Hale, E. M.; Tierney, D. L.; Liu, B.; Cao, Z.; Cheng, M.-J.; Goddard, W. A., 3rd; Liu, W., *J. Am. Chem. Soc.* **2019,** *141* (7), 3153-3159; (b) Liu, S.; Liu, H.; Liu, S.; Lu, Z.; Lu, C.; Leng, X.; Lan, Y.; Shen, Q., *J. Am. Chem. Soc.* **2020,** *142* (21), 9785-9791.

(25) Liu, Z.; Chen, H.; Lv, Y.; Tan, X.; Shen, H.; Yu, H.-Z.; Li, C., *J. Am. Chem. Soc.* **2018,** *140* (19), 6169-6175.

(26) (a) Liu, Y.; Wang, Y.; Yin, Y.; Pan, J.; Zhang, J., *Energy Fuels* **2018,** *32* (2),

1999-2008; (b) Wang, Y.; Wang, Y.; Liu, Y., *Chem. Eng. J.* **2020,** *393*, 124740.

(27) Paeth, M.; Carson, W.; Luo, J.-H.; Tierney, D.; Cao, Z.; Cheng, M.-J.; Liu, W., *Chem. Eur. J.* **2018,** *24* (45), 11559-11563.

(28) Zhang, S.-L.; Bie, W.-F., *RSC Adv.* **2016,** *6* (75), 70902-70906.

(29) (a) Kornfilt, D. J. P.; MacMillan, D. W. C., *J. Am. Chem. Soc.* **2019,** *141* (17), 6853-6858; (b) Kautzky, J. A.; Wang, T.; Evans, R. W.; MacMillan, D. W. C., *J. Am. Chem. Soc.* **2018,** *140* (21), 6522-6526.

(30) Wang, Y.-F.; Lonca, G. H.; Chiba, S., *Angew. Chem. Int. Ed.* **2014,** *53* (4), 1067-1071.

(31) Zhang, C.-P.; Cai, J.; Zhou, C.-B.; Wang, X.-P.; Zheng, X.; Gu, Y.-C.; Xiao, J.-C., *Chem. Commun.* **2011,** *47* (33), 9516-9518.

(32) Gaussian 09, Revision D. 01, M. J. Frisch et. al. Gaussian, Inc., 2013.

(33) Lee, C.; Yang, W.; Parr, R. G., *Phys. Rev. B Condens. Matter* **1988,** *37* (2), 785-789.

(34) Grimme, S.; Antony, J.; Ehrlich, S.; Krieg, H., *J. Chem. Phys.* **2010,** *132* (15), 154104.

(35) (a) Wadt, W. R.; Hay, P. J., *J. Chem. Phys.* **1985,** *82* (1), 284-298; (b) Hay, P. J.; Wadt, W. R., *J. Chem. Phys.* **1985,** *82* (1), 299-310.

(36) Yanai, T.; Tew, D. P.; Handy, N. C., *Chem. Phys. Lett.* **2004,** *393* (1), 51-57.

(37) Trasatti, S., *Pure Appl. Chem.* **1986,** *58* (7), 955-966.

(38) Anderson, G. M.; Cameron, I.; Murphy, J. A.; Tuttle, T., *RSC Adv.* **2016,** *6* (14), 11335-11343.

Appendix – NMR spectra

Chapter 2

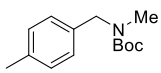

4bb
($CDCl_3$, 300 MHz)

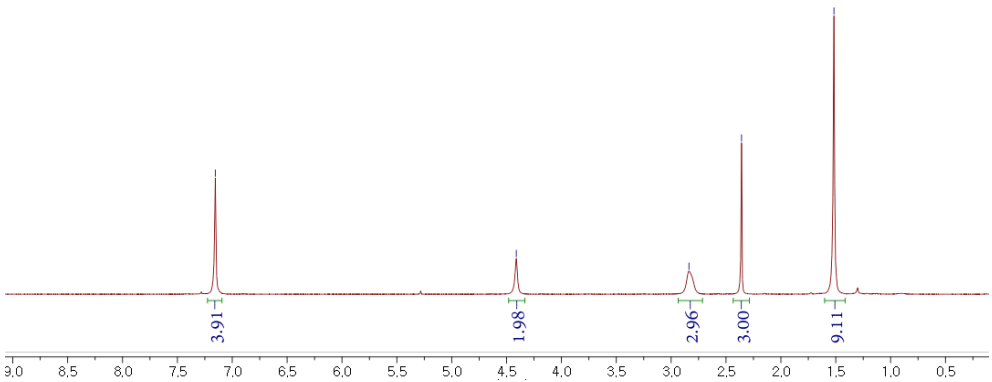

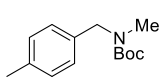

4bb
($CDCl_3$, 75 MHz)

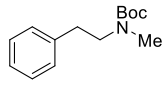

8bb
($CDCl_3$, 500 MHz)

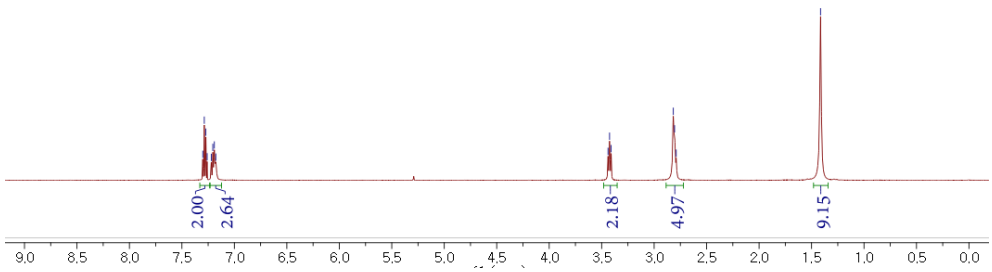

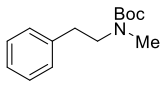

8bb
($CDCl_3$, 75 MHz)

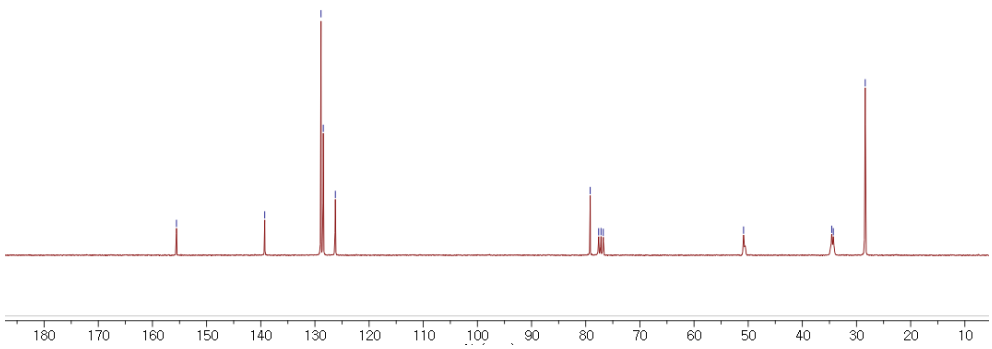

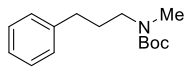

9bb
($CDCl_3$, 300 MHz)

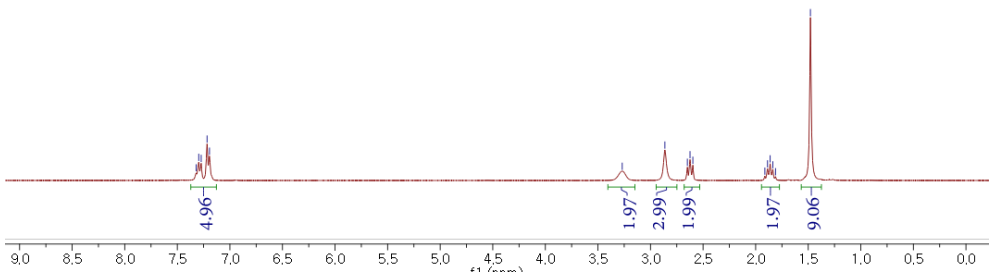

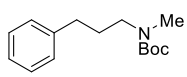

9bb
($CDCl_3$, 75 MHz)

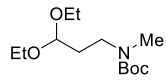

11bb
($CDCl_3$, 500 MHz)

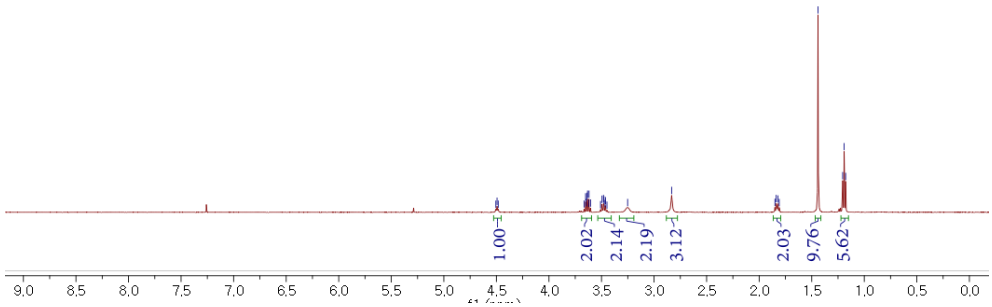

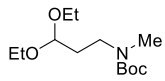

11bb
($CDCl_3$, 125 MHz)

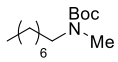

12bb
($CDCl_3$, 300 MHz)

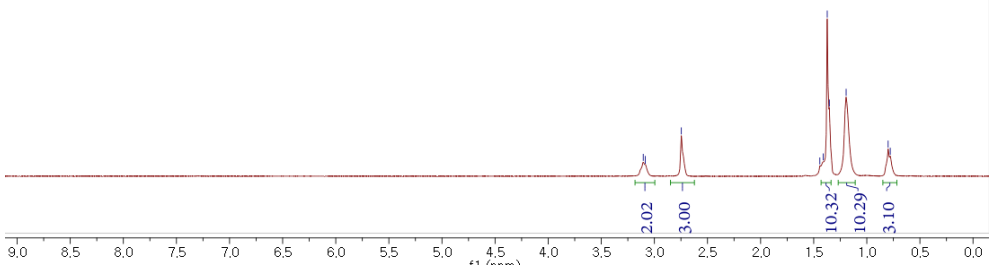

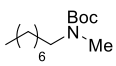

12bb
($CDCl_3$, 75 MHz)

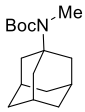

15bb
($CDCl_3$, 500 MHz)

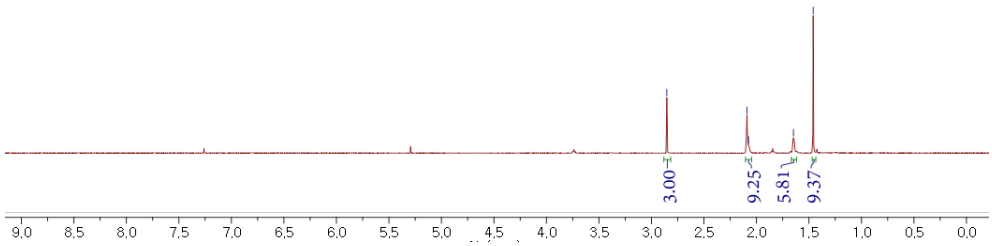

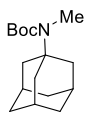

15bb
($CDCl_3$, 125 MHz)

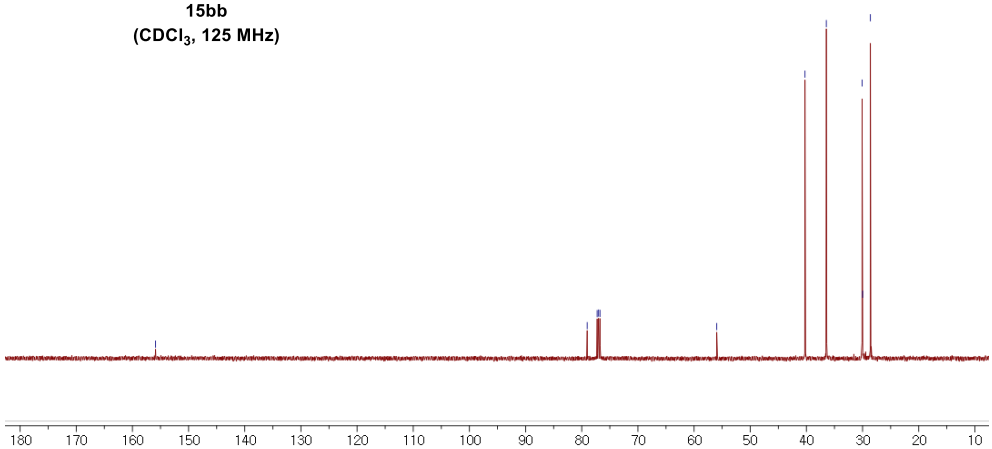

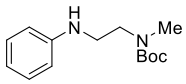

20bb
($CDCl_3$, 300 MHz)

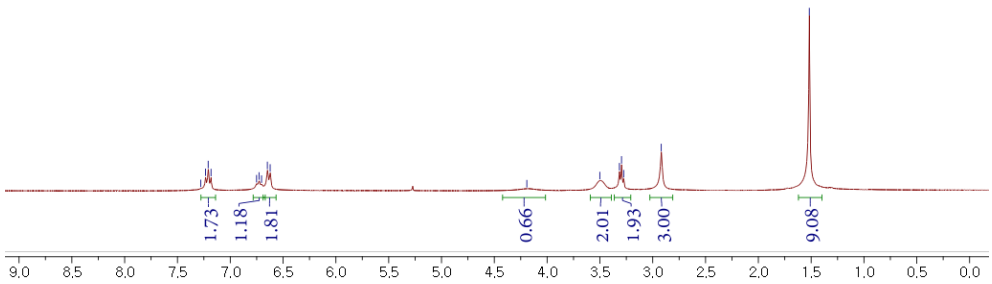

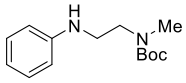

20bb
($CDCl_3$, 75 MHz)

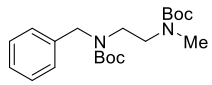

21bb
($CDCl_3$, 500 MHz)

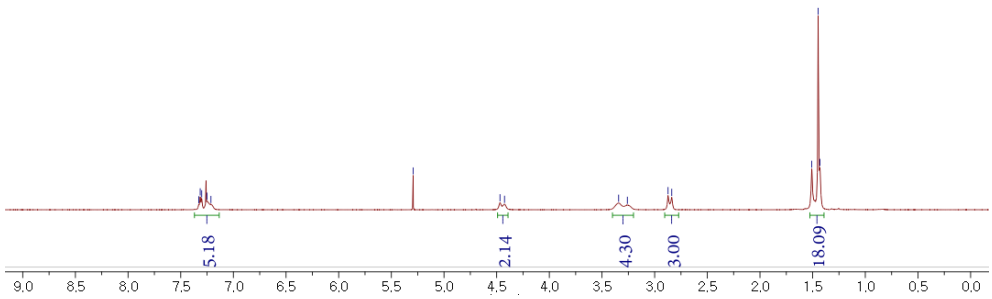

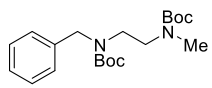

21bb
($CDCl_3$, 75 MHz)

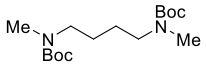

29bb
($CDCl_3$, 500 MHz)

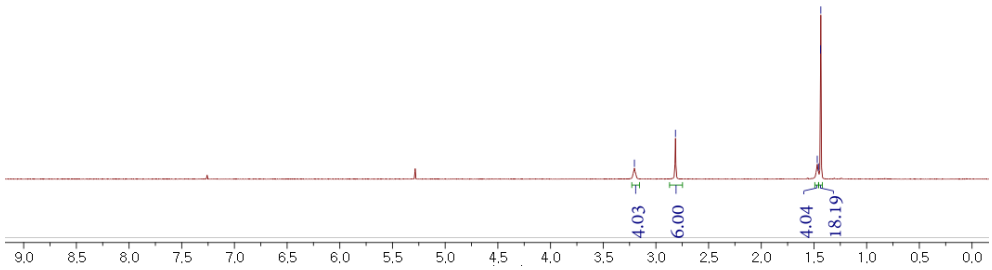

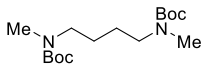

29bb
($CDCl_3$, 75 MHz)

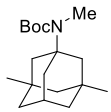

31bb
($CDCl_3$, 500 MHz)

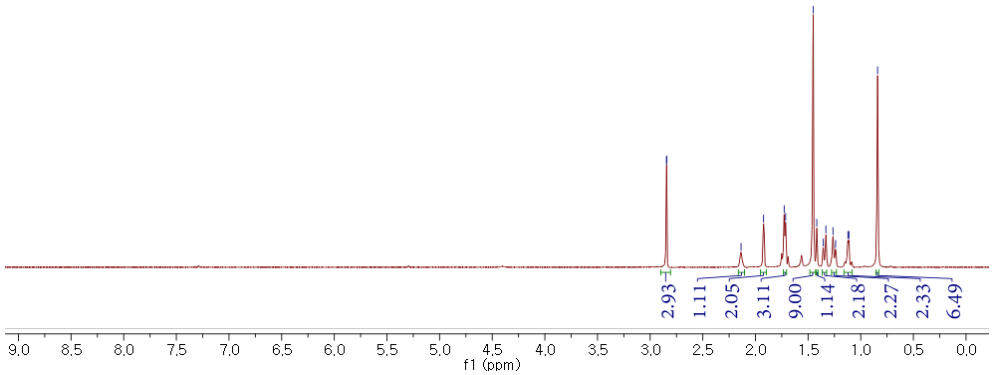

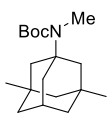

31bb
($CDCl_3$, 125 MHz)

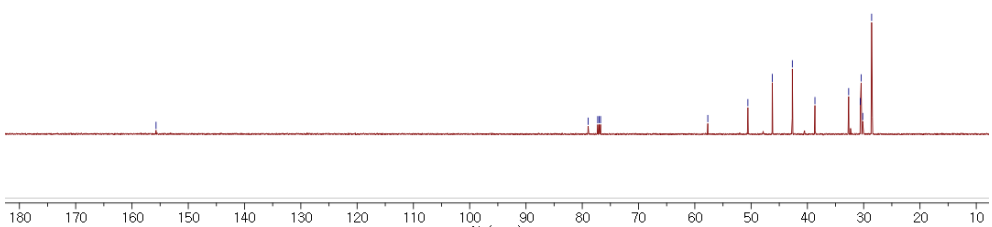

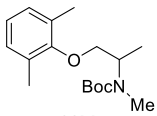

32bb
($CDCl_3$, 500 MHz)

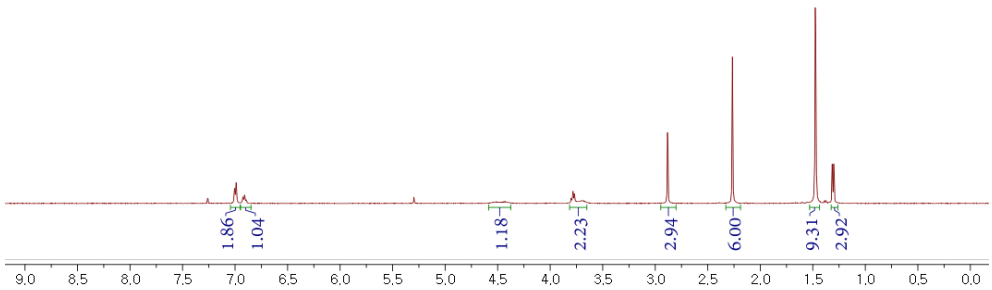

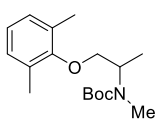

32bb
($CDCl_3$, 75 MHz)

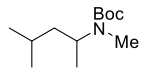

33bb
($CDCl_3$, 500 MHz)

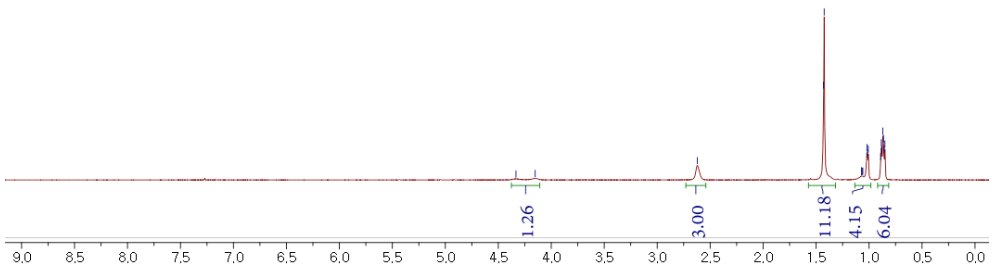

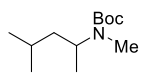

33bb
($CDCl_3$, 125 MHz)

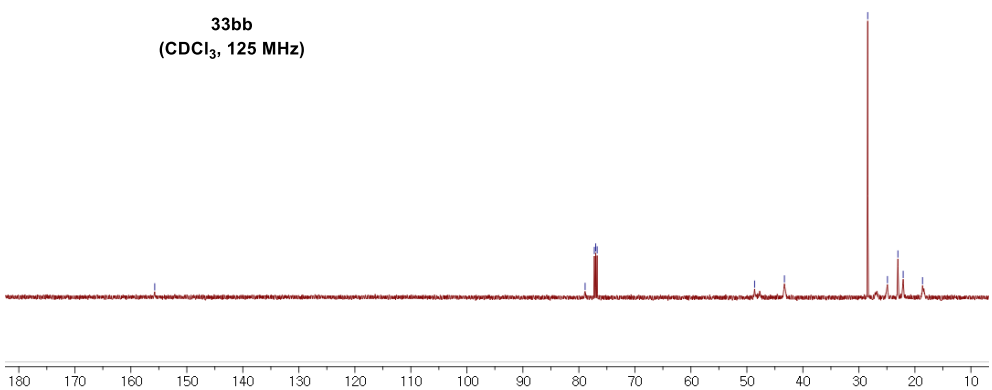

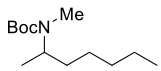

34bb
($CDCl_3$, 500 MHz)

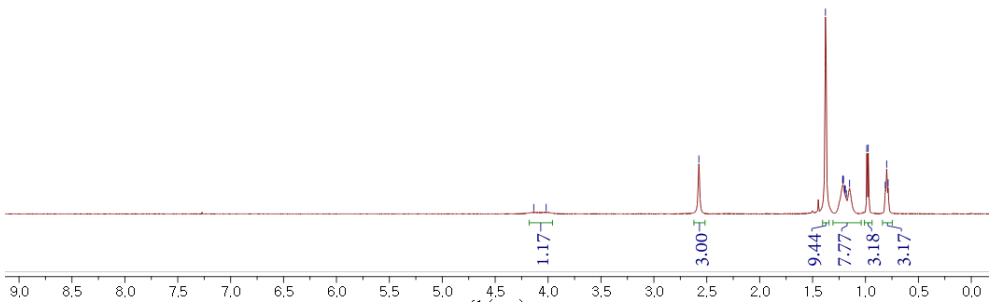

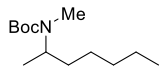

34bb
($CDCl_3$, 125 MHz)

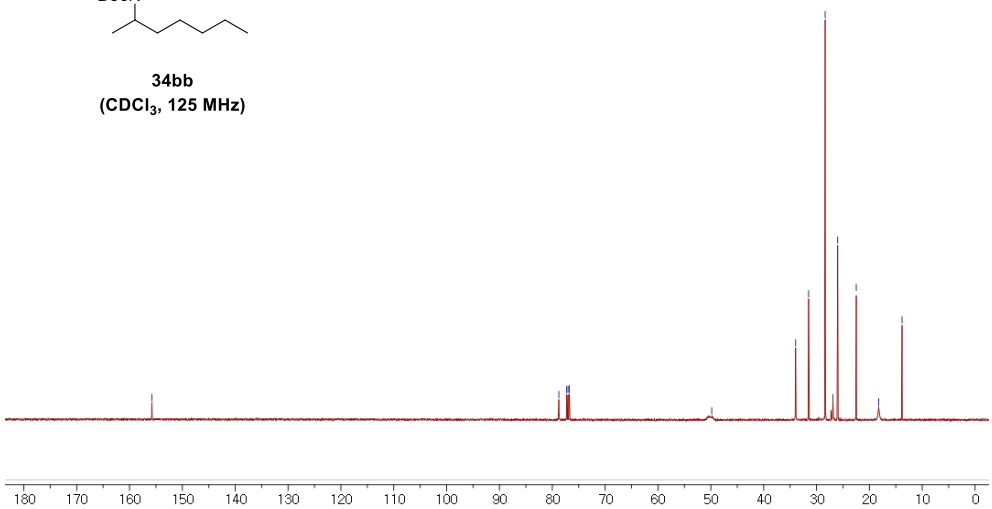

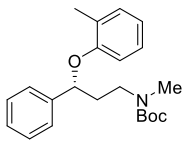

35bb
($CDCl_3$, 300 MHz)

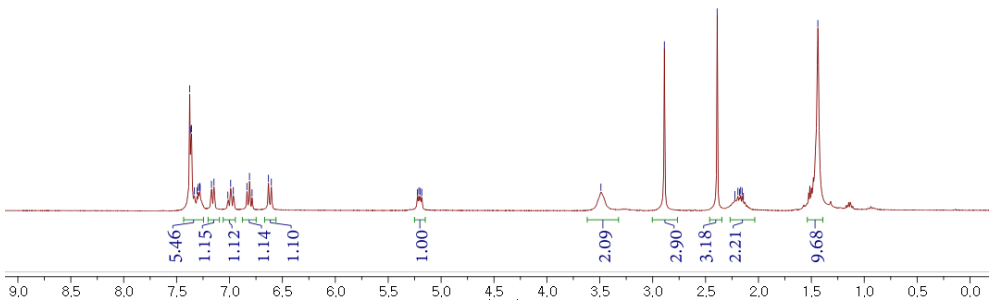

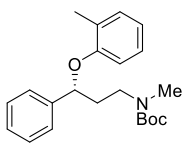

35bb
($CDCl_3$, 75 MHz)

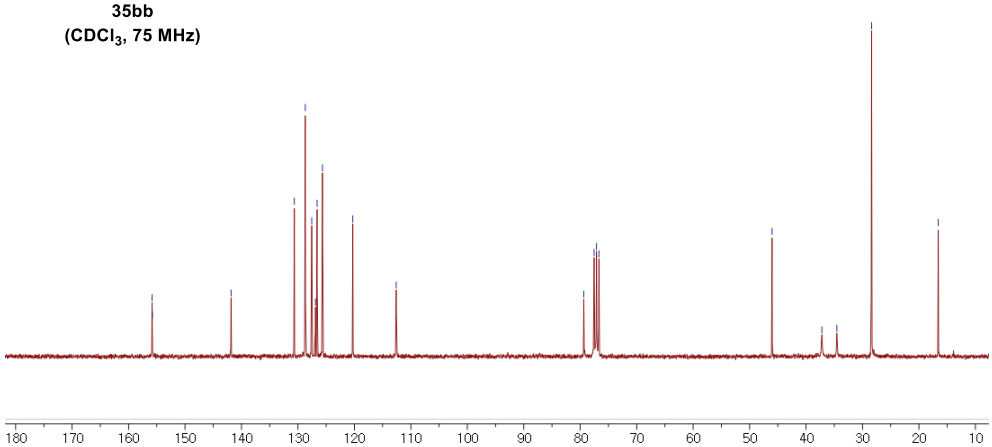

Chapter 3

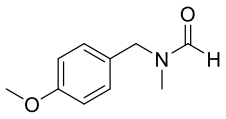

2d
($CDCl_3$, 300 MHz)

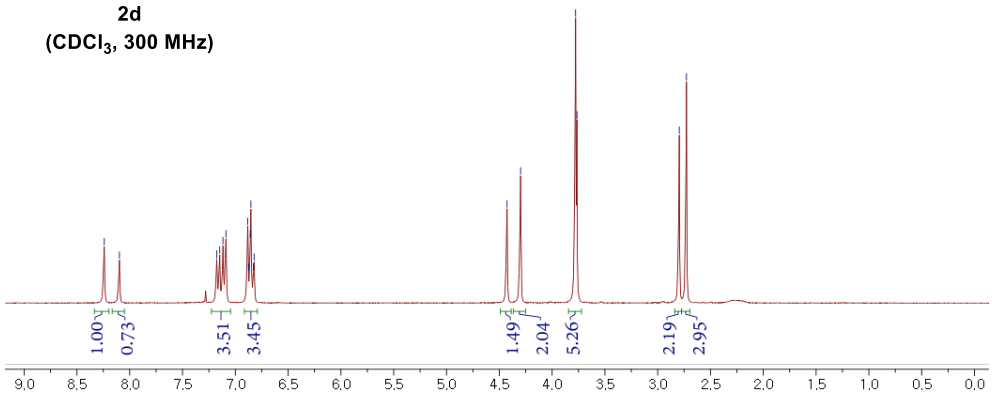

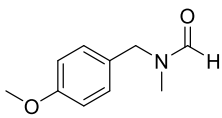

2d
($CDCl_3$, 125 MHz)

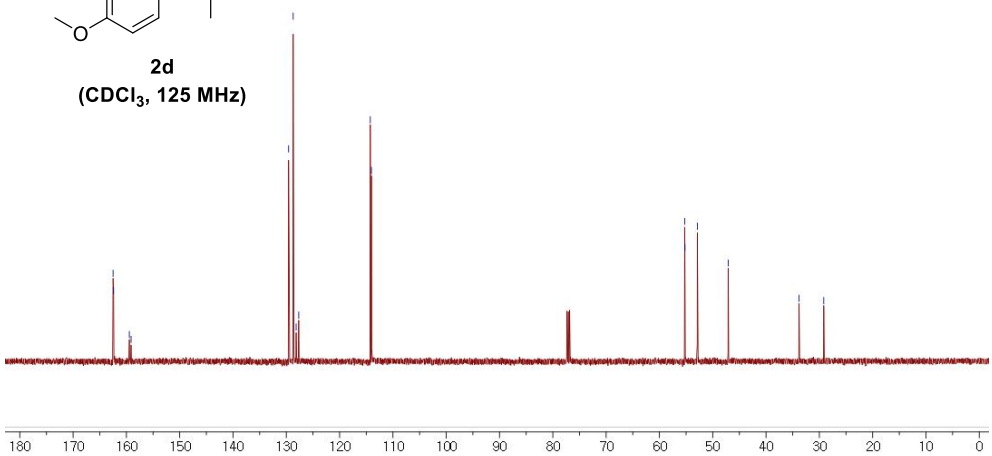

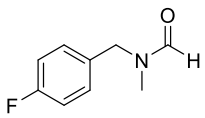

3d
($CDCl_3$, 400 MHz)

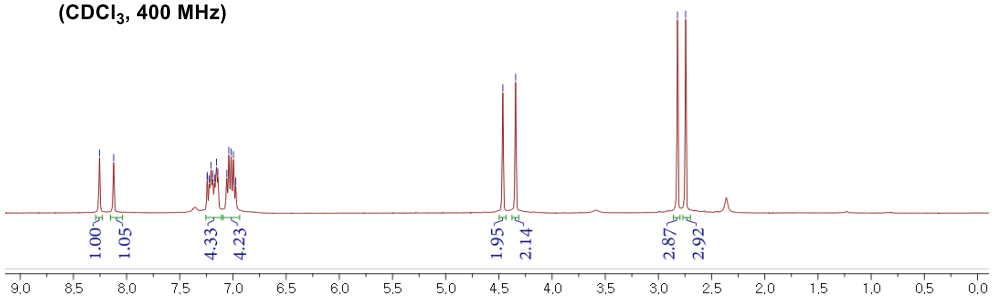

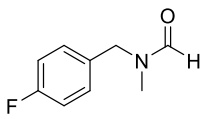

3d
($CDCl_3$, 100 MHz)

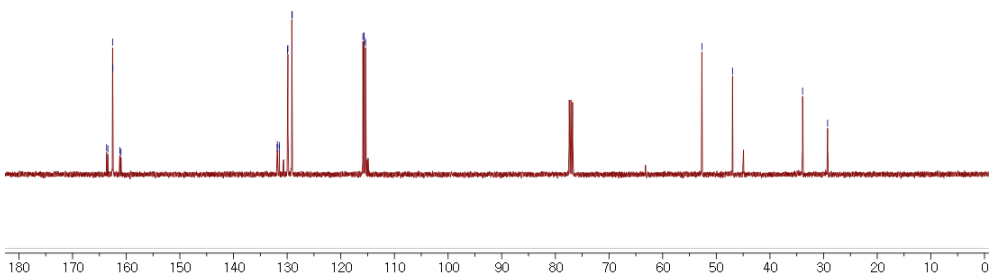

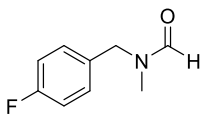

3d
($CDCl_3$, 375 MHz)

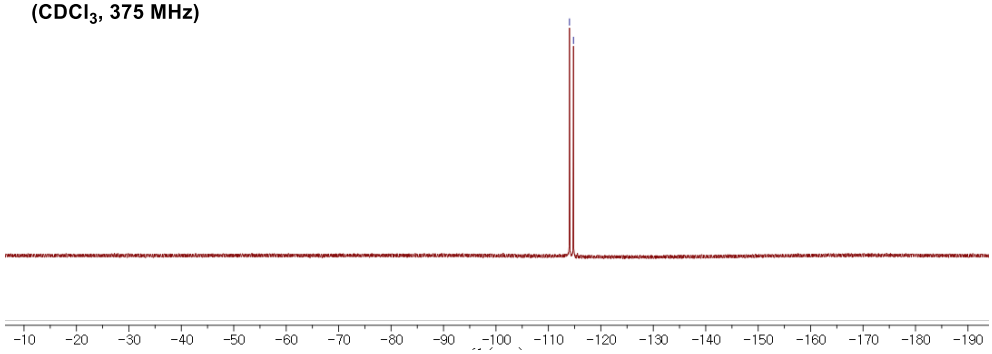

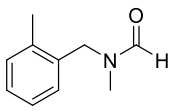

5d
($CDCl_3$, 300 MHz)

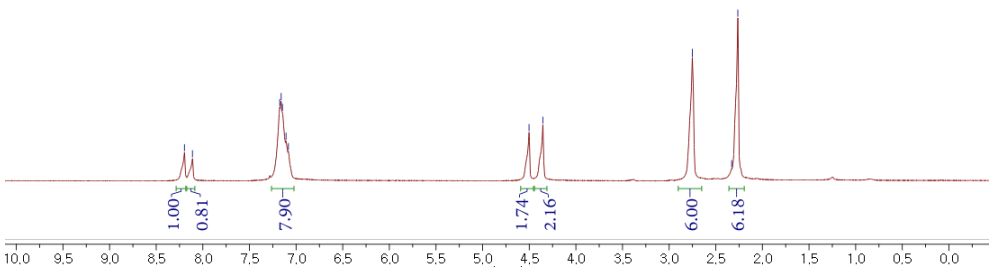

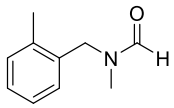

5d
($CDCl_3$, 125 MHz)

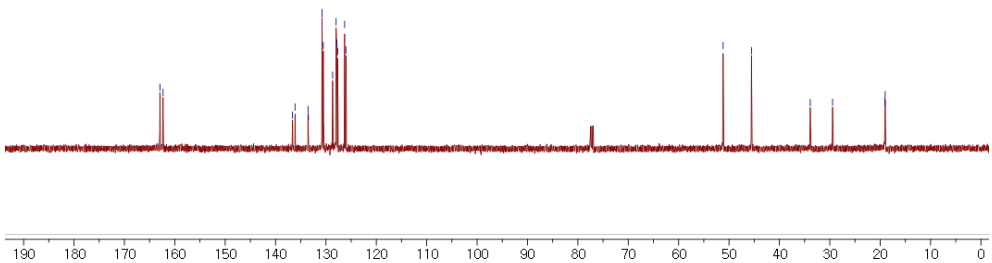

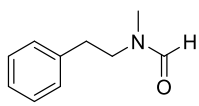

6d
($CDCl_3$, 400 MHz)

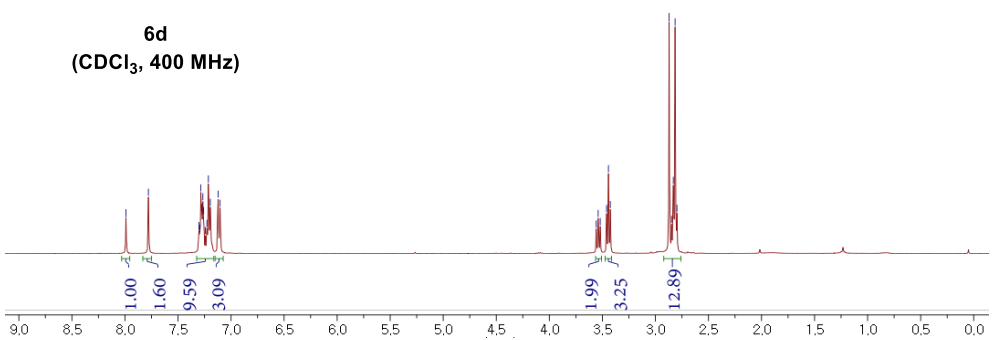

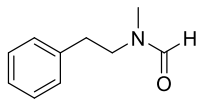

6d
($CDCl_3$, 100 MHz)

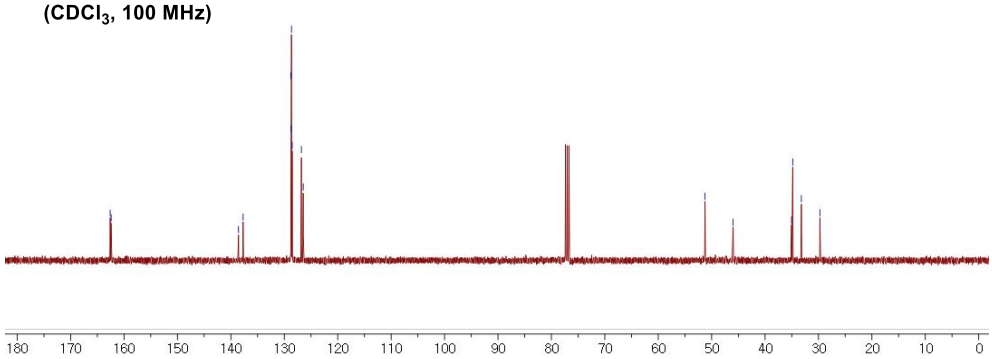

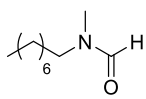

8d
($CDCl_3$, 300 MHz)

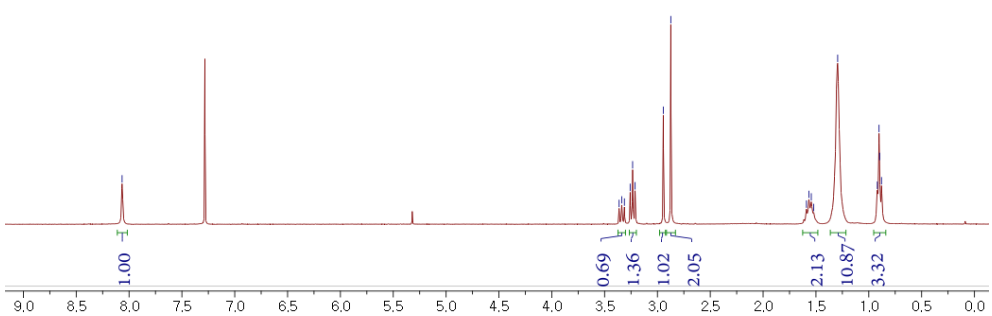

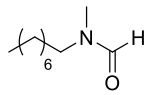

8d
($CDCl_3$, 75 MHz)

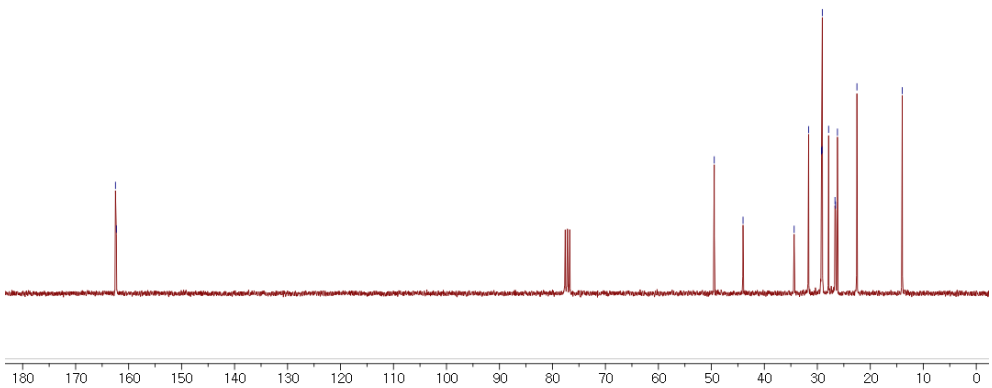

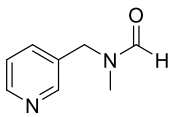

9d
($CDCl_3$, 300 MHz)

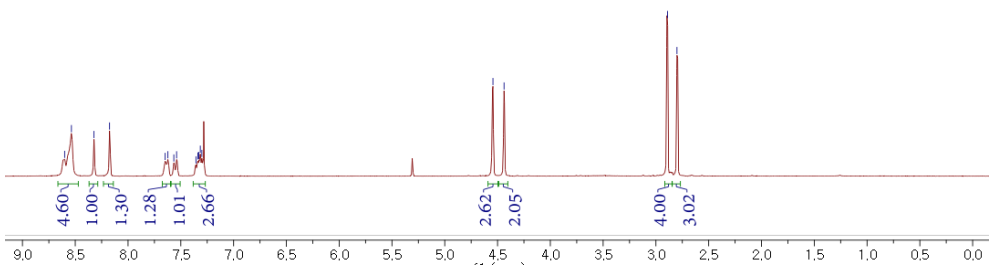

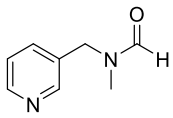

9d
($CDCl_3$, 75 MHz)

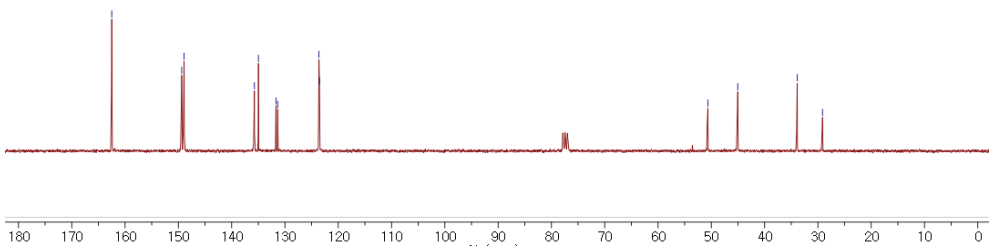

Chapter 5

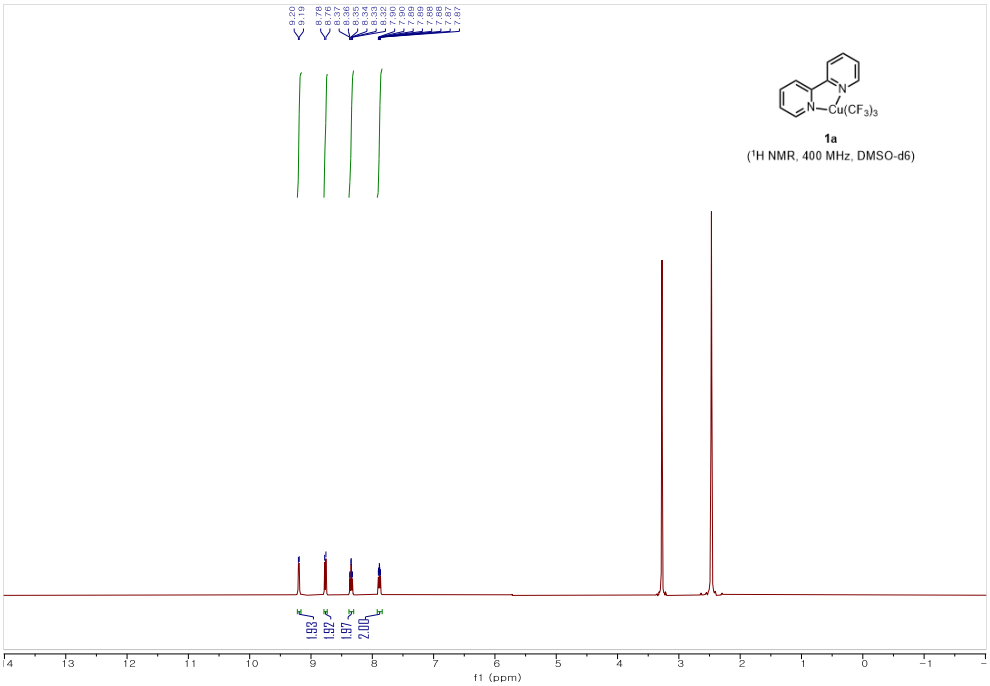
9.20
9.19
8.78
8.77
8.37
8.36
8.35
8.34
8.33
8.32
7.90
7.89
7.89
7.88
7.88
7.87
7.87
1.93
1.92
1.97
2.00
f1 (ppm)
1a
(1H NMR, 400 MHz, DMSO-d6)

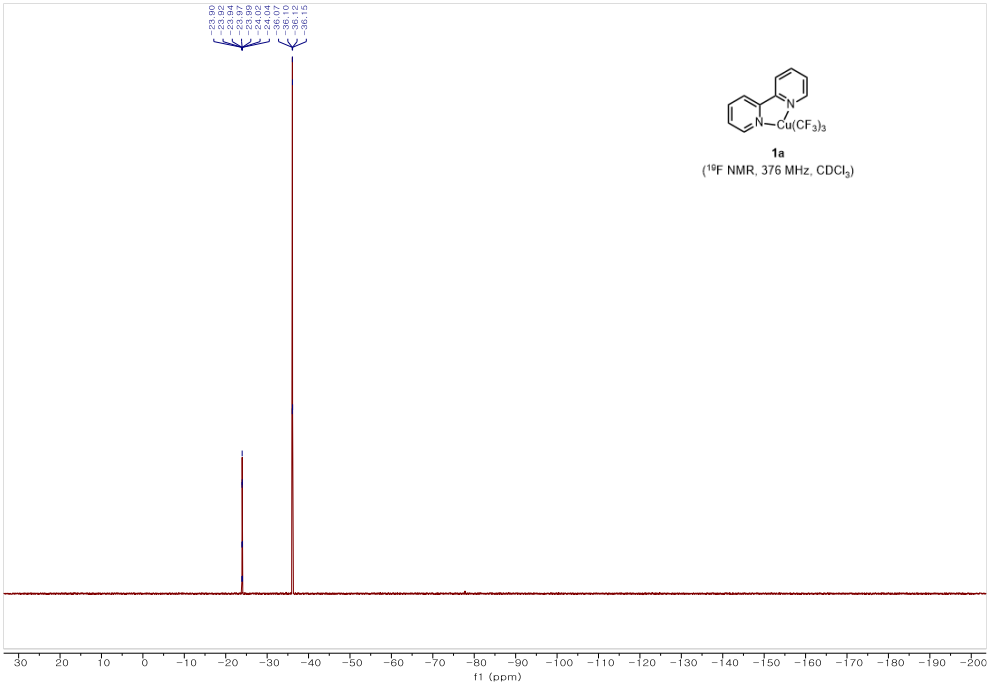
-23.90
-23.92
-23.94
-23.97
-23.99
-24.02
-24.04
-36.07
-36.10
-36.12
-36.15
f1 (ppm)
1a
(19F NMR, 376 MHz, CDCl3)

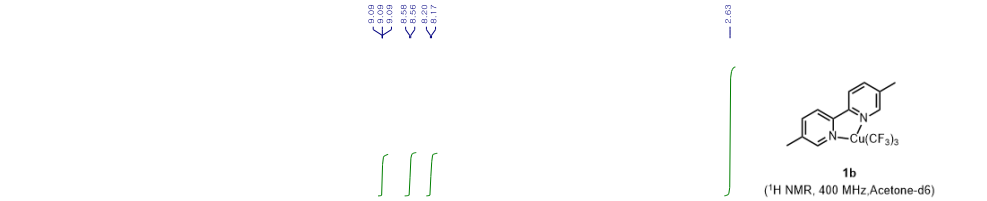

1b
(^{1}H NMR, 400 MHz,Acetone-d6)

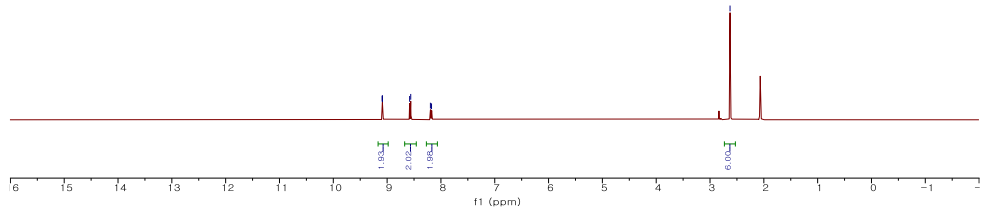

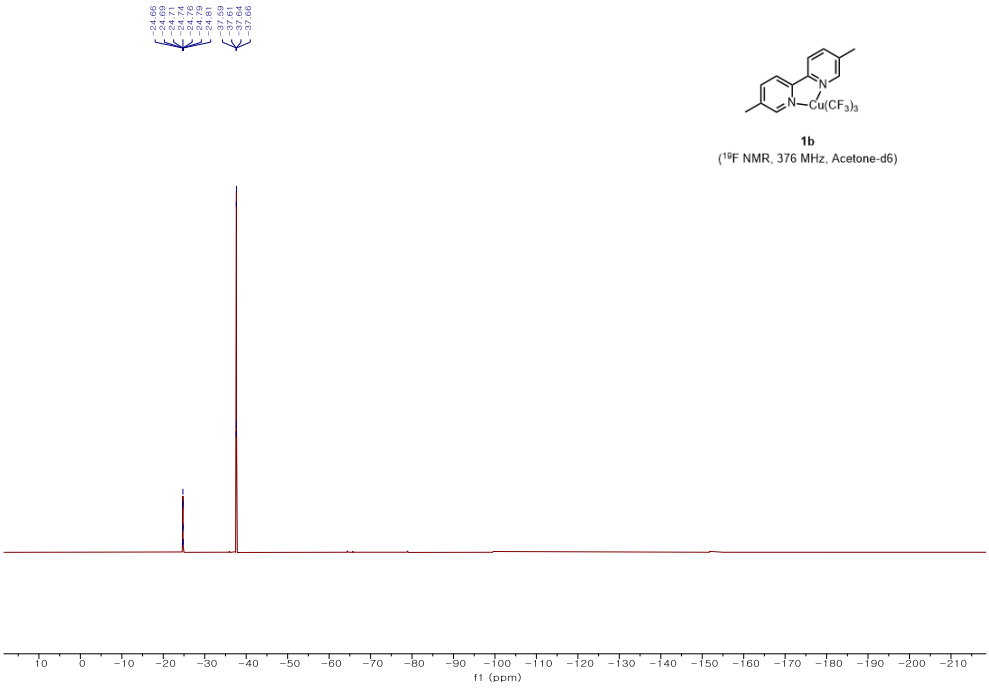

1b
(^{19}F NMR, 376 MHz, Acetone-d6)

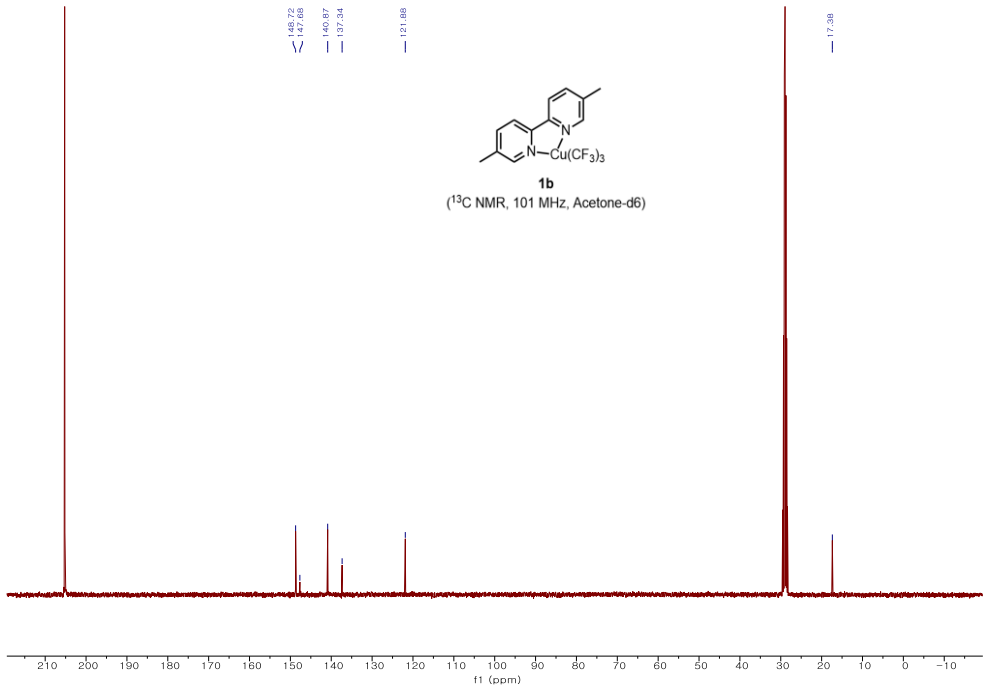

1b
(^{13}C NMR, 101 MHz, Acetone-d6)

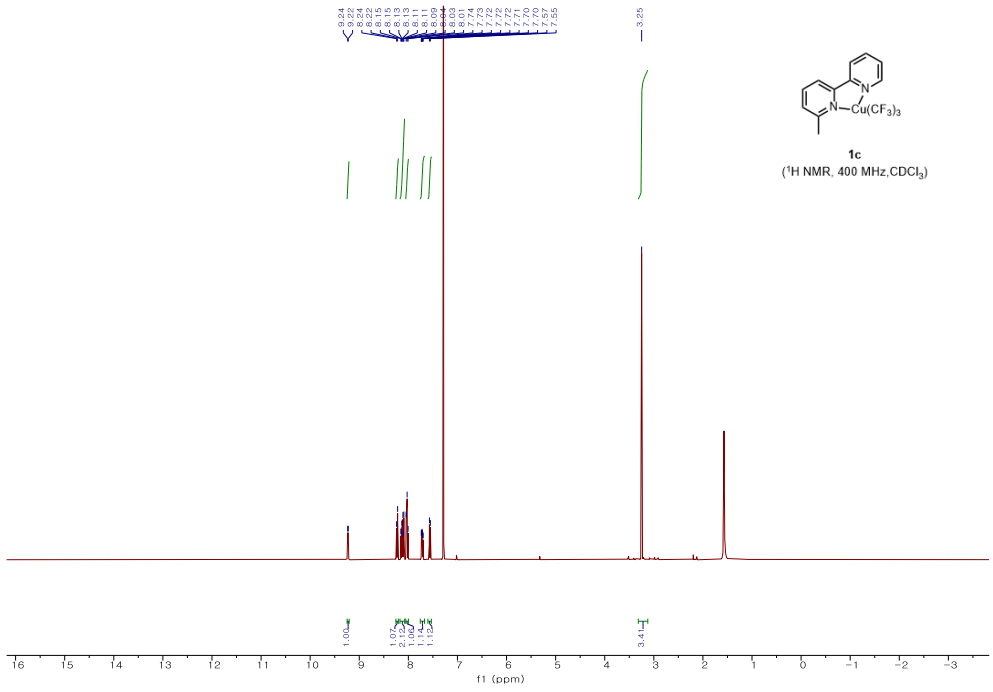

1c
(^{1}H NMR, 400 MHz,$CDCl_3$)

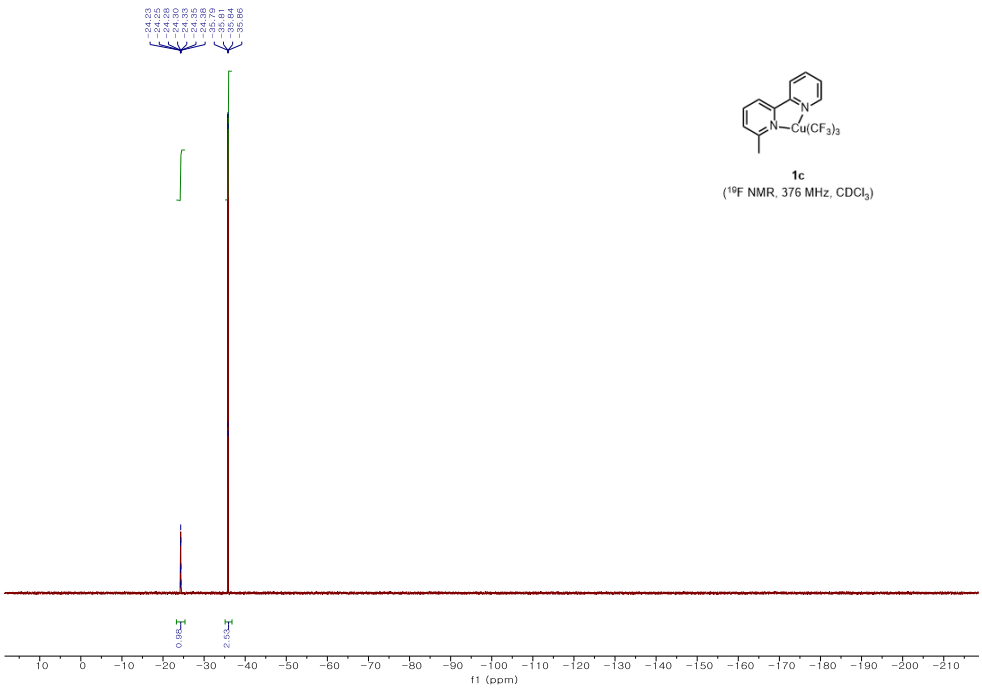

1c

(^{19}F NMR, 376 MHz, $CDCl_3$)

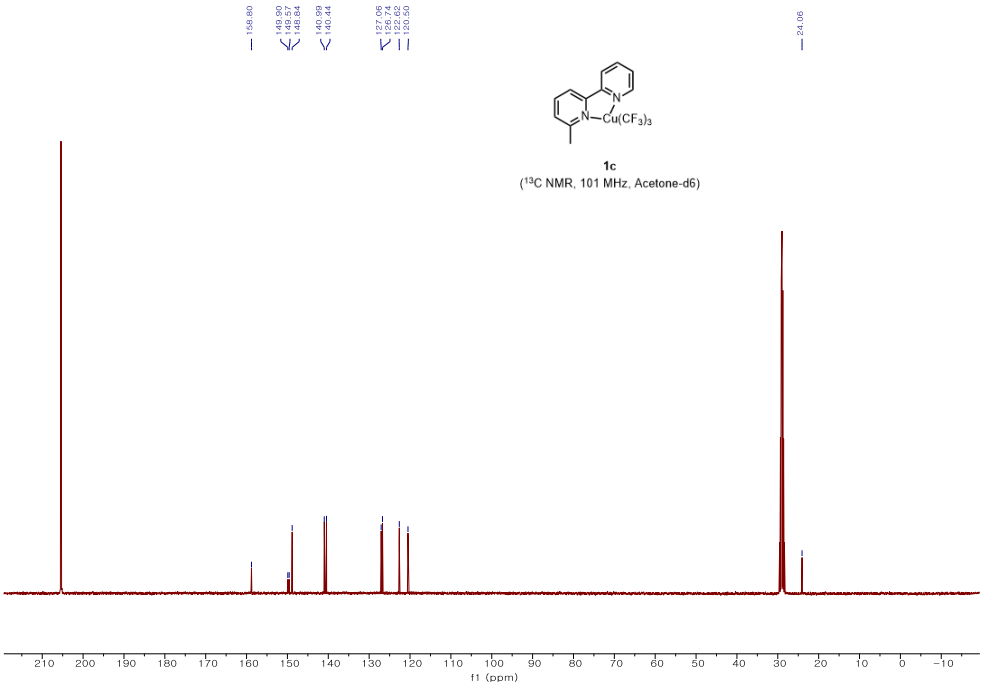

1c

(^{13}C NMR, 101 MHz, Acetone-d6)

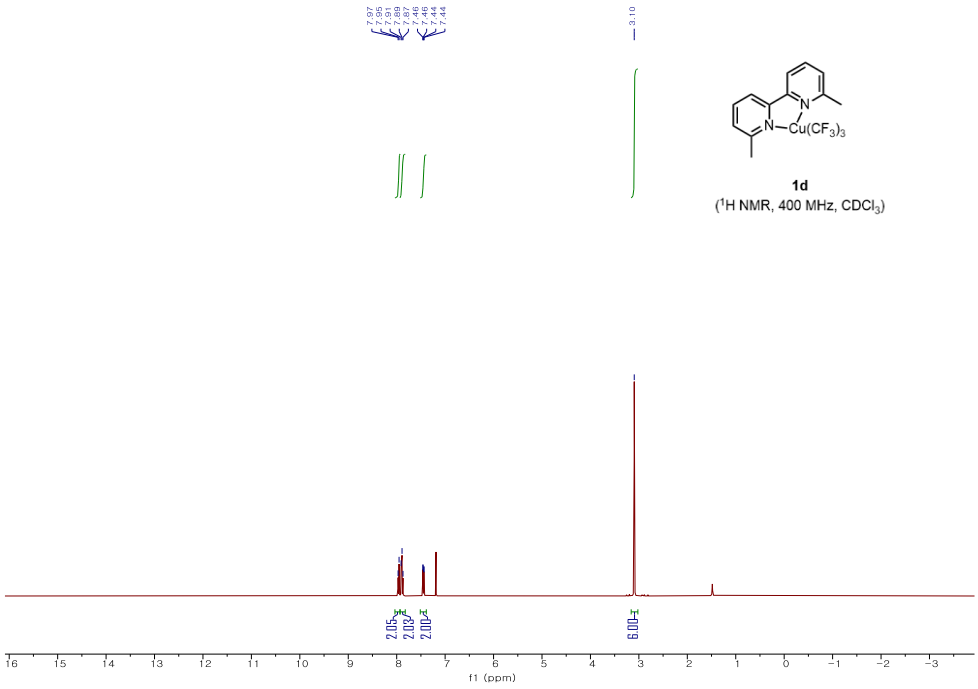

1d
(^{1}H NMR, 400 MHz, $CDCl_3$)

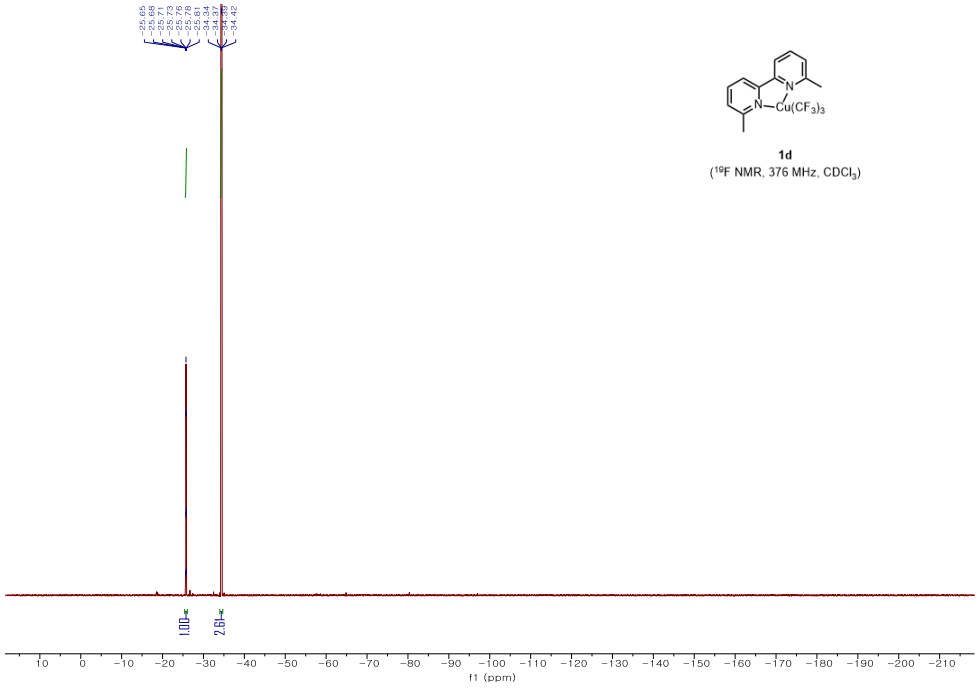

1d
(^{19}F NMR, 376 MHz, $CDCl_3$)

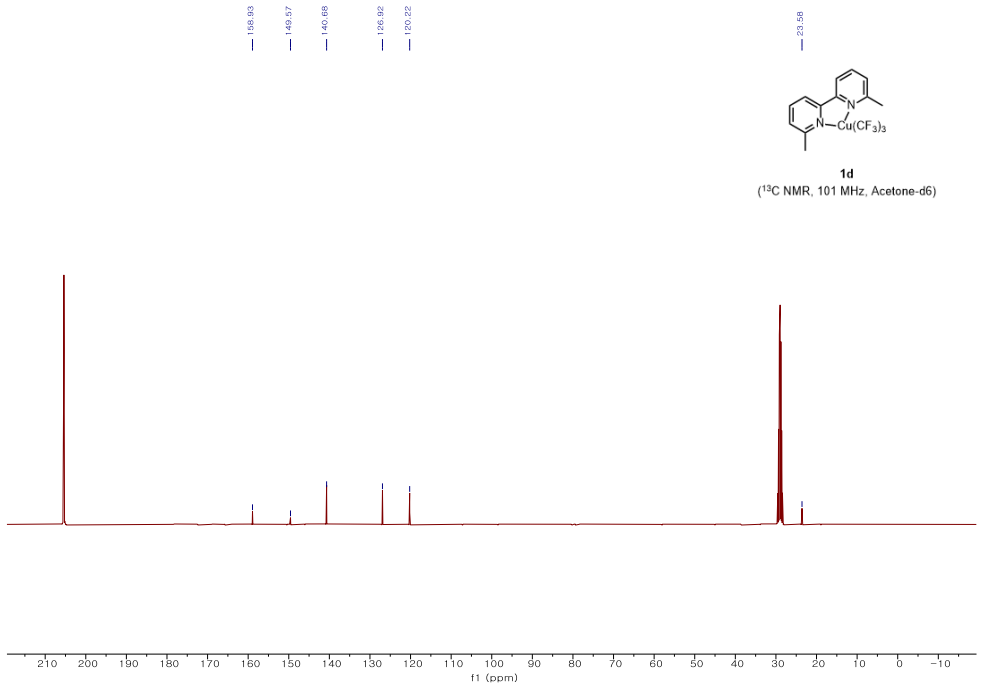

1d
(^{13}C NMR, 101 MHz, Acetone-d6)

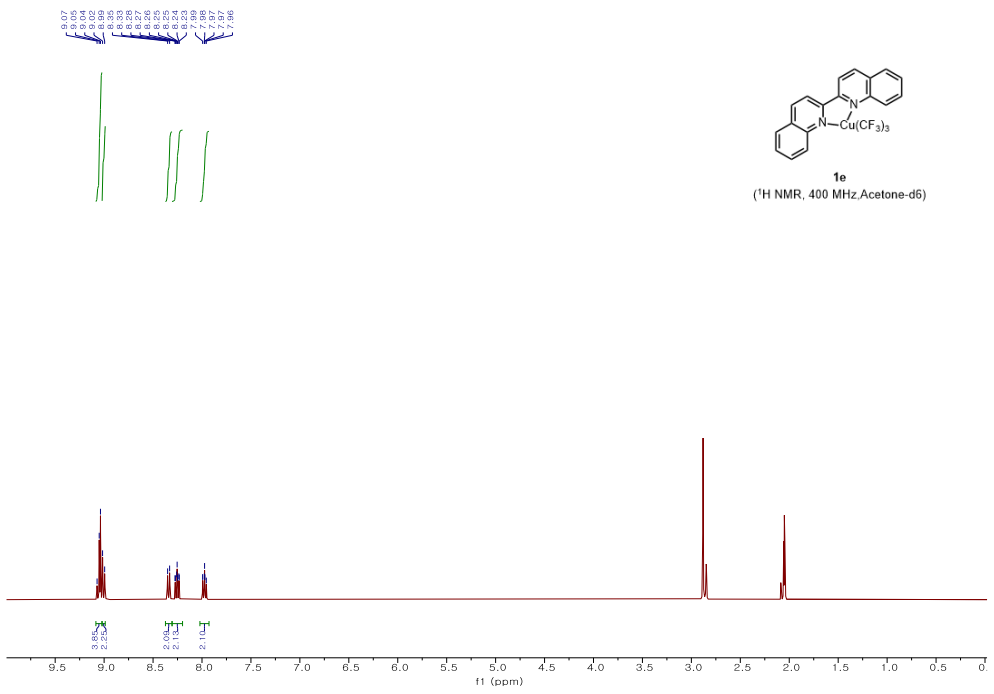

1e
(^{1}H NMR, 400 MHz,Acetone-d6)

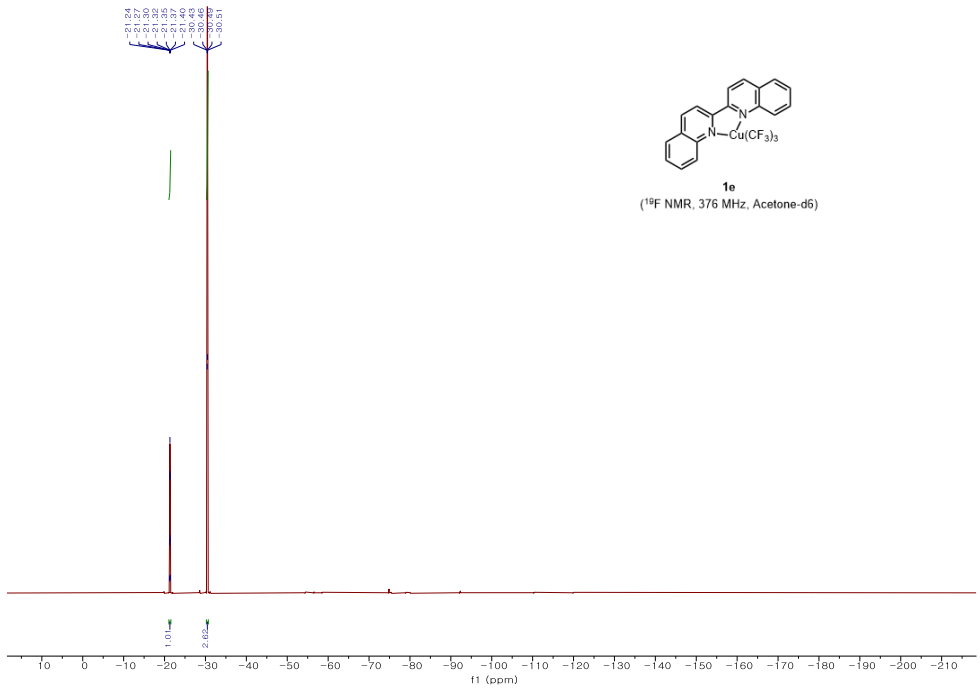

1e

(^{19}F NMR, 376 MHz, Acetone-d6)

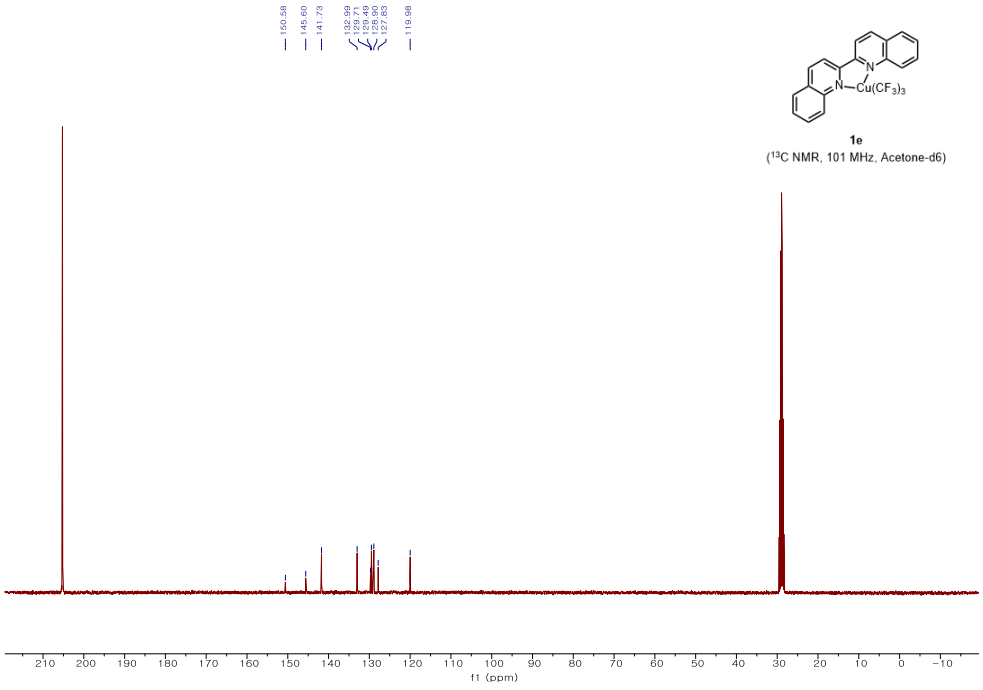

1e

(^{13}C NMR, 101 MHz, Acetone-d6)

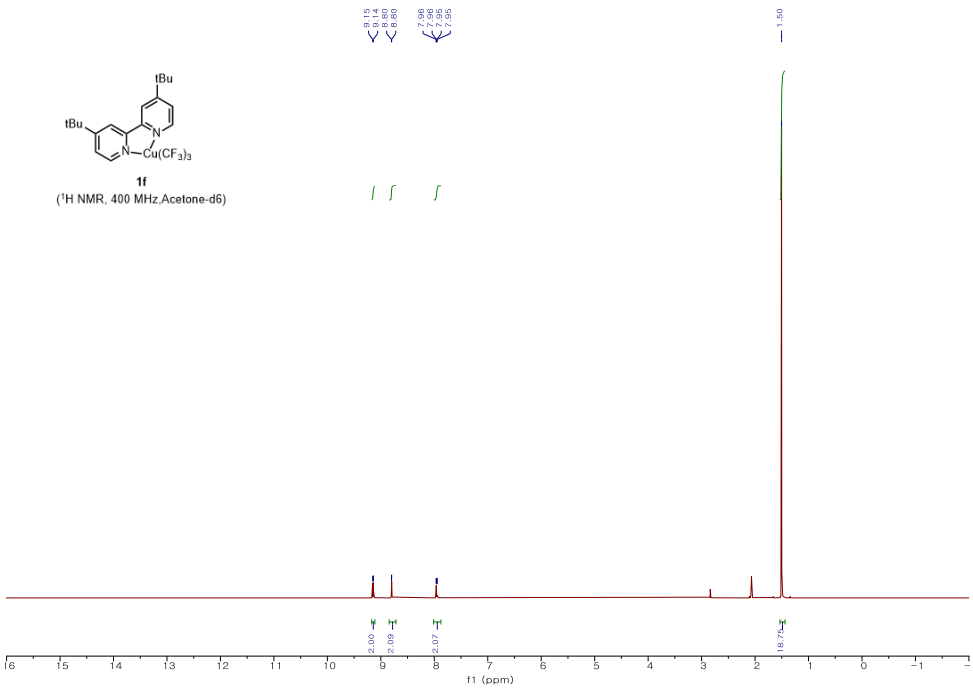
tBu
tBu
N
N
Cu(CF3)3
1f
(1H NMR, 400 MHz,Acetone-d6)
9.15
9.14
8.80
8.80
7.96
7.96
7.95
7.95
1.50
2.00
2.09
2.07
18.70
f1 (ppm)

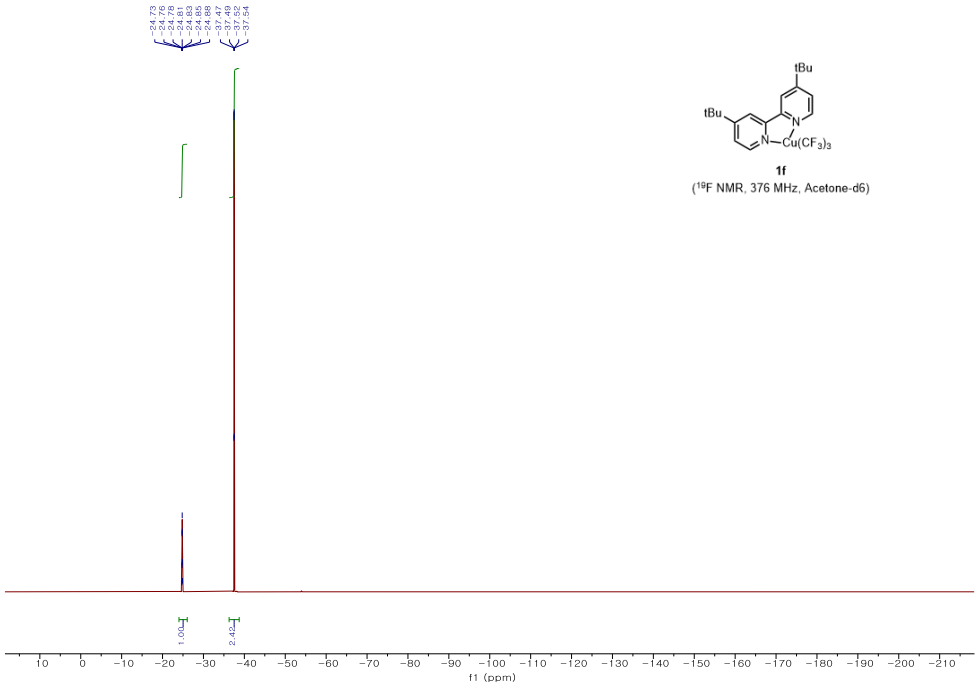
-24.73
-24.76
-24.78
-24.81
-24.83
-24.85
-24.88
-37.47
-37.49
-37.52
-37.54
tBu
tBu
N
N
Cu(CF3)3
1f
(19F NMR, 376 MHz, Acetone-d6)
1.00
2.42
f1 (ppm)

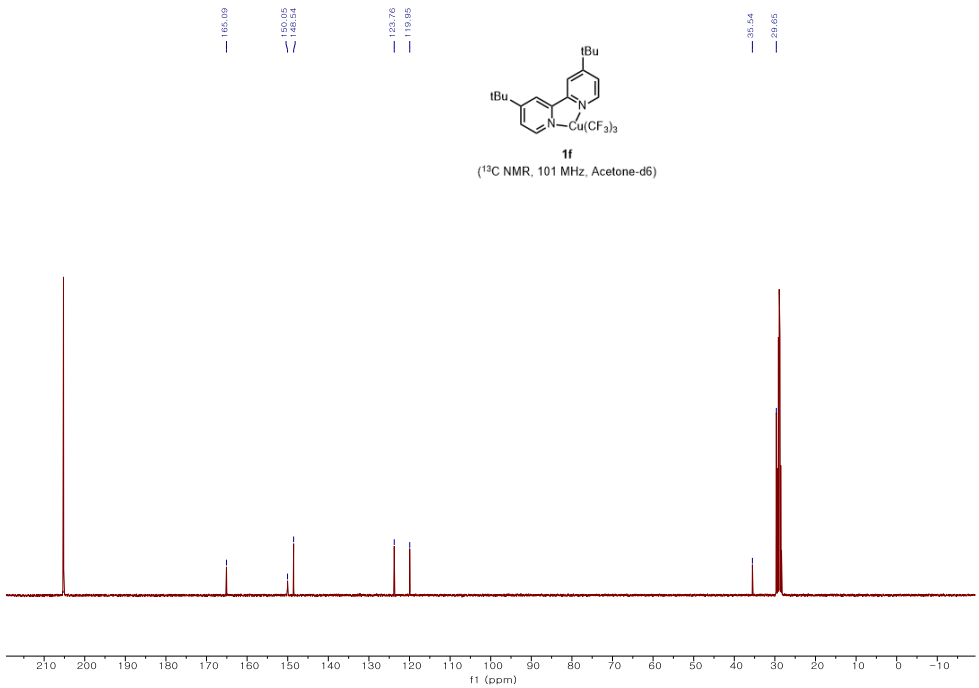

1f
(^{13}C NMR, 101 MHz, Acetone-d6)

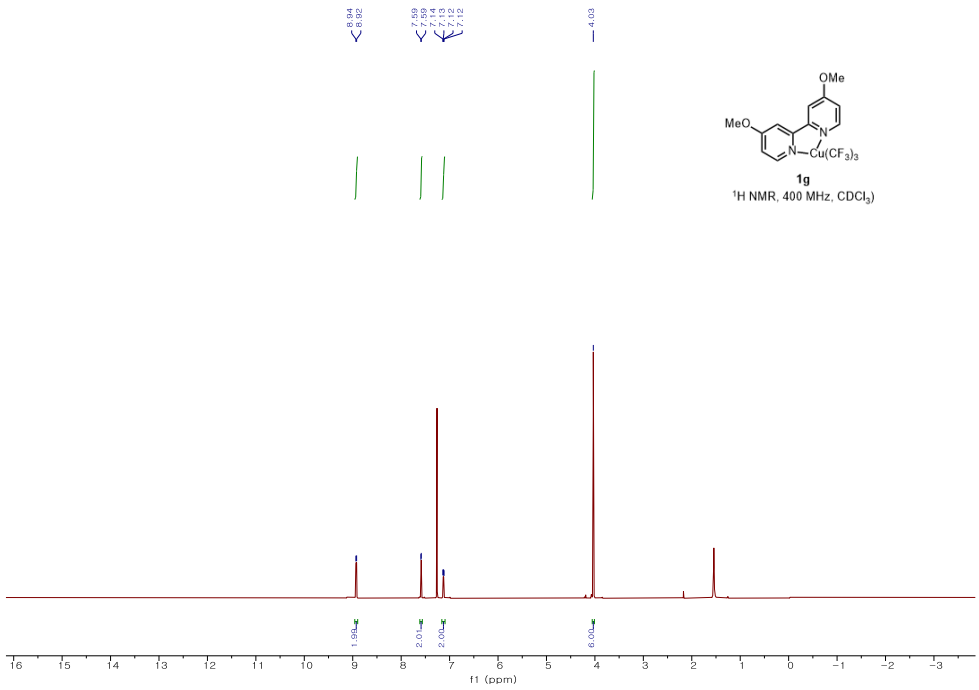

1g
(^{1}H NMR, 400 MHz, $CDCl_3$)

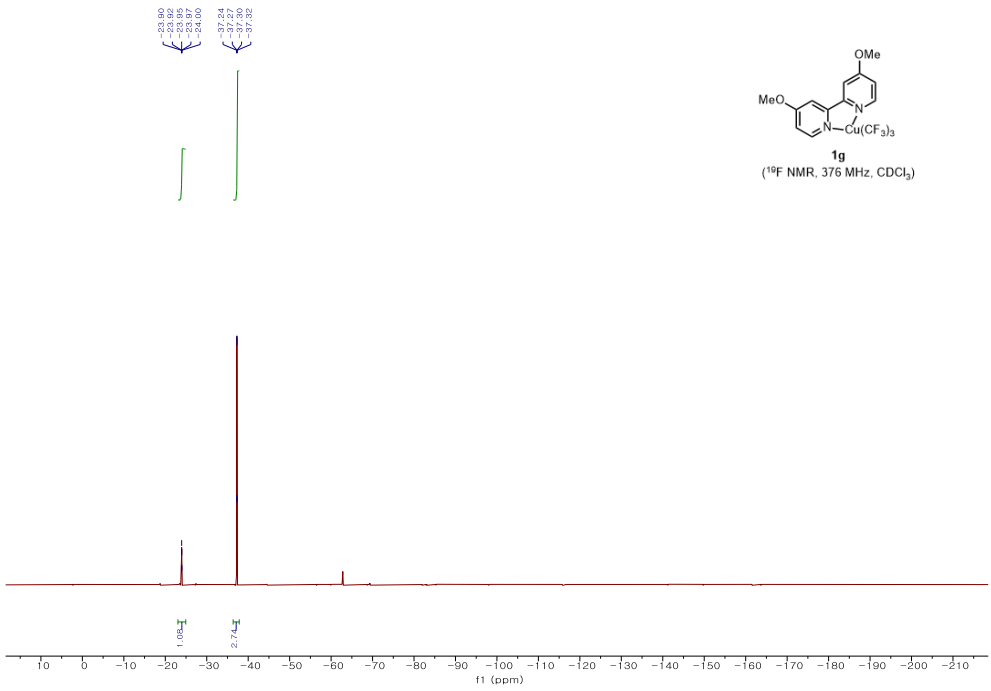

1g
(^{19}F NMR, 376 MHz, $CDCl_3$)

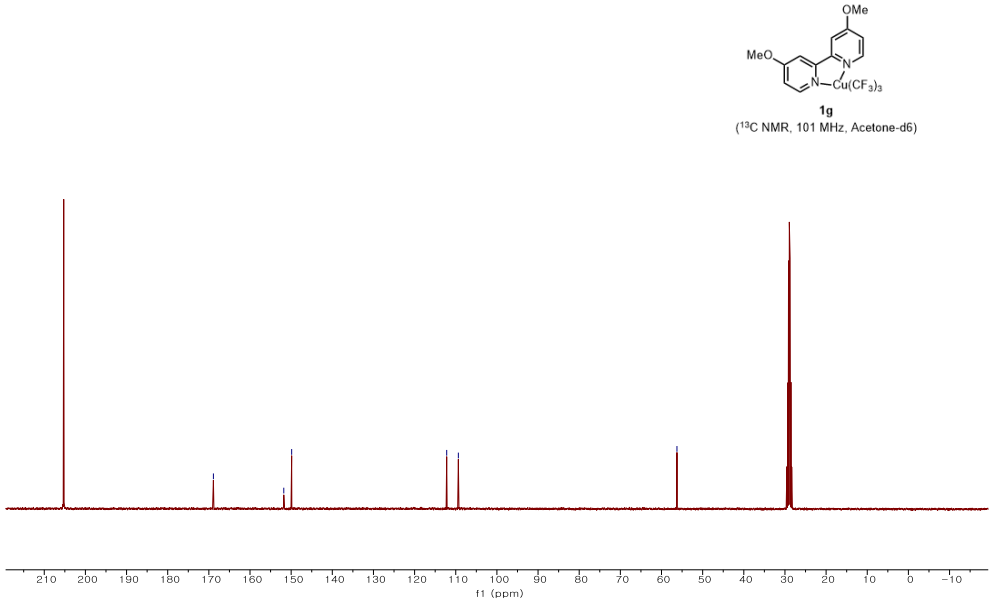

1g
(^{13}C NMR, 101 MHz, Acetone-d6)

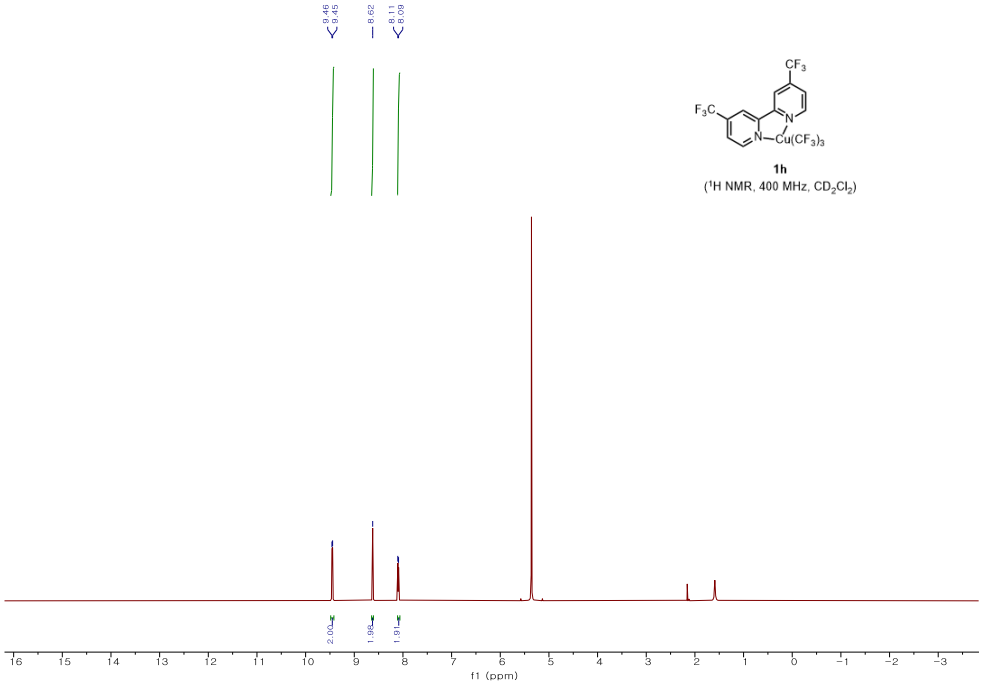

1h
(^{1}H NMR, 400 MHz, CD_2Cl_2)

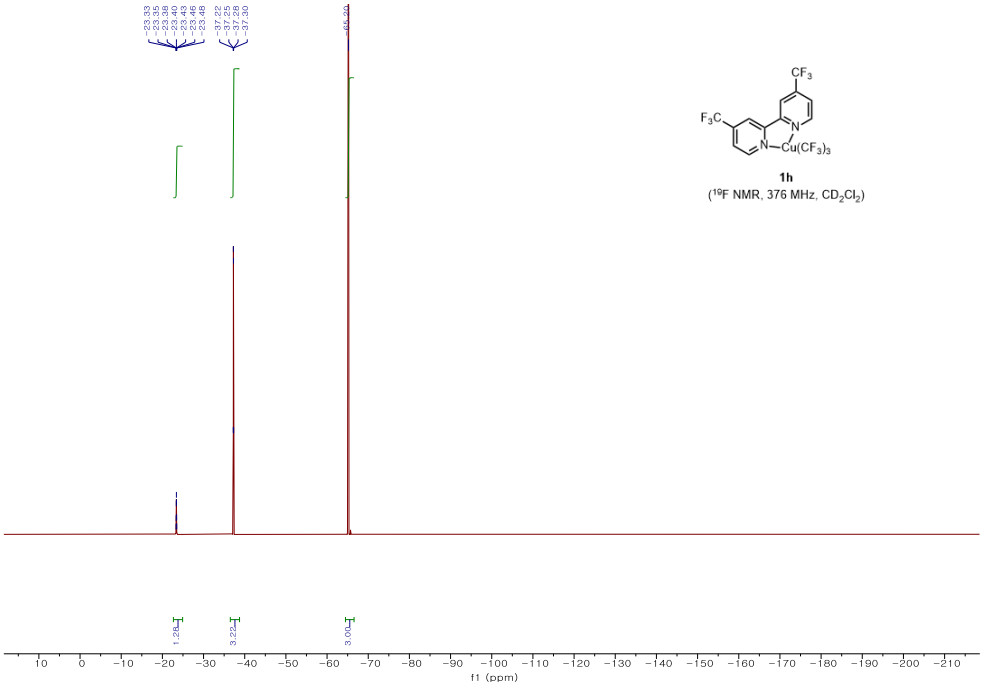

1h
(^{19}F NMR, 376 MHz, CD_2Cl_2)

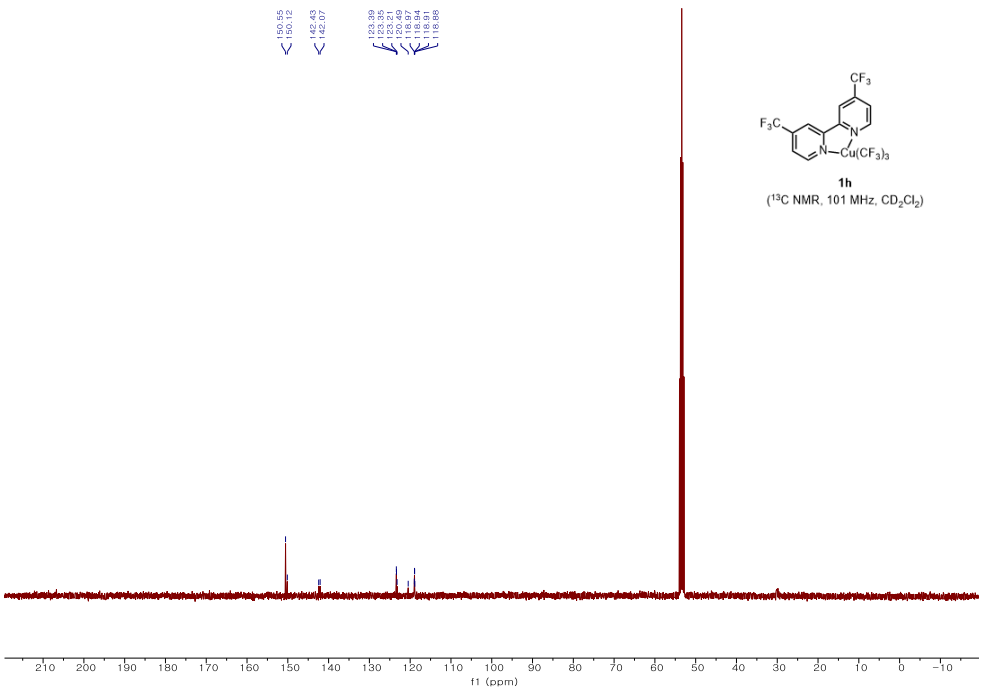

1h
(^{13}C NMR, 101 MHz, CD_2Cl_2)

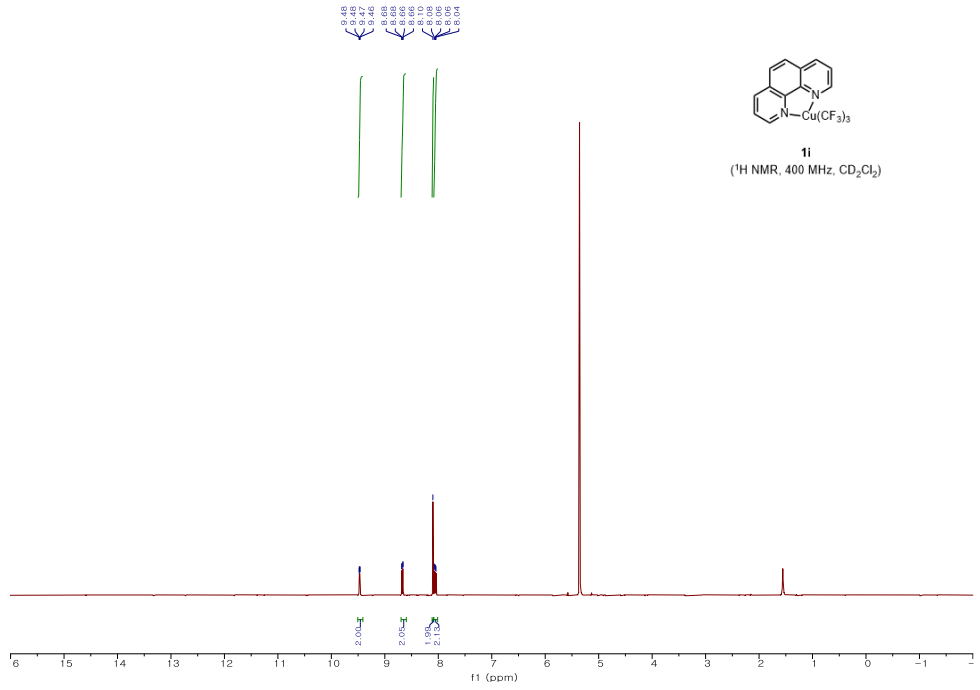

1i
(^{1}H NMR, 400 MHz, CD_2Cl_2)

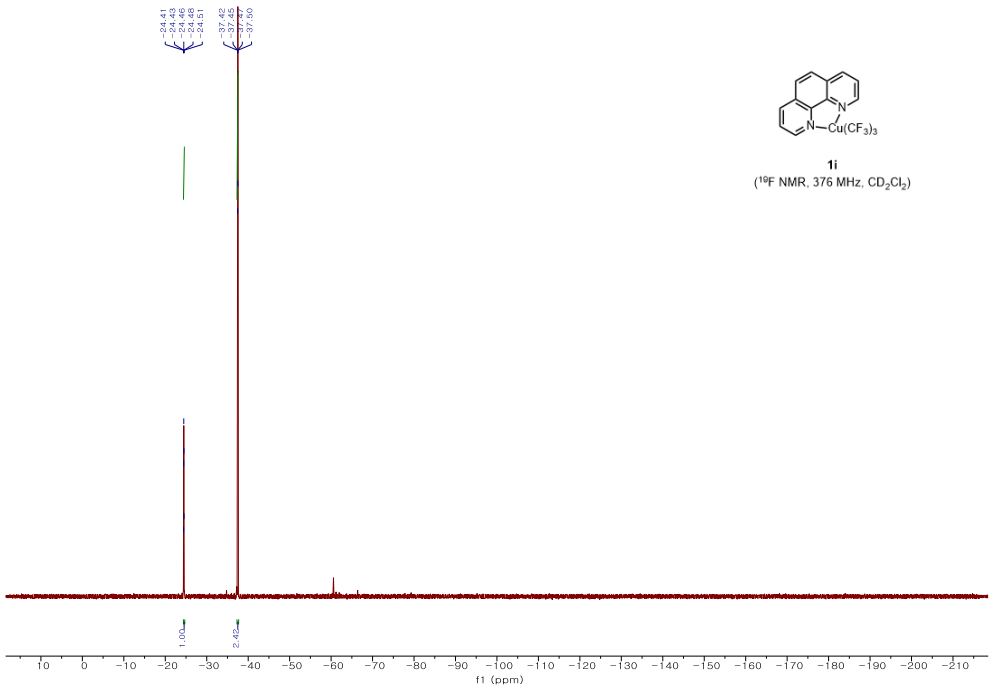

1i
(^{19}F NMR, 376 MHz, CD_2Cl_2)

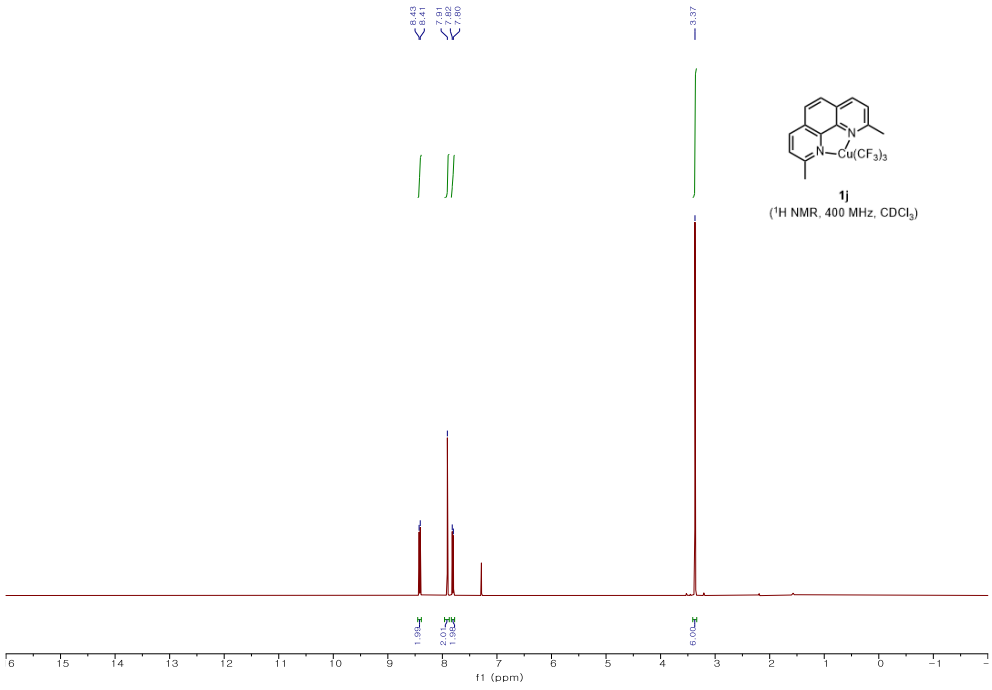

1j
(^{1}H NMR, 400 MHz, $CDCl_3$)

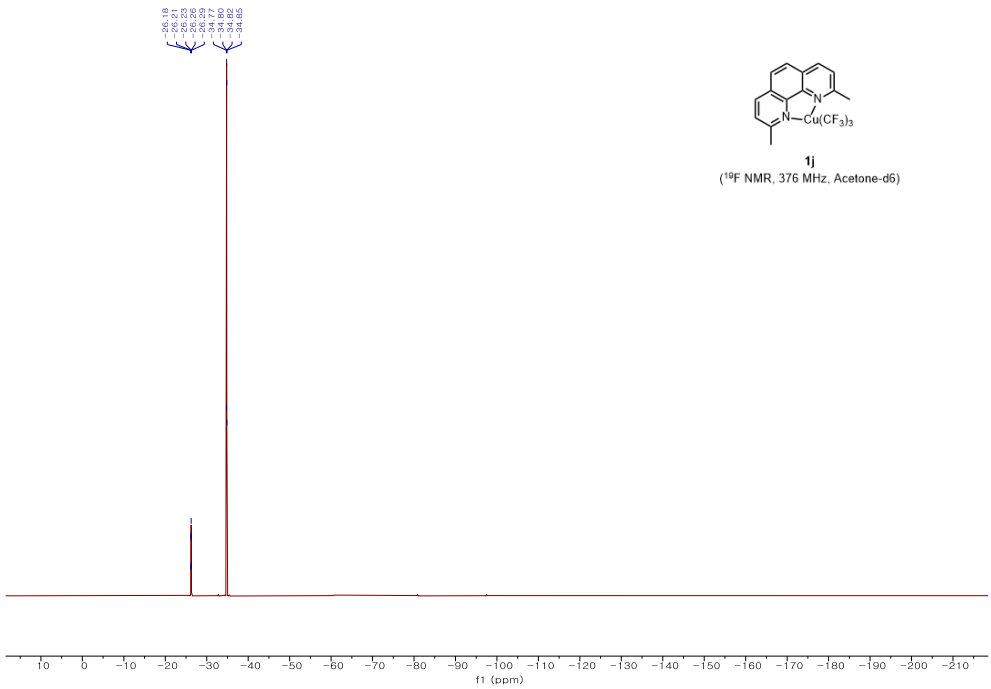

1j
(^{19}F NMR, 376 MHz, Acetone-d6)

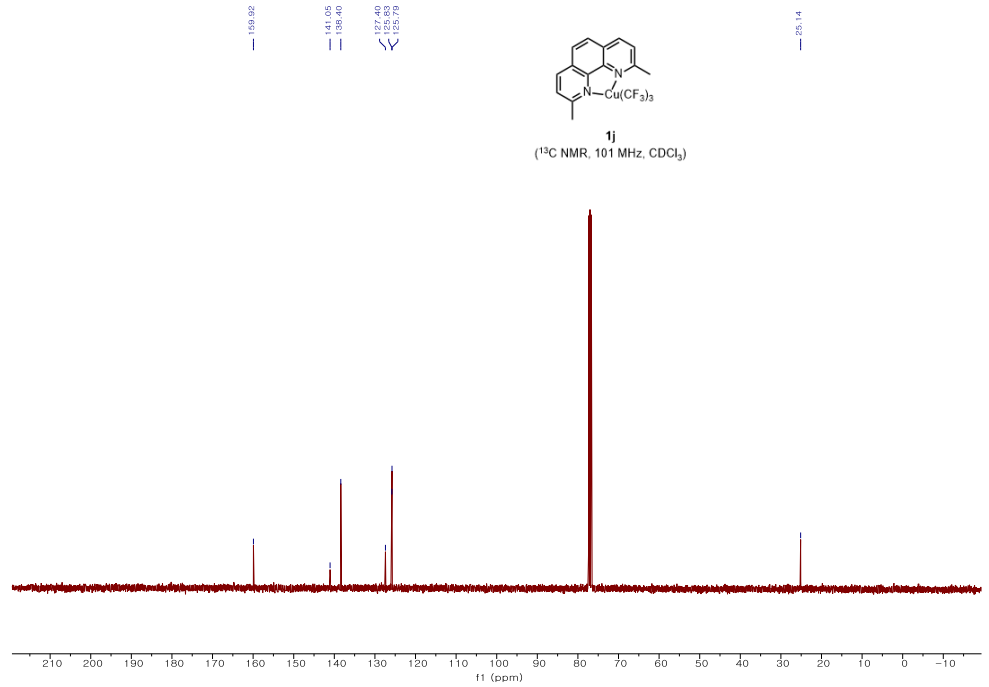

1j
(^{13}C NMR, 101 MHz, $CDCl_3$)

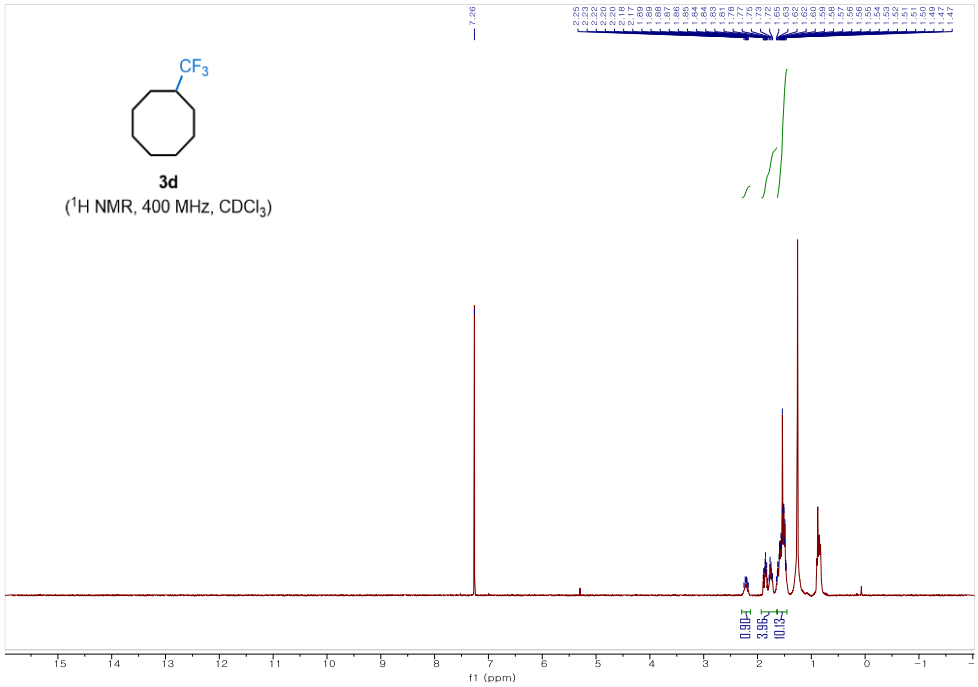
CF3
3d
(1H NMR, 400 MHz, CDCl3)
f1 (ppm)

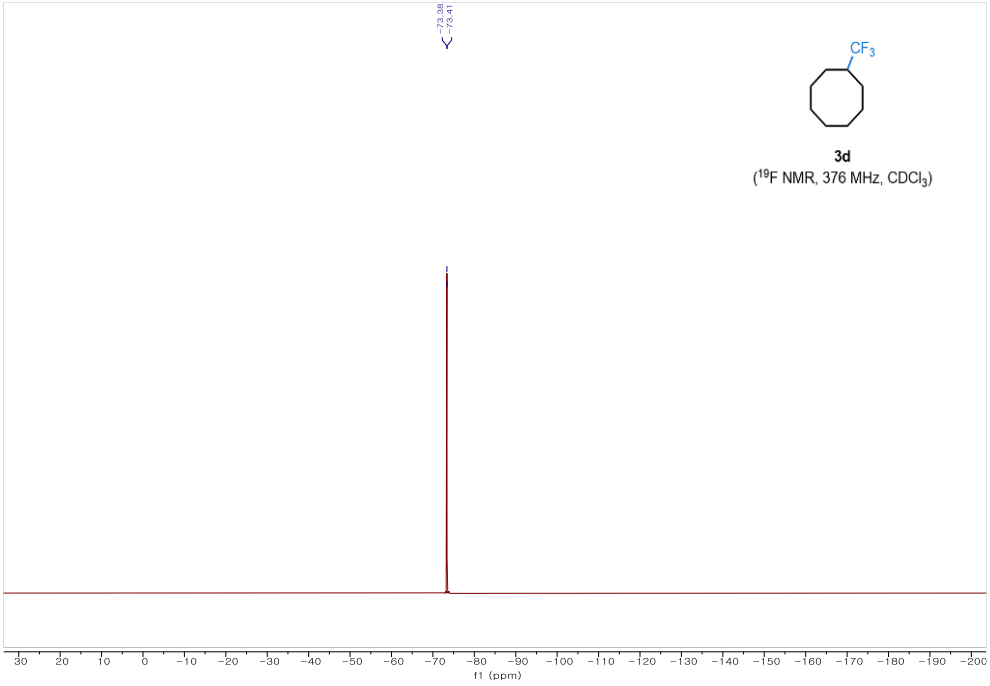
CF3
3d
(19F NMR, 376 MHz, CDCl3)
f1 (ppm)

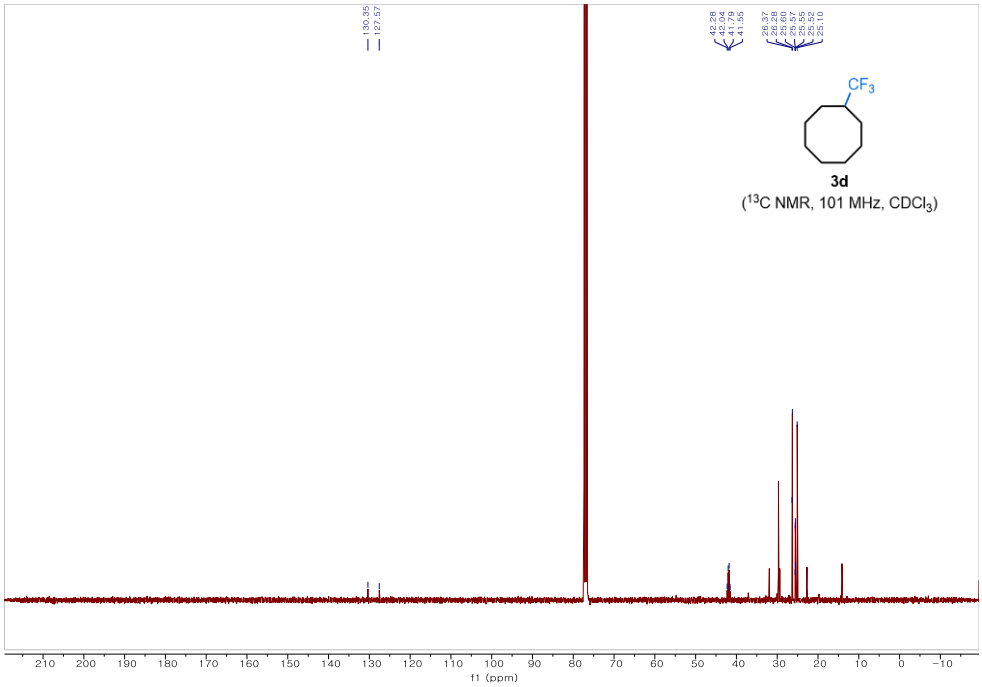
CF3
3d
(13C NMR, 101 MHz, CDCl3)
f1 (ppm)

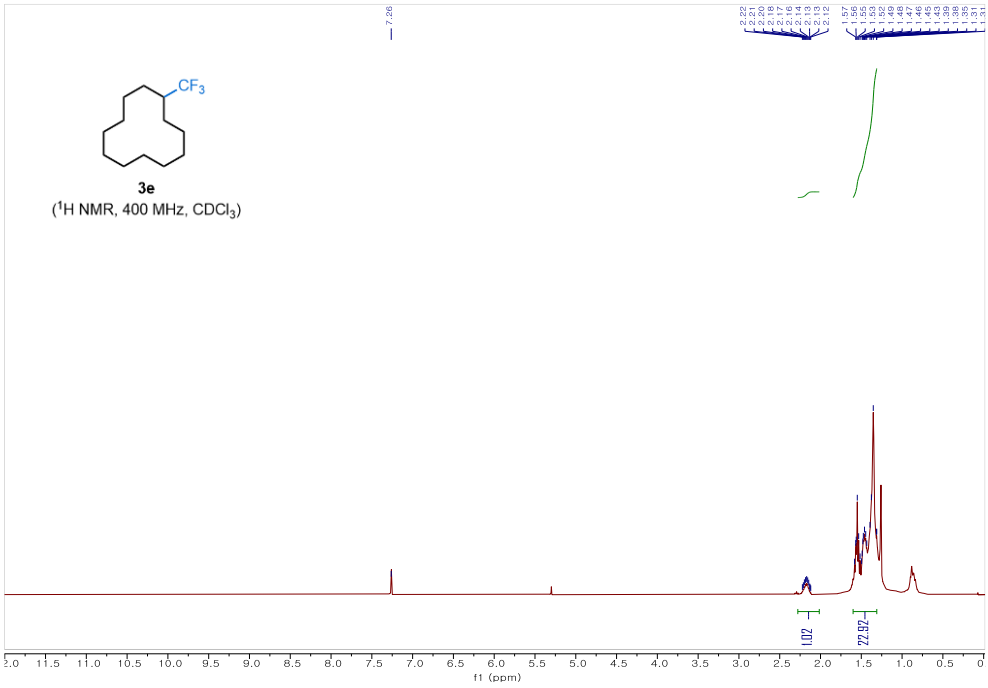
CF3
3e
(1H NMR, 400 MHz, CDCl3)
1.02
22.82
f1 (ppm)

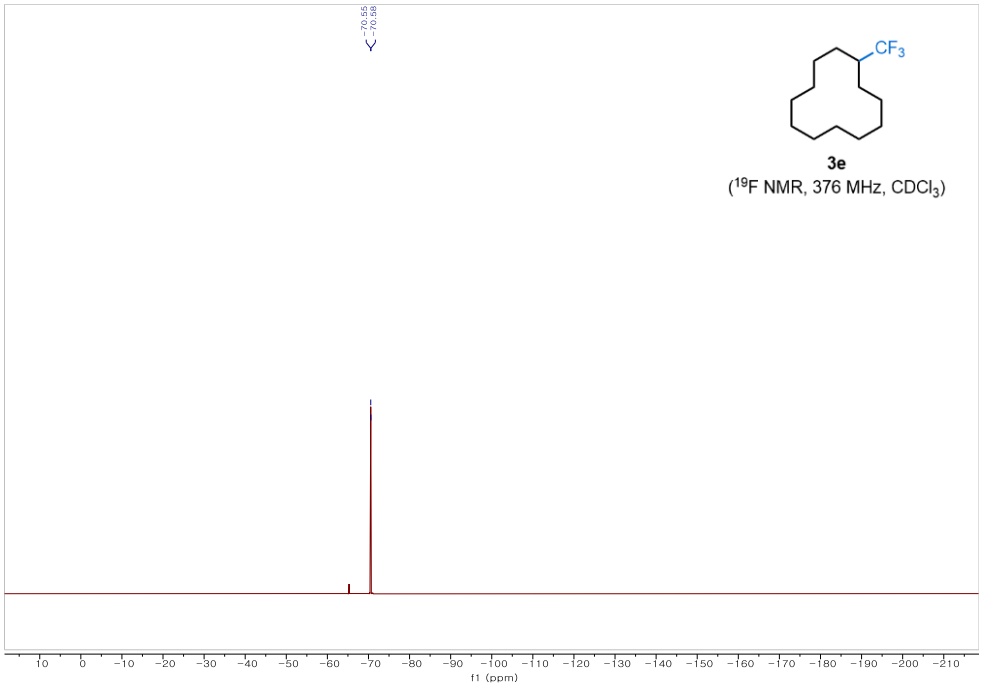
-70.55
-70.58
CF3
3e
(19F NMR, 376 MHz, CDCl3)
f1 (ppm)

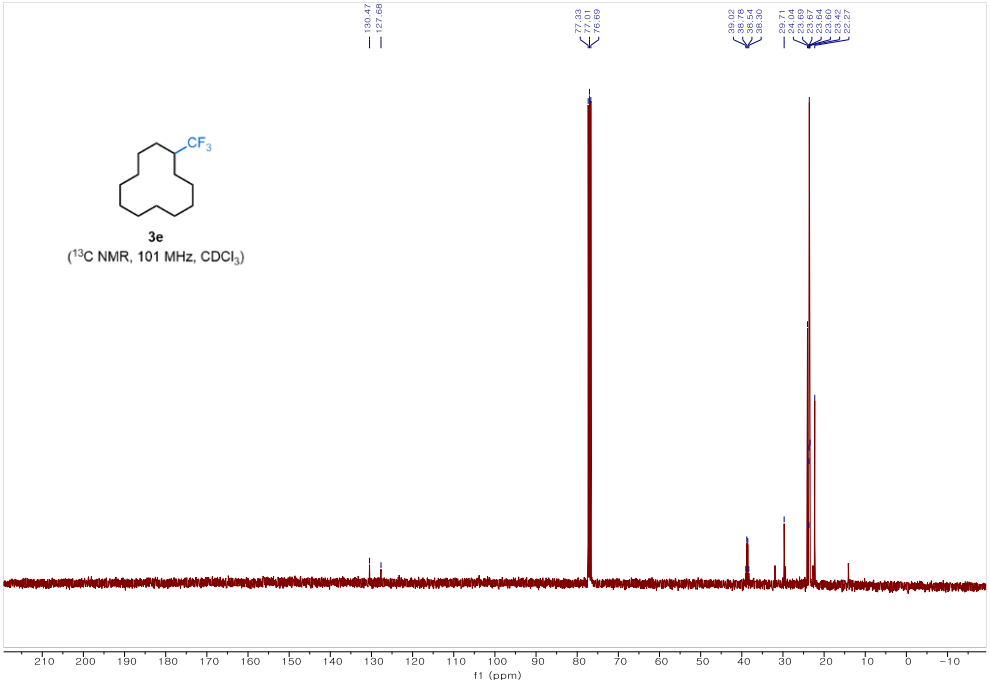
130.47
127.68
77.33
77.01
76.69
39.02
38.78
38.54
38.30
29.71
24.44
23.69
23.67
23.64
23.60
23.42
22.27
CF3
3e
(13C NMR, 101 MHz, CDCl3)
f1 (ppm)

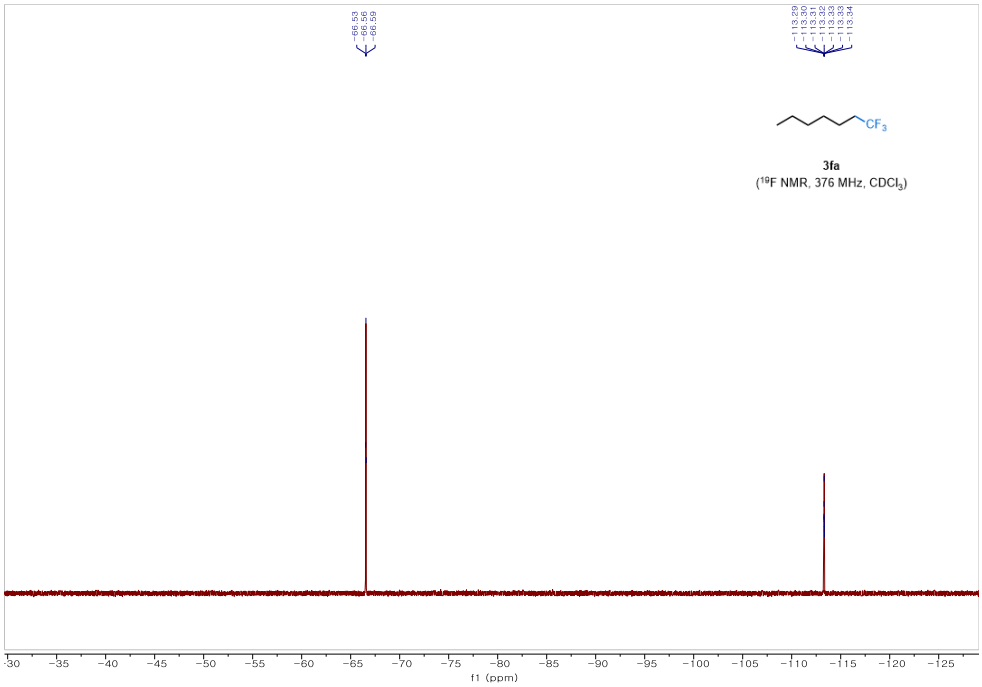

3fa
(^{19}F NMR, 376 MHz, $CDCl_3$)

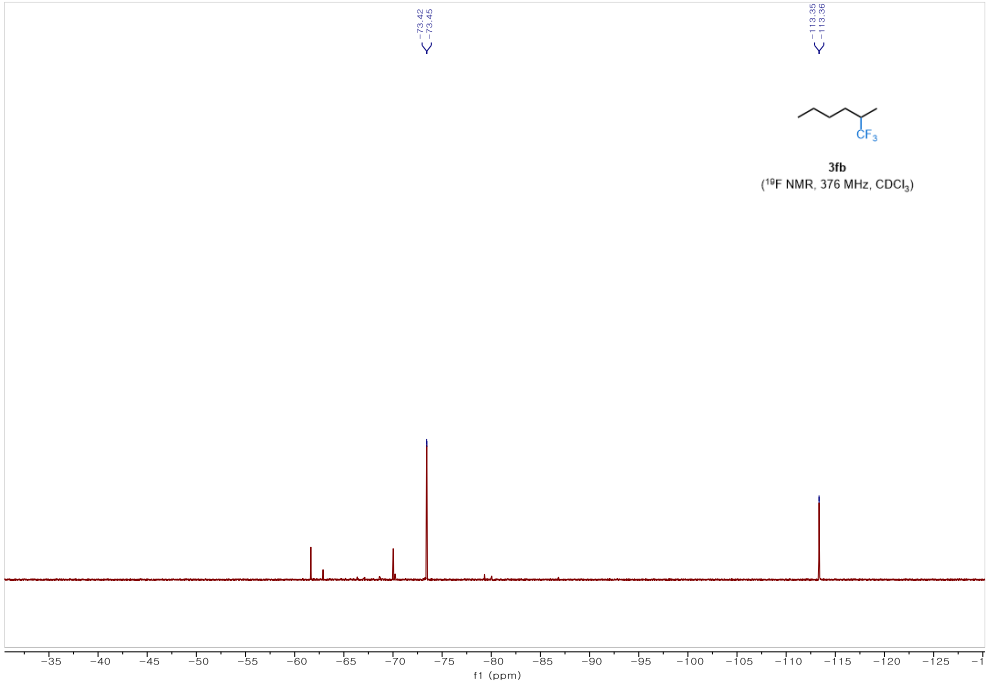

3fb
(^{19}F NMR, 376 MHz, $CDCl_3$)

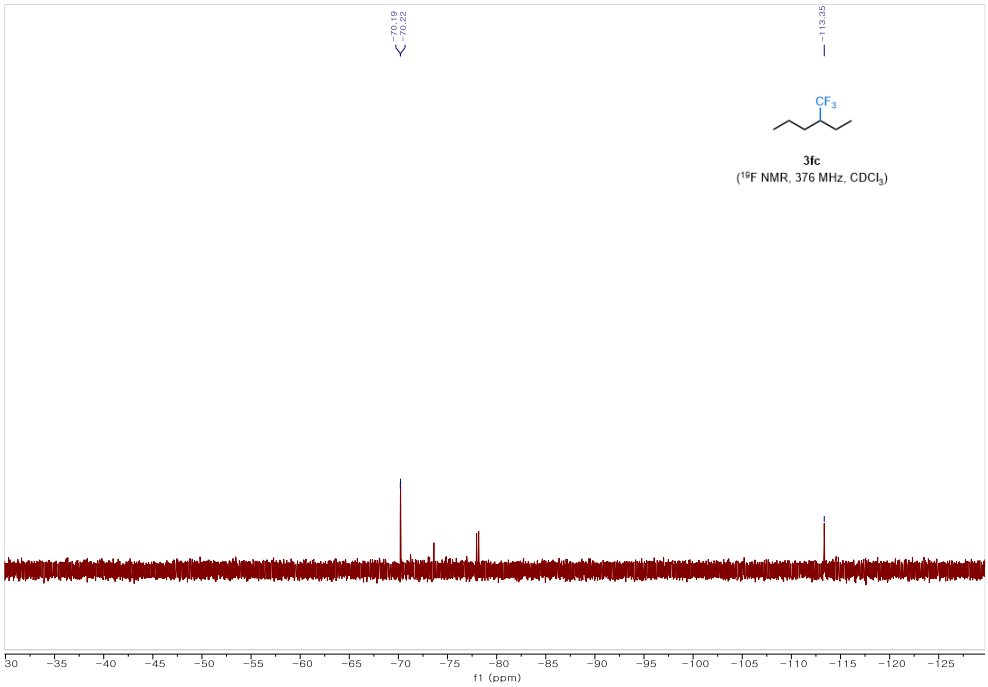
-70.19
-70.22
-113.35
CF3
3fc
(19F NMR, 376 MHz, CDCl3)
f1 (ppm)

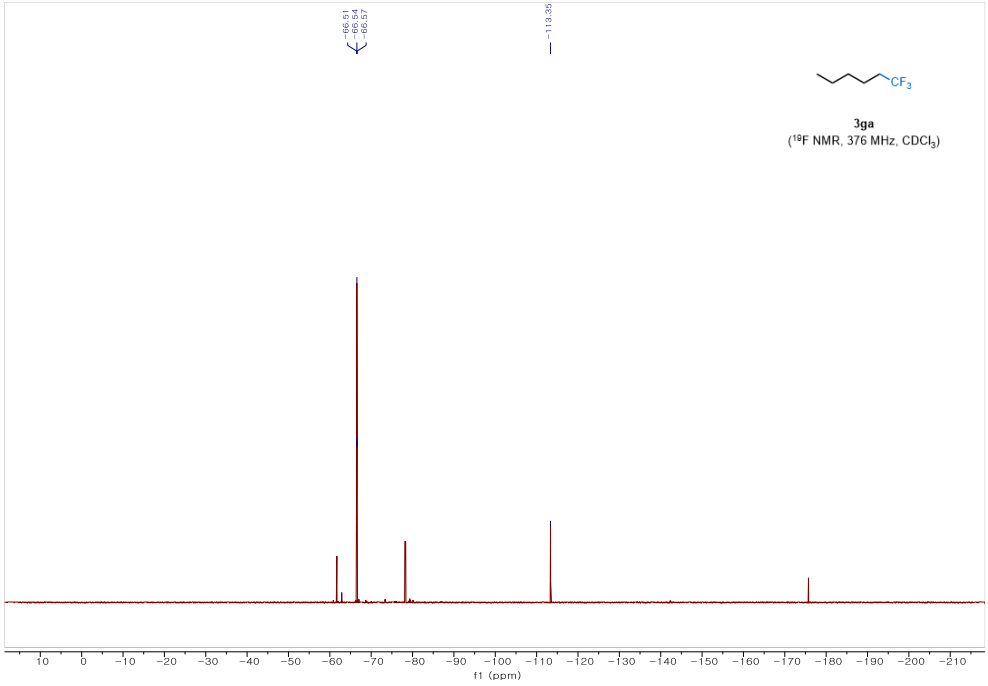
-66.51
-66.54
-66.57
-113.35
CF3
3ga
(19F NMR, 376 MHz, CDCl3)
f1 (ppm)

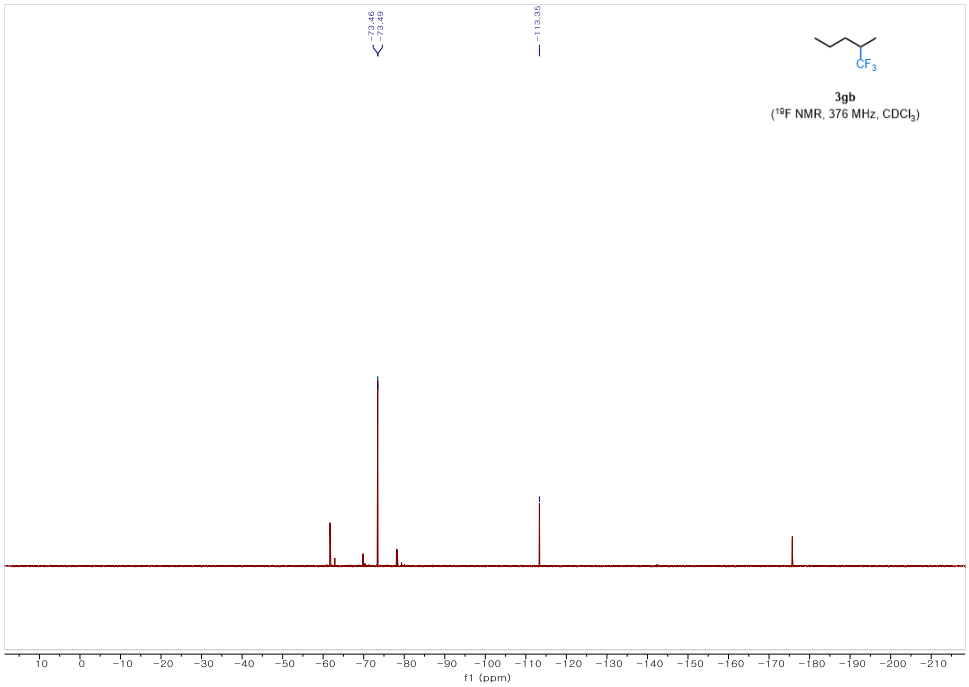
-73.46
-73.49
-113.35
CF3
3gb
(19F NMR, 376 MHz, CDCl3)
10 0 -10 -20 -30 -40 -50 -60 -70 -80 -90 -100 -110 -120 -130 -140 -150 -160 -170 -180 -190 -200 -210
f1 (ppm)

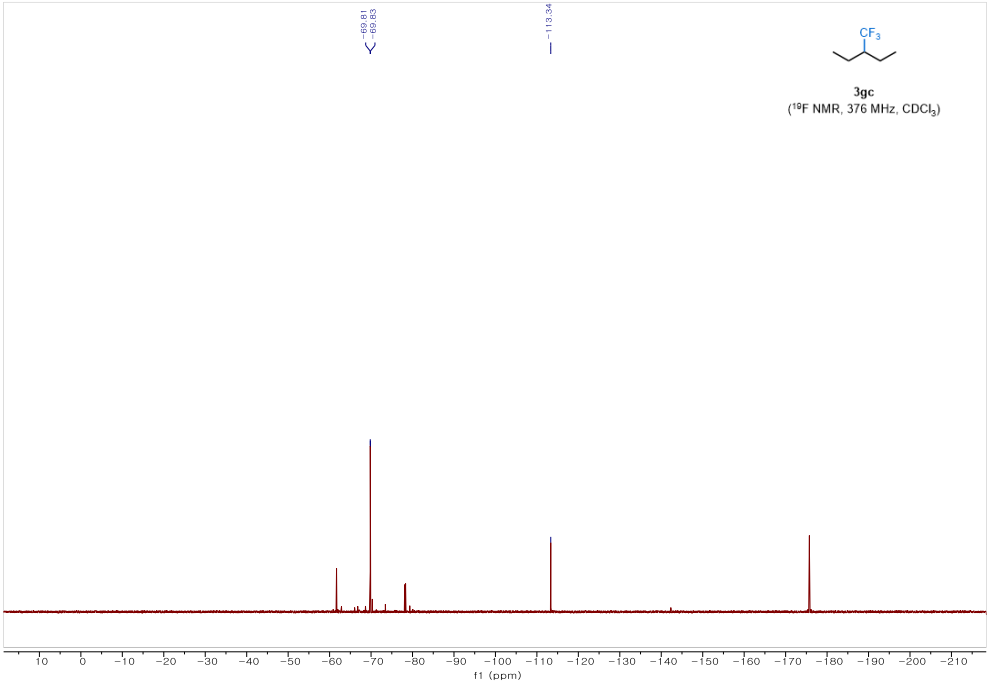
-69.81
-69.83
-113.34
CF3
3gc
(19F NMR, 376 MHz, CDCl3)
10 0 -10 -20 -30 -40 -50 -60 -70 -80 -90 -100 -110 -120 -130 -140 -150 -160 -170 -180 -190 -200 -210
f1 (ppm)

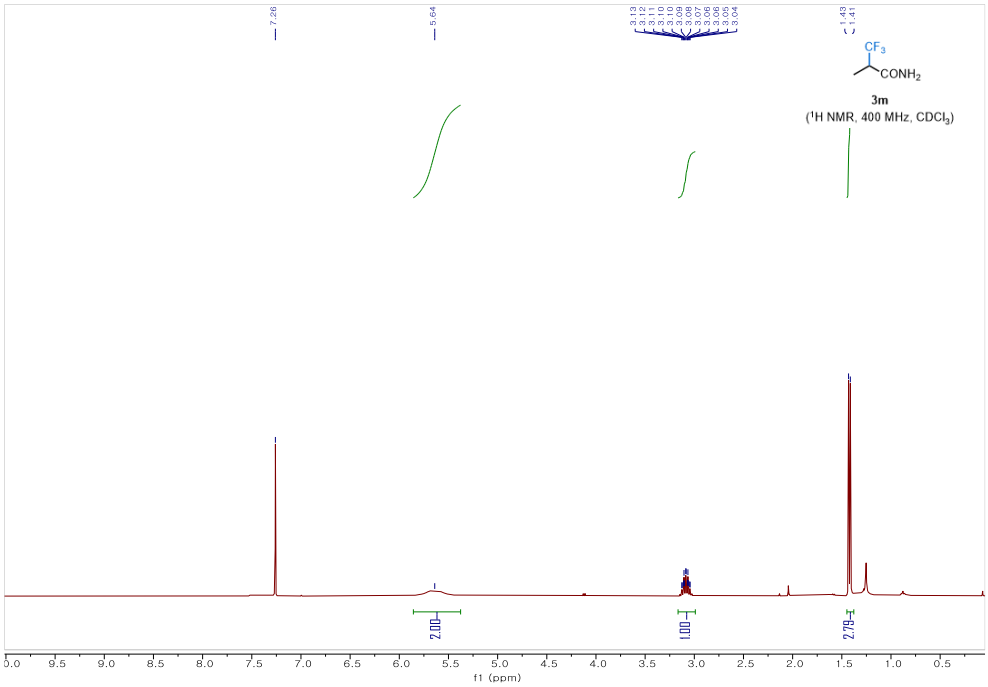
7.26
5.64
3.13
3.12
3.11
3.10
3.09
3.08
3.07
3.06
3.05
3.04
1.43
1.41
CF3
CONH2
3m
(1H NMR, 400 MHz, CDCl3)
2.00
1.00
2.79
f1 (ppm)

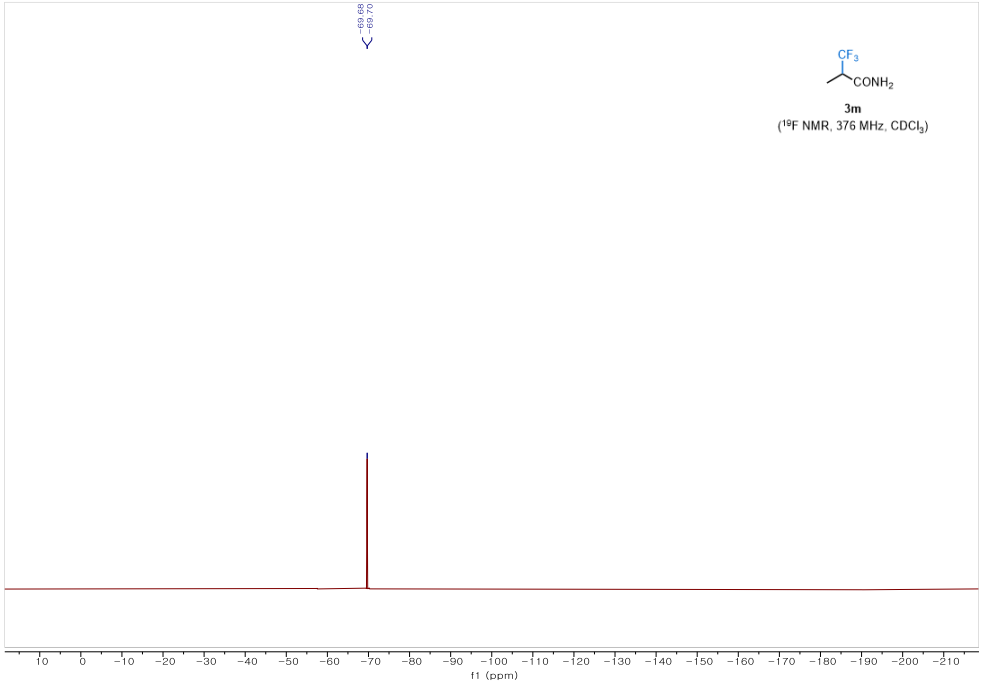
-69.68
-69.70
CF3
CONH2
3m
(19F NMR, 376 MHz, CDCl3)
f1 (ppm)

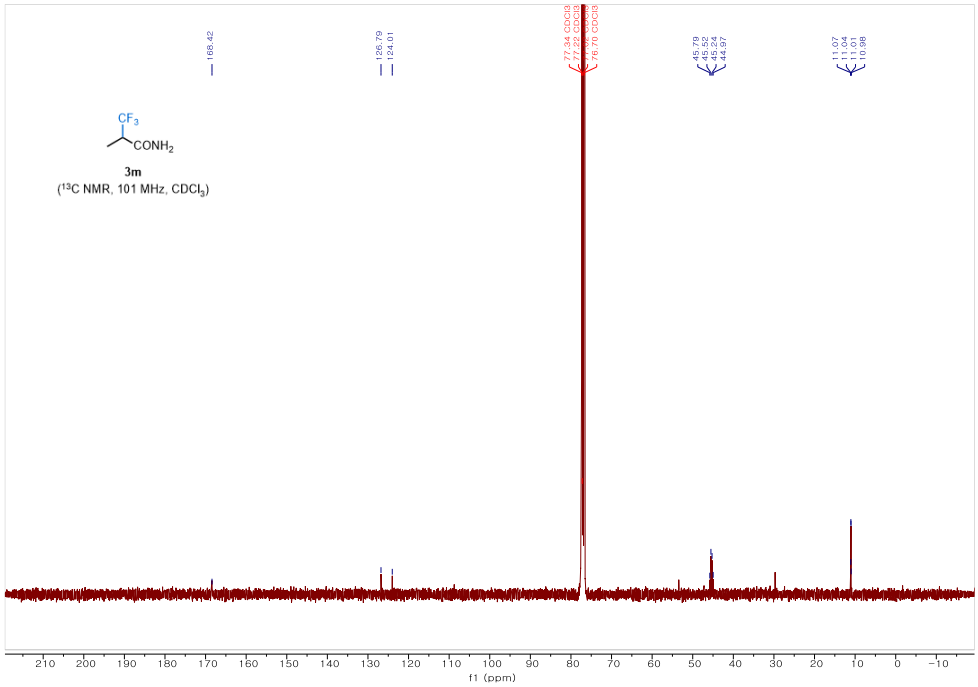
168.42
126.79
124.01
77.34 CDCl3
77.02 CDCl3
76.70 CDCl3
45.79
45.53
45.24
44.97
11.07
11.04
11.01
10.98
CF3
CONH2
3m
(13C NMR, 101 MHz, CDCl3)
f1 (ppm)

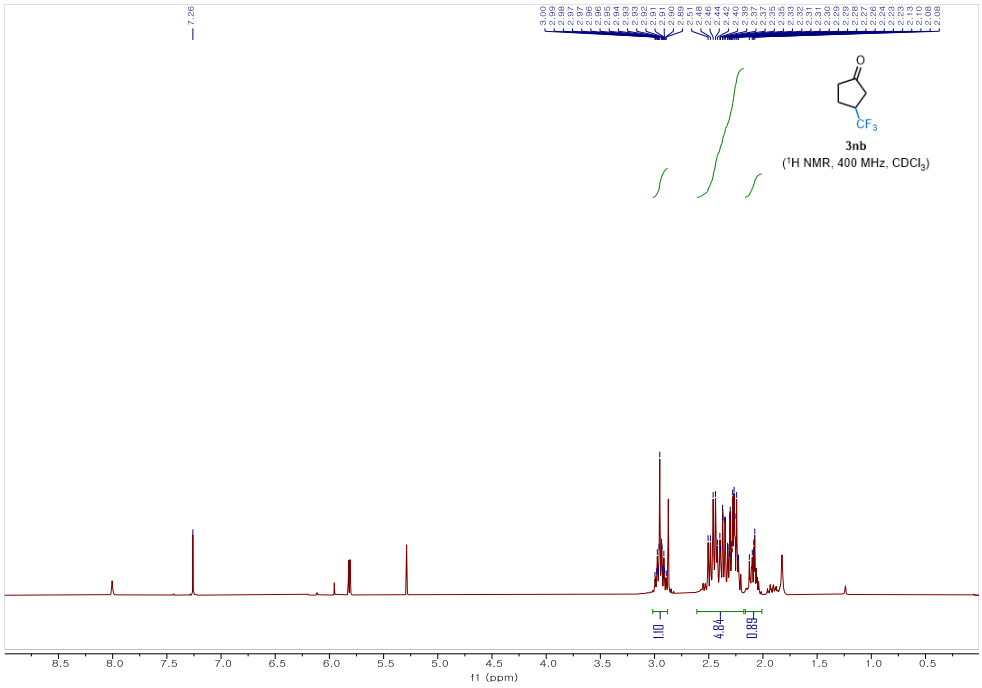
7.26
O
CF3
3nb
(1H NMR, 400 MHz, CDCl3)
1.00
4.84
0.89
f1 (ppm)

^{19}F NMR (376 MHz, $CDCl_3$) δ -72.41 (d, J = 8.7 Hz).

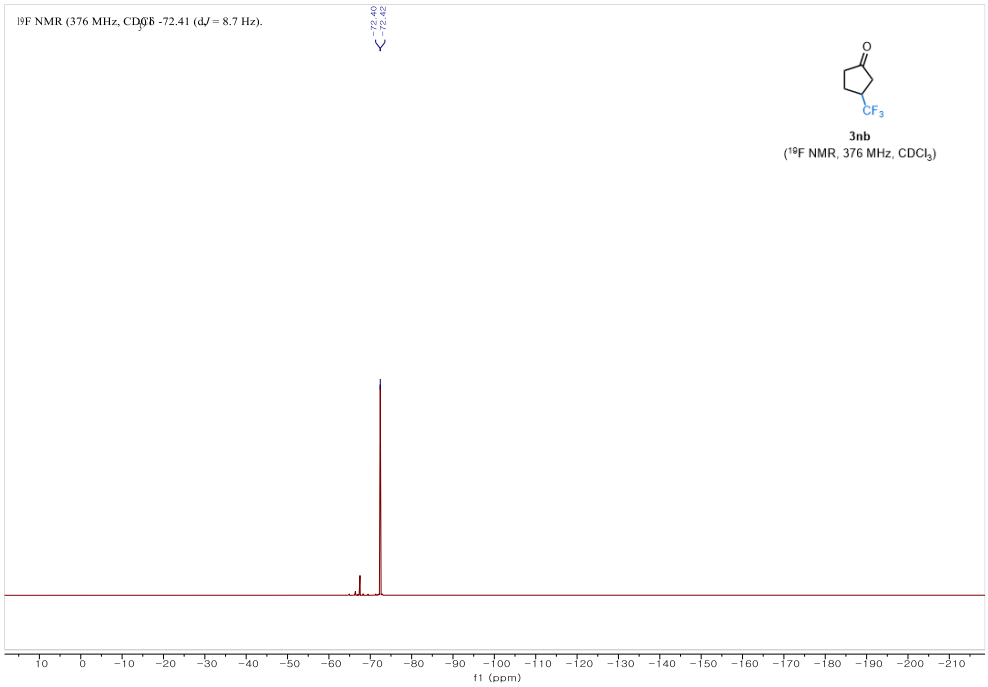

3nb
(^{19}F NMR, 376 MHz, $CDCl_3$)

^{13}C NMR (101 MHz, $CDCl_3$) δ 214.55, 127.26 (d, J = 276.9 Hz), 40.08 (d, J = 28.1 Hz), 37.91, 37.06, 22.40.

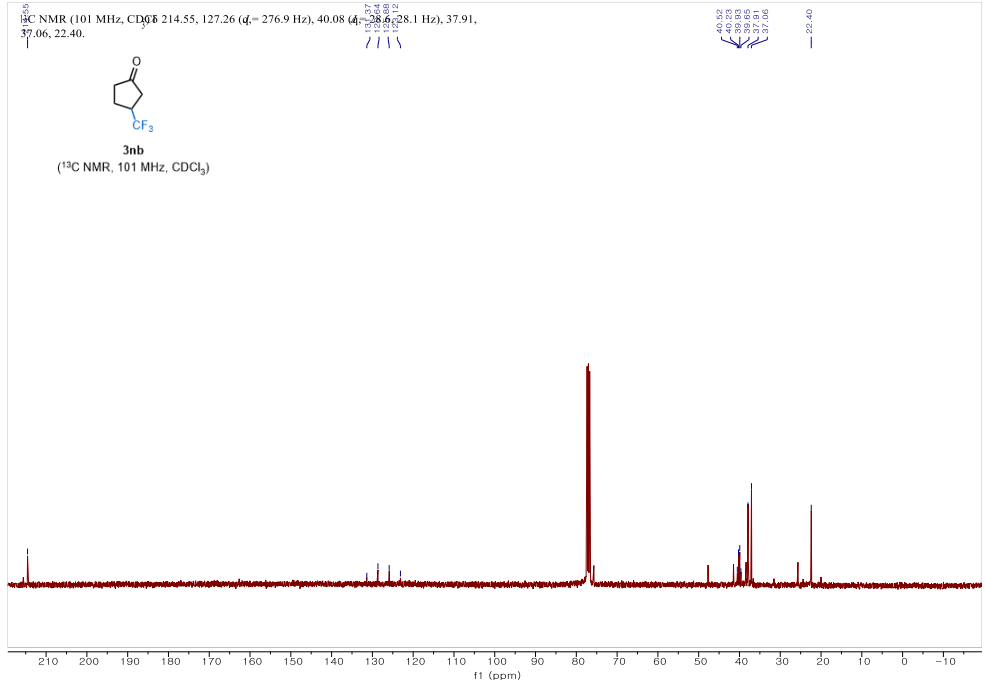

3nb
(^{13}C NMR, 101 MHz, $CDCl_3$)

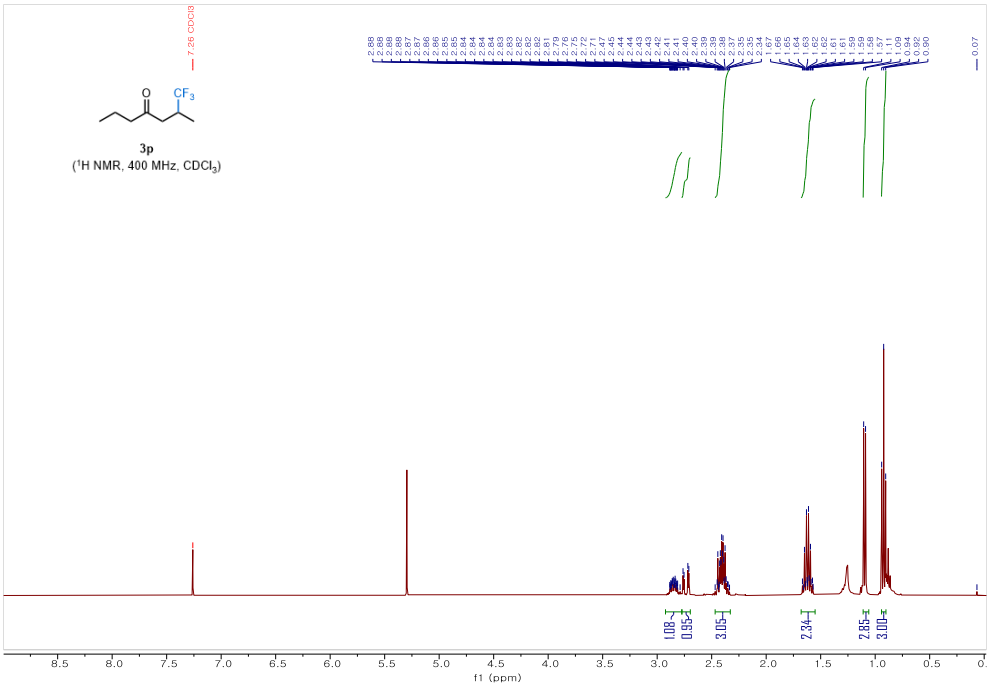
7.26 CDCl3
O
CF3
3p
(1H NMR, 400 MHz, CDCl3)
0.07
1.08
0.95
3.05
2.34
2.85
3.00
f1 (ppm)

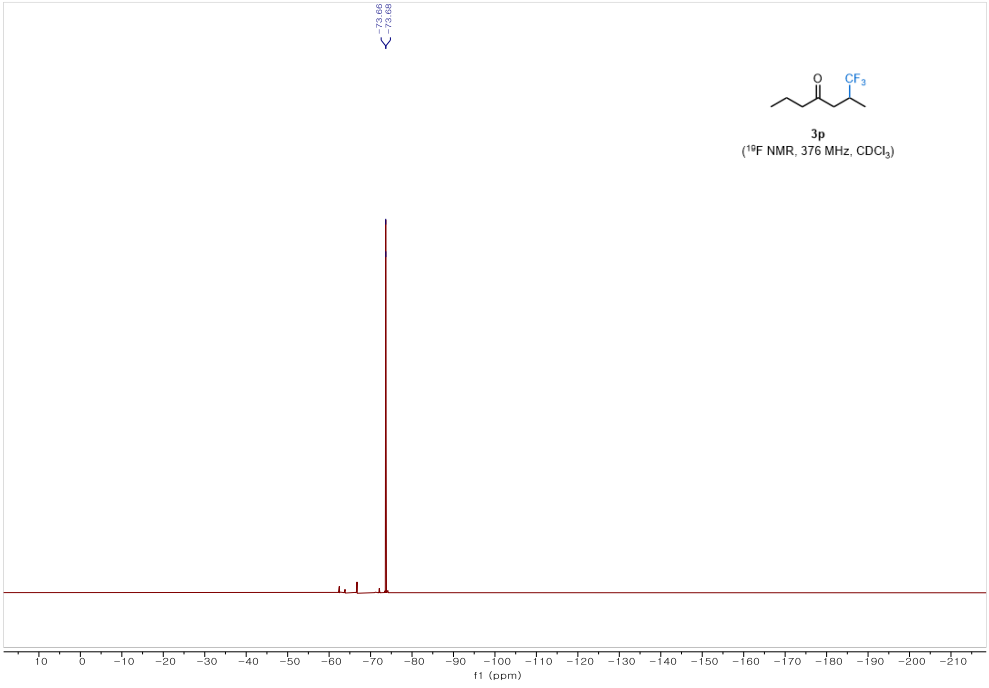
-73.66
-73.68
O
CF3
3p
(19F NMR, 376 MHz, CDCl3)
f1 (ppm)

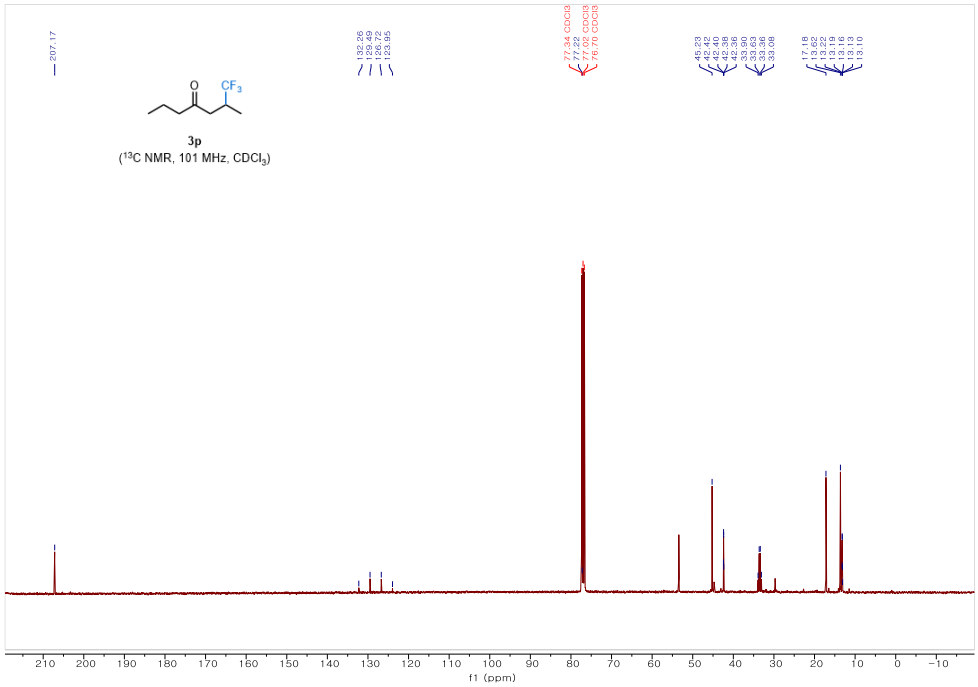
207.17
132.26
132.49
126.72
123.95
77.34 CDCl3
77.02 CDCl3
76.70 CDCl3
45.23
42.42
42.40
42.36
42.33
33.63
33.36
33.08
17.18
17.02
13.22
13.19
13.16
13.13
13.10
O
CF3
3p
(13C NMR, 101 MHz, CDCl3)
f1 (ppm)

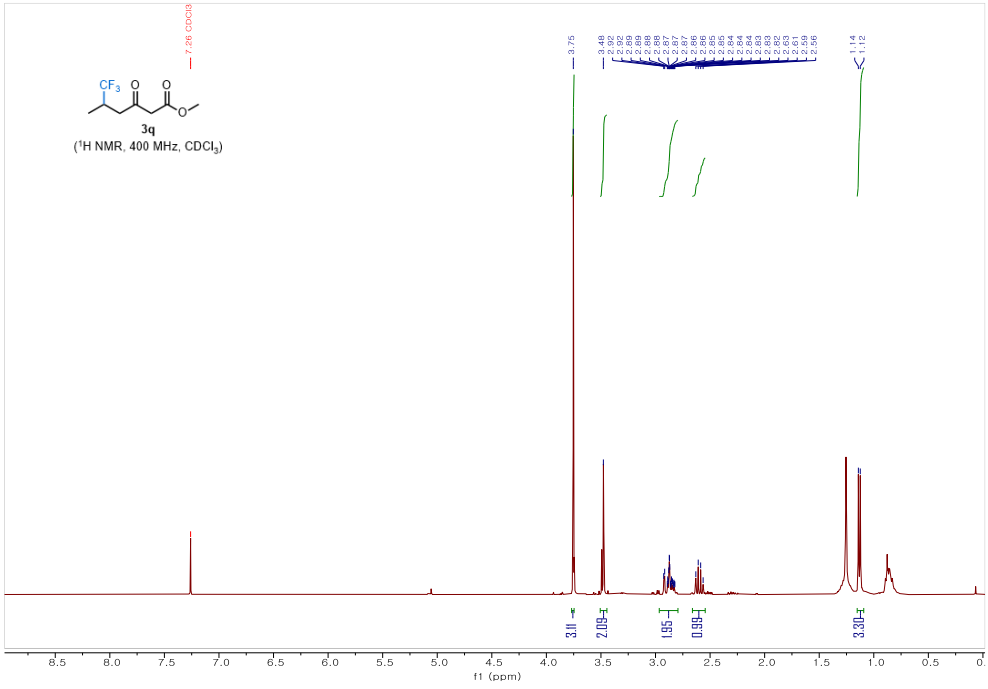
7.26 CDCl3
3.75
3.49
3.32
2.92
2.89
2.88
2.87
2.86
2.85
2.84
2.83
2.82
2.63
2.61
2.59
2.56
1.14
1.12
CF3
O
O
O
3q
(1H NMR, 400 MHz, CDCl3)
3.11
2.09
1.95
0.99
3.30
f1 (ppm)

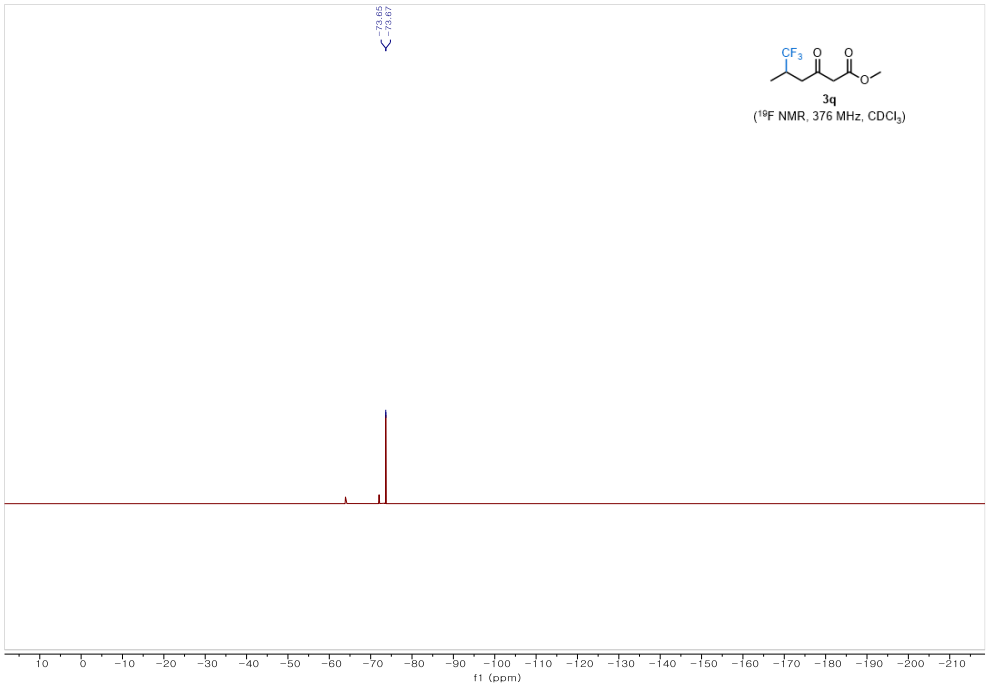
-73.65
-73.67
CF3 O O
O
3q
(19F NMR, 376 MHz, CDCl3)
10 0 -10 -20 -30 -40 -50 -60 -70 -80 -90 -100 -110 -120 -130 -140 -150 -160 -170 -180 -190 -200 -210
f1 (ppm)

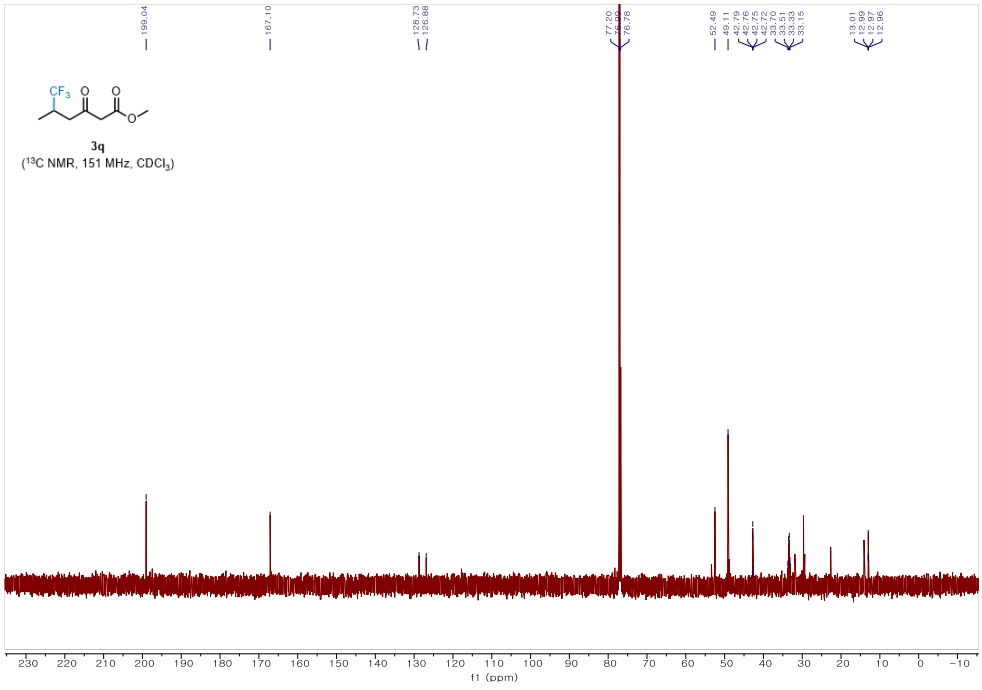
199.04
167.10
128.73
128.68
77.00
76.69
76.78
52.49
49.11
42.79
42.75
42.75
42.72
33.70
33.51
33.33
33.15
13.01
12.99
12.97
12.96
CF3 O O
O
3q
(13C NMR, 151 MHz, CDCl3)
230 220 210 200 190 180 170 160 150 140 130 120 110 100 90 80 70 60 50 40 30 20 10 0 -10
f1 (ppm)

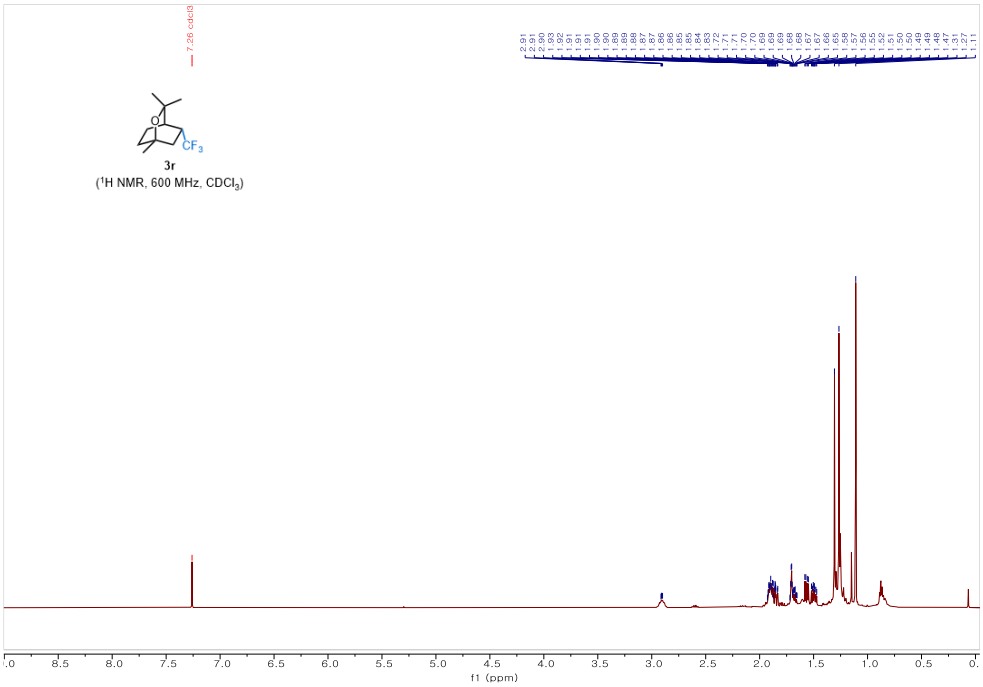
7.26 cdcl3
2.91
2.91
2.90
1.92
1.91
1.91
1.91
1.90
1.90
1.89
1.89
1.88
1.87
1.87
1.86
1.86
1.85
1.85
1.84
1.83
1.72
1.71
1.71
1.70
1.70
1.69
1.69
1.68
1.68
1.67
1.67
1.66
1.65
1.58
1.57
1.56
1.55
1.52
1.51
1.50
1.49
1.48
1.48
1.47
1.47
1.27
1.11
CF3
3r
(1H NMR, 600 MHz, CDCl3)
f1 (ppm)

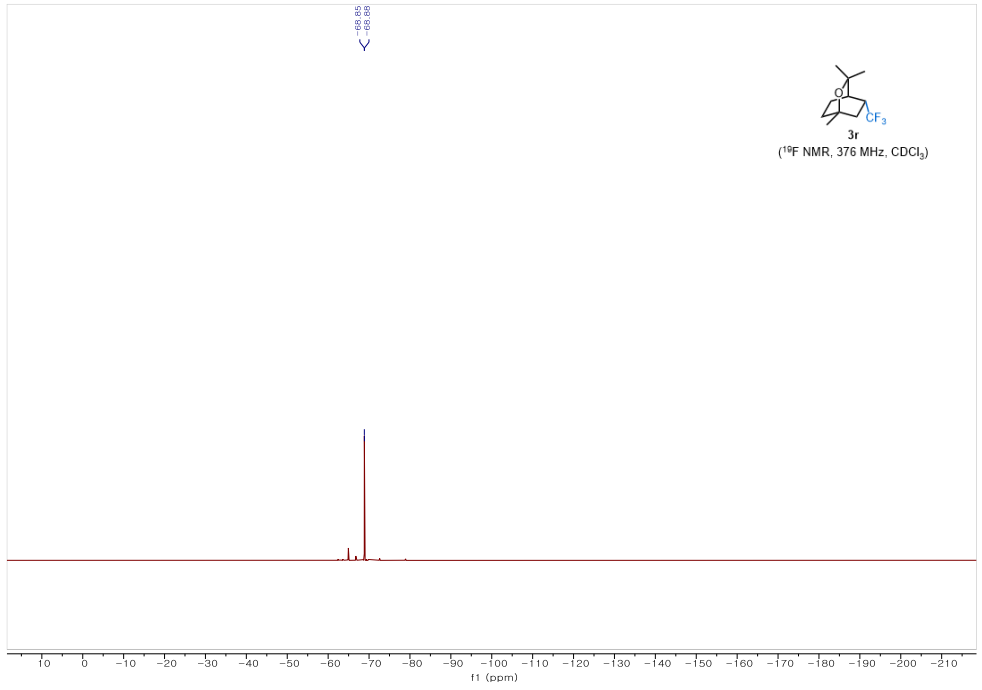
-68.85
-68.86
CF3
3r
(19F NMR, 376 MHz, CDCl3)
f1 (ppm)

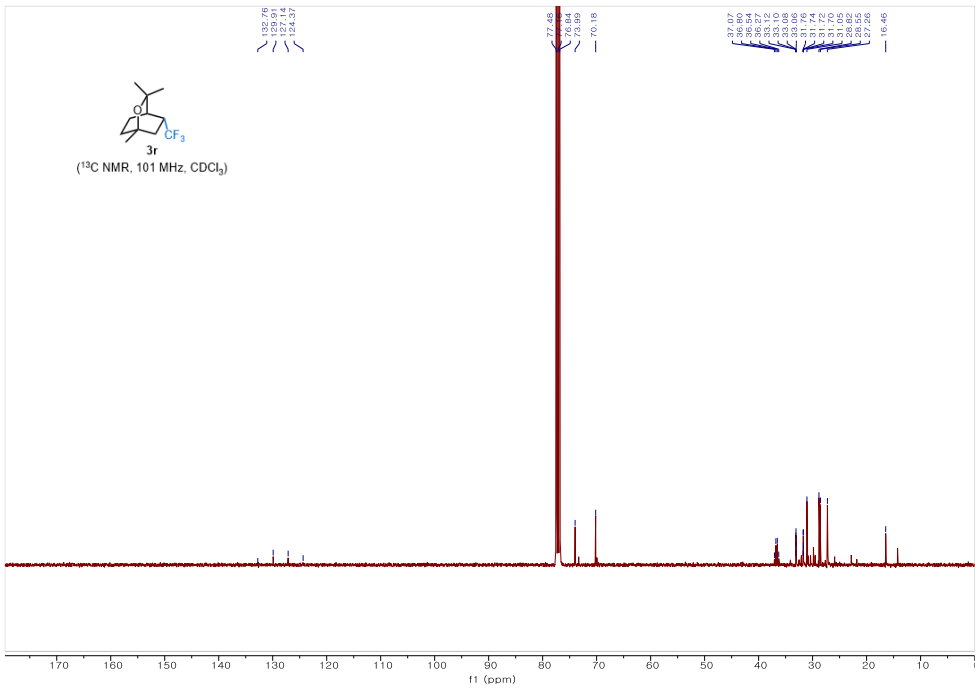
132.76
129.91
127.14
124.37
77.48
77.16
76.84
73.99
70.18
37.07
36.80
36.54
36.27
33.12
33.10
33.08
33.06
31.74
31.72
31.70
31.05
28.82
28.55
27.26
16.46
CF3
3r
(13C NMR, 101 MHz, CDCl3)
170
160
150
140
130
120
110
100
90
80
70
60
50
40
30
20
10
f1 (ppm)

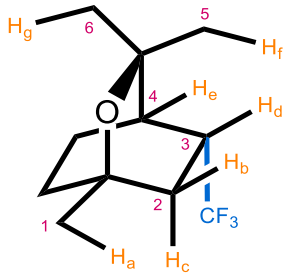

3r

(HSQC, $CDCl_3$)

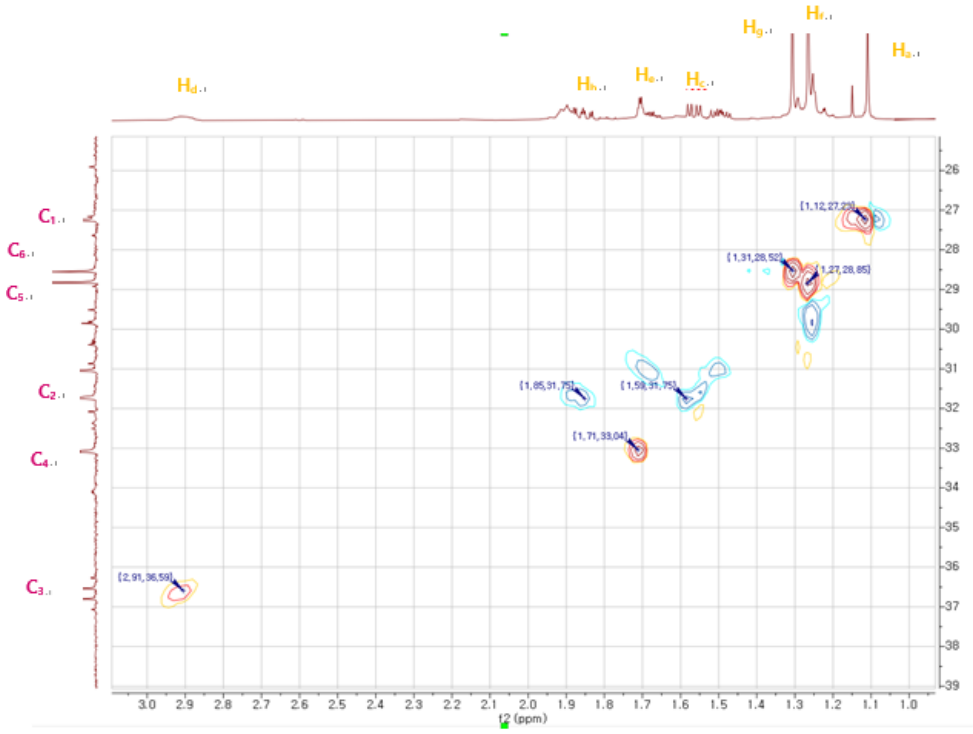

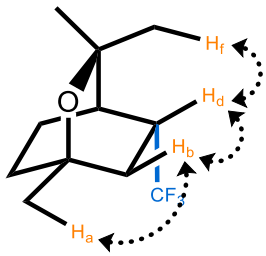

3r

(NOESY, $CDCl_3$)

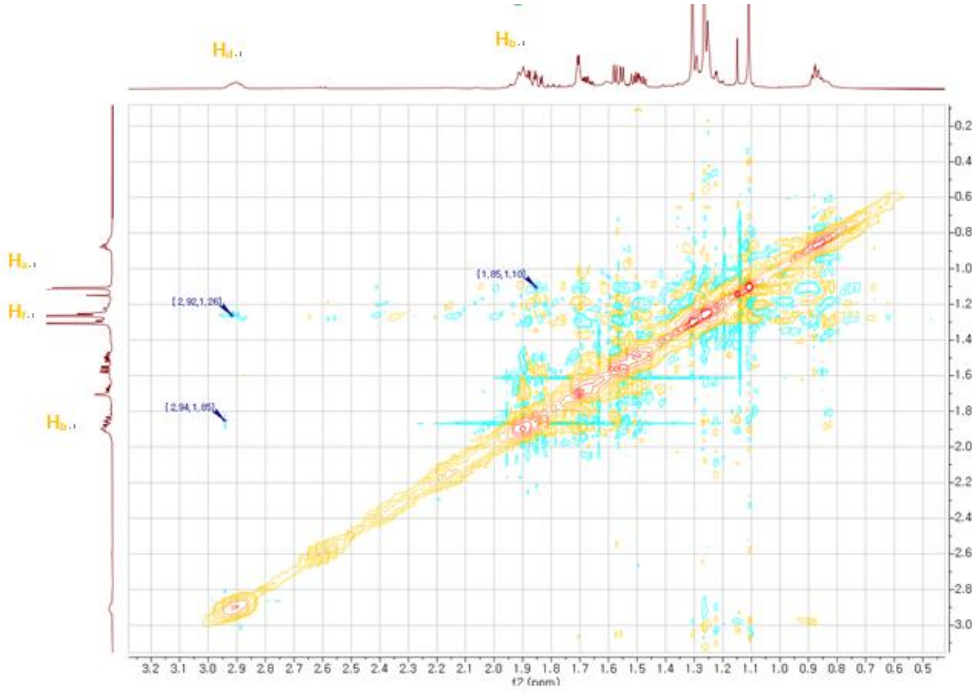

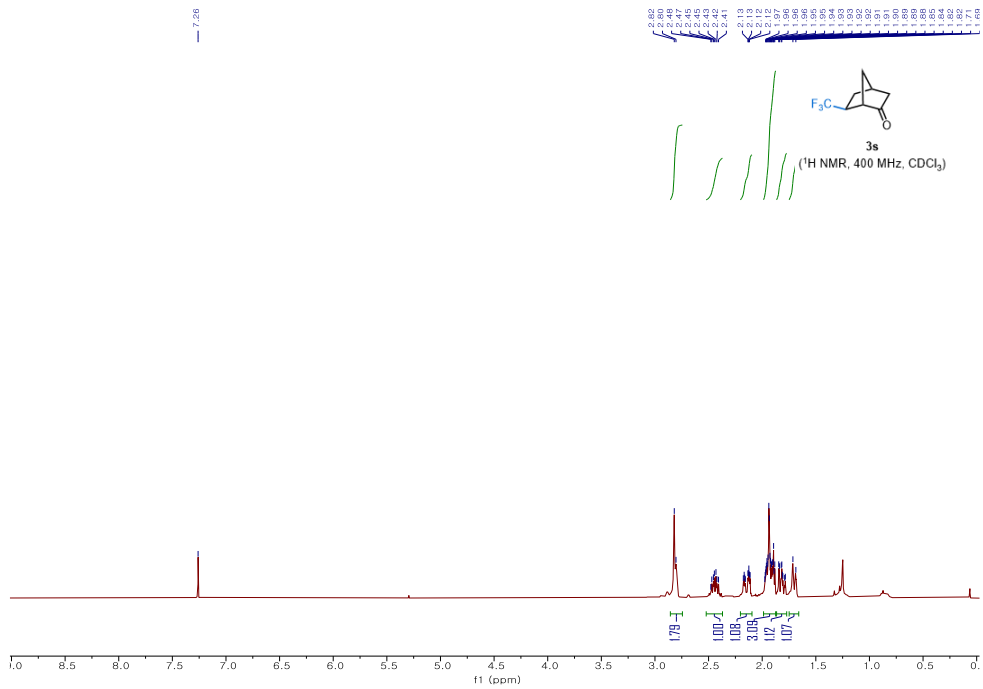
7.26
2.82
2.80
2.49
2.47
2.45
2.45
2.43
2.42
2.41
2.13
2.13
2.12
2.12
2.07
1.96
1.96
1.95
1.94
1.93
1.92
1.91
1.90
1.89
1.88
1.85
1.84
1.82
1.82
1.71
1.64
F3C
O
3s
(1H NMR, 400 MHz, CDCl3)
1.79
1.00
1.08
3.05
1.12
1.07
f1 (ppm)

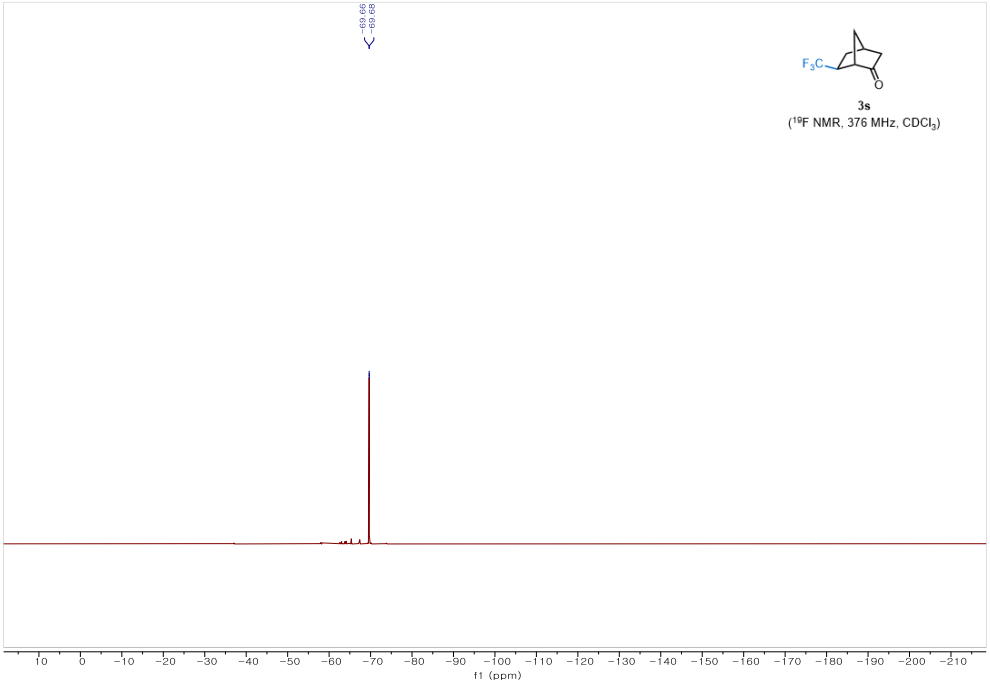
-69.66
-69.68
F3C
O
3s
(19F NMR, 376 MHz, CDCl3)
f1 (ppm)

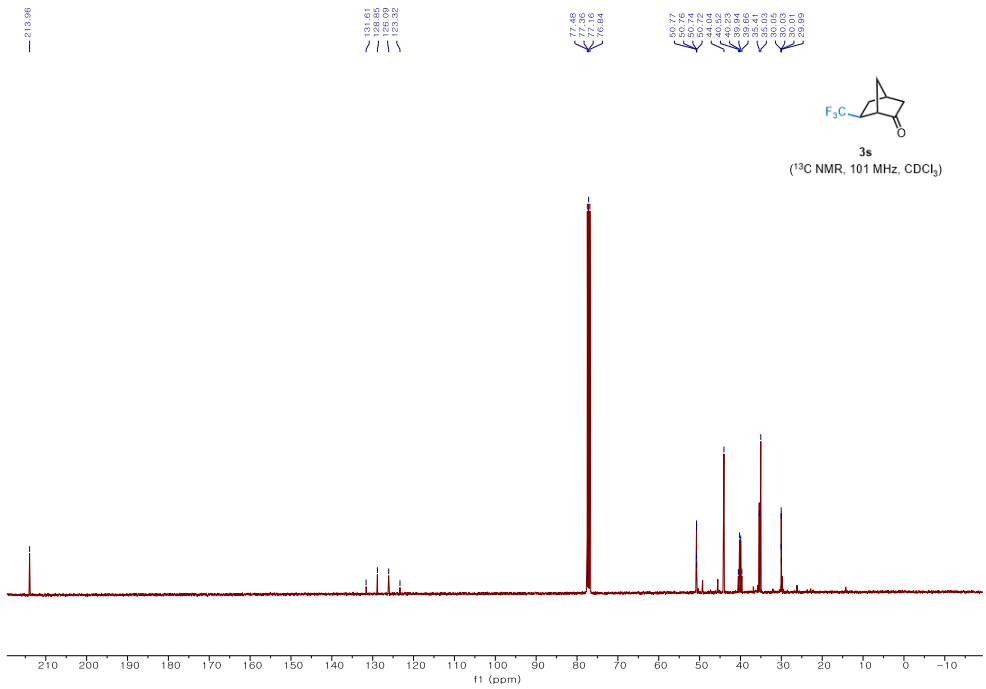

3s

(^{13}C NMR, 101 MHz, $CDCl_3$)

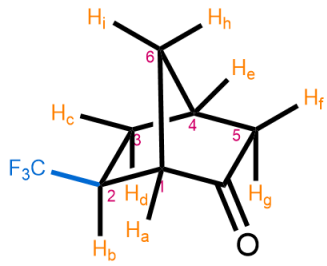

3s

(HSQC, $CDCl_3$)

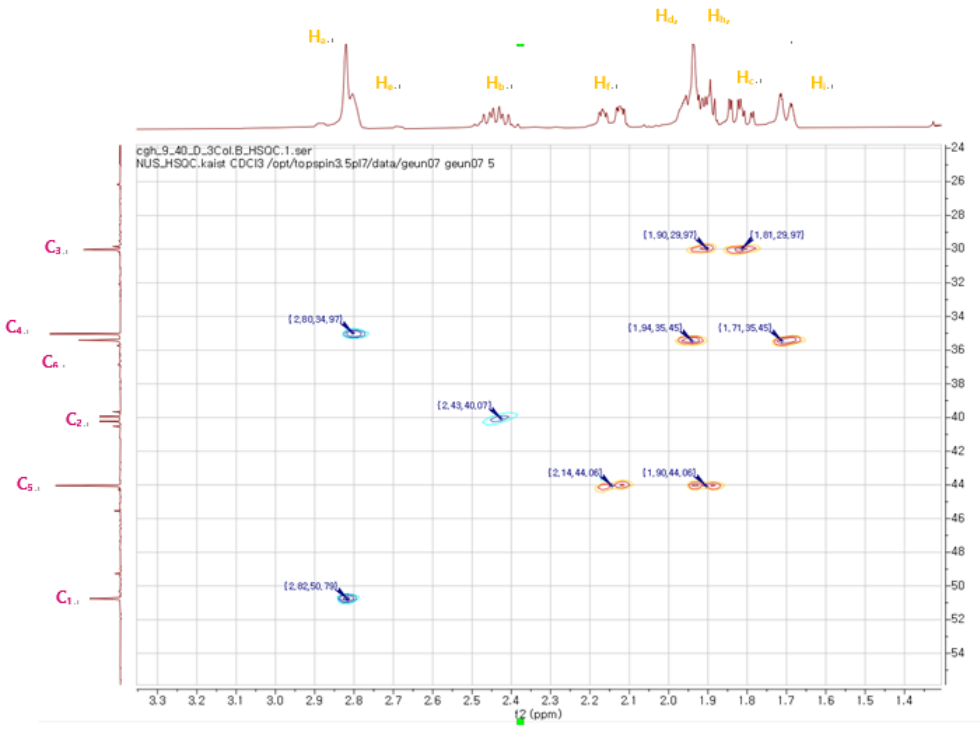

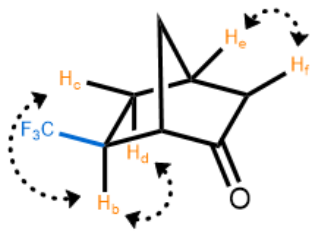

3s

(COSY, $CDCl_3$)

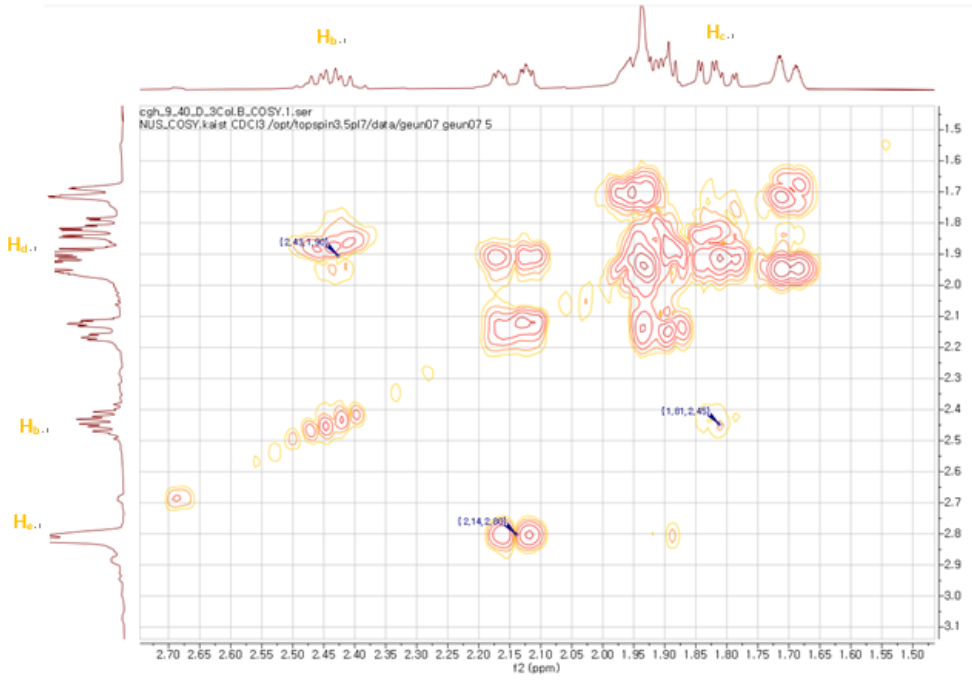

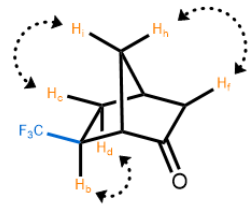

3s

(NOESY, $CDCl_3$)

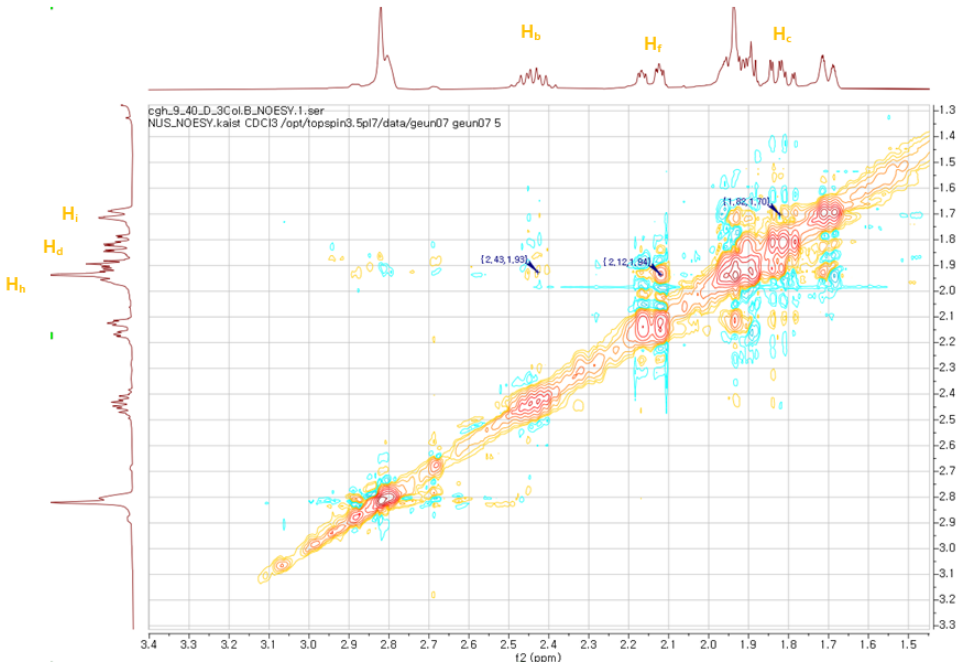

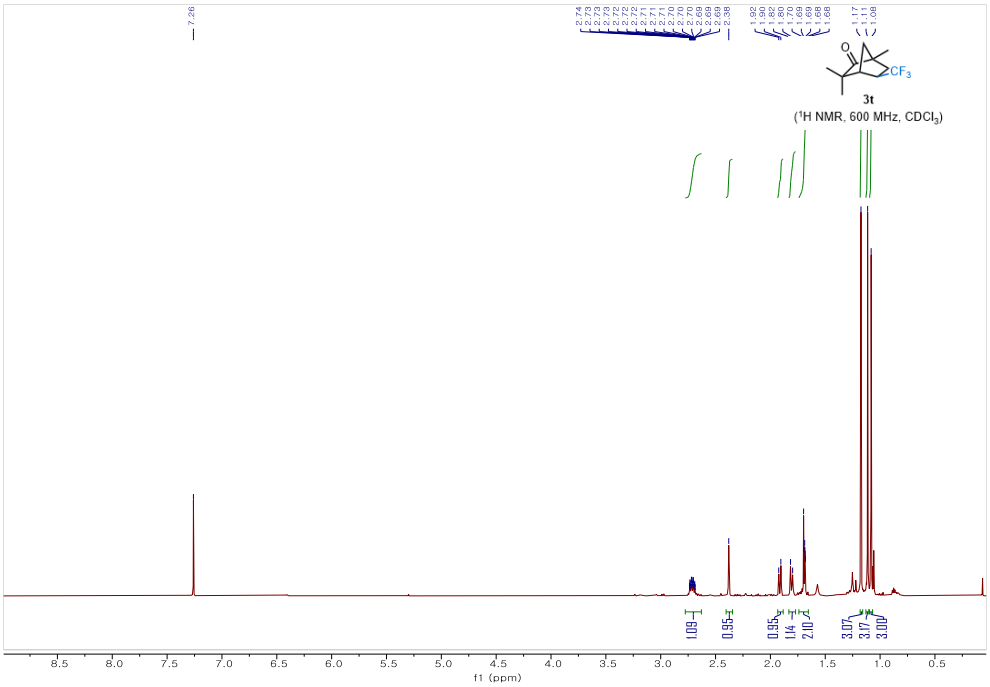
3t
(1H NMR, 600 MHz, CDCl3)
f1 (ppm)

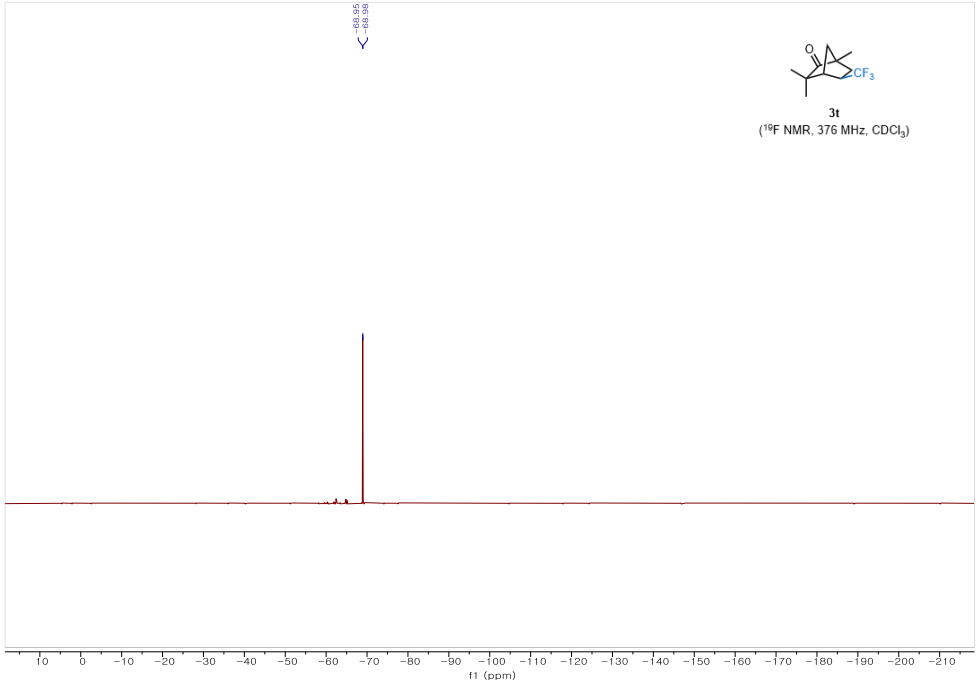
3t
(19F NMR, 376 MHz, CDCl3)
f1 (ppm)

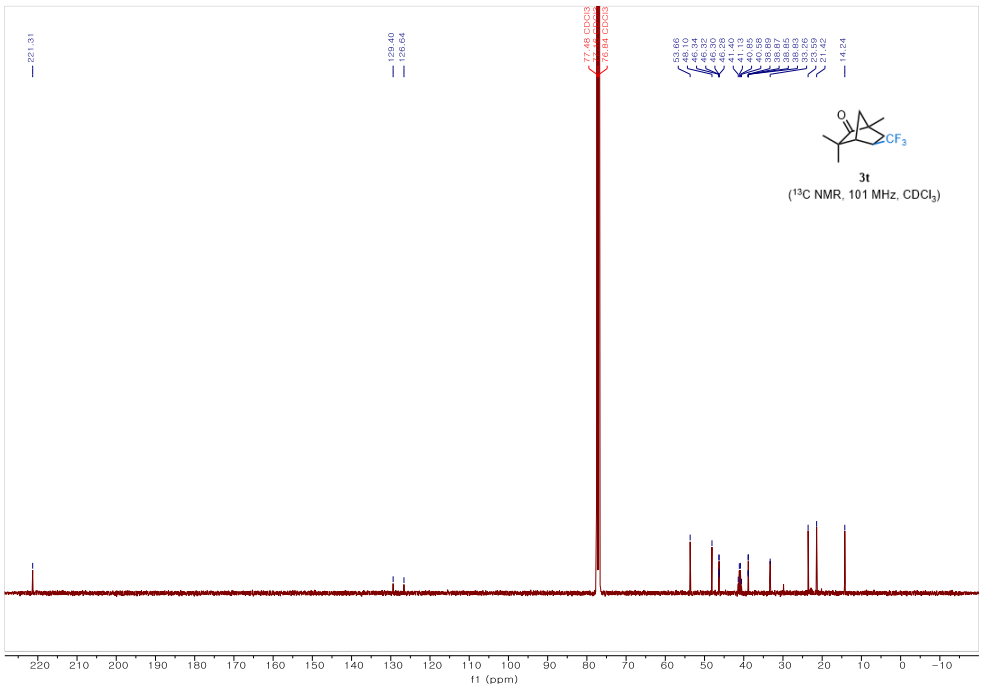
221.31
129.40
126.64
77.48 CDCl3
77.16
76.84 CDCl3
53.66
48.10
46.34
46.32
46.30
46.28
41.64
41.13
40.85
40.65
38.89
38.87
38.85
38.83
38.35
23.59
21.42
14.24
O
CF3
3t
(13C NMR, 101 MHz, CDCl3)
f1 (ppm)

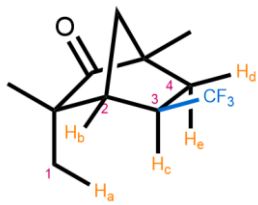

3t

(HSQC, $CDCl_3$)

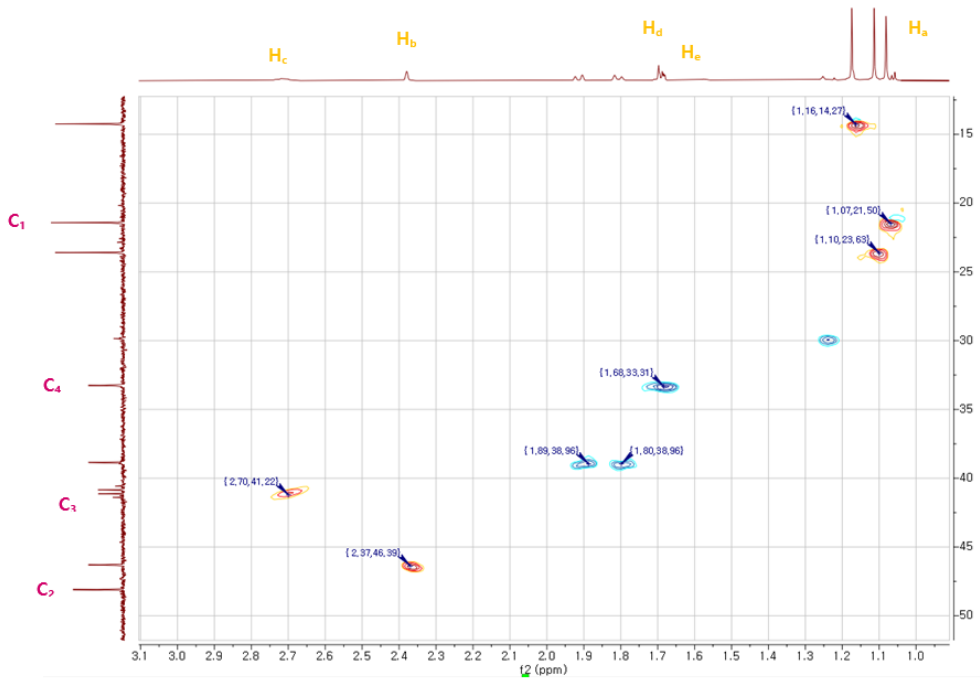

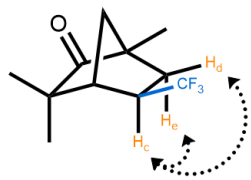

3t

(COSY, $CDCl_3$)

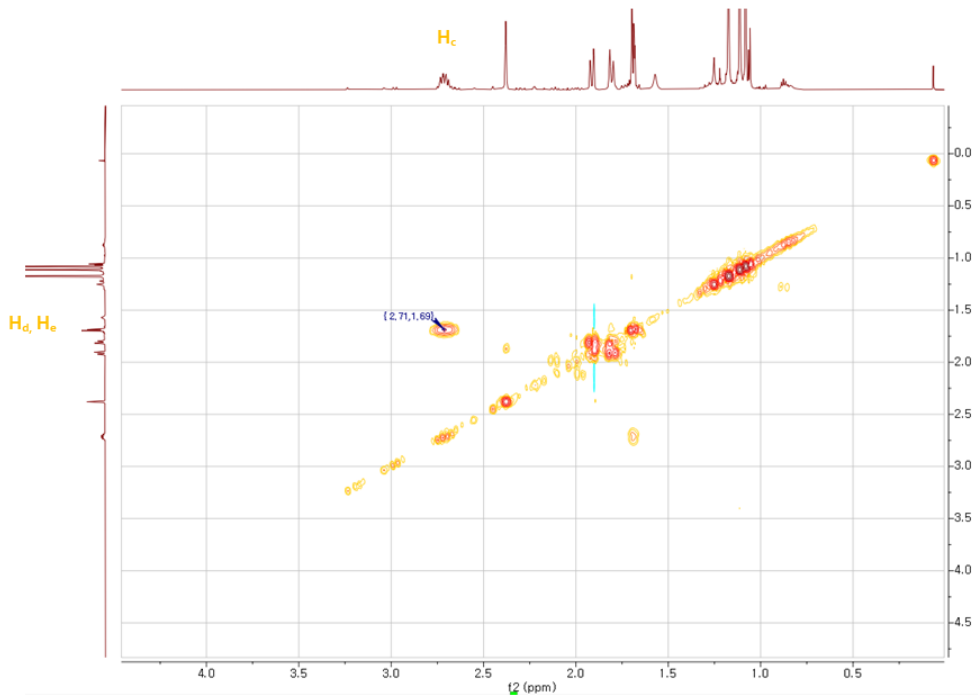

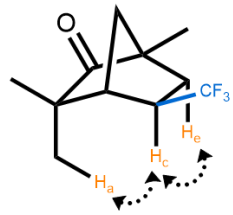

3t

(NOESY, $CDCl_3$)

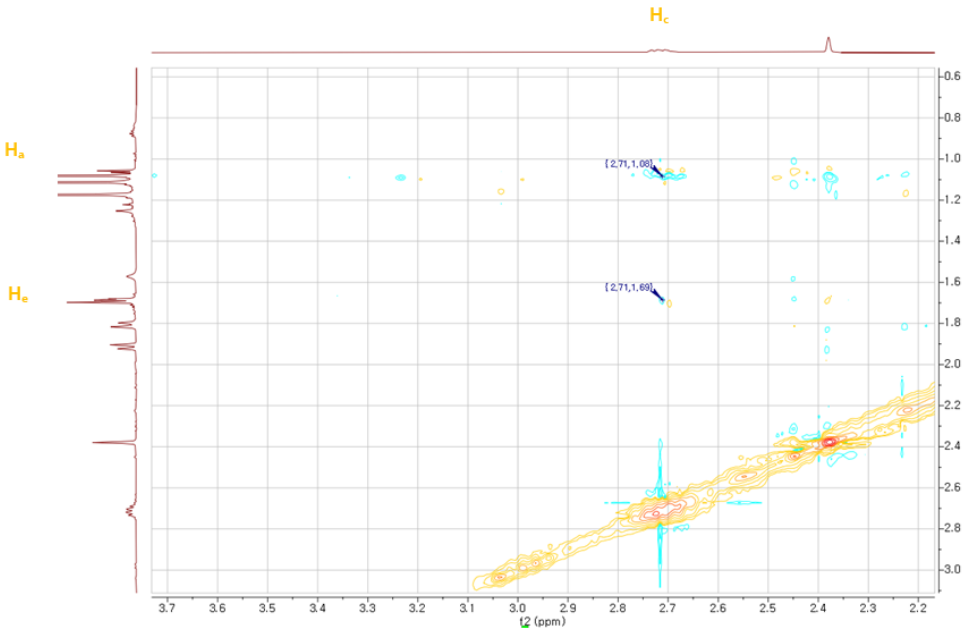

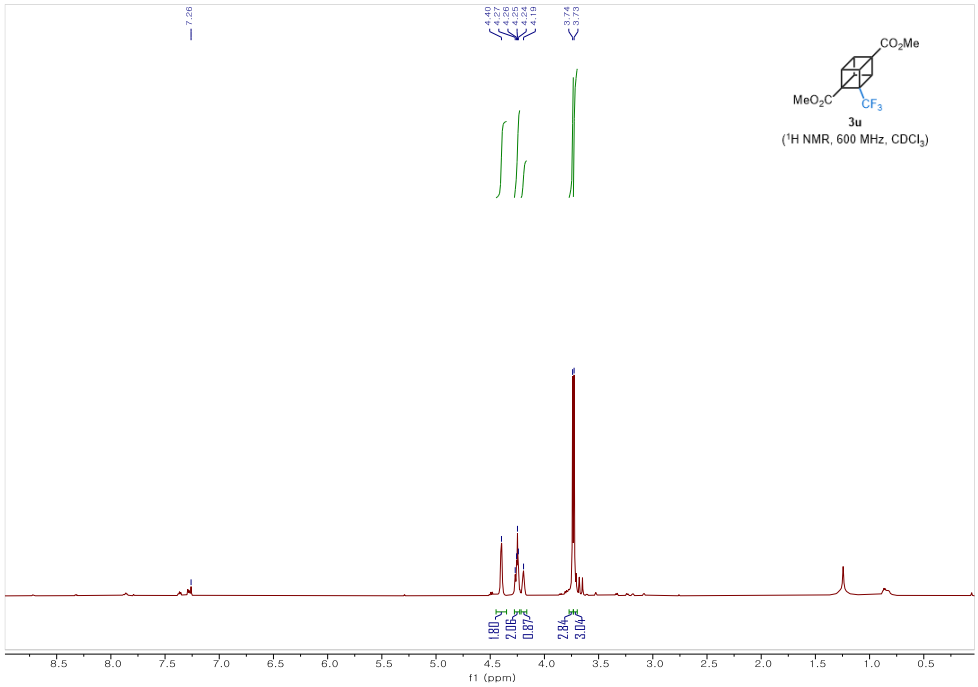
7.26
4.40
4.27
4.26
4.25
4.24
4.19
3.74
3.70
CO2Me
MeO2C
CF3
3u
(1H NMR, 600 MHz, CDCl3)
1.80
2.06
0.87
2.84
3.04
8.5
8.0
7.5
7.0
6.5
6.0
5.5
5.0
4.5
4.0
3.5
3.0
2.5
2.0
1.5
1.0
0.5
f1 (ppm)

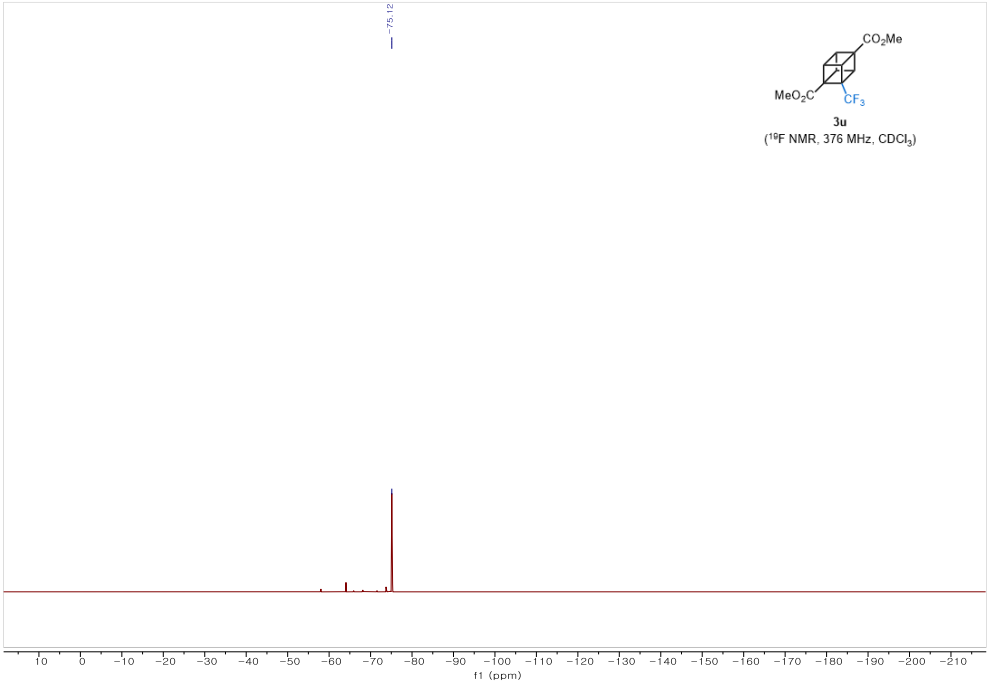
-75.12
CO2Me
MeO2C
CF3
3u
(19F NMR, 376 MHz, CDCl3)
10
0
-10
-20
-30
-40
-50
-60
-70
-80
-90
-100
-110
-120
-130
-140
-150
-160
-170
-180
-190
-200
-210
f1 (ppm)

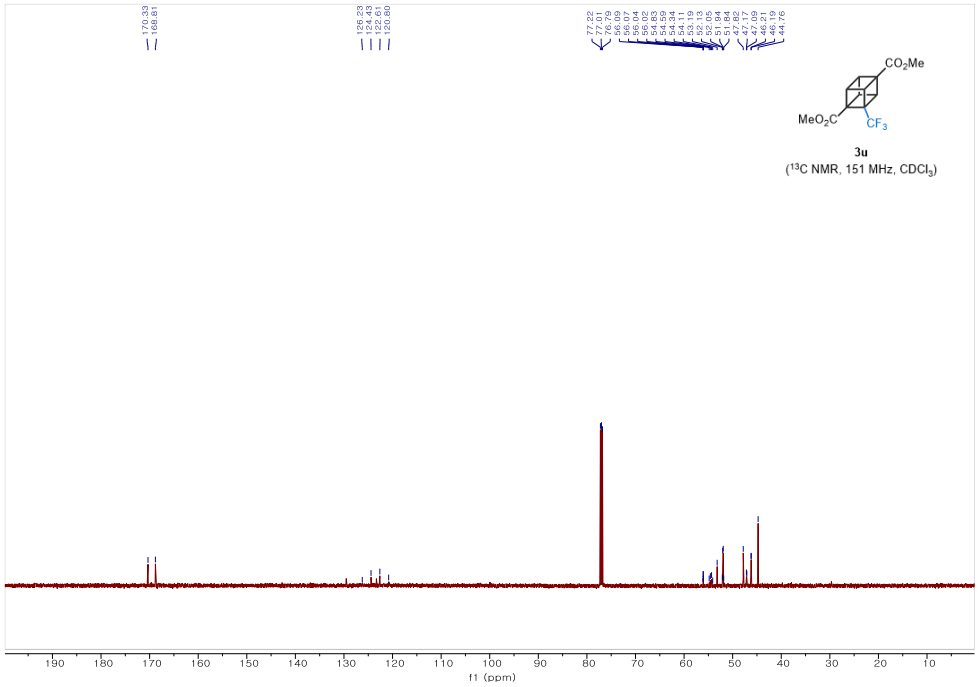
170.33
168.81
126.23
124.43
122.61
120.80
77.22
77.01
76.79
56.09
56.07
56.04
55.92
54.83
54.60
54.34
54.11
53.19
52.13
52.05
51.94
51.84
47.82
47.77
47.09
46.21
45.19
44.76
CO2Me
MeO2C
CF3
3u
(13C NMR, 151 MHz, CDCl3)
190
180
170
160
150
140
130
120
110
100
90
80
70
60
50
40
30
20
10
f1 (ppm)

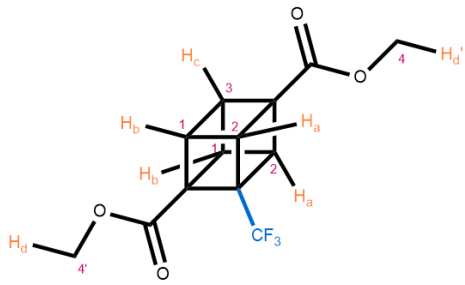

3u

(HSQC, $CDCl_3$)

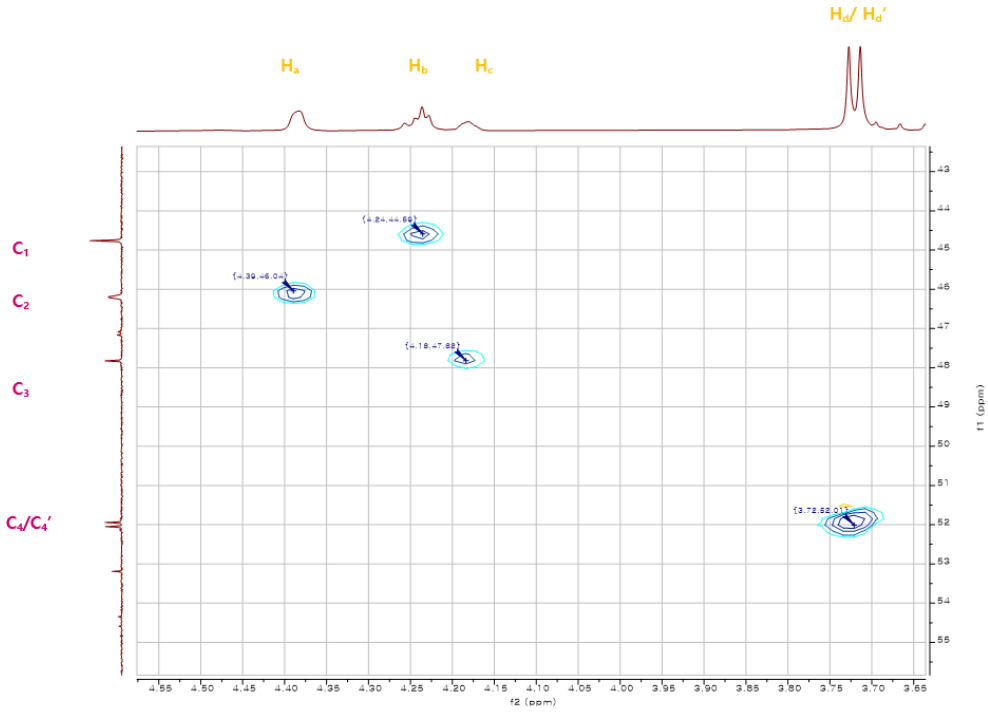

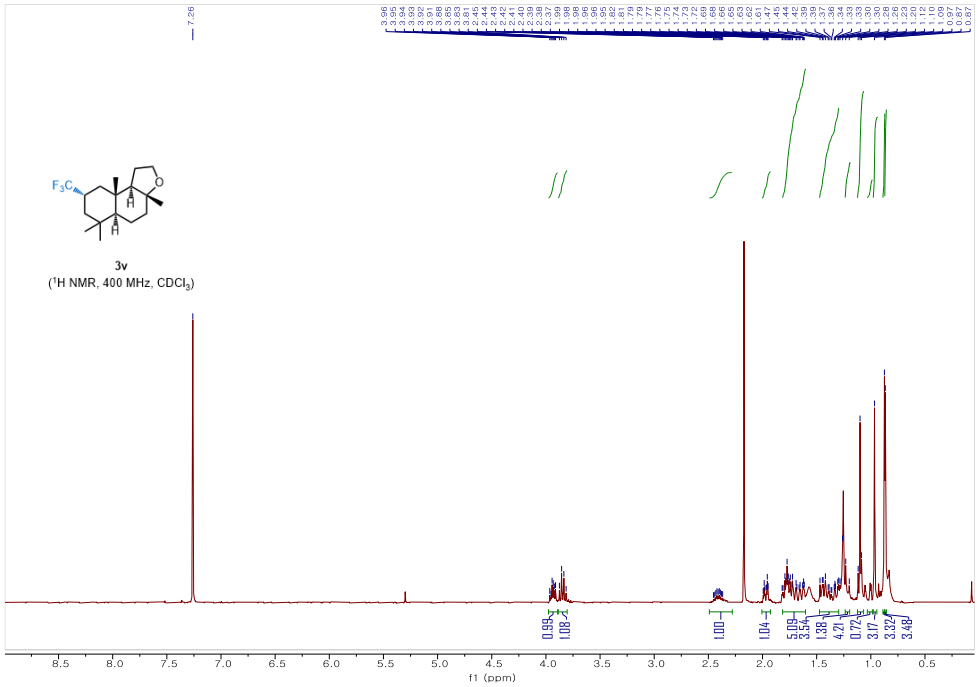
7.26
F3C
H
H
O
3v
(1H NMR, 400 MHz, CDCl3)
0.99
1.08
1.00
1.04
5.09
3.54
1.38
4.21
0.72
3.17
3.32
3.48
8.5
8.0
7.5
7.0
6.5
6.0
5.5
5.0
4.5
4.0
3.5
3.0
2.5
2.0
1.5
1.0
0.5
f1 (ppm)

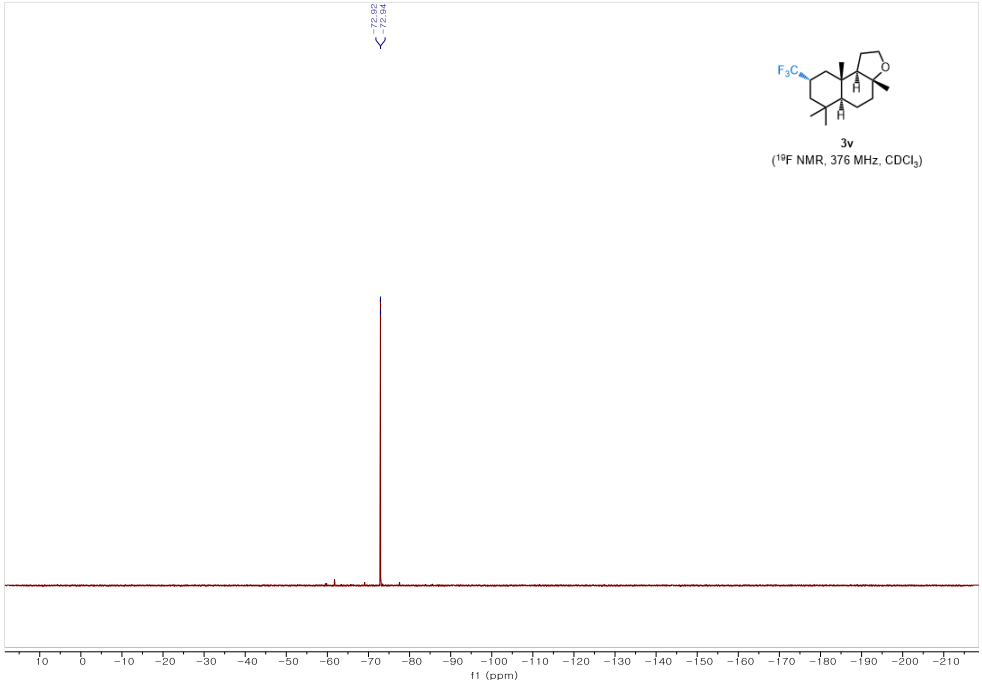
-72.92
-72.94
F3C
H
H
O
3v
(19F NMR, 376 MHz, CDCl3)
10
0
-10
-20
-30
-40
-50
-60
-70
-80
-90
-100
-110
-120
-130
-140
-150
-160
-170
-180
-190
-200
-210
f1 (ppm)

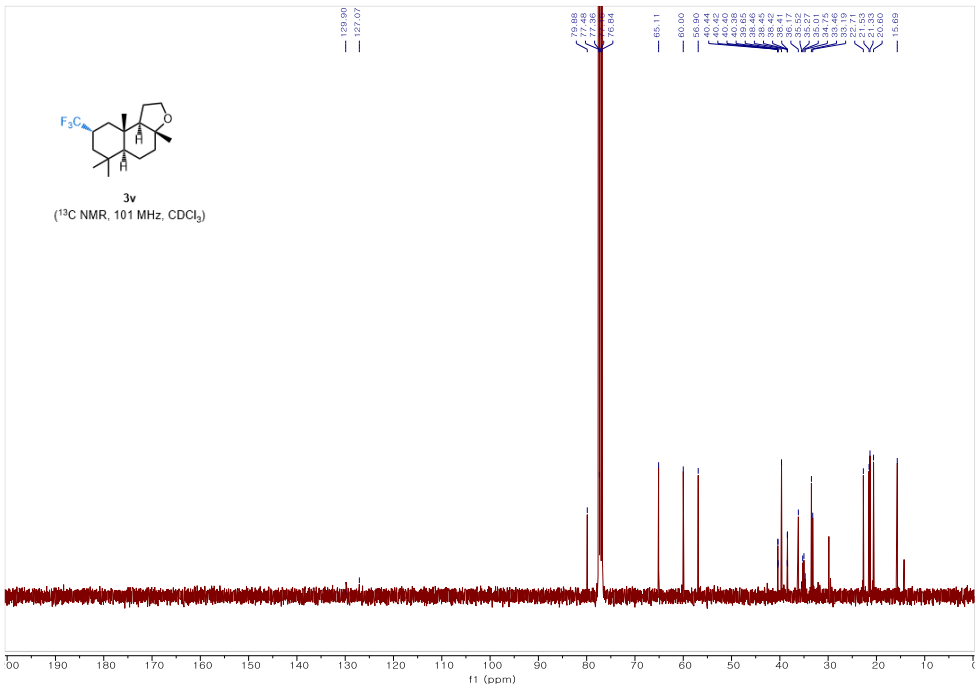
128.90
127.07
79.88
77.48
77.16
76.84
65.11
60.00
56.90
40.44
40.42
40.40
40.28
39.45
38.46
38.45
38.41
37.17
35.52
35.27
35.01
34.75
33.46
33.19
22.71
21.53
21.33
20.80
15.69
F3C
O
H
H
3v
(13C NMR, 101 MHz, CDCl3)
f1 (ppm)

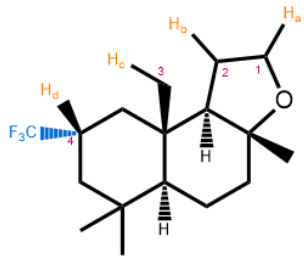

3v

(HSQC, $CDCl_3$)

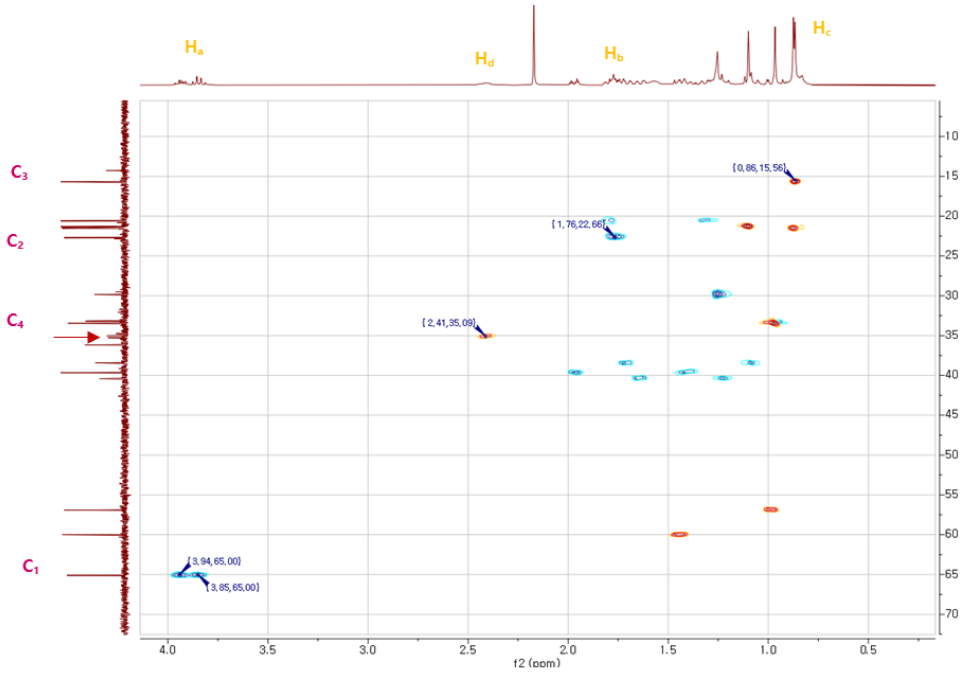

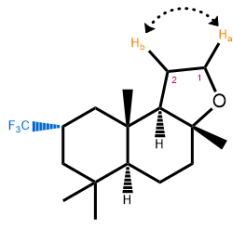

3v
(COSY, $CDCl_3$)

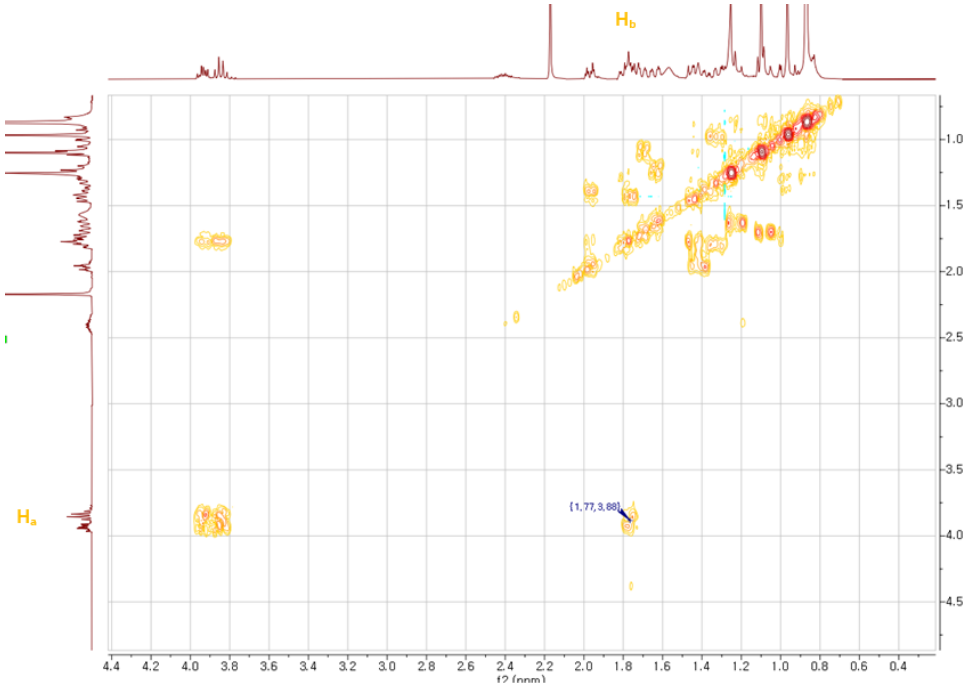

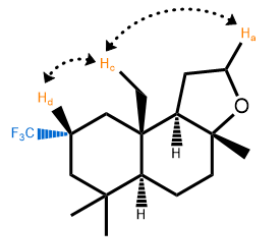

3v
(NOESY, $CDCl_3$)

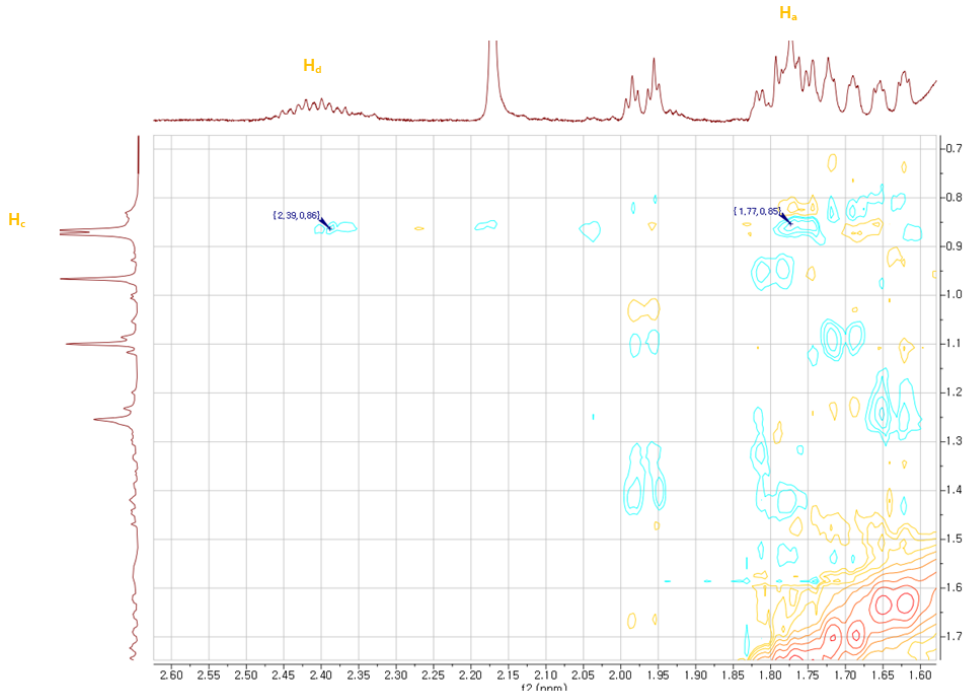

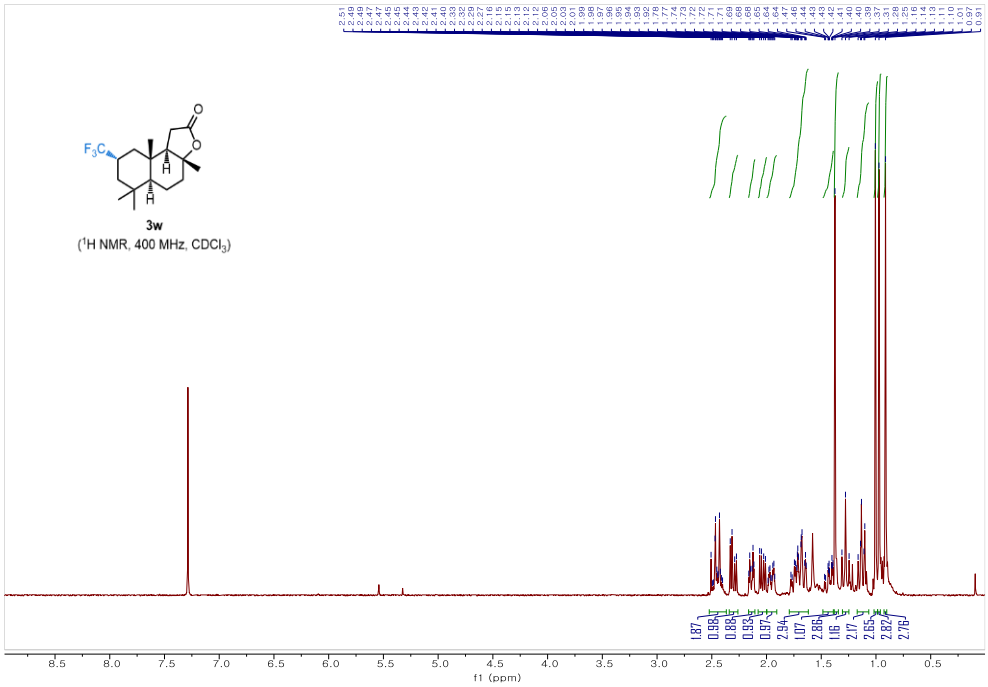
F3C
H
H
3w
(1H NMR, 400 MHz, CDCl3)
1.87
0.96
0.88
0.93
0.97
2.94
1.07
2.86
1.16
2.17
2.65
2.82
2.76
f1 (ppm)

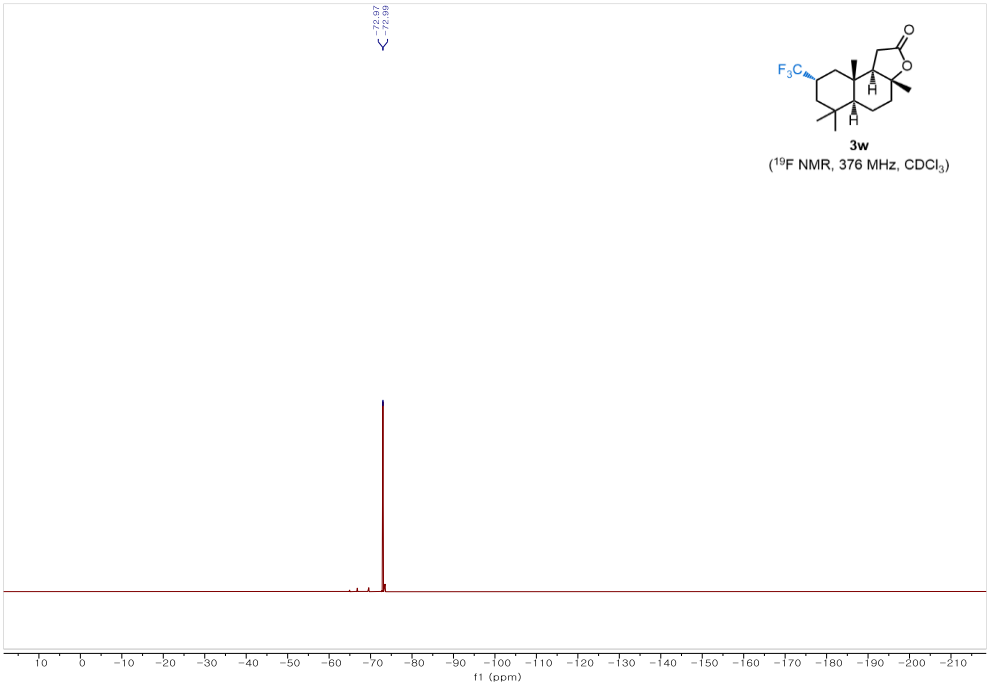
-72.97
-72.99
F3C
H
H
3w
(19F NMR, 376 MHz, CDCl3)
f1 (ppm)

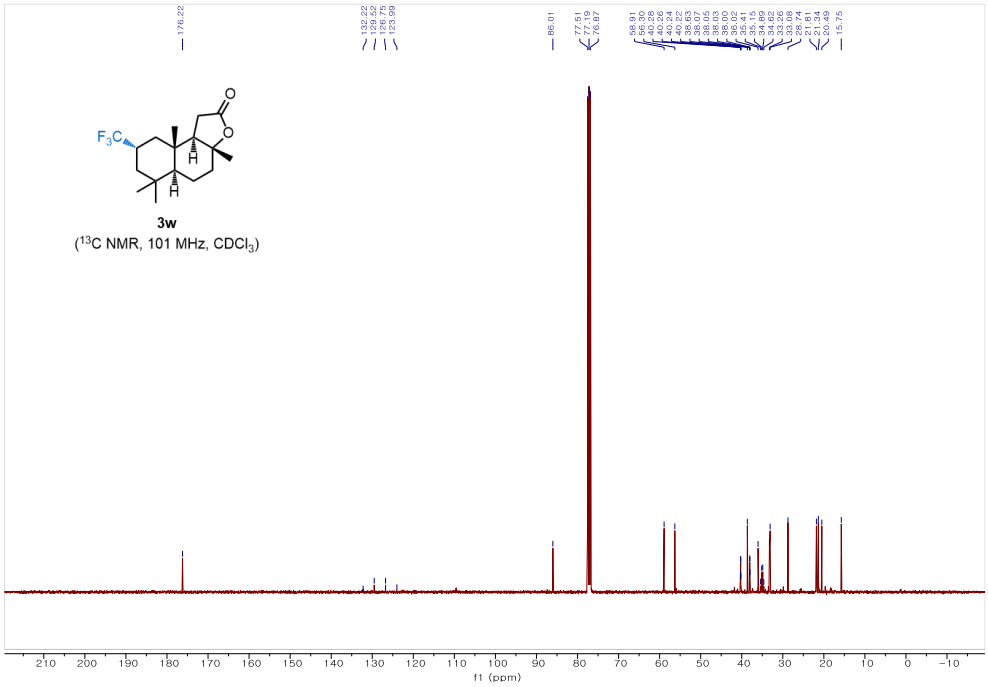

3w

(^{13}C NMR, 101 MHz, $CDCl_3$)

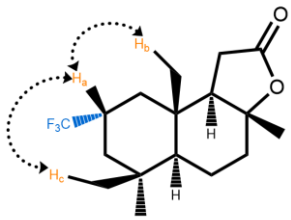

3w

(NOESY, $CDCl_3$)

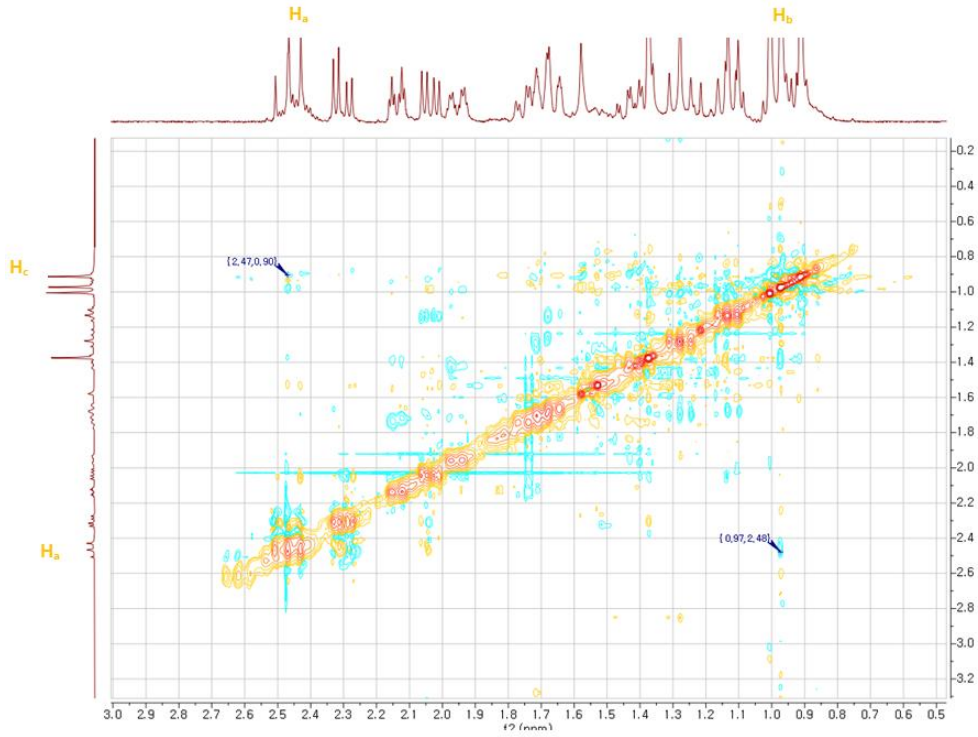

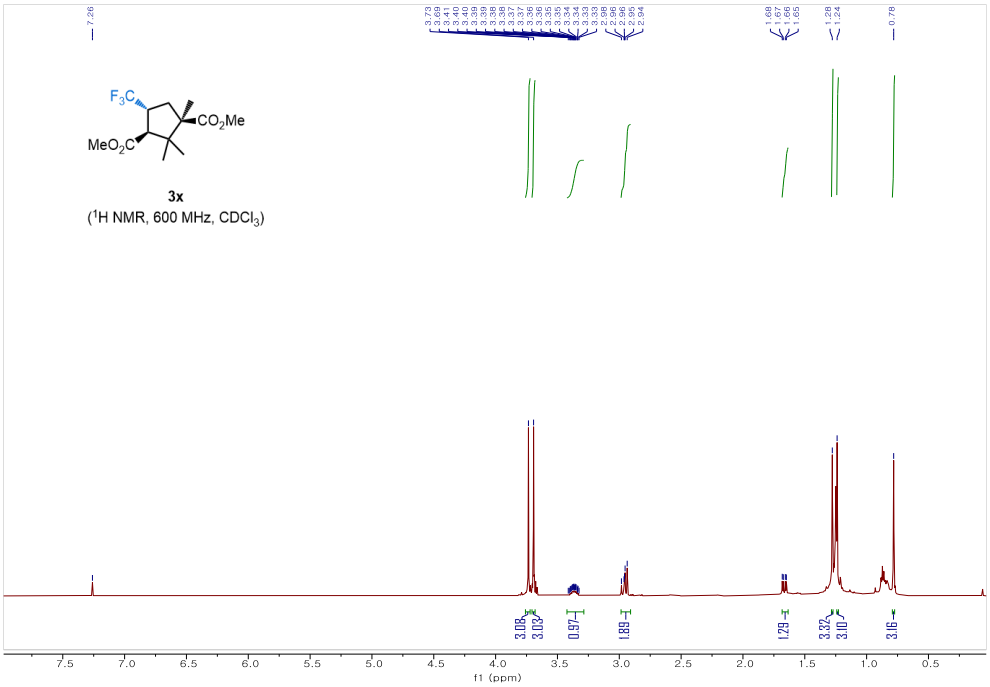
F3C
CO2Me
MeO2C
3x
(1H NMR, 600 MHz, CDCl3)
7.26
3.73
3.69
3.41
3.40
3.40
3.39
3.39
3.38
3.38
3.37
3.37
3.36
3.35
3.35
3.35
3.34
3.34
3.33
3.33
2.96
2.96
2.95
2.94
1.69
1.67
1.66
1.65
1.28
1.24
0.78
3.08
3.02
0.97
1.88
1.79
3.32
3.10
3.16
7.5
7.0
6.5
6.0
5.5
5.0
4.5
4.0
3.5
3.0
2.5
2.0
1.5
1.0
0.5
f1 (ppm)

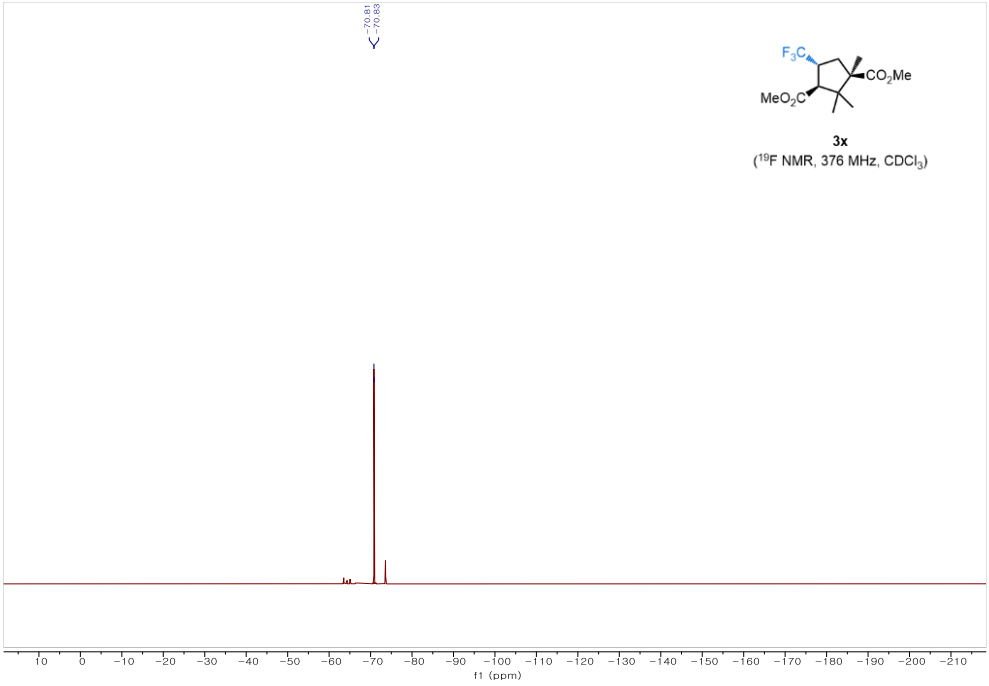
-70.81
-70.83
F3C
CO2Me
MeO2C
3x
(19F NMR, 376 MHz, CDCl3)
10
0
-10
-20
-30
-40
-50
-60
-70
-80
-90
-100
-110
-120
-130
-140
-150
-160
-170
-180
-190
-200
-210
f1 (ppm)

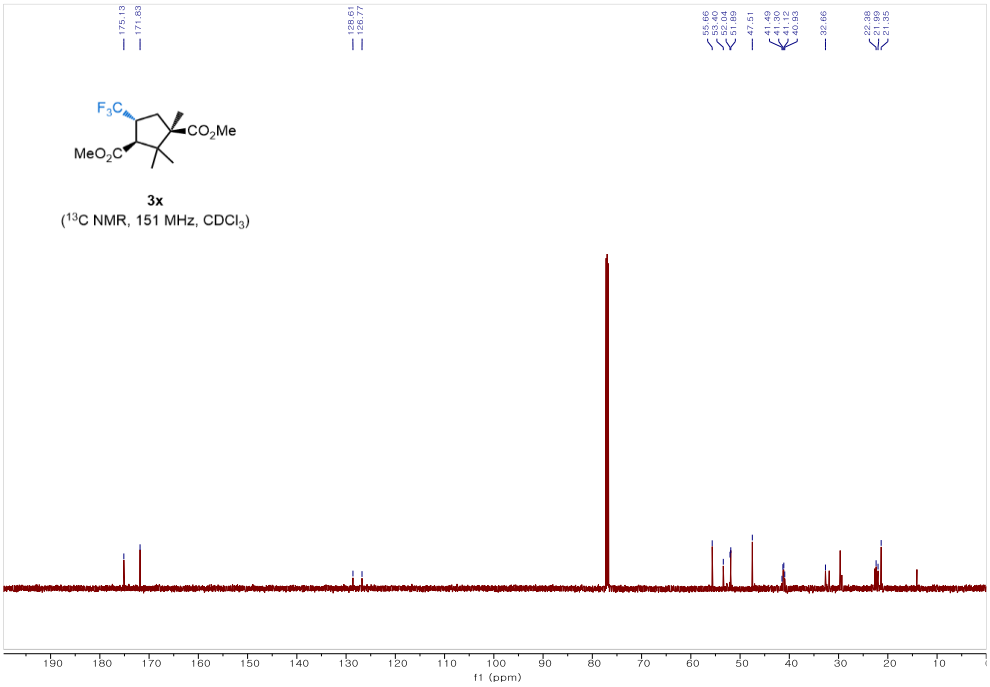
175.13
171.83
128.61
126.77
55.66
53.40
52.14
51.69
47.51
41.49
41.30
41.12
40.93
32.66
22.38
21.69
21.35
F3C
CO2Me
MeO2C
3x
(13C NMR, 151 MHz, CDCl3)
190
180
170
160
150
140
130
120
110
100
90
80
70
60
50
40
30
20
10
f1 (ppm)

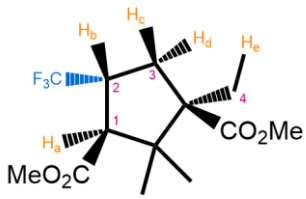

3x

(HSQC, $CDCl_3$)

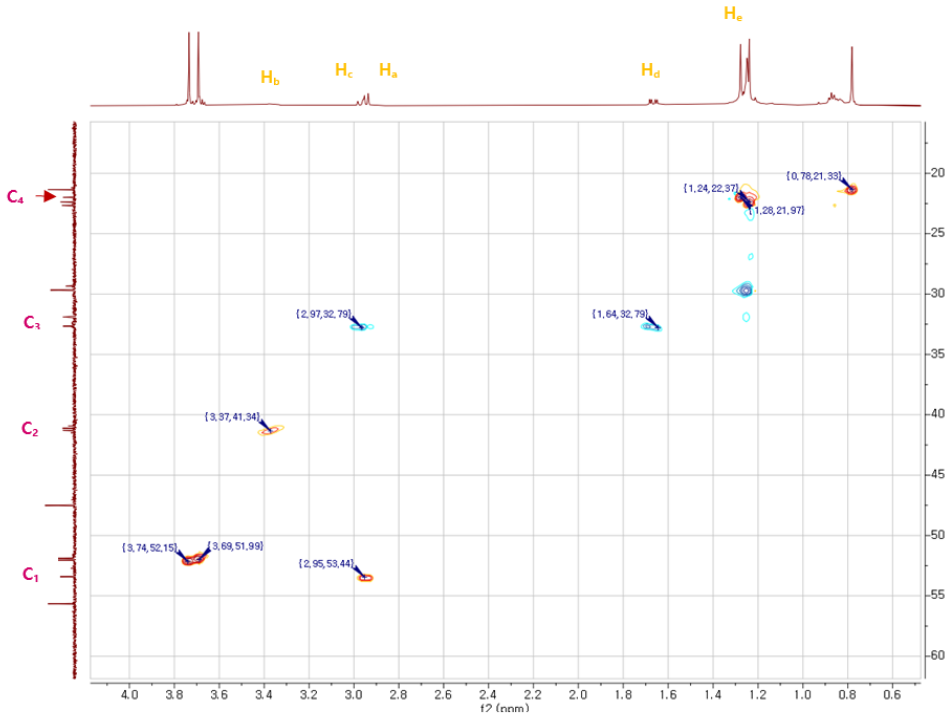

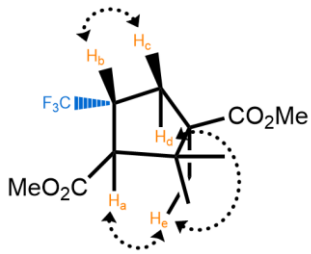

3x

(NOESY, $CDCl_3$)

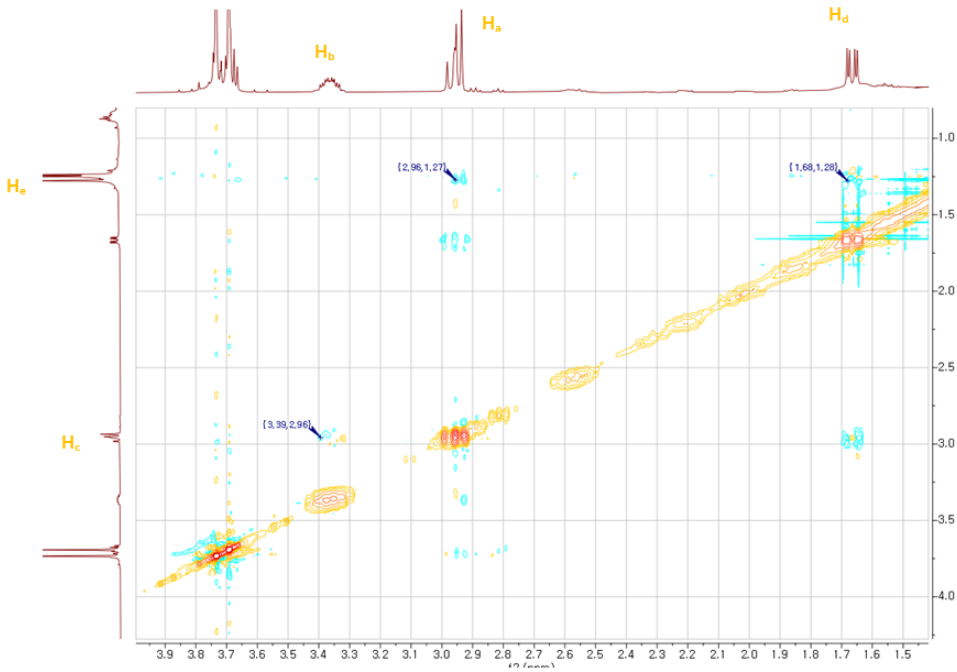

국문 초록

유기물의 C1 작용기화 반응 개발: N-메틸화, N-포밀화, 그리고 C(sp^3)-H 트리플루오르메틸화

본 논문에서는 유기금속 복합체를 이용한 새로운 C1 작용기화 반응을 개발하였다. 파트 1에서는 메탄올을 C1 원천으로 이용한 촉매적 활성화 방법에 대해 논한다. 메탄올은 다양한 분야에서 활용되는 생분해성 물질로, 경제적이고 지속 가능한 화합물로 주목을 받는다. 1 장에서는 메탄올이 유기 합성에 도입되는 대표적인 반응 예시들을 기술한다. 2 장에서는 메탄올과 루테늄 촉매를 이용한 다양한 아민의 단일 N-메틸화 반응에 대해서 기술한다. 메탄올은 탈수소화 반응을 통해 포름알데이드로 활성화가 되고, 메커니즘 연구를 통해서 수소 가스를 이용한 속도론적 반응성 조절이 본 선택성의 핵심임이 제안된다. 같은 루테늄 촉매는 간단한 반응 조건의 조절을 통해서 메탄올이 아민의 N-포밀화, N,N-이중메틸화, N,N-포밀메틸화 반응에도 활용될 수 있는 것을 보였다 (3 장).

파트 2에서는 유기 물질에 C1 트리플루오르메틸 작용기를 도입하여 $C(sp^3)$–CF_3 결합을 만드는 반응에 대해서 기술한다. 트리풀루오르메틸 작용화는 의약 개발 등 여러 분야에서의 활용성을 이유로 유기 합성에서 중요성이 대두되고 있다. 4 장에서는 최근의 $C(sp^3)$–CF_3 결협 형성 방법에 대해서 정리한다. C–H 활성화 트리플루오르메틸화는 중요한 해당 작용기를 복잡한 분자에 한번에 도입 할 수 있는 방법을 제시할 수 있어 이상적인 작용기화 반응으로 여겨지고 있다. 5 장에서는 구리-트리플루오르메틸 복합체와 빛을 이용하여 활성화되지 않은 일반적인 알케인의 $C(sp^3)$–H 트리플루오르메틸화 반응에 대해서 기술한다. 본 합성 방법은 도전적인 반응이 간단한 조건에서 가능하도록 하였고, 다양한 생활성 및 복잡한 분자의 작용기화를 통해 그 활용성을 보인다.

주요어 : C1 화학, 메탄올, 메틸화. 포밀화, C–H 활성화 반응, 트리플루오르메틸화. 구리, 가시 광선

학 번 : 2016-20368